

# Artificial ligands and biological interactors of GABARAP: Insights from a structural, biophysical, and imaging perspective

Inaugural-Dissertation

Zur Erlangung des Doktorgrades  
der Mathematisch-Naturwissenschaftlichen Fakultät  
der Heinrich-Heine-Universität Düsseldorf

vorgelegt von

**Alina Üffing**

aus Bocholt

Düsseldorf, Juli 2024

aus dem Institut für Physikalische Biologie  
der Heinrich-Heine-Universität Düsseldorf

Gedruckt mit der Genehmigung der  
Mathematisch-Naturwissenschaftlichen Fakultät der  
Heinrich-Heine-Universität Düsseldorf

Berichterstatter

Prof. Dr. Dieter Willbold

Prof. Dr. Andreas Reichert

Tag der mündlichen Prüfung: 27.08.2024



## Eidesstattliche Erklärung

Ich versichere an Eides statt, dass die Dissertation von mir selbstständig und ohne unzulässige fremde Hilfe unter Beachtung der Grundsätze zur Sicherung guter wissenschaftlicher Praxis an der Heinrich-Heine-Universität Düsseldorf erstellt worden ist.

Ferner erkläre ich, dass ich in keinem anderen Dissertationsverfahren mit oder ohne Erfolg versucht habe, diese Dissertation einzureichen.

Düsseldorf, den

---

(Alina Üffing)

# Acknowledgements

An dieser Stelle möchte ich mich bei all jenen bedanken, die mich in den letzten Jahren unterstützt und zur Entstehung dieser Arbeit beigetragen haben.

Zuerst danke ich Prof. Dr. Dieter Willbold für die Möglichkeit meine Dissertation am Institut für Physikalische Biologie (HHU) und am IBI-7 (Forschungszentrums Jülich) anzufertigen, seine fachliche Beratung und die Möglichkeit an internationalen Konferenzen teilzunehmen.

Außerdem danke ich Prof. Dr. Andreas Reichert für die Übernahme des Zweitgutachtens sowie die lehrreichen Besprechungen im Laufe der letzten Jahre.

Ein ganz besonderer Dank gilt Dr. Silke Hoffmann. Ohne deine unermüdliche Unterstützung und zahlreichen Diskussionen wäre diese Arbeit nicht zu dem geworden, was sie ist. Durch deine motivierende Art ist meine wissenschaftliche Neugier so groß wie nie.

Zudem danke ich Prof. Dr. Oliver Weiergräber für die schöne Zusammenarbeit, die lehrreichen Gespräche und vor allem die Geduld, mir vieles in der Strukturbiologie auch dreimal zu erklären.

Ein weiterer Dank gilt Dr. Thomas Gensch, Dr. Melanie Schwarten, Dr. Philipp Neudecker und Lisa Gold sowie der gesamten Kritzer-Gruppe für die konstruktive Zusammenarbeit an den Manuskripten in dieser Arbeit. Außerdem möchte ich mich bei allen aktuellen und ehemaligen Kolleginnen und Kollegen des IBI-7 (und IBI-1) bedanken: Insbesondere bei Joana Wilms, Assalla Abu Shamseye, Julia Große, Greta Willner und Markus Tusche für die gute Zusammenarbeit sowie bei Dr. Jochen Dobner, Dr. Julia L. Sanwald und Dr. Indra M. Simons, welche mir den „GABARAP-Einstieg“ erleichtert haben. Ein weiterer Dank geht an die Mitglieder des Sonderforschungsbereichs 1208.

Ein herzlicher Dank geht außerdem an Franziska Kaesler, Sebastian Kloubert, Gabriel Crespo López-Urrutia und Esther Wollert für's Zuhören und Dazwischenreden, für ernste Gespräche und gemeinsames Lachen.

Zu guter Letzt möchte ich den wunderbaren Menschen danken, welche mich außerdem durch die letzten Jahre begleitet haben. Meinen Freundinnen und Freunden – mit euch ist das Leben einfach schöner. Meinem Freund, Marcel – du verdienst einen Preis dafür, dass du mich während all meiner Abschlussarbeiten unterstützt und ertragen hast. Meiner Schwester Sarah und meinen Eltern für's Zuhören, Ermutigen und immer da sein.

## Summary

The  $\gamma$ -aminobutyric acid type A receptor-associated protein (GABARAP) is one out of seven human autophagy related 8 (ATG8) proteins, which can be divided into the GABARAP and microtubule-associated protein 1 light chain 3 (MAP1LC3/LC3) subfamilies. The seven paralogs show high structural similarity and all consist of a ubiquitin-like fold with two additional, less conserved N-terminal  $\alpha$ -helices, which participate in protein-protein and protein-lipid interactions. Furthermore, the ATG8 proteins can be covalently conjugated to membranes by an E1-E2-E3-like enzyme cascade after exposure of a C-terminal glycine. Many interaction partners bind to the two hydrophobic pockets (HP1 and HP2) on the surface of the ATG8s via a moderately conserved so-called LC3-interacting region (LIR), supporting a wide range of affinities. This explains, at least partially, how the paralogs fulfill their non-redundant functions in autophagy-related and -unrelated processes, and can be exploited to develop selective binders for the two subfamilies or even for individual members.

In this work, interactions of GABARAP were studied from different perspectives: First, from a structural perspective by investigating artificial ligands of ATG8s, namely stapled (i.e., internally crosslinked) peptides including Pen3-*ortho* and Pen8-*ortho*. These peptides, which only differ in the position of two methyl groups, bind GABARAP and LC3B with different selectivity, with Pen3-*ortho* preferring GABARAP 100-fold over LC3B, while Pen8-*ortho* binds both paralogs with similar affinities. The X-ray structures of the two stapled peptides in complex with GABARAP revealed different binding modes—one resembling the orientation of natural ligands and the other showing antiparallel orientation relative to the  $\beta$ 2-strand of GABARAP. Additionally, the small-molecule compound GW5074 was analyzed regarding its interaction with GABARAP. Chemical shift perturbation determined by a heteronuclear single quantum coherence (HSQC) nuclear magnetic resonance (NMR) titration of  $^{15}\text{N}$ -GABARAP with GW5074 revealed engagement of HP1, complementing data on the structure-activity relationships of arylidene-indolinone ligands of GABARAP and LC3B.

Concurrently, the epidermal growth factor receptor (EGFR) was investigated as a putative direct biological interactor of GABARAP from both a structural and a biophysical perspective. Preceding this work, enhanced degradation of the EGFR after EGF stimulation had been reported for cells lacking GABARAP, but not its paralogs. *In-vitro* affinity measurements with an EGFR-derived LIR peptide revealed selectivity for GABARAP and its closest paralog GABARAPL1. Additionally, the X-ray structure of a chimeric protein generated by fusion of the putative EGFR LIR with GABARAP revealed canonical binding to HP1 and HP2 of GABARAP. HSQC NMR titrations of the putative EGFR LIR peptide and GABARAP further supported this notion, offering a potential explanation for the reported phenotype.

Finally, a bivalent GABARAP-mTagBFP2-GABARAP construct was applied to study putative interactions from a live-cell imaging perspective. Interestingly, the construct strongly highlighted microtubules, which have been reported to interact with GABARAP in early *in-vitro* studies. Positively charged residues in the N-terminal region of GABARAP suggested to be responsible in these studies proved to be crucial for the peculiar localization of the bivalent construct in living cells. Additionally, microtubule association was dependent on the choice of mTagBFP2 as a fluorophore.

In conclusion, this work provides insights from different perspectives that enhance our understanding of the multifaceted human ATG8 protein family—with a focus on GABARAP. The findings reported herein can be applied in future research to further investigate biological processes involving these proteins and to develop powerful modulators for application in cell biology and medicine.

## Zusammenfassung

Das *γ-aminobutyric acid type A receptor-associated protein* (GABARAP) ist eines von sieben humanen Autophagie assoziierten (ATG8) Proteinen, welche sich in die GABARAP und *microtubule-associated protein 1 light chain 3* (MAP1LC3/LC3) Unterfamilien unterteilen lassen. Die sieben Paraloge weisen eine hohe strukturelle Ähnlichkeit auf und besitzen eine ubiquitinähnliche Faltung mit zwei zusätzlichen, weniger konservierten N-terminalen  $\alpha$ -Helices, welche an Protein-Protein und Protein-Lipid Interaktionen beteiligt sind. Des Weiteren können die ATG8 Proteine nach Freilegung eines C-terminalen Glycins durch eine E1-E2-E3-ähnlichen Enzymkaskade kovalent an Membranen konjugiert werden. Viele Interaktionspartner binden an zwei hydrophobe Taschen (HP1 und HP2) auf der Oberfläche der ATG8 mithilfe einer moderat konservierten LC3-interagierenden Region (LIR), die ein breites Spektrum an Affinitäten abdeckt. Dies erklärt zumindest teilweise, wie die Paraloge ihre nicht-redundanten Funktionen in autophagischen und nicht-autophagischen Prozessen erfüllen und kann für die Entwicklung selektiver Bindungspartner für die zwei Unterfamilien oder sogar individuelle Mitglieder der ATG8s genutzt werden.

In dieser Arbeit wurden Interaktionen von GABARAP aus verschiedenen Perspektiven untersucht: Erstens aus einer strukturellen Perspektive durch die Untersuchung artifizieller Liganden, genauer *stapled* (d.h. intern vernetzten) Peptiden, unter anderem Pen3-*ortho* und Pen8-*ortho*. Diese Peptide, welche sich nur in der Position zweier Methylgruppen unterscheiden, binden GABARAP und LC3B mit verschiedenen Selektivitäten, wobei Pen3-*ortho* GABARAP 100-fach gegenüber LC3B präferiert, während Pen8-*ortho* beide Paraloge mit vergleichbarer Affinität bindet. Die Röntgenkristallstruktur der beiden *stapled* Peptide in einem Komplex mit GABARAP zeigte verschiedene Bindungsmodi — einer ähnelt der Ausrichtung natürlicher Liganden, der andere zeigt eine antiparallele Ausrichtung zu GABARAPs  $\beta$ 2-Strang. Außerdem wurde das *small-molecule compound* GW5074 in Bezug auf seine Interaktion mit GABARAP untersucht. Die Änderung der chemischen Verschiebung, welche mittels *heteronuclear single quantum coherence* (HSQC) NMR Titration von  $^{15}\text{N}$ -GABARAP mit GW5074 bestimmt wurde, zeigte die Einbindung der HP1. Dies ergänzt Daten zur Struktur-Aktivität Beziehung von Aryliden-Indolinon-Liganden mit GABARAP und LC3B.

Gleichzeitig wurde der *epidermal growth factor receptor* (EGFR) als möglicher direkter biologischer Interaktionspartner von GABARAP, sowohl aus struktureller als auch aus biophysikalischer Sicht untersucht. Im Vorhinein dieser Arbeit wurde ein verstärkter Abbau von EGFR nach EGF-Stimulation, spezifisch in GABARAP-defizienten, aber nicht Paralog-defizienten Zellen berichtet. *In-vitro* Affinitätsmessungen mit einem EGFR abgeleiteten LIR-Peptid zeigten eine Selektivität für GABARAP und sein nächstes Paralog GABARAPL1. Darüber hinaus ergab die Röntgenkristallstruktur eines chimären Proteins, welches als Fusion des mutmaßlichen EGFR-LIR Peptids mit GABARAP

generiert wurde, eine kanonische Bindung an GABARAPs HP1 und HP2. HSQC NMR Titration des mutmaßlichen EGFR-LIR-Peptids zu GABARAP unterstützten diese Beobachtung und bieten eine mögliche Erklärung für den beschriebenen Phänotyp.

Zuletzt wurde ein bivalentes GABARAP-mTagBFP2-GABARAP zur Untersuchung möglicher Interaktionen aus einer Lebendzellmikroskopie Perspektive angewendet. Interessanterweise hob das Konstrukt Mikrotubuli stark hervor, von denen in frühen *in-vitro*-Studien berichtet wurde, dass sie mit GABARAP interagieren. Positiv geladene Seitenketten in der N-terminalen Region von GABARAP, welche in diesen Studien für die Assoziation mit Mikrotubuli verantwortlich gemacht wurden, erwiesen sich entscheidend für die besondere Lokalisierung des bivalenten Konstrukts in Zellen. Darüber hinaus war die Mikrotubuli Assoziation abhängig vom Fluorophor, im speziellen mTagBFP2.

Zusammenfassend bietet diese Arbeit Einsichten aus verschiedenen Perspektiven, welche unser Verständnis der vielen Facetten humaner ATG8 Proteine erweitern — mit besonderem Fokus auf GABARAP. Die hier erlangten Erkenntnisse können in Zukunft genutzt werden, um biologische Prozesse, an denen diese Proteine beteiligt sind, weiter zu untersuchen und wirksame Modulatoren für die Anwendungen in der Zellbiologie und Medizin zu entwickeln.

# Contents

<b>Summary.....</b>	<b>I</b>
<b>Zusammenfassung.....</b>	<b>III</b>
<b>Contents .....</b>	<b>V</b>
<b>List of Abbreviations.....</b>	<b>VII</b>
<b>List of Figures .....</b>	<b>X</b>
<b>1 Introduction .....</b>	<b>1</b>
1.1. The human ATG8 protein family .....	1
1.1.1. The GABARAP and LC3 subfamilies.....	1
1.1.2. Structural features and interaction sites .....	2
1.2. Human ATG8 proteins and autophagy .....	7
1.2.1. Conjugation of human ATG8s to autophagic membranes .....	9
1.2.2. Roles of GABARAP and LC3 during the different steps of autophagy .....	10
1.3. Unconventional roles of human ATG8 proteins .....	13
1.3.1. Conjugation of human ATG8s to single membranes .....	14
1.3.2. Interplay of autophagy and endocytic trafficking.....	15
1.4. Studying human ATG8 protein function .....	17
1.4.1. From phenotypes to molecular mechanisms .....	17
1.4.2. From molecular interaction to modulation of function .....	18
1.5. Modulation of autophagy as a therapeutic strategy .....	19
<b>2 Aims.....</b>	<b>21</b>
<b>3 Results .....</b>	<b>23</b>
3.1. Structure-based design of stapled peptides that bind GABARAP and Inhibit autophagy .....	23
3.2. Exploring arylidene-indolinone ligands of autophagy proteins LC3B and GABARAP .....	37
3.3. GABARAP interacts with EGFR — supporting the unique role of this hAtg8 protein during receptor trafficking .....	49
3.4. Highlighting the hidden: monitoring the avidity-driven association of a fluorescent GABARAP tandem with microtubules in living cells .....	73
<b>4 Summary and Conclusion.....</b>	<b>113</b>
<b>5 List of Publications and Presentations .....</b>	<b>119</b>
5.1. Publications.....	119
5.2. Preprints/submitted manuscripts.....	119
5.3. Poster Presentations.....	120
<b>5 References .....</b>	<b>121</b>





## List of Abbreviations

<b>ADRB2</b>	beta-2 adrenergic receptor
<b>AnkG</b>	Ankyrin-G
<b>AnkB</b>	Ankyrin-B
<b>ARL8B</b>	ADP-ribosylation factor-like protein 8B
<b>ATG/ATG</b>	autophagy related protein/ <i>gene</i>
<b>ATG8 (Atg8)</b>	autophagy related 8 protein
<b>ATP</b>	adenosine triphosphate
<b>ATTEC</b>	autophagosome-tethering chimera
<b>BafA1</b>	bafilomycin A1
<b>BLI</b>	biolayer interferometry
<b>CASM</b>	conjugation of ATG8 to single membranes
<b>EGFR</b>	epidermal growth factor receptor
<b>ESCRT-I</b>	endosomal sorting complex required for transport I
<b>ER</b>	endoplasmic reticulum
<b>ERK1/2</b>	extracellular signal-regulated kinase 1/2
<b>FAM134B</b>	reticulophagy regulator 1
<b>FDB</b>	FIP200 binding domain
<b>FIP200</b>	FAK family kinase-interacting protein of 200 kDa
<b>FLCN</b>	folliculin
<b>FNIP</b>	folliculin-interacting protein
<b>FUNDC1</b>	FUN14 domain-containing protein 1
<b>FYCO1</b>	FYVE and coiled-coil domain-containing protein 1
<b>GABA<sub>A</sub>-receptor</b>	γ-aminobutyric acid type A receptor
<b>GABARAP</b>	γ-aminobutyric acid type A receptor-associated protein
<b>GATE-16</b>	Golgi-associated ATPase enhancer of 16 kDa
<b>GEC-1</b>	glandular epithelial cell protein 1
<b>GFP</b>	green fluorescent protein

<b>GRB2</b>	growth factor receptor-bound protein 2
<b>HGF</b>	hepatocyte growth factor
<b>HP1 and HP2</b>	hydrophobic pocket 1 and 2
<b>HSQC</b>	heteronuclear single quantum coherence
<b>JIP1</b>	JNK-interacting protein 1
<b>LANDO</b>	LC3-associated endocytosis
<b>LAP</b>	LC3-associated phagocytosis
<b>LDELS</b>	LC3-dependent extracellular vesicle loading and secretion
<b>LDS</b>	LIR docking site
<b>LIR</b>	LC3-interacting region
<b>MAP1A/B</b>	microtubule associated protein 1A/B
<b>MAP1ALC1</b>	microtubule-associated protein 1A light chain 1
<b>MAP1BLC2</b>	microtubule-associated protein 1B light chain 2
<b>MAP1LC3/LC3</b>	microtubule-associated protein 1 light chain 3
<b>MET</b>	mesenchymal-epithelial transition factor
<b>mTOR</b>	mammalian target of rapamycin
<b>NBR1</b>	next to BRCA1 gene 1 protein
<b>NDP52</b>	nuclear domain 10 protein 52
<b>NIX</b>	NIP-3-like protein X
<b>NMR</b>	nuclear magnetic resonance
<b>NSF</b>	N-ethylmaleimide-sensitive factor
<b>OPTN</b>	optineurin
<b>PE</b>	phosphatidylethanolamine
<b>PIK3C3/VPS34</b>	phosphatidylinositol 3-kinase catalytic subunit type 3
<b>PI3KC3-C1</b>	class III phosphatidylinositol PI3-kinase complex I
<b>PI3P</b>	phosphatidylinositol-3-phosphate
<b>PI4KIII<math>\beta</math></b>	phosphatidylinositol 4-kinase III $\beta$
<b>PI4KII<math>\alpha</math></b>	phosphatidylinositol 4-kinase II $\alpha$

<b>PI4P</b>	phosphatidylinositol-4-phosphate
<b>PLEKHM1</b>	pleckstrin homology domain-containing family M member 1
<b>PROTAC</b>	proteolysis targeting chimera
<b>PS</b>	phosphatidylserine
<b>PTM</b>	posttranslational modification
<b>RFP</b>	red fluorescent protein
<b>SI</b>	supplemental information
<b>SCOC</b>	short coiled-coil protein
<b>SLC2A1</b>	solute carrier family 2 member 1
<b>SNAP29</b>	synaptosomal-associated protein 29
<b>SQSTM1/p62</b>	sequestosome-1
<b>STX17</b>	syntaxin-17
<b>STING</b>	stimulator of interferon genes protein
<b>TBC1D5</b>	TBC1 domain family member 5
<b>TECPR1</b>	tectonin beta-propeller repeat-containing protein 1
<b>UDS</b>	UIM docking site
<b>UIM</b>	ubiquitin-interacting motif
<b>ULK</b>	Unc-51-like kinase
<b>VAMP8</b>	vesicle-associated membrane protein 8
<b>VPS37A</b>	vacuolar protein sorting-associated protein 37A
<b>VPS15</b>	PI3-kinase p150 subunit
<b>WIPI2/4</b>	WD repeat domain containing phosphoinositide-interacting protein 2/4
<b>α-SNAP</b>	alpha-soluble NSF attachment protein

## List of Figures

<b>Figure 1.</b> Structural and sequence overview of human ATG8 proteins. ....	<b>3</b>
<b>Figure 2.</b> Interaction sites of GABARAP and its binding partners.....	<b>7</b>
<b>Figure 3.</b> Schematic overview of the autophagic process. ....	<b>9</b>
<b>Figure 4.</b> Conjugation of ATG8 proteins to autophagic membranes. ....	<b>10</b>
<b>Figure 5.</b> Conjugation of ATG8 proteins to single membranes (CASM). ....	<b>15</b>
<b>Figure 6.</b> Overview of paralog mRNA expression in selected cell lines and tissues and ATG8 related publications. ....	<b>113/114</b>
<b>Figure 7.</b> Overview of artificial (pink background) and putative biological interactors of GABARAP (green background) investigated in this work.....	<b>117</b>

# 1 Introduction

## 1.1. The human ATG8 protein family

Autophagy related (ATG) proteins comprise a group of evolutionarily conserved proteins involved in the eponymous process of autophagy and have initially been discovered in the yeast *Saccharomyces cerevisiae* (Tsukada and Ohsumi, 1993, Thumm et al., 1994). Atg8 was among the first discovered proteins in yeast, and soon after, mammalian homologs were described and characterized (Kabeya et al., 2000, Kabeya et al., 2004, Lang et al., 1998, He et al., 2003). Humans possess seven ATG8 paralogs, which can be divided into the  $\gamma$ -aminobutyric acid type A receptor-associated protein (GABARAP) and microtubule-associated protein 1 light chain 3 (MAP1LC3/LC3) subfamilies, with the former comprising GABARAP, GABARAPL1 and GABARAPL2 (Xin et al., 2001) and the latter LC3A, LC3B, LC3B2 and LC3C (He et al., 2003). Notably, LC3B2, which differs from LC3B by only one amino acid residue, and LC3C only show very low and/or tissue-specific expression. In the following the two human ATG8 subfamilies and their structural features and interactions will be described to demonstrate the versatility and uniqueness defining this protein family.

### 1.1.1. The GABARAP and LC3 subfamilies

While yeast possesses one Atg8 protein, several homologs have emerged in the evolution of multicellular organisms (Shpilka et al., 2011). Varying numbers of Atg8-like proteins exist in higher eukaryotes with up to 22 in plants (Kellner et al., 2017) and only two in *Caenorhabditis elegans* (Wu et al., 2015). Phylogenetic analysis of the seven human paralogs indicated closest relation between GABARAP and GABARAPL1 in the GABARAP subfamily and LC3A and LC3B in the LC3 subfamily, while GABARAPL2 and LC3C branched into separate clades. Consistently, sequence identity is diverse ranging from 31% between GABARAP and LC3B to 87% between GABARAP and GABARAPL1 and 83% between LC3A and LC3B (Jatana et al., 2020).

Several of the ATG8 proteins were described before or in parallel to their identification as homologs of yeast Atg8 and connecting them to autophagy. As its name implies, GABARAP was first described as a protein associated with the  $\gamma$ -aminobutyric acid type A (GABA<sub>A</sub>) receptor (Wang et al., 1999, Wang and Olsen, 2000) and has subsequently been shown to be important for anterograde trafficking of the receptor (Ye et al., 2021, Leil et al., 2004, Chen et al., 2000). Similarly, GABARAPL1, initially named glandular epithelial cell protein 1 (GEC-1), encoded by an estrogen regulated gene (Pellerin et al., 1993, Vernier-Magnin et al., 2001) has been reported to be involved in trafficking of both the GABA<sub>A</sub> and  $\kappa$ -opioid receptor (Chen et al., 2006, Mansuy et al., 2004). GABARAPL2 was originally proposed to modulate intra-Golgi transport and accordingly termed Golgi-associated ATPase enhancer of weight 16 kDa (GATE-16; Sagiv et al., 2000). The microtubule-associated

protein 1 light chain 3 (MAP1LC3/LC3) protein subfamily, hereafter referred to as the LC3 subfamily, was originally copurified with bovine brain microtubules (Kuznetsov and Gelfand, 1987). While light chains 1 and 2 (MAP1ALC1 and MAP1BLC2) associate with microtubule associated proteins 1A and 1B (MAP1A and MAP1B), respectively, LC3 was shown to co-purify with both. Additionally, in contrast to LC1 and LC2, expression of LC3 was found to not be linked to the heavy chain genes (Mann and Hammarback, 1996, Mann and Hammarback, 1994), indicating a distinct function early on.

Soon after the discovery of autophagy related proteins in yeast, including Atg8, homologs of yeast proteins in higher eukaryotes were identified and characterized regarding their function during autophagy—including the members of the LC3 and GABARAP subfamilies in humans (Kabeya et al., 2000, Kabeya et al., 2004, Tanida et al., 2003, Tanida et al., 2002, Tanida et al., 2001). The fact that in humans seven paralogs have emerged, compared to a single one in yeast, raises the question of functional divergence versus redundancy of the subfamilies as well as individual ATG8s. Proteomic analysis of the interactome of the ATG8s revealed that about one third of each of the identified proteins interacted specifically with the GABARAP and the LC3 subfamily, respectively, and one third interacted with both subfamilies (Behrends et al., 2010). While different expression levels and tissue distributions offer one explanation for the specific interactions, structural features of the individual paralogs may also regulate binding and thereby support distinct functions in both autophagy-related and -unrelated processes.

### 1.1.2. Structural features and interaction sites

The versatile roles of ATG8 proteins are, at least partially, based on their structural features and interaction sites, many of which are evolutionarily conserved (Noda et al., 2010, Zhang et al., 2022). All ATG8s share a ubiquitin-like fold with one or two additional N-terminal helices (Paz et al., 2000, Krichel et al., 2019, Coyle et al., 2002; Figure 1A). The sequence of the N-terminal helices is the least conserved part among the paralogs, with higher sequence variation within the LC3 subfamily compared to the GABARAPs (Jatana et al., 2020; Figure 1B) and has been suggested to be important for selective interactions with binding partners (Sugawara et al., 2004, Shvets et al., 2011). The N-terminal helix  $\alpha 2$  aligning with the ubiquitin-fold forms hydrophobic pocket 1 (HP1), which together with hydrophobic pocket 2 (HP2) within the ubiquitin-like domain constitutes the interface of interaction with proteins harboring an LC3-interacting region (LIR) motif (Pankiv et al., 2007, Ichimura et al., 2008, Noda et al., 2010), termed LIR docking site (LDS). Additionally, ATG8 proteins are able to interact with proteins containing a ubiquitin-interacting motif (UIM) via another less well characterized interaction site located opposite to the LDS, namely the UIM docking site (UDS; Marshall et al., 2019). Finally, a function-defining feature of ATG8 proteins is their conjugation to lipids, by a ubiquitin-like E1-E2-E3 enzyme conjugation system (Tanida et al., 2002, Tanida et al.,

2001, Hanada et al., 2007, Fujita et al., 2008b, Otomo et al., 2013), via a terminal glycine once exposed after processing by the cysteine protease ATG4 (Kabeya et al., 2004).

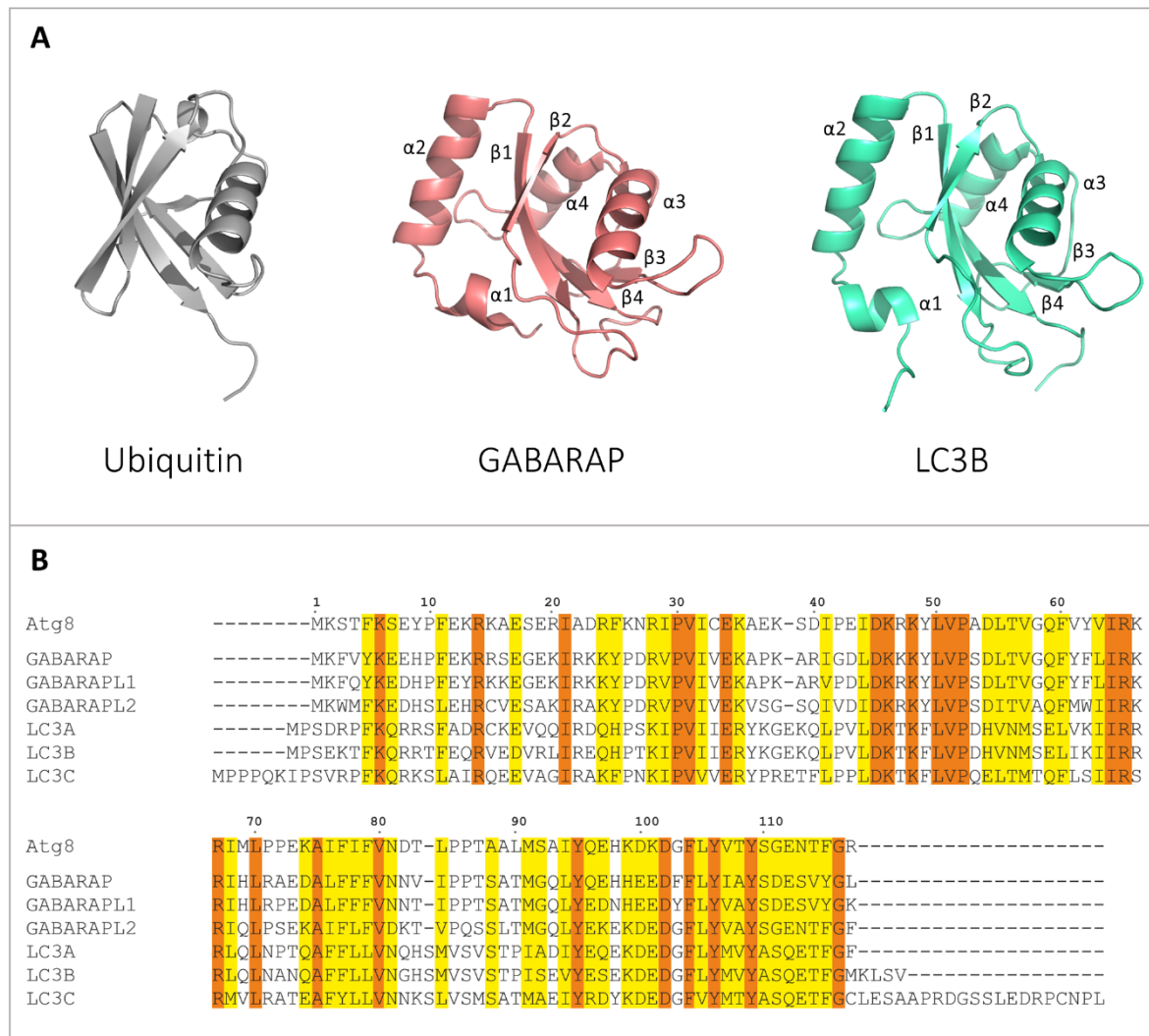


**Figure 1. Structural and sequence overview of human ATG8 proteins. (A)** Cartoon structural models of Ubiquitin (PDB ID: 1UBQ, Vijay-Kumar et al., 1987), GABARAP (PDB ID: 1KOT, Stangler et al., 2002), and LC3B (PDB ID: 1V49, Kouno et al., 2005). For GABARAP and LC3B  $\alpha$ -helices and  $\beta$ -strands are marked. Images were created using the PyMOL Molecular Graphics System, Version 3.0 Schrödinger, LLC. **(B)** Sequence alignment of *Saccharomyces cerevisiae* Atg8 and human ATG8 proteins generated with Clustal Omega (Sievers and Higgins, 2014, Madeira et al., 2022). Identical residues are marked in orange and similar ones in yellow.

As this work mostly focusses on GABARAP, an exemplary overview of the interaction sites mapped on the surface of this paralog is shown in Figure 2A. The N-terminal region of GABARAP, together with a loop region following the  $\beta$ 1 strand, has been reported to be involved in membrane expansion and thereby regulating autophagosome size (Zhang et al., 2023). Additionally, early *in-vitro* studies have revealed that the association of GABARAP with microtubules as well as the ability to induce tubulin polymerization are dependent on the N-terminal region of GABARAP, likely through interactions of positively charged residues with the negatively charged C-terminal tails of the tubulin monomers (Coyle et al., 2002, Wang and Olsen, 2000).

In case of GABARAP, HP1 of the abovementioned LDS is lined by Glu17, Ile21, Pro30, Lys48, Leu50, Phe104 and has been shown to preferentially bind indole-based substances and aromatic side chains of amino acids (Thielmann et al., 2008). HP2 is formed by Tyr49, Val51, Pro52, Leu55, Phe60, Leu63 and Ile64 (Thielmann et al., 2008, Noda et al., 2008) and is extended by an additional hydrophobic residue (Phe62) in the GABARAPs compared to the LC3 subfamily, possibly regulating subfamily selective binding (Wirth et al., 2019). These two hydrophobic pockets build the interface for the majority of interactions of ATG8s with other proteins (Johansen and Lamark, 2020, Birgisdottir et al., 2013, Rogov et al., 2023), harboring a LIR motif (Figure 2B). Since the description of the first LIR in sequestosome-1 (SQSTM1/p62), where binding to LC3B is mediated by a W-X<sub>1</sub>-X<sub>2</sub>-L motif, with W (Trp) and L (Leu) interacting with HP1 and HP2, respectively, and X being any amino acid, as well as an acidic cluster preceding the conserved core motif (Pankiv et al., 2007, Ichimura et al., 2008), a wide variety of LIRs have been described. Structural studies and mutational analysis have refined the canonical core motif to  $\Theta_0$ -X<sub>1</sub>-X<sub>2</sub>- $\Gamma_3$ , with  $\Theta_0$  representing aromatic residues (Trp/Phe/Tyr) and  $\Gamma_3$  (Ile/Leu/Val) large hydrophobic residues. The X<sub>1</sub> and X<sub>2</sub> core LIR residues, often represented by acidic or hydrophobic residues, as well as the residues N- and C-terminal to the core LIR are less conserved (Johansen et al., 2017, Johansen and Lamark, 2020, Birgisdottir et al., 2013, Alemu et al., 2012). Notably, with the growing number of characterized LIRs, the importance of these residues for regulating binding affinity and selectivity for the different paralogs/subfamilies, has become apparent. The residues in the immediate N-terminal vicinity of the core LIR are often acidic and enhance binding with the ATG8 through the basic surface surrounding the hydrophobic pockets (Johansen and Lamark, 2020). Additionally, favorable binding to LC3s over GABARAPs has been reported when X<sub>3</sub> and X<sub>4</sub> are acidic (Wirth et al., 2019, Cheng et al., 2016). The core LIR position X<sub>1</sub> is frequently occupied by Val or Ile in case of proteins showing selective binding for the GABARAP subfamily, though exceptions are known (Rogov et al., 2017a). In contrast, X<sub>2</sub>, despite being the most promiscuous position of the core LIR, appears to be a stronger determinant for LC3 binding, as substitution to Gly or Pro in the pleckstrin homology domain-containing family M member 1 (PLEKHM1) LIR was disruptive to binding LC3s but only mildly affected binding of the GABARAPs (Johansen and Lamark, 2020, Rogov et al., 2017a). Regarding the region C-terminal to the core LIR, X<sub>4</sub> appears to play a role for selectivity, with Pro in this position being favorable for GABARAP binding (Wirth et al., 2019). X<sub>7</sub> is frequently occupied by acidic residues, and charge-mediated interactions with a conserved Arg residue adjacent to HP2 (Arg67 in GABARAP) likely support binding (Cheng et al., 2016). Furthermore, in FAM134B (also called reticulophagy regulator 1), ankyrin-G (AnkG) and ankyrin-B (AnkB), X<sub>7</sub> marks the start of an amphipathic helix, which has been proposed to facilitate extraordinarily strong binding (Li et al., 2018).

Both binding affinity and selectivity of proteins towards ATG8s can additionally be regulated through phosphorylation of certain LIR residues (Rogov et al., 2013, Rogov et al., 2017b, Kuang et



al., 2016, Wild, 2011, Wirth et al., 2021, Zhou et al., 2023, Birgisdottir et al., 2019, Zhu et al., 2013, Yang et al., 2015, Chino et al., 2022). Positive regulation of binding is frequently facilitated by phosphorylation of residues in the region N-terminal to the core LIR, where Ser/Thr residues are common, with the strongest effects seen for phosphorylation of residues immediately preceding the core LIR (Birgisdottir et al., 2013, Rogov et al., 2023). One example is the phosphorylation of Ser177 ( $X_{-1}$ ) of optineurin (OPTN), which leads to a five-fold increase in affinity to LC3B and has been shown to be involved in the clearance of cytosolic *Salmonella* (Wild, 2011, Rogov et al., 2013). Phospho-mimicking mutations of Ser244 and Ser249 of phosphatidylinositol 3-kinase catalytic subunit type 3 (PIK3C3/VPS34) result in 15- to 20-fold increase in affinity to GABARAP/GABARAPL1 and LC3C (Birgisdottir et al., 2019). In case of the mitophagy receptor NIP-3-like protein X (NIX/BNIP3L), an even more drastic about 100-fold increase in affinity to LC3B as a result of Ser34 ( $X_{-2}$ ) and Ser35 ( $X_{-1}$ ) phosphorylation has been reported (Rogov et al., 2017b). In contrast, phosphorylation of Tyr18 of FUN14 domain-containing protein 1 (FUNDC1) in position  $\Theta_0$  of its core LIR negatively regulates binding to LC3B, possibly serving as a molecular switch in mitophagy (Kuang et al., 2016). Another putative example of negative regulation through phosphorylation has been proposed for the hepatocyte growth factor receptor (HGF) MET (mesenchymal-epithelial transition factor) in the context of liver cancer. While phosphorylated putative core LIR residues  $\Theta_0$  and  $X_1$  (Tyr1234 and Tyr1235) contribute to growth factor signaling, their dephosphorylation induces autophagy (Huang et al., 2019). Despite being less common, an impact of phosphorylation C-terminal to the core LIR on ATG8 binding has also been reported. Interestingly, phosphorylation of Ser18 of short coiled-coil protein (SCOC) leads to positive regulation of binding specifically to the LC3 subfamily proteins but not the GABARAPs (Wirth et al., 2021). Notably, several studies on the effects of phosphorylation on binding are limited to one ATG8 subfamily or paralog (Kuang et al., 2016, Wild, 2011, Rogov et al., 2017b, Wu et al., 2014), thus it remains to be determined whether all paralogs are similarly affected in these cases.

In addition to canonical LIR motifs, non-canonical ones have been described, including the LC3C specific CLIR in nuclear domain 10 protein 52 (NDP52/CALCOCO2), which only engages HP2 (von Muhlinen et al., 2012), and the apoptosis regulator Bcl-2 LIR, which preferentially binds GABARAP and GABARAPL1 and only occupies HP1 (Ma et al., 2013). Regarding its orientation relative to GABARAP, the synthetic peptide K1 is noteworthy since it binds in a non-canonical fashion, antiparallel to the  $\beta_2$  strand of GABARAP (Weiergräber et al., 2008).

While LIR-LDS interactions have been and continue to be thoroughly characterized, with more and more complex structures of GABARAP (and paralogs) with LIR-harboring peptides being resolved, structural data for the UDS-UIIM interaction is still lacking. However, interactions with GABARAP and LC3A dependent on predicted UIMs have been identified by yeast-two-hybrid assays, with epsin-1-3 and rabenosyn interacting with both paralogs and ataxin-3 and ataxin-3L binding

GABARAP only (Marshall et al., 2019). Interestingly, ATG4B has been suggested to interact with both the LDS and UDS region of ATG8s (Satoo et al., 2009, Skytte Rasmussen et al., 2017), even though no UIM has been identified for ATG4B. Due to the ability of ATG4B to stabilize pools of unlipidated GABARAP, protecting them from proteasomal degradation, the UDS has been proposed as an interaction site for receptors for proteasomal degradation, possibly without ubiquitylation (Skytte Rasmussen et al., 2017, Johansen and Lamark, 2020). Conversely, ubiquitylation of Lys13 and Lys23 by the E3 ligase MIB1 and subsequent degradation has been reported in the absence of pericentriolar material 1 protein (PCM1), which appears to stabilize GABARAP through a LIR-LDS based interaction and thereby regulates autophagosome formation (Joachim et al., 2017). Another posttranslational modification (PTM), namely acetylation and deacetylation of Lys46 and Lys48, has been proposed to be important for shuttling of GABARAP between nucleus and the cytoplasm where it can undergo conjugation to membranes (Baeken et al., 2020, Ali et al., 2024). This conjugation to membranes can be viewed either as a PTM of GABARAP/ATG8s, as lipids (e.g. phosphatidylethanolamine or phosphatidylserine (Durgan et al., 2021, Ichimura et al., 2000) are covalently conjugated to the C-terminal glycine exposed by ATG4, or as a modification of membranes similar to the modification of proteins by ubiquitin—recently termed Atg8ylation (Kumar et al., 2021). In the following chapters, conjugation of ATG8s to autophagic membranes, often referred to as double membranes, and single membranes and the corresponding functions in autophagy-related and -unrelated processes will be discussed, with particular attention to non-redundant functions of the individual ATG8 proteins.

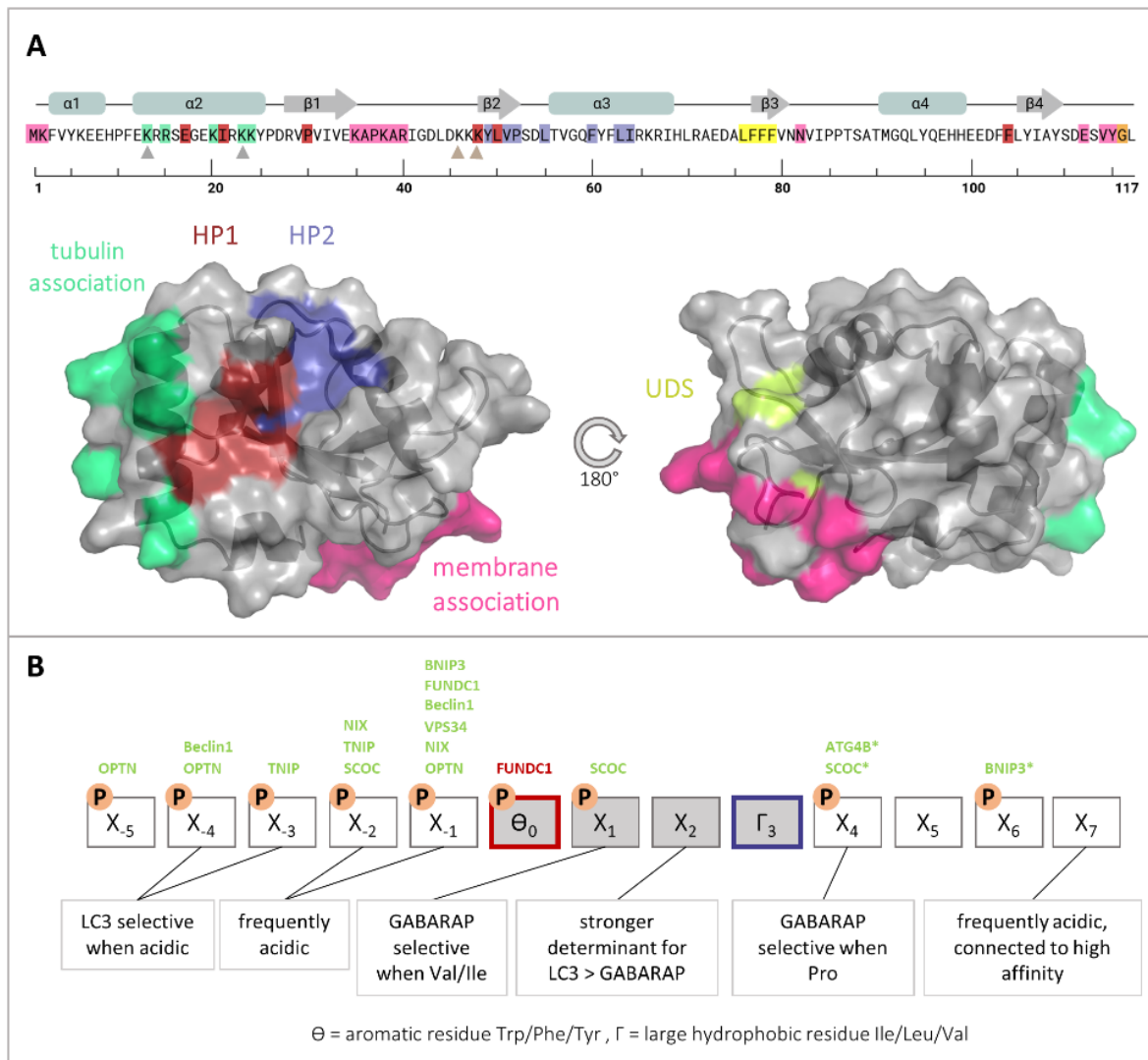


**Figure 2. Interaction sites of GABARAP and its binding partners.** (A) Verified and putative interaction sites of GABARAP mapped to the primary structure and molecular surface. (PDB ID: 1KOT, Stangler et al., 2002). HP1 (red), HP2 (blue), tubulin association site (green), UDS (yellow), lipidation site (orange), and membrane association site (pink) are marked. Additionally, ubiquitylation sites (gray arrows) and putative acetylation sites (brown arrows) are indicated. Images were created using the PyMOL Molecular Graphics System, Version 3.0 Schrödinger, LLC and BioRender.com. (B) The conserved LIR sequence of ATG8 interaction partners. The core LIR motif is marked in gray with colored frames indicating residues interacting with HP1 (red) and HP2 (blue). Residues modulated by phosphorylation are indicated by 'P' with selected examples of interacting proteins indicated above, in green in case of positive regulation and red in case of negative regulation. Asterisk indicates subfamily/paralog specific positive regulation. Below the sequence, the significance of individual positions regarding binding affinity and selectivity is indicated. For details and references refer to the main text.

## 1.2. Human ATG8 proteins and autophagy

The evolutionary conserved process of macroautophagy, hereafter referred to as autophagy, is a degradative process for maintenance of cellular homeostasis. The term 'autophagy' was defined around 60 years ago as engulfment of cytoplasmic contents by double membrane structures, namely autophagosomes, and their delivery to the lysosome for degradation (De Duve, 1963, Arstila and Trump, 1968). While these early studies were mostly based on morphological investigations by electron microscopy, a breakthrough for understanding the molecular mechanisms behind this process was achieved by identification of autophagy-related genes (ATGs) and the respective

proteins in yeast (Tsukada and Ohsumi, 1993, Harding et al., 1995, Thumm et al., 1994) as well as their mammalian and human counterparts (Mizushima et al., 1998, Mizushima et al., 2011). Since then, extensive research on autophagy and the related proteins has led to the current understanding of the process—from initiation of phagophore formation over its expansion, and closure to transport of the resulting autophagosome to the lysosome and subsequent fusion (Figure 3). Autophagy can be non-selective, mainly as a response to starvation, or selective with a wide range of cargos ranging from protein aggregates to whole organelles and invading pathogens (Feng et al., 2014, Mizushima and Komatsu, 2011, Jin et al., 2013, Johansen and Lamark, 2020, Bjorkoy et al., 2005, Ma et al., 2022, Lazarou et al., 2015, Deosaran et al., 2013, Tumbarello et al., 2015, Thurston et al., 2009). Please note that in the following chapters referring to cell-based and *in-vitro* studies, human protein names will be used for simplicity, even though some studies additionally include other mammalian cell lines or proteins.

In humans, the Unc-51-like kinase (ULK) complex, comprising ULK1/2, FAK family kinase-interacting protein of 200 kDa (FIP200/RB1CC1), ATG13, and ATG101, is initially recruited to the phagophore initiation site at endoplasmic reticulum (ER) subdomains enriched in phosphatidylinositol-synthase (Chan et al., 2007, Ganley et al., 2009, Nishimura et al., 2017). While occurring independently of the ULK kinase function, downstream ATG proteins and the phospholipid phosphatidylinositol-3-phosphate (PI3P), the determinants regulating this recruitment remain incompletely understood (Nishimura and Tooze, 2020, Melia et al., 2020). ATG9A vesicles appear to be involved in these initial steps, in that they deliver phosphatidylinositol 4-kinase III $\beta$  (PI4KIII $\beta$ ) to the phagophore nucleation site, leading to phosphatidylinositol-4-phosphate (PI4P) generation. PI4KIII $\beta$  and PI4P have been proposed to be involved in ULK complex recruitment, possibly through association of the ATG13 N-terminus with negatively charged phospholipids like PI4P (Judith et al., 2019, Karanasios et al., 2013). Additionally, ATG9A together with ATG2 and WD repeat domain phosphoinositide-interacting protein 4 (WIPI4) mediate lipid transfer from the ER (and possibly other source membranes) to the expanding phagophore (Gomez-Sanchez et al., 2018, Maeda et al., 2019, Maeda et al., 2020, Chowdhury et al., 2018).

The ULK complex recruits and activates the class III phosphatidylinositol 3-kinase complex I (PI3KC3-C1), consisting of VPS34, Beclin1, PI3-kinase p150 subunit (VPS15) and ATG14 (Baskaran et al., 2014), by phosphorylation, leading to the generation of PI3P on the phagophore membrane (Russell et al., 2013). Subsequently, PI3P binds WD repeat domain containing phosphoinositide-interacting protein 2 (WIPI2), which in turn associates with ATG16L1 of the ATG12-ATG5-ATG16L1 complex and thereby regulates conjugation of ATG8 proteins to the phagophore membrane (Dooley et al., 2014). Subsequently, the ATG8s are involved in phagophore expansion (Zhang et al., 2023, Weidberg et al., 2011), recognition of selective cargoes (Gatica et al., 2018, Ravenhill et al.,

2019, Johansen and Lamark, 2020), autophagosome closure (Fujita et al., 2008b, Weidberg et al., 2011) and transport (Pankiv et al., 2010, Fu et al., 2014), and fusion with the lysosome (Nguyen et al., 2016).

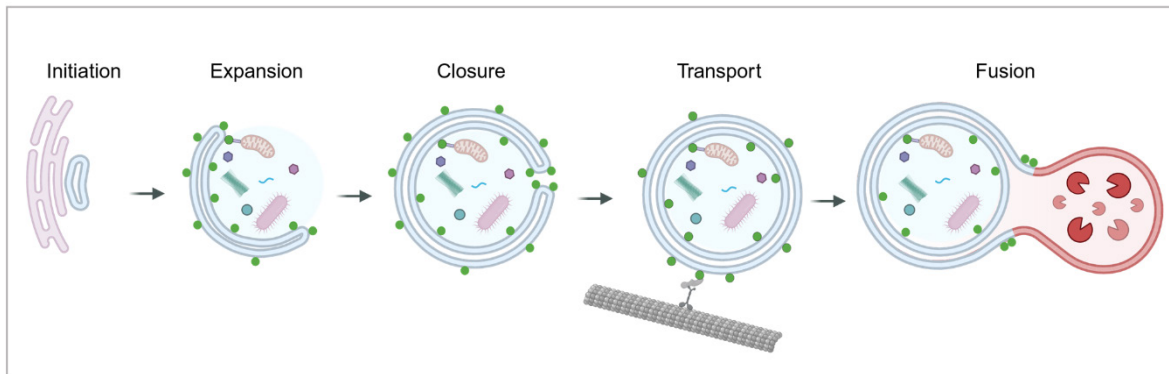


**Figure 3. Schematic overview of the autophagic process.** Initiation of phagophore formation is followed by expansion and finally closure of the autophagosome. Subsequently, autophagosomes are transported for fusion with the lysosome, where autophagosomal content, ranging from protein aggregates to whole organelles and pathogens, is degraded. Cargo recruitment can be either non-selective, or selective with the help of cargo receptors, which in turn associate with ATG8 proteins (green circles) decorating autophagic membranes. Involvement of ATG8 proteins has also been proposed for expansion, closure, transport of the phagophore/autophagosome and fusion with the lysosome. Image was created with BioRender.com.

### 1.2.1. Conjugation of human ATG8s to autophagic membranes

During autophagy, ATG8s are conjugated to double membrane sheets by a ubiquitin-like E1-E2-E3 enzyme cascade (Figure 4). Initially, a C-terminal glycine is exposed by the cysteine protease ATG4 (Kabeya et al., 2004), which can also delipidate conjugated ATG8s (Kauffman et al., 2018, Tamargo-Gomez et al., 2021). The glycine is then covalently bound to a cysteine of the E1-like activating enzyme ATG7 under adenosine triphosphate (ATP) consumption (Mizushima, 2020, Tanida et al., 2001, Tanida et al., 2014). Next, ATG8 proteins are transferred to the E2-like enzyme ATG3, whose association with curved membranes through an N-terminal amphipathic helix is critical for ATG8 lipidation (Nath et al., 2014, Hervás et al., 2017, Tanida et al., 2003). ATG3 interacts with ATG12 of the ATG12-ATG5-ATG16L1 complex, which functions as the E3-like enzyme conjugating ATG8s to phosphatidylethanolamine (PE; Otomo et al., 2013, Hanada et al., 2007, Zheng et al., 2019). Notably, ATG7 also functions as an E1-like enzyme in the conjugation of ATG12 to ATG5, with ATG10 as the E2-like enzyme and no known E3-like enzyme (Mizushima et al., 1998). Subsequently, ATG12-ATG5 associates with a dimeric ATG16L1 to form the E3-like complex for the ATG8 conjugation system (Mizushima et al., 2003, Dooley et al., 2014). ATG16L1 determines the site of ATG8 conjugation to the autophagosomal membrane through interaction with WIPI2 or FIP200, in both cases mediated by its FIP200 binding domain (FBD; Dooley et al., 2014, Fujita et al., 2008b, Lystad et al., 2019, Gammoh et al., 2013). *In-vitro* reconstitution of the ATG8 membrane conjugation system has revealed that WIPI2 and the PI3KC3-C1 complex mutually enhance their recruitment to the membrane and thereby accelerate ATG12-ATG5-ATG16L1 binding and ATG8 lipidation. Beyond

its recruitment, WIPI2 appears to allosterically activate the ATG12-ATG5-ATG16L1 complex (Fracchiolla et al., 2020). Thus, conjugation to autophagic membranes relies on the ULK complex, PI3P generation by PI3KC3-C1 and WIPI2.

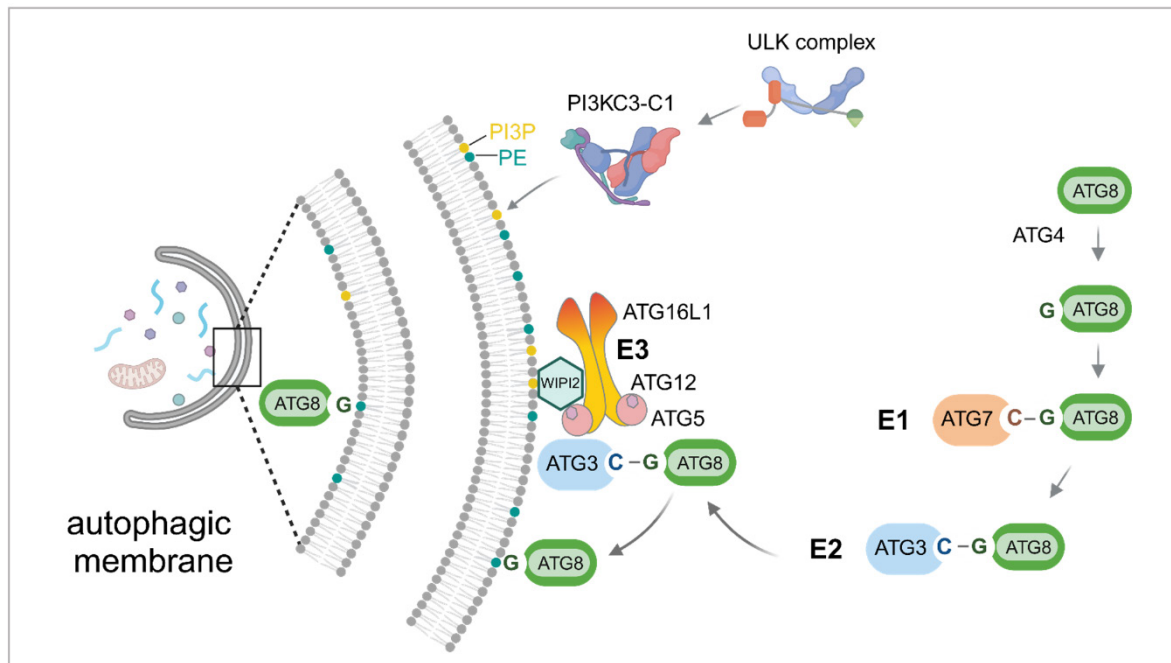


**Figure 4. Conjugation of ATG8 proteins to autophagic membranes.** ATG8 proteins are conjugated by an E1 E2 E3-like enzyme cascade after initial exposure of the C-terminal glycine by the action of ATG4. ATG7 functions as E1, ATG3 as E2 and the ATG12-ATG5-ATG16L1 complex as E3. Via its FIP200 binding domain (FBD), ATG16L1 associates with WIPI2, which in turn is recruited by PI3P. Double-membrane conjugation thus depends on PI3P generation by the class III phosphatidylinositol 3-kinase complex I (PI3KC3-C1) and its activation by the ULK complex (Shi et al., 2020). Image was created with BioRender.com.

### 1.2.2. Roles of GABARAP and LC3 during the different steps of autophagy

ATG8 proteins are involved in the different steps of autophagy—from phagophore expansion to fusion with the lysosome (Figure 3). Even though lipidation of ATG8s occurs downstream of ULK complex and PI3KC3-C1 complex recruitment to the phagophore initiation site (Itakura and Mizushima, 2010, Nishimura et al., 2017), ATG8s can interact with components of these complexes through their LIRs (Alemu et al., 2012, Kraft et al., 2012, Birgisdottir et al., 2019). This points towards positive feedback loops for recruitment of the complexes, additional downstream functions of the ULK and PI3KC3-C1 complexes during autophagosome maturation and/or negative regulation through degradation of the complexes themselves by autophagy (Martens and Fracchiolla, 2020, Nishimura and Tooze, 2020). While LC3 subfamily proteins have been shown to be negative regulators of ULK activity, GABARAP subfamily members positively regulate ULK (Grunwald et al., 2020). Interestingly, activity of the ULK kinase has been proposed to inhibit the delipidating enzyme ATG4, which is also recruited to autophagic membranes through interaction with ATG8s, during phagophore expansion (Pengo et al., 2017, Sanchez-Wandelmer et al., 2017). Additionally,

prevention of ATG4-mediated delipidation appears to be regulated through phosphorylation of LC3C and GABARAPL2 by serine/threonine-protein kinase TBK1, aiding in the maintenance of lipidated LC3C/GABARAPL2 on the growing phagophore (Herhaus et al., 2020). After conjugation to the phagophore ATG8s, in conjunction with the ATG9-ATG2 axis (Maeda et al., 2020, Noda, 2021), are important for phagophore expansion through membrane tethering functions of their N-termini. On the one hand, GABARAP and LC3 subfamily proteins have been proposed to associate with two distinct lipid bilayers, thereby achieving expansion through fusion of their host membrane with vesicles (Weidberg et al., 2011). In line with that, a study on yeast Atg8 reports tubulovesicular structure formation through insertion of two aromatic residues (Phe77, Phe79) into the membrane to which Atg8 is conjugated, with its N-terminus facing away from the membrane, possibly aiding lipid supply during phagophore expansion (Maruyama et al., 2021). On the other hand, association with the same membrane that the respective ATG8 is conjugated to has been reported to also mediate membrane expansion (Zhang et al., 2023).

In addition to these roles during biogenesis of the autophagosome, ATG8s are also important for selective cargo recruitment (Birgisdottir et al., 2013, Pankiv et al., 2007, Johansen and Lamark, 2020, Kirkin and Rogov, 2019). This is facilitated by cargo receptors, which tether the cargo to the growing phagophore membrane by binding to ATG8s via LIR motifs. The first identified cargo receptor was p62/SQSTM1 (Bjorkoy et al., 2005, Pankiv et al., 2007), which was followed by many others including the now well characterized OPTN (Korac et al., 2013), next to BRCA1 gene 1 protein (NBR1; Kirkin et al., 2009), and NDP52 (Thurston et al., 2009). Beside these soluble cargo receptors, there are also membrane-bound cargo receptors located on organelles, for example FAM134B for ER-phagy (Khaminets et al., 2015) and NIX for mitophagy (Novak et al., 2010, Schwarten et al., 2009). The exact roles of the different ATG8 paralogs in selective cargo receptor recruitment are not clear. However, the selectivity of NDP52 for LC3C, which is crucial for innate immunity against *Salmonella*, is an example of paralog-specific cargo receptor binding (von Muhlinen et al., 2012).

When ATG8s are depleted, cells accumulate immature, open autophagosomes, indicating a role of these proteins in the closure of the expanded phagophore (Fujita et al., 2008a, Weidberg et al., 2010). A recent study has shown that both GABARAP and LC3 subfamily proteins interact with the endosomal sorting complex required for transport I (ESCRT-I) component vacuolar protein sorting-associated protein 37A (VPS37A) to seal autophagosomes and maintain them in a sealed state (Javed et al., 2023). Furthermore, an interaction between GABARAP and ATG2 has been suggested to be critical for formation and closure of the expanded phagophore (Bozic et al., 2020).

Before fusion of the matured autophagosome with the lysosome, they are transported along microtubules. Here, LC3s are involved through interaction with JNK-interacting protein 1 (JIP1), thereby regulating dynein driven minus-end transport (Fu et al., 2014), and through binding the

Rab7 effector FYVE and coiled-coil domain-containing protein 1 (FYCO1) mediating plus-end transport (Pankiv et al., 2010). Finally, ATG8 proteins are important for autophagosome-lysosome fusion and subsequent degradation of autophagolysosomal contents by recruiting various factors for fusion, with GABARAP playing a prominent role, as rescue of knockout of all ATG8s was more efficient with GABARAPs than with LC3s (Nguyen et al., 2016, Vaites et al., 2018). These factors include the phosphatidylinositol 4-kinase II $\alpha$  (PI4KII $\alpha$ ; Wang et al., 2015), the large scaffolding protein PLEKHM1, which preferentially binds to GABARAP in a LIR-dependent manner (McEwan et al., 2015, Nguyen et al., 2016, Rogov et al., 2017a), and the SNARE protein syntaxin-17 (STX17; Gu et al., 2019, Kumar et al., 2018). PLEKHM1 additionally binds the HOPS complex as a tethering factor (McEwan et al., 2015) and the small GTPase ADP-ribosylation factor-like protein 8B (ARL8B) on lysosomes (Marwaha et al., 2017). STX17 is only recruited to mature autophagosome, thereby preventing premature fusion with lysosomes, and recruits the cytosolic SNARE synaptosomal-associated protein 29 (SNAP29; Itakura et al., 2012). Additionally, the complex is stabilized by oligomeric ATG14, which primes the complex for interaction with the lysosomal SNARE vesicle-associated membrane protein 8 (VAMP8) and promotes fusion of the autophagosome with the lysosome (Diao et al., 2015).

After fusion the SNAREs are disassembled by N-ethylmaleimide-sensitive factor (NSF) together with its cofactor, the  $\alpha$ -soluble NSF attachment protein ( $\alpha$ -SNAP; Baker and Hughson, 2016). Notably, GABARAP has been reported to bind NSF (Kittler et al., 2001), hinting toward its involvement in SNARE disassembly (Johansen and Lamark, 2020, Thielmann et al., 2009).

Due to multiple, context-dependent roles of participating proteins and the complexity of the process in general, reports on the roles of ATG8s during autophagy can appear contradicting, regarding the essentiality of ATG8s for autophagy (Weidberg et al., 2010, Nguyen et al., 2016, Szalai et al., 2015, Vaites et al., 2018, Lee and Lee, 2016). With regard to the early steps of autophagy, namely phagophore formation and expansion, some studies have reported that ATG8s are essential (Sou et al., 2008, Komatsu et al., 2005), while others have concluded that they are not strictly required (Nguyen et al., 2016, Collier et al., 2021). In contrast, most studies agree on the indispensability of ATG8s during later steps of autophagy, ultimately leading to cargo degradation (Tsuboyama et al., 2016, Nguyen et al., 2016, Weidberg et al., 2010), though there are examples of some cargos being degraded without involvement of the ATG8s (Ohnstad et al., 2020, Honda et al., 2014). These discrepancies can be accounted to context-dependent (e.g. specific cargos, specific tissue, health/disease related) differences in the autophagic process as well as methodological differences between the studies (e.g. depletion of components of the conjugation machinery vs. depletion of the ATG8, different analyzed timepoints).



Recently, Nguyen and Lazarou offered a reconciling hypothesis for the function of ATG8s in autophagy, proposing that ATG8s are dispensable for autophagosome formation, but act on the efficiency of the process. In contrast, concerning autophagosome-lysosome fusion, the presence of ATG8s is considered mandatory, but their lipidation is not. The latter however can enhance the fusion process through recruiting fusion factors with increased avidity (Nguyen and Lazarou, 2022). While there are many open questions regarding the specific roles of the different paralogs during autophagy, a central role for GABARAP has become clear on a functional level and is supported by the fact that many of the core autophagy components, including the ULK complex (Alemu et al., 2012), the PI3KC3-C1 complex (Birgisdottir et al., 2019), ATG4 (Skytte Rasmussen et al., 2017) and ATG2 (Bozic et al., 2020), preferentially bind to GABARAP subfamily proteins over LC3 subfamily proteins (Johansen and Lamark, 2020).

### 1.3. Unconventional roles of human ATG8 proteins

While autophagy is a process for degradation of intracellular cargoes, extracellular material can be engulfed and degraded by endocytosis. Historically, autophagy and endocytosis were considered separate pathways with the lysosome as the shared degradative compartment (De Duve, 1963). This view, however had to be revised after observation of LC3B conjugation to single endolysosomal membranes in different contexts (Florey and Overholtzer, 2012), namely phagocytosis of pathogens (Sanjuan et al., 2007, Gong et al., 2011) and apoptotic cells (Martinez et al., 2011, Florey et al., 2011) referred to as LC3-associated phagocytosis (LAP), entosis and macropinocytosis (Florey et al., 2011). Due to the involvement of autophagy related proteins and the degradative nature of the described processes, they are frequently referred to as non-canonical autophagy. Conjugation of ATG8s to single membranes (CASM) has now been established as the term describing the molecular features shared by these processes, which are distinct from conjugation to autophagic membranes during canonical autophagy (Durgan and Florey, 2022, Durgan et al., 2021) and will be discussed in the following chapter. Interestingly, single-membrane conjugation has also been shown to be involved during endocytosis and recycling of certain plasma membrane receptors and this process was termed LC3-associated endocytosis (LANDO; Heckmann et al., 2020, Heckmann et al., 2019). Furthermore, CASM has been proposed to be involved in secretion of extracellular vesicles (Guo et al., 2017, Gardner et al., 2023, Leidal et al., 2020), accordingly called LC3-dependent extracellular vesicle loading and secretion (LDELS; Leidal and Debnath, 2020) and antigen presentation (Fletcher et al., 2018, Ma et al., 2012).

Notably, most studies on CASM focus on LC3 proteins (Wang et al., 2022), however GABARAP has been shown to be conjugated to single membranes in the same manner as LC3s (Sakuma et al.,

2024, Kuwahara and Iwatsubo, 2024). In case of folliculin (FLCN) - folliculin-interacting protein (FNIP) tumor suppressor sequestration, single membrane conjugation of GABARAP even appears to be specifically required (Goodwin et al., 2021).

### 1.3.1. Conjugation of human ATG8s to single membranes

Since the first reports on non-canonical autophagy and conjugation of ATG8 proteins to single membranes, diverse stimuli, processes and contexts with both distinct and shared molecular features have been described. Recently, a unifying mechanism for CASM centering around the E3-like complex component ATG16L1 and the V-ATPase has been proposed (Durgan and Florey, 2022; Figure 5). The upstream stimuli activating CASM are diverse and depend on the specific process. When induced by ionophores, lysosomotropic drugs or stimulator of interferon genes protein (STING), CASM is independent of VPS34 activity and PI3P formation (Goodwin et al., 2021, Florey et al., 2015), while LAP relies on Rubicon controlled VPS34 activity (Yang et al., 2012, Inomata et al., 2020). Subsequently, the mechanism of V-ATPase dependent membrane conjugation of ATG8s appears to be shared for different contexts (Durgan and Florey, 2022, Fletcher et al., 2018, Fracchiolla and Martens, 2018, Hooper et al., 2022). As with canonical autophagy, conjugation relies on the E1-E2-E3-like enzyme cascade. However, instead of interacting with membrane-bound WIPI2 via its FBD (see Figure 4), ATG16L1 interacts with V-ATPase depending on K490 in its WD40 domain, previously reported to be important for non-canonical autophagy (Hooper et al., 2022, Fletcher et al., 2018). During *Salmonella* infection this interaction is blocked by the bacterial effector SopF, hinting toward a function of CASM in innate immunity (Xu et al., 2019). Due to the fact that lysosomotropic drugs, ionophores (Florey et al., 2015, Jacquin et al., 2017) and pathogenic factors (Ulferts et al., 2021) activate CASM but the V-ATPase inhibitor BafilomycinA1 (BafA1) inhibits it (Goodwin et al., 2021, Fischer et al., 2020), a proton transport-independent function of the V-ATPase is likely (Durgan and Florey, 2022). Interestingly, another V-ATPase inhibitor, namely saliphenylhalamide, which like BafA1 raises the lysosomal pH by blocking proton pump activity (Xie et al., 2004) activates CASM (Hooper et al., 2022). While BafA1 dissociates the V-ATPase membrane subunit  $V_0$  from the cytosolic  $V_1$  subunit, saliphenylhalamide stabilizes the assembled V-ATPase, implying that V-ATPase assembly plays a role during CASM (Hooper et al., 2022). This idea is further supported by the fact that increased  $V_1$  recruitment has been observed during STING activation-induced CASM (Fischer et al., 2020), LAP (Hooper et al., 2022) and after treatment with the ionophore monensin (Timimi et al., Preprint 2023). A direct interaction between the  $V_1H$  subunit of the V-ATPase and ATG16L1 only occurs when  $V_0$  and  $V_1$  are assembled and in cells lacking  $V_1H$ , recruitment of ATG16L1 failed after influenza infection and monensin treatment (Timimi et al., Preprint 2023). Thus, conjugation of ATG8 proteins to single membranes is independent of the ULK complex and WIPI2, but depends on the interaction of ATG16L1 with the V-ATPase via its WD40

domain (Durgan and Florey, 2022). A further defining feature is that ATG8s are not only conjugated to phosphatidylethanolamine (PE) but also phosphatidylserine (PS), with the physiological function of this modification remaining to be investigated (Durgan and Florey, 2021, Durgan et al., 2021). Notably, a different mechanism of ATG8 conjugation to damaged single membrane lysosomes has been recently described, which is independent of ATG16L1 and V-ATPase. Upon treatment with lysosomotropic compounds and subsequent sphingomyelin exposure, ATG8s are conjugated by the action of a E3-like complex containing tectonin beta-propeller repeat-containing protein 1 (TECPR1) in place of ATG16L1 (Kaur et al., 2023).

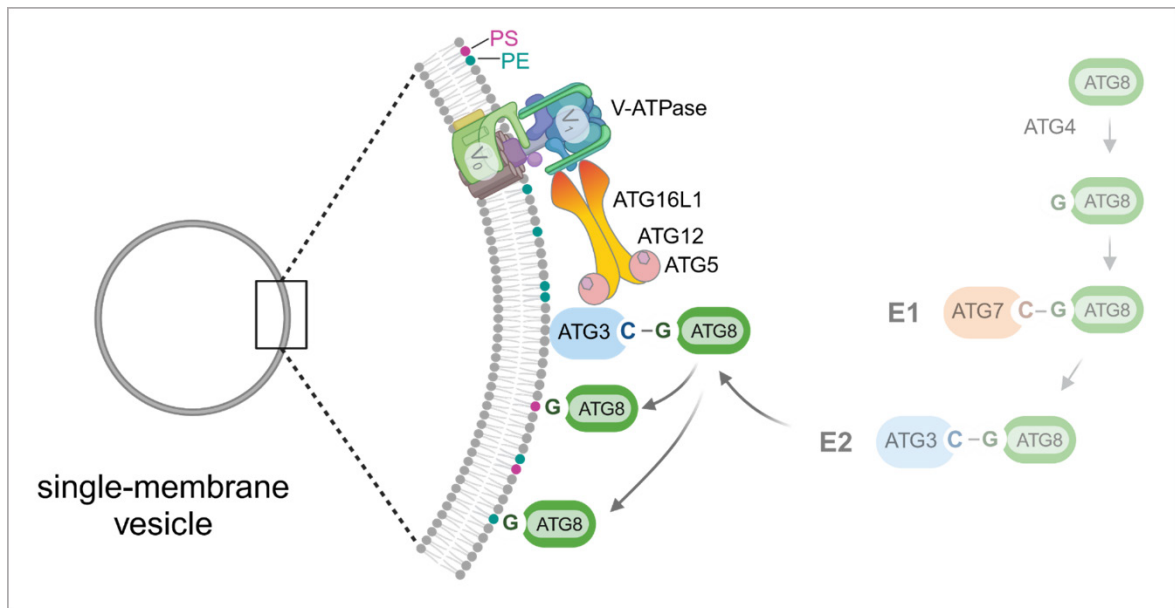


**Figure 5. Conjugation of ATG8 proteins to single membranes (CASM).** As shown in Figure 4, conjugation occurs by an E1-E2-E3-like enzyme cascade. Here, the WD40 domain of ATG16L1 binds to the V<sub>1</sub> subunit of the V-ATPase. ATG8s are conjugated to both phosphatidylethanolamine (PE, turquoise) and phosphatidylserine (PS, pink). Image was created with BioRender.com.

### 1.3.2. Interplay of autophagy and endocytic trafficking

Endocytic trafficking and autophagy share several molecular features (Birgisdottir and Johansen, 2020, Fraser et al., 2017). The role of ATG8 proteins and the conjugation machinery in non-canonical autophagy processes and CASM is one such example and has been discussed above. Additionally, endocytic trafficking and autophagy intersect at several stages and appear to depend on each other (Birgisdottir and Johansen, 2020, Tooze et al., 2014, Sakuma et al., 2024). On the one hand, endosomal vesicles supply lipids and proteins during autophagosome formation and maturation (Noda, 2017, Kuroki et al., 2018, Gordon and Seglen, 1988). On the other hand, endolysosomal membranes can be degraded by autophagy when they are damaged (e.g. lysophagy; Chauhan et al., 2016, Maejima et al., 2013). Additionally, the autophagy machinery and/or ATG8 proteins have been proposed to regulate trafficking of various plasma membrane proteins, including receptors, though the exact role is poorly understood and appears to be highly dependent

on the context and the protein of interest (Carosi et al., 2024, Fraser et al., 2019, Coelho et al., 2022).

The retromer-interacting protein TBC1 domain family member 5 (TBC1D5) and its role in regulating receptor recycling is an example of this complexity. TBC1D5 is a Rab GTPase-activating protein, which colocalizes with endosomes under basal conditions and with autophagosomes upon starvation, proposedly in a LIR-LDS dependent manner (Popovic et al., 2012). It was shown that TBC1D5 shuttles to autophagosomes during glucose deprivation, thereby releasing retromer and increasing recycling of the glucose transporter solute carrier family 2 member 1 (SLC2A1) to the plasma membrane (Roy et al., 2017). In contrast, TBC1D5 remains bound to retromer during nutrient starvation and is captured by autophagy, which leads to decreased recycling of the beta-2 adrenergic receptor (ADRB2) to the plasma membrane, likely in a LIR-independent manner (Carosi et al., 2024).

Association with ATG8 proteins has additionally been reported for several receptors, including the  $\kappa$ -opioid (Chen et al., 2006, Chen et al., 2011, Huang et al., 2022), vanilloid (Lainez et al., 2010), angiotensin (Cook et al., 2008), transferrin (Green et al., 2002), HGF (Barrow-McGee et al., 2016, Bell et al., 2019), GABA<sub>A</sub> (Wang et al., 1999, Ye et al., 2021) and EGF receptors (Dobner et al., 2020). In case of the GABA<sub>A</sub> receptor, anterograde trafficking from the Golgi complex to the cell surface appears to be regulated through a direct LIR-LDS based interaction with GABARAP (Ye et al., 2021). For the transferrin and HGF receptors LIR based interactions have been proposed (Huang et al., 2019, Gardner et al., 2023) alongside reports indicating engagement of the LC3C C-terminal tail in endosome localization for autophagic degradation of the receptors under starvation conditions (Coelho et al., 2022, Coelho and Park, 2023). In case of the EGFR, endogenously tagged GABARAP was shown to co-migrate with the labeled ligand of the EGFR and endogenous EGFR coimmunoprecipitated with overexpressed GABARAP, hinting towards an interaction between the two. Notably, depletion of GABARAP, but not GABARAPL1 and GABARAPL2 led to enhanced EGFR degradation and altered signaling in cells (Dobner et al., 2020). Interestingly, extracellular signal-regulated kinase (ERK1/2) cascade components have also been shown to increasingly colocalize with ATG8 proteins after growth factor stimulation (Martinez-Lopez et al., 2013).

While many open questions remain regarding the involvement of ATG8 proteins in endocytic trafficking of receptors, they appear to be involved in both the autophagic regulation of their plasma membrane abundance depending on nutrient availability (Coelho and Park, 2023) and in anterograde transport, likely independent of autophagy (Ye et al., 2021, Chen et al., 2011). The latter is supported by the observation that cells lacking GABARAP-type proteins show altered Golgi morphology and surfaceome composition (Sanwald et al., 2020).

## 1.4. Studying human ATG8 protein function

Since their discovery, a wide range of methods have been developed and applied to study ATG8 proteins and have shaped the current understanding of these proteins, their interactions and the processes they are involved in (Ktistakis and Florey, 2019, Klionsky et al., 2021a, Johansen et al., 2017). Using ATG8 proteins, either overexpressed or endogenously tagged, as baits for affinity enrichment and subsequent analysis by mass spectrometry has been one strategy to identify interaction networks of ATG8 proteins under different conditions (Behrends et al., 2010, Eck et al., 2020).

Today, many phenotypic observations can be related to a cellular function and an underlying molecular mechanism. Nevertheless, open questions remain regarding canonical and non-canonical autophagy, paralog-specific roles of ATG8 proteins in different contexts, and the regulation of their versatile functions (Cuervo et al., 2024, Johansen and Lamark, 2020, Martens and Fracchiolla, 2020). In the following chapters, two general strategies, complementing each other to broaden the understanding of human ATG8 proteins and their functions, will be summarized.

### 1.4.1. From phenotypes to molecular mechanisms

Classically, morphological and phenotypic observations precede the investigation of the underlying molecular mechanisms and interactions. As described above, this also holds true in the context of autophagy research in general (Tsukada and Ohsumi, 1993, Ohsumi, 2014). In case of ATG8s, the observation of two distinct forms of LC3B by immunoblot analysis, combined with microscopy revealing localization of green fluorescent protein (GFP)-LC3B at autophagosomal membranes (Kabeya et al., 2000), paved the way for elucidation of the conjugation system in mammalian cells (Tanida et al., 2003, Tanida et al., 2002). Moreover, this led to the wide-spread use of both GFP-LC3B as a marker for autophagic membranes (Mizushima, 2004, Klionsky et al., 2021a) and red fluorescent protein (RFP)-GFP-LC3B, exploiting the different pH sensitivities of the fluorophores, as a readout for autophagic flux (Kimura et al., 2007).

The development of methods for gene manipulation in mammalian cells, including siRNA-based knockdown (Elbashir et al., 2001) and CRISPR/Cas9 mediated knockout (Doudna and Charpentier, 2014) of genes, has enabled screening for genes and respective proteins generating specific phenotypes related to canonical or non-canonical autophagy (Orvedahl et al., 2011, Ulferts et al., 2021). Additionally, individual proteins or protein families can be knocked out to study their specific functions. In the case of ATG8 proteins, studies applying knockout of individual proteins, either of the two subfamilies, or all ATG8s have revealed different functions of these proteins. Knockout of all ATG8 proteins in HeLa cells revealed that ATG8s are crucial for autophagosome-lysosome fusion but not autophagosome formation and cargo recognition, in PINK1/Parkin-mediated mitophagy as

well as starvation induced autophagy. Furthermore, the GABARAP subfamily appears to be the main driver during these processes, as only GABARAP—but not LC3-subfamily knockout has led to a significant phenotype (Nguyen et al., 2016). Accordingly, degradation of protein aggregates appears to mostly rely on members of the GABARAP subfamily rather than the LC3s (Vaites et al., 2018). Mechanistically, these observations can at least partially be linked to GABARAP, either alone or along with its two paralogs GABARAPL1 and GABARAPL2, selectively interacting with factors required for autophagosome-lysosome fusion, like PI4KII $\alpha$  (Wang et al., 2015, Behrends et al., 2010) and PLEKHM1 (Nguyen et al., 2016, Rogov et al., 2017a). LAP represents another example of phenotypic observations, namely rapid recruitment of a GFP-tagged LC3B to phagocytosed pathogens (Sanjuan et al., 2007) and entotic cells (Florey et al., 2011), that initiated extensive research revealing mechanistic insights (Durgan and Florey, 2021, Durgan et al., 2021, Hooper et al., 2022). In contrast, the mechanisms behind other ATG8-related phenotypes and their connections to other functions of these proteins remain to be investigated. These include the observation of disrupted Golgi morphology and altered surface protein abundance in GABARAP subfamily knockout cells (Sanwald et al., 2020) as well as altered EGFR degradation and signaling after stimulation, specifically in GABARAP-deficient cells (Dobner et al., 2020).

#### 1.4.2. From molecular interaction to modulation of function

Exploring molecular interactions and their determinants to predict physiological functions is another approach for studying ATG8 proteins. Through phage display approaches, screening randomized peptide libraries, the GABARAP ligands NIX (Schwarten et al., 2009), clathrin heavy chain (Mohrlüder et al., 2007a) and calreticulin (Mohrlüder et al., 2007b) have been identified and binding determinants characterized. After description of the LIR consensus motif for ATG8 binding (Noda et al., 2010, Alemu et al., 2012), a web tool for *in silico* identification of LIR containing proteins was developed, allowing selection of putative ATG8 interactors for further experimental verification (Kalvari et al., 2014). In addition to identification of putative biological interactor of ATG8s, there have been efforts to develop artificial interactors. Fluorescently labelled sensors based on peptides identified by phage-display have been introduced as tools for monitoring the localization of individual ATG8s, revealing paralog-specific functions (Stolz et al., 2017). Moreover, screening of small-molecule compound libraries for ATG8 binders represents another strategy to identify modulators of canonical as well as non-canonical functions (Steffek et al., 2023, Hartmann et al., 2021). Such approaches have gained additional relevance with the emergence of autophagy as a potential therapeutic target (Kocak et al., 2022).

## 1.5. Modulation of autophagy as a therapeutic strategy

Soon after the discovery of the first autophagy-related genes and respective proteins in yeast and in mammalian cells, connections to cancer (Liang et al., 1999, Yue et al., 2003) and neurodegenerative diseases were drawn (Ravikumar et al., 2002, Komatsu et al., 2006). Despite a lack of methods to measure autophagic activity in humans, extensive research involving mouse models as well as analysis of mutations in disease have now linked autophagy to a wide variety of additional human pathologies including cardiovascular, pulmonary, musculoskeletal, infectious, and metabolic disorders (Klionsky et al., 2021b, Yamamoto et al., 2023). In the following, the roles of autophagy in neurodegeneration and cancer will be summarized along with strategies for its modulation as a therapeutic approach.

Regarding cancer, autophagy plays a dual, highly context-dependent role, with both tumor-promoting and tumor-suppressive functions (Yang and Klionsky, 2020, Debnath et al., 2023). Autophagic tumor suppression is established through various mechanisms, including removal of damaged proteins and organelles, maintaining genomic stability, and regulating the immune response (Galluzzi et al., 2015). Even though mutations of core autophagy genes are rare in human cancers (Lebovitz et al., 2015), several studies have provided evidence for an antitumor effect of autophagy. Increased tumor formation in mice after heterozygous disruption of the PI3KC3-C1 complex component Beclin1 (Qu et al., 2003, Yue et al., 2003) or deletion of Atg7 (Takamura et al., 2011) are two examples of such studies. Additionally, autophagy is stimulated by the tumor suppressor p53 upon cellular stress like DNA damage (Crichton et al., 2006, Kenzelmann Broz et al., 2013).

In contrast, once a tumor has developed, autophagy promotes tumor progression by supporting the metabolic demands in the microenvironment resulting from insufficient oxygen and nutrient supply (Russell and Guan, 2022, Yang and Klionsky, 2020). Accordingly, depleting mice of Atg7 has been shown to attenuate tumor growth in different cancers (Yang et al., 2014, Karsli-Uzunbas et al., 2014). It is important to note that autophagy may also influence tumor cell survival by promoting resistance to chemotherapy (Rubinsztein et al., 2012, Rebecca and Amaravadi, 2016). Due to the versatile roles of ATG8 proteins in autophagy, their involvement in cancer is not far-fetched. Indeed, ATG8 proteins can be a marker for either poor or good prognosis regarding tumor progression, depending on the type and stage of the disease (Jacquet et al., 2021).

Due to its ambivalent role in cancer, both activation and inhibition of autophagy are considered as therapeutic strategies (Rebecca and Amaravadi, 2016, Kocak et al., 2022). On the one hand, autophagy appears to be required for an immune response against the cancer cells during certain treatments (Masuelli et al., 2017, Michaud et al., 2011), on the other hand autophagy inhibition appears to be useful for sensitizing certain cancer cells for chemotherapy (Verbaanderd et al., 2017). Treatment with chloroquine or hydroxychloroquine, which decrease autophagosome-

lysosome fusion (Mauthe et al., 2018), are clinically applied for this purpose (Xu et al., 2018). However, due to some reported side-effects (Leung et al., 2015), only partial therapeutic response in many cases and multiple, not fully elucidated mechanisms of action (Verbaanderd et al., 2017), efforts are being made to find more specific inhibitors (Kocak et al., 2022). Targeting ATG8 proteins has been one approach in this direction (Cerulli et al., 2020, Gray et al., 2021), which succeeded in positive complementation of treatment with chemotherapeutic drugs in cancer cell lines and mice (Gray et al., 2021). The connection between upregulation of specific ATG8 paralogs and poor prognosis in certain cancer types represents a rationale for developing paralog-specific modulators (Jacquet et al., 2021).

A connection between neurodegeneration and autophagy became evident with reports of autophagic clearance of aggregation-prone proteins (Ravikumar et al., 2002) and neurodegeneration in mice depleted of core autophagy proteins Atg5 (Hara et al., 2006) and Atg7 (Komatsu et al., 2006). While the specific mechanisms are incompletely understood and dependent on the specific disease, autophagy has now been linked to a variety of neurodegenerative disorders, including Parkinson's, Alzheimer's and Huntington's disease (Klionsky et al., 2021b, Yang and Klionsky, 2020, Menzies et al., 2015). Deposition of protein aggregates and dysfunctional mitochondria are characteristic of these diseases, and impaired autophagy may contribute to this pathology (Menzies et al., 2015, Sliter et al., 2018, Fang et al., 2019, Narendra et al., 2008). Accordingly, mutations of autophagy-related proteins have been associated with different neurodegenerative diseases (Yamamoto et al., 2023, Stamatakou et al., 2020). Induction of autophagy, e.g. through mammalian target of rapamycin (mTOR) inhibition, has been shown to mitigate symptoms of neurodegeneration in mice and has therefore been proposed as a therapeutic strategy (Caccamo et al., 2010, Ravikumar et al., 2004), with several autophagy activators currently undergoing preclinical and clinical trials (Kocak et al., 2021). Targeted protein degradation is a newly emerging field in the context of autophagy-modulating drugs. While proteolysis targeting chimeras (PROTACs) are high molecular weight compounds which utilize the ubiquitin-proteasome system and involve target ubiquitylation (Nalawansa and Crews, 2020, Ding et al., 2020), autophagosome-tethering chimeras (ATTECs) are smaller molecules which function independently of ubiquitylation and have the potential to degrade larger targets as they rely on macroautophagy (Kocak et al., 2021). Up to now, degradation of aggregated proteins and mitochondria has been shown using the ATTEC strategy (Mei et al., 2023, Li et al., 2019, Tan et al., 2023). Targets are usually tethered to phagophores via ATG8 proteins, either through ATG8 binding peptides or small-molecule compounds (Schwalm et al., 2023b, Schwalm et al., Preprint 2023a).



## 2 Aims

Since its discovery 25 years ago, a plethora of interactions of the human ATG8 protein GABARAP have been described. These include artificial ligands which are of potential interest for therapeutic applications and biological interactors important for cellular functions of GABARAP. Understanding the molecular determinants of these interactions can aid in both further development of modulators and explaining biological processes.

Investigating the interaction of GABARAP with the stapled peptides Pen3-*ortho* and Pen8-*ortho* and the small-molecule compound GW5074 from a structural perspective and thereby elucidating the structural features determining the binding mode and functionality of these ligands represents the first aim of this work.

The second aim, namely the structural and biophysical characterization of the interaction between GABARAP and a putative physiological binding partner, is inspired by the phenotype of enhanced EGFR degradation after stimulation—specifically in GABARAP single knockout cells—previously observed in our institute. To understand whether a direct interaction can provide an explanation for this phenotype, GABARAP as well as its paralogs will be analyzed regarding their binding affinities to EGFR derived peptides. Additionally, the molecular interactions between GABARAP and one of these peptides will be analyzed.

Finally, a live cell imaging-based approach using a bivalent GABARAP-mTagBFP2-GABARAP construct will be employed to highlight interactions that may be overlooked by conventional tagging strategies. The microtubule cytoskeleton may represent such a twilight zone, as interaction with GABARAP has been reported in early *in-vitro* studies, but evidence in cells is sparse. In this work the factors determining the interaction between microtubules and GABARAP-mTagBFP2-GABARAP will be investigated.



### 3 Results

#### 3.1. Structure-based design of stapled peptides that bind GABARAP and Inhibit autophagy

<b>Authors</b>	Hawley Brown, Mia Chung, <b>Alina Üffing</b> , Nefeli Batistatou, Tiffany Tsang, Samantha Daskocil, Weiqun Mao, Dieter Willbold, Robert C. Bast Jr., Zhen Lu, Oliver H. Weiergräber, Joshua A. Kritzer
<b>Journal</b>	Journal of the American Chemical Society
<b>Year of Publication</b>	2022
<b>DOI</b>	10.1021/jacs.2c04699
<b>Impact Factor</b>	15.0 (2022)
<b>Contribution</b>	Expression and purification of GABARAP, screening for crystallization conditions, diffraction data collection (remote at ESRF), data processing, structure refinement and validation
<b>Reprint Permission</b>	Reprinted with permission from <i>J. Am. Chem. Soc.</i> 2022, 144, 32, 14687–14697. Copyright 2022, American Chemical Society

Note that only the main text is included in this dissertation, SI material can be found here:

<https://pubs.acs.org/doi/full/10.1021/jacs.2c04699>



## Structure-Based Design of Stapled Peptides That Bind GABARAP and Inhibit Autophagy

Hawley Brown, Mia Chung, Alina Üffing, Nefeli Batistatou, Tiffany Tsang, Samantha Daskocil, Wei-qun Mao, Dieter Willbold, Robert C. Bast, Jr., Zhen Lu, Oliver H. Weiergräber, and Joshua A. Kritzer\*

**Cite This:** *J. Am. Chem. Soc.* 2022, 144, 14687–14697

**Read Online**

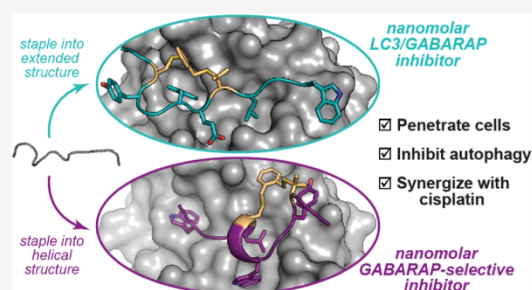
ACCESS |

Metrics & More

Article Recommendations

Supporting Information

**ABSTRACT:** The LC3/GABARAP family of proteins is involved in nearly every stage of autophagy. Inhibition of LC3/GABARAP proteins is a promising approach to blocking autophagy, which sensitizes advanced cancers to DNA-damaging chemotherapy. Here, we report the structure-based design of stapled peptides that inhibit GABARAP with nanomolar affinities. Small changes in staple structure produced stapled peptides with very different binding modes and functional differences in LC3/GABARAP paralog selectivity, ranging from highly GABARAP-specific to broad inhibition of both subfamilies. The stapled peptides exhibited considerable cytosolic penetration and resistance to biological degradation. They also reduced autophagic flux in cultured ovarian cancer cells and sensitized ovarian cancer cells to cisplatin. These small, potent stapled peptides represent promising autophagy-modulating compounds that can be developed as novel cancer therapeutics and novel mediators of targeted protein degradation.



### INTRODUCTION

Autophagy is a dynamic cellular process by which cytosolic material is transported to the lysosomal compartment for degradation. Bulk autophagy recycles biomolecules into building blocks in response to starvation, while selective autophagy removes misfolded proteins, damaged organelles, and intracellular pathogens.<sup>1</sup> Dysregulation of autophagy is a hallmark of many diseases, including neurodegenerative diseases, infectious diseases, and cancer.<sup>1</sup> During carcinogenesis, autophagy is thought to be protective as down-regulating autophagy increases oxidative stress, DNA damage, and chromosomal instability.<sup>2</sup> However, established tumors can become overly reliant on autophagy to survive an environment with low nutrients, hypoxia, and high oxidative stress.<sup>2</sup>

There is a great deal of evidence that autophagy inhibition could be a promising therapeutic strategy for advanced-stage cancers. For example, genetic knockdown of essential autophagy genes attenuates tumor growth and extends survival in pancreatic ductal adenocarcinoma, lung cancer, and melanoma.<sup>3–5</sup> Autophagy is induced in response to DNA-damaging chemotherapy, and autophagy has been implicated in cisplatin resistance in breast and ovarian cancers.<sup>6,7</sup> Multiple clinical trials using the nonspecific autophagy inhibitors chloroquine and hydroxychloroquine in combination with chemotherapy have shown an overall improved response

compared to chemotherapy alone for pancreatic cancer, glioblastoma, breast cancer, and other malignancies.<sup>8–11</sup> However, hydroxychloroquine and related drugs broadly affect endolysosomal processes and are not specific to autophagy, and they can cause significant side effects at doses required for autophagy inhibition.<sup>12,13</sup> Novel, autophagy-specific inhibitors are highly sought-after to better understand the effects of autophagy inhibition on advanced cancers and to develop therapeutics with improved efficacy and better side effect profiles.<sup>14</sup>

One strategy for specific autophagy inhibition is interruption of key protein–protein interactions.<sup>14</sup> Members of the Atg8 protein family, including the mammalian LC3 (LC3A, LC3B, LC3C) and GABARAP (GABARAP, GABARAP-L1, GABARAP-L2/GATE-16) subfamilies, are involved in key protein–protein interactions at several steps in autophagy, including initiation, formation and elongation of the phagophore, cargo recruitment, autophagosome trafficking, and lysosomal fusion (Figure 1).<sup>15</sup> Mammalian LC3 and GABARAP proteins, which

Received: May 2, 2022

Published: August 2, 2022



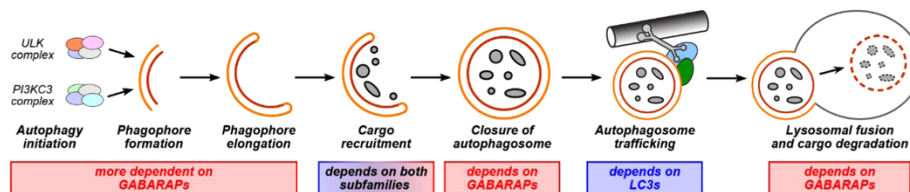


**Figure 1.** Roles of LC3/GABARAP proteins in autophagy. Autophagy pathways proceed through a multistep process that involves protein–protein interactions of LC3/GABARAP proteins at every step. Some of the known differential roles for proteins from the LC3 and GABARAP subfamilies are noted.<sup>18–20</sup>

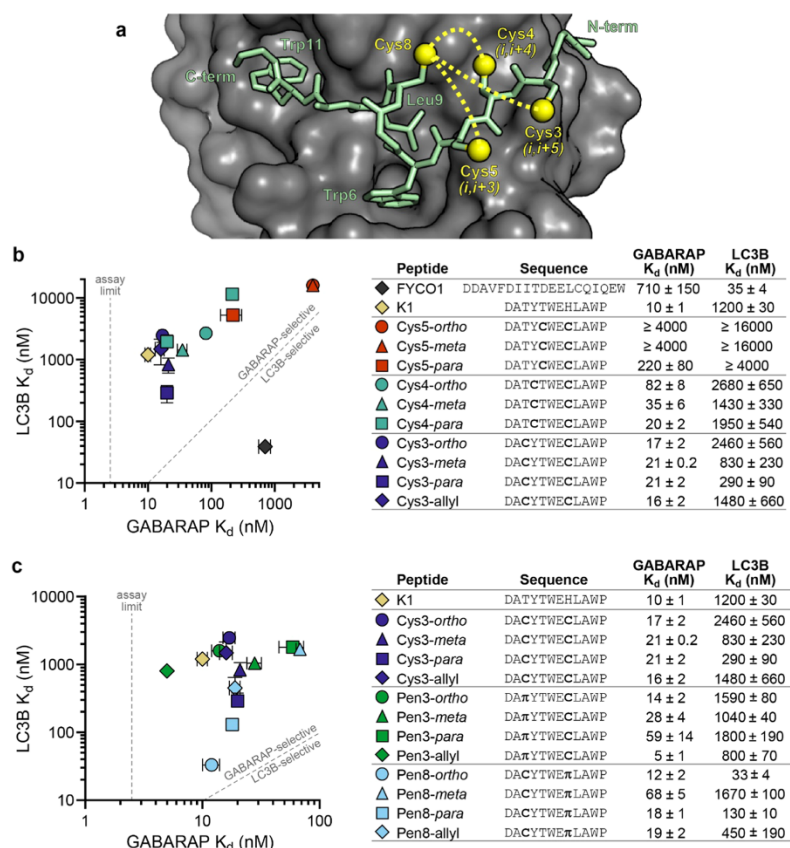


**Figure 2.** Diversity-oriented stapling of K1. (a) The structure of K1 bound to GABARAP<sup>28</sup> suggested that replacing residue 8 with Cys and then stapling it to a second Cys residue at either position 3, position 4, or position 5 could potentially stabilize the overall structure (yellow dotted lines). Cysteine side chains are depicted at all four positions, with sulfur atoms indicated by yellow spheres. (b) Cysteine-substituted K1 analogues were stapled using the linkers *ortho*-, *meta*-, or *para*-dimethylbenzene, and affinities for recombinant GABARAP and LC3B were measured using fluorescence polarization. Allyl-modified Cys3 peptide was tested as an unstapled control. Peptides K1 and FYCO1 were tested as GABARAP-selective and LC3B-selective controls, respectively. (c) Penicillamine-substituted analogues of peptide Cys3 were stapled, and their binding affinities for GABARAP and LC3B were measured.  $\pi$  denotes penicillamine. Peptides were prepared with fluorescein on their N-termini (Figure S1 and Table S1). Data are shown as the average and standard error of the mean for three or more independent trials. Primary data are shown in Figures S4–S17.

we will refer to collectively as LC3/GABARAP proteins, recognize a conserved motif known as the LC3-interacting region (LIR).<sup>16,17</sup> Proteins with LIR motifs that bind LC3 and/or GABARAP proteins include ATG4, which promotes autophagy initiation and phagophore formation, selective

autophagy adaptors such as p62 which recruit proteins to be degraded, and trafficking machinery including FYCO1 and the HOPS complex.<sup>18–20</sup> Thus, disruption of protein–protein interactions involving LC3/GABARAP proteins has been recognized as a promising strategy for autophagy inhibition.

For example, blocking protein–protein interactions of LC3/GABARAP proteins using engineered binding proteins sensitized acute myeloid leukemia cells to chemotherapy.<sup>21</sup> Additionally, the application of LC3-binding peptides sensitized ovarian cancer cells to cisplatin treatment.<sup>19</sup> GABARAP and LC3 subfamilies are important for autophagy in mammalian cells, with different yet overlapping roles (Figure 1). The different roles of GABARAPs and LC3s in cancer progression are poorly understood, so inhibitors selective to each subfamily are important for studying how they control autophagy in cancer and other pathologies.<sup>22</sup>

LIR motifs bind Atg8-family proteins in an extended conformation anchored by conserved hydrophobic side chains.<sup>16,17,23</sup> Several studies have explored structural determinants of selectivity for LC3 and GABARAP proteins, and generally, it was observed that GABARAPs are able to accommodate a wider variety of LIR ligands.<sup>23–25</sup> In previous work, we described structure–activity relationships for an LC3-specific LIR motif derived from FYCO1, a Rab7 effector protein that mediates autophagosome trafficking.<sup>26</sup> We also described peptides with side-chain-to-side-chain crosslinks, or “stapled” peptides, with improved affinity, selectivity for LC3B over GABARAP, proteolytic stability, and cytosolic delivery. In this work, we report two new classes of stapled peptides that inhibit LC3/GABARAP proteins with nanomolar affinity, one GABARAP-selective class and another that inhibits both subfamilies. Notably, while most implementations of a stapled peptide strategy involve helical peptides,<sup>27</sup> here we employ a “diversity-oriented stapling” approach that allows the synthesis and evaluation of stapled peptides with a variety of three-dimensional structures. This methodology enabled the discovery of two distinct families of stapled GABARAP ligands. We obtained crystal structures, which revealed that high affinity and selectivity were governed by small changes in the chemical structures of the staples, producing two different, high-affinity binding modes. These peptides resist biological degradation, penetrate the cytosol, inhibit autophagy, and are synergistic with DNA-damaging chemotherapy in ovarian cancer cells.

## RESULTS

**Peptide K1 is an Artificial, GABARAP-Selective Ligand.** The highest-affinity natural ligands for LC3B/GABARAP proteins are large, negatively charged peptides. We sought to design smaller, less charged ligands that would be more suitable as pharmacological agents, so we started with the non-natural GABARAP ligand K1, which was discovered in a phage display selection by Weiergräber et al.<sup>28</sup> The binding mode of K1 is unique compared to all known native ligands in three respects: K1 binds with a single turn of a  $3_{10}$  helix instead of an extended conformation, K1 binds with the opposite N-to-C orientation compared to natural ligands, and K1 induces GABARAP to widen a key hydrophobic pocket to accommodate a Trp residue in addition to the canonical aliphatic residue (Figures 2a and S3). We tested fluorescein-tagged K1 in a direct fluorescence polarization (FP) assay with recombinant, His-tagged GABARAP and LC3B and found that it bound GABARAP with a  $K_d$  of  $10 \pm 1$  nM and LC3B with a  $K_d$  of  $1200 \pm 30$  nM (Figure 2b), which made it an ideal starting point for designing stapled GABARAP inhibitors.<sup>23,29</sup>

**Diversity-Oriented Stapling of K1.** While K1 has a high affinity for GABARAP, applications of peptides with all-natural amino acids can be limited by their biological stability and cell

penetration (see below). Covalent linking of side chains, or “peptide stapling,” is a promising strategy to minimize these limitations.<sup>27</sup> While most stapled peptides are  $\alpha$ -helical, we and others have shown that appropriately designed staples can improve the properties of peptides in other conformations as well.<sup>26,30–34</sup> Based on the crystal structure of K1 bound to GABARAP,<sup>28</sup> we designed peptides Cys5, Cys4, and Cys3, which stapled K1 in  $(i,i+3)$ ,  $(i,i+4)$ , and  $(i,i+5)$  positions, respectively (Figure 2a). We stapled each peptide using dithiol bis-alkylation<sup>34</sup> with *ortho*-, *meta*-, and *para*-dimethylbenzene linkers, allowing for a “diversity-oriented stapling” approach, where the staple geometry was varied (Figure 2a).<sup>31,35,36</sup> Stapling in  $(i,i+3)$  positions (the Cys5 peptides) reduced binding to both GABARAP and LC3B compared to K1. Stapling in  $(i,i+4)$  positions (the Cys4 peptides) produced stapled peptides with similar LC3B binding across staple geometries but different GABARAP binding with the best affinity afforded by the longer *para* linker. By contrast, for the Cys3 peptides, which were stapled in  $(i,i+5)$  positions, the unstapled control (Cys3-allyl) and all three stapled peptides bound GABARAP with nanomolar affinity, but the staple geometry modulated LC3B binding across an order of magnitude (Figure 2b).

From these initial designs, it was clear that shorter staples were generally less compatible with GABARAP binding. We explored the effects of longer linkers by stapling  $(i,i+4)$  positions with homocysteine instead of cysteine in either the 4th or 8th position (peptides Hcy4 and Hcy8, respectively, Figure S8). Homocysteine in either position significantly improved GABARAP binding for peptides with an *ortho* staple but not with *meta* or *para* staples. Homocysteine position and staple geometry had large effects on LC3B binding, with Hcy8-*para* having increased LC3B affinity ( $230 \pm 30$  nM) compared to other  $(i,i+4)$  stapled peptides (Figure S8).

Because both Cys3-*meta* and Cys4-*meta* each showed only a moderate decrease in GABARAP affinity compared to K1, we hypothesized that a peptide with three cysteine substitutions stapled using a (1,3,5)-trimethylbenzene linker might also be tolerated.<sup>34,37</sup> We found that both the unstapled Cys3.4.8-allyl and stapled Cys3.4.8-*tmb* peptides had GABARAP-binding affinities comparable to Cys3-*meta* and Cys4-*meta*, and the stapled Cys3.4.8-*tmb* maintained 35-fold binding selectivity for GABARAP over LC3B (Figure S8).

**$\beta$ -Branching in the Staple Modulates Binding and Selectivity.** Next, we hypothesized that  $\beta$ -branching in the stapled residues might modulate affinity and selectivity. Replacing Cys3 with penicillamine, a  $\beta$ -branched analogue of cysteine, increased binding affinity to GABARAP while maintaining selectivity over LC3B for all staple geometries and the allylated, unstapled control (Figure 2c). We confirmed that this was due to stabilization of  $\beta$ -strand structure by testing unstapled K1 analogues with *tert*-butyl glycine and *tert*-butyl alanine in the 3 position, which had similar affinities and selectivities (Figure S8). Unexpectedly, replacing Cys8 with penicillamine not only maintained high affinity for GABARAP but also improved LC3B binding affinity by nearly 2 orders of magnitude (compare Cys3-*ortho* and Pen8-*ortho*, Figure 2c). This effect was highly dependent on the structure of the rest of the staple, with only moderate LC3B binding observed for Pen8-*para* and poor LC3B binding for Pen8-*meta*. Ultimately, introducing  $\beta$ -branching into the staple produced not only Pen3-*ortho*, a 14 nM ligand for GABARAP with 100-fold selectivity for GABARAP over LC3B, but also Pen8-*ortho*,



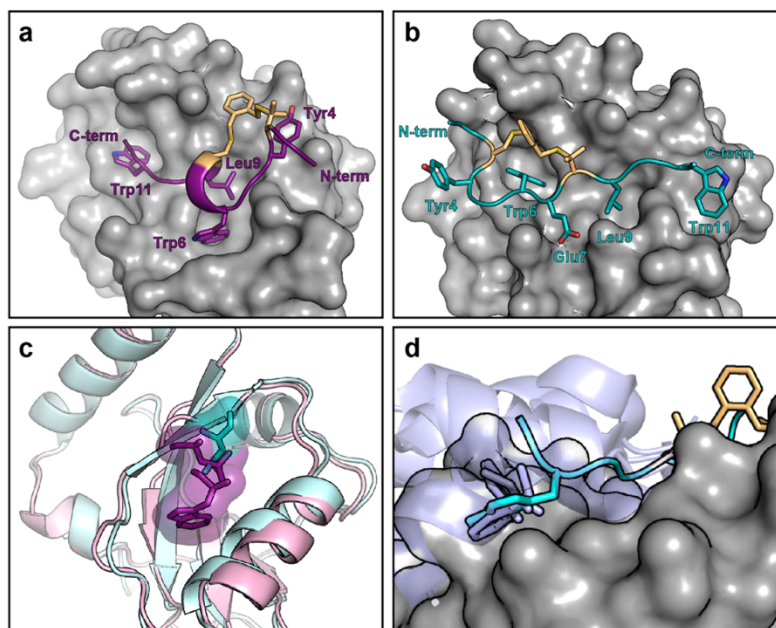


**Figure 3.** Pen3-*ortho* and Pen8-*ortho* bind GABARAP in different binding modes. (a) Crystal structure of Pen3-*ortho* bound to GABARAP. (b) Crystal structure of Pen8-*ortho* bound to GABARAP. GABARAP is depicted in surface rendering. (c) Pen3-*ortho* induces a conformational change in GABARAP that expands the central hydrophobic pocket relative to other ligands, including Pen8-*ortho*. Residues that bind this pocket from Pen3-*ortho* and Pen8-*ortho* are shown in purple and cyan, respectively, and GABARAPs bound to Pen3-*ortho* and Pen8-*ortho* are shown in pink and cyan ribbons, respectively. (d) Trp11 of Pen8-*ortho* (cyan) accesses a binding pocket that has only previously been observed to be engaged with a C-terminal helix of natural ligands (ligands from AnkB, FAM134B, SEC62, RTN3, and STX17 shown in lavender).<sup>29,38–40</sup> In all structures, some side chains are omitted for clarity.

which had 12 nM affinity for GABARAP and 33 nM affinity for LC3B. Surprisingly, these two peptides differed only in the placement of two methyl groups within the staple.

**Crystal Structures Reveal Two Different Binding Modes.** Because Pen3-*ortho* and Pen8-*ortho* are so similar but have different selectivity, we explored their binding modes by obtaining their crystal structures bound to GABARAP. These structures revealed two completely different binding modes. Pen3-*ortho*, the GABARAP-selective stapled peptide, binds GABARAP with a single turn of a  $3_{10}$  helix in a manner highly similar to parent peptide K1 (Figures 3a and S3). Unexpectedly, Pen8-*ortho* binds in the opposite orientation using a more extended conformation in a manner similar to natural LIR motifs (Figures 3b and S3). These observations are consistent with the penicillamine in the eighth position disrupting the helical structure and forcing a different binding mode for Pen8-*ortho*. Because they bind in opposite orientations, Pen3-*ortho* and Pen8-*ortho* use different side chains to engage GABARAP's two hydrophobic pockets. Pen8-*ortho* fills one pocket with Trp6 and the other with Leu9, while Pen3-*ortho* fills the first pocket with Trp11 and the second with both Trp6 and Leu9. This second hydrophobic pocket is expanded in the Pen3-*ortho*-bound structure to accommodate both side chains (Figure 3c). Notably, Trp11 in Pen8-*ortho* binds in a third hydrophobic pocket not typically accessed by canonical LIR motifs. This third pocket is part of a larger binding surface used by some longer natural ligands,<sup>29,38,39</sup> but these binding interactions typically use aliphatic residues that

bind as part of a longer C-terminal helix—the binding interaction with a single Trp residue has never been seen before (Figure 3d).

The crystal structures offer a potential explanation for why Pen3-*ortho*, which binds in the artificial, K1-like conformation, is selective for GABARAP over LC3B, while Pen8-*ortho*, which binds in the natural, more extended conformation, binds with high affinity to both GABARAP and LC3B. We surmise that LC3B is unable to bind ligands in the K1-like conformation with high affinity due to an inability to undergo induced fit to accommodate the Trp side chain in the central hydrophobic pocket (Figure 2c). Notably, in both structures, the staple makes extended van der Waals contacts with GABARAP, implying that the staple contributes directly to the binding affinity for both ligands.

**Structure-Based Design Using 4-Mercaptoproline (4MP).** Based on the dihedral angles of bound Pen3-*ortho* and Ramachandran plots of proline and pre-proline residues,<sup>41,42</sup> we hypothesized that a 4-mercaptoproline (4MP) residue within the staple would favor Pen3-*ortho*'s GABARAP-selective binding conformation. 4MP conformationally restricts both the backbone and the staple, and we recently reported its use as a valuable building block for peptide stapling for non- $\alpha$ -helical peptides.<sup>32</sup> Testing a panel of Pen3-*ortho* analogues with 4MP in the third position (parent peptide MP3), we found that 4MP substitution maintained high GABARAP affinity while decreasing binding affinity to LC3B for all staple geometries (Figure 4a). These data, along with the observation



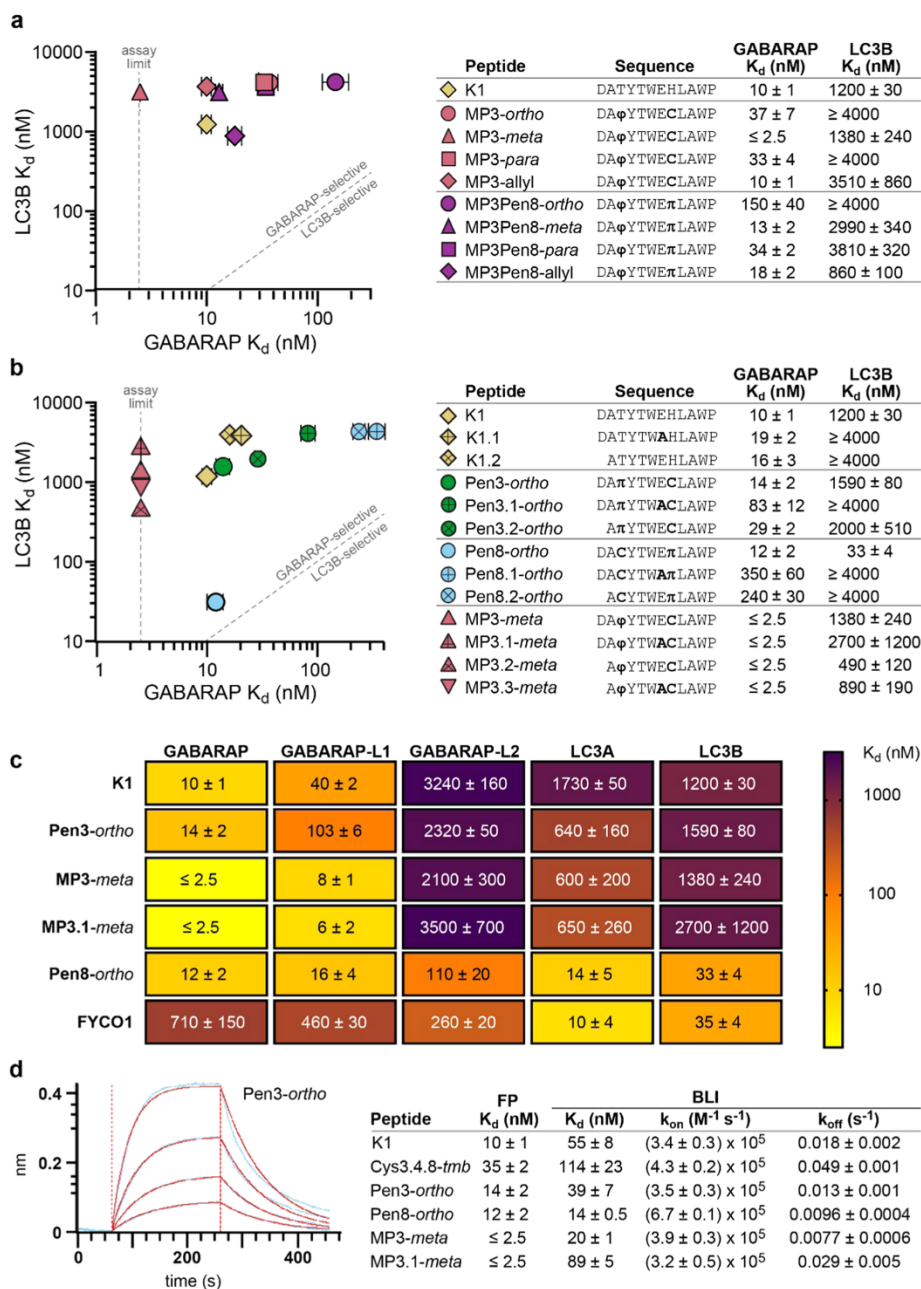


**Figure 4.** Structure-based design of improved GABARAP ligands. (a) Stapled peptides containing 4-mercaptoproline (4MP) and their affinities for recombinant GABARAP and LC3B as measured by FP.  $\phi$  denotes 4MP, and  $\pi$  denotes penicillamine. (b) Stapled peptides with a decreased negative charge and their affinities for recombinant GABARAP and LC3B. (c) Affinities of selected peptides were measured for five human paralogs in the GABARAP/LC3 family using FP assays. For FP assays, peptides were prepared with fluorescein on their N-termini (Figure S1 and Table S1). (d) Example data (blue curves), curve fits (red curves), and binding data (table) for a biolayer interferometry (BLI) assay with selected biotinylated peptides (Figure S1 and Table S2) and recombinant GABARAP. All data are shown as the average and standard error of the mean for three or more independent trials. Primary data and additional BLI results are shown in Figures S20–S22 and Table S10.

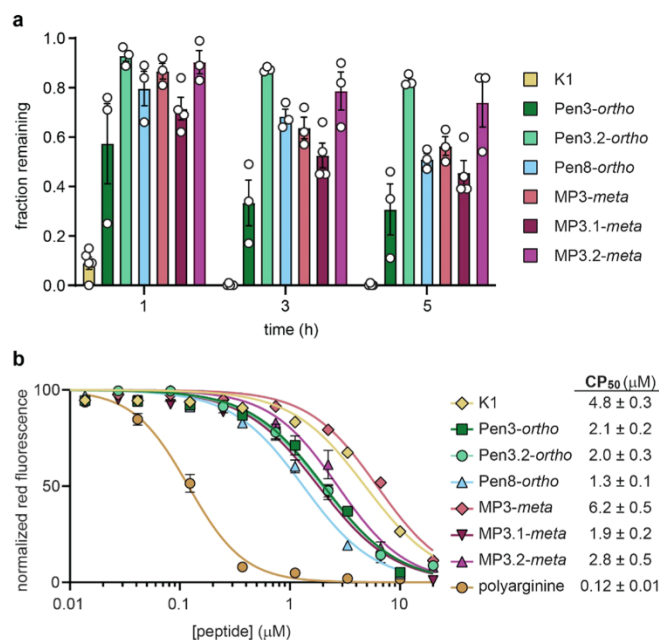


**Figure 5.** Biological stability and cytosolic penetration of GABARAP inhibitors. (a) Chloroalkane-tagged peptides (Figure S1 and Table S3) were incubated with HeLa cell lysates for 1, 3, and 5 h, and HPLC was used to quantitate the fraction of peptide remaining. (b) Cytosolic penetration after 24 h incubation of chloroalkane-tagged peptides with HeLa cells, as measured using the chloroalkane penetration assay (CAPA).<sup>44,45</sup> CAPA measures cytosolic penetration by monitoring the extent to which cytosolic HaloTag protein is blocked by chloroalkane-tagged peptide, with 100% fluorescence indicating no cytosolic penetration and 0% fluorescence indicating penetration sufficient to block all cytosolic HaloTag. CP<sub>50</sub> values are derived from the curve fits shown.<sup>44,45</sup> Chloroalkane-tagged polyarginine is shown as a positive control.<sup>44,45</sup> All data are shown as the average and standard error of at least three independent trials. Results of individual trials and additional data at a 4 h time point are shown in Figures S24 and S25 and Table S11.

that 4MP substitution abolished the nanomolar LC3B affinity of Pen8-ortho (compare to MP3Pen8-ortho, Figure 4a), suggested that 4MP promotes the helical Pen3-ortho binding conformation and disfavors the extended Pen8-ortho binding conformation. The highest-affinity ligand, MP3-meta, had a binding affinity for GABARAP that was too strong to be measured by direct FP ( $K_d \leq 2.5$  nM; see below for measurement using an orthogonal assay) and at least 1000-fold selectivity for GABARAP over LC3B (Figure 4a).

Prior to moving forward with biological assays, we sought to further lessen the overall negative charge. We noticed that residues Asp1 and Glu7 appear to make much more extensive polar contacts in the Pen8-ortho structure compared to the Pen3-ortho structure, as is commonly observed for the binding of canonical LIR motifs.<sup>23,39</sup> For example, GABARAP Arg67 forms a salt bridge with Glu7 in Pen8-ortho but not Pen3-ortho (Figure S3). Thus, we hypothesized that we could reduce charge and improve selectivity by truncating the N-terminal Asp and/or replacing Glu7 with Ala. Both substitutions only moderately affected K1's binding affinity for GABARAP, and Pen3-ortho analogues with either substitution showed 2- to 6-fold decreases in GABARAP affinity while maintaining specificity for GABARAP over LC3B (Figure 4b). Strikingly, both substitutions had larger effects on Pen8-ortho, decreasing GABARAP affinity by 20- to 30-fold while also losing all measurable binding affinity to LC3B. These results confirm the prediction that these negatively charged residues play

important roles in binding LC3B but less so for GABARAP, especially when ligands bind in the non-natural, K1-like conformation. For the highest-affinity ligand, MP3-meta, either or both substitutions maintained high-affinity GABARAP binding and at least 200-fold selectivity over LC3B (Figure 4b).

#### Selectivity Across Human LC3/GABARAP Analogues.

We next sought to characterize binding affinities of the stapled peptides for additional human LC3/GABARAP paralogs. We set up similar FP assays with recombinant LC3A, GABARAP-L1, and GABARAP-L2 and tested selected stapled peptides and controls (Figure 4c). K1, Pen3-ortho, and MP3-meta all share a similar selectivity pattern, binding GABARAP and GABARAP-L1 in the low-to-mid nanomolar range, and GABARAP-L2, LC3A, and LC3B mostly in the micromolar range. By contrast, we found that Pen8-ortho bound the five paralogs tested with  $K_d$  values between 12 and 110 nM. In fact, stapled peptide Pen8-ortho bound LC3B and LC3A with similar affinity as the natural, LC3-selective FYCO1 peptide (Figure 4c).

#### Orthogonal Binding Assay: Biolayer Interferometry.

The binding affinity measured for K1 in FP assays is different than the  $K_d$  in the original report by Weiergräber et al., which used surface plasmon resonance.<sup>28</sup> These results suggested that the fluorescein attached to peptides for the FP assay may improve binding to GABARAP. To control for these effects, we used biolayer interferometry (BLI) as an orthogonal binding

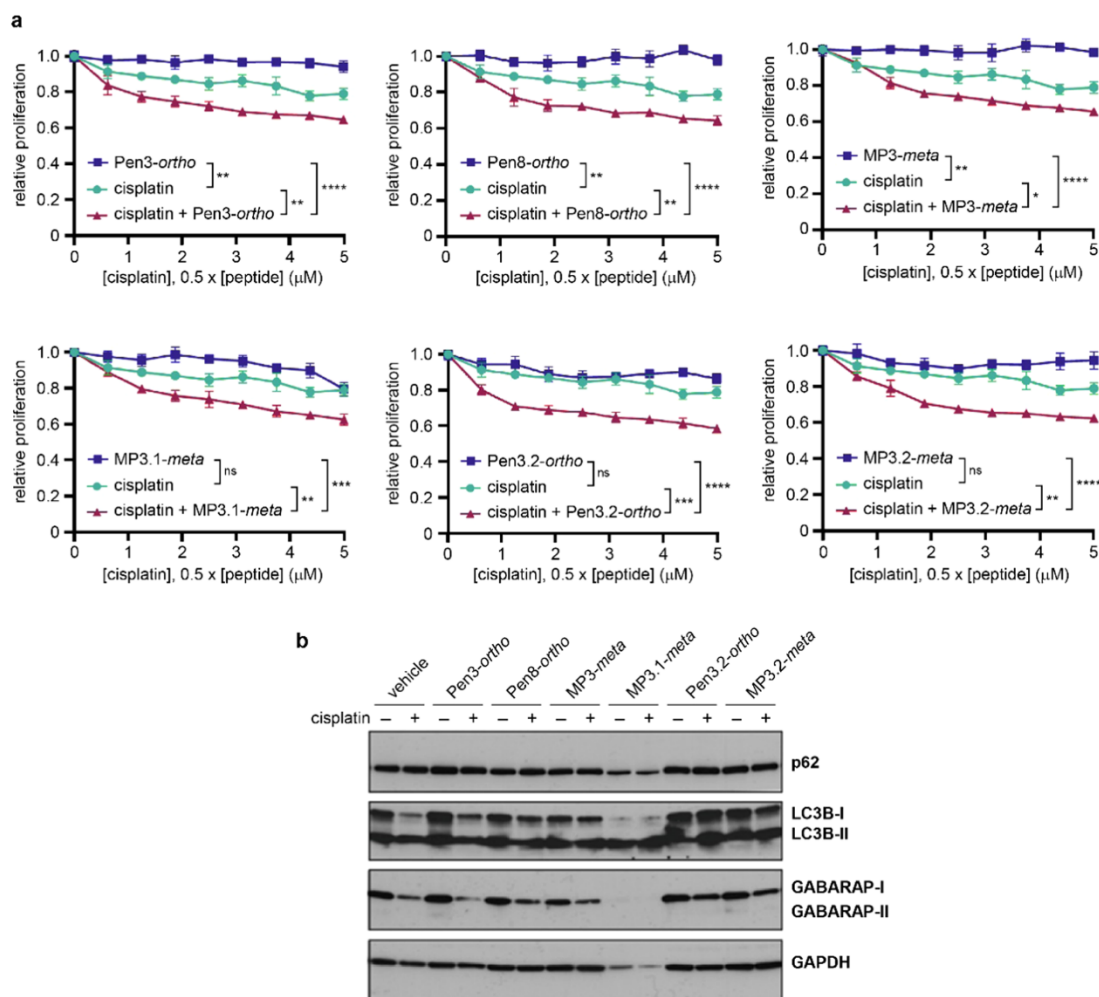


**Figure 6.** Effects of stapled peptides on ovarian cancer cells. (a) Relative cell proliferation after treatment of OVCAR8 cells with peptide alone (1.25–10  $\mu$ M), cisplatin alone (0.6–5  $\mu$ M), or cisplatin plus peptide (1:2 ratio of cisplatin to peptide). ns denotes not significant, \* $p$  < 0.05, \*\* $p$  < 0.01, \*\*\* $p$  < 0.001, and \*\*\*\* $p$  < 0.0001, one-way ANOVA with multiple comparisons. All peptides showed synergistic effects with cisplatin; combination indices are shown in Figure S31. Data are shown as the average and standard error of four technical replicates, and data are representative of two biological replicates (Figure S31). (b) Western blots of OVCAR8 cells treated with 25  $\mu$ M peptide and/or 10  $\mu$ M cisplatin for 48 h. Blot is representative of two biological replicates (Figure S32).

assay that employed biotinylated peptides (Figure S1 and Table S2).  $K_d$  values measured by BLI were, in general, 3- to 10-fold higher than  $K_d$  values measured by FP, consistent with N-terminal fluorescein contributing to binding (Figure 4d and Table S10). Importantly, the binding affinities of the highest-affinity ligands were at the titration limit of the FP assay, so BLI offered a more accurate method for comparing their binding affinities. The GABARAP-binding affinities of K1, Pen3-ortho, Pen8-ortho, and MP3-meta were measured by BLI at  $55 \pm 8$ ,  $39 \pm 7$ ,  $14 \pm 0.5$ , and  $20 \pm 1$  nM, respectively. BLI data also provided insight into binding kinetics, revealing that slower off-rates appear to be primary drivers for affinity improvements for stapled analogues of K1. Pen8-ortho was the only stapled peptide with enhanced on-rate, which may be due

to its canonical LIR binding mode not requiring induced fit of GABARAP (Figure 3c).

**Resistance to Biological Degradation.** Proteolytic degradation is a liability for peptides, but artificial amino acids and staples can provide resistance. We measured the stability of selected GABARAP ligands following 1, 3, and 5 h incubation in freshly prepared HeLa cell lysate, a high-stringency assay for measuring susceptibility to biological degradation.<sup>26,32,43</sup> K1 was degraded rapidly, with only 9% remaining after 1 h. Incorporating artificial amino acids such as *tert*-butyl alanine conferred some protease resistance, with 34% remaining at 1 h and 4% at 5 h (Figure S28). Stapling conferred even more resistance. At 5 h, between 35 and 80% of stapled peptides remained intact (Figure 5a). Interestingly, the

bicyclic peptide Cys3.4.8-*tmf* (see above) had less peptide remaining at 5 h than most of the stapled peptides (Figure S28)—in this case, bicyclic stapling did not confer an added advantage compared to single staples with respect to biological degradation.

**Penetration to the Cytosol.** In many cases, peptide stapling also increases cytosolic penetration.<sup>26,27,31</sup> We examined the cytosolic penetration of our stapled GABARAP-binding peptides using the chloroalkane penetration assay (CAPA), a robust assay that measures penetration to the cytosol without interference from the material trapped at the cell surface or in endosomes.<sup>44</sup> Importantly, while linear peptide K1 was the most prone to degradation, it was among the least cell-penetrant peptides tested (Figure 5b). This result helps to rule out degradation artifacts and supports the CAPA data report on the internalization of intact peptides.<sup>45,46</sup> We found that, with the exception of MP3-*meta*, all stapled peptides had significantly improved cytosolic penetration compared to K1 (Figure 5b). Removing negative charges had modest effects, improving cytosolic penetration by 2–3 fold for some but not all stapled peptides. Overall, the CAPA data showed that stapled GABARAP ligands effectively access the cytosol when incubated for 24 h at concentrations as low as 1 to 2 micromolar.

**Synergy with DNA-Damaging Agents and Effects on Autophagy.** Prior work indicated that autophagy is associated with cisplatin resistance in ovarian cancer and that autophagy inhibition can be synergistic with DNA-damaging chemotherapy in several solid tumors.<sup>6,21,30</sup> To determine whether GABARAP-binding stapled peptides have similar applications, we examined the effects of peptides alone and with cisplatin on cell growth in the OVCAR8 ovarian cancer cell line. Peptides alone showed limited effects on tumor cell growth up to 10  $\mu$ M. However, all peptides enhanced cisplatin-induced growth inhibition at concentrations as low as 2.5  $\mu$ M (Figures 6a and S31). Synergistic effects between peptides and cisplatin were confirmed by calculating combination indices, which were well below 1 for all peptides tested, with MP3.2-*meta* having the highest degree of synergy (Figure S31).

Because LC3B and GABARAP are involved in every step of autophagy (Figure 1), it was not clear precisely how LC3B/GABARAP inhibitors would affect autophagy. We treated OVCAR8 cells with cisplatin and/or stapled peptides and analyzed the autophagy markers p62, LC3B, and GABARAP by Western blotting (Figures 6b and S32). MP3.1-*meta* showed apparent cytotoxicity at 25  $\mu$ M, as evidenced by low intensity in the GAPDH loading control. In all other samples, p62 levels were relatively unchanged, implying that cisplatin and cisplatin plus peptide had minimal effects on selective autophagy mediated by p62. However, as previously shown in OVCAR8,<sup>30</sup> when cells are treated with cisplatin at sub-lethal doses, cisplatin decreases LC3B-I and GABARAP-I, which indicates induction of non-p62-dependent autophagy. When cotreated with sub-lethal doses of cisplatin and stapled peptides Pen8-*ortho*, Pen3.2-*ortho*, MP3-*meta*, or MP3.2-*meta*, OVCAR8 cells had increased LC3B-I compared to cells treated with cisplatin alone (Figure 6b). Treating cells with cisplatin and Pen3.2-*ortho* or MP3.2-*meta* also reversed the decrease in GABARAP-I observed in cells treated with cisplatin alone. These results suggest that K1-derived stapled peptides can partially block autophagy induction by cisplatin, which is a plausible mechanism for their synergistic effects on cell proliferation.

## DISCUSSION

Despite decades of work on stapled  $\alpha$ -helices, the structural and functional consequences of stapling nonhelical peptides remain difficult to predict. In this case, a diversity-oriented stapling strategy allowed for development of two classes of high-affinity GABARAP ligands: Pen8-*ortho*, which binds both GABARAPs and LC3s with nanomolar affinity, and the more GABARAP-selective Pen3-*ortho* and its analogues, including MP3-*meta*. The striking difference in binding modes for Pen8-*ortho* and Pen3-*ortho*, despite a difference of the locations of only two methyl groups, underscores the ability of a diversity-oriented stapling approach to broadly access conformational space for peptides, especially peptides lacking extended  $\alpha$ -helices. These stapled peptides are among the most potent binders of LC3/GABARAP proteins described to date. Notably, native ligands with similar or higher affinity have an extended C-terminal helix (Figure 3d), are twice the size of the stapled peptides reported here, and have eight or more negative charges, making them unlikely to be useful for pharmacological inhibition.<sup>23,29</sup> For Pen8-*ortho*, binding affinity appears to derive from the ability to access three hydrophobic pockets, and for Pen3-*ortho*, binding affinity appears to derive from engagement of a large, cryptic hydrophobic pocket that is not observed for native ligands. Both inhibitors also make extensive contact with GABARAP via their hydrophobic staples.

Our applications of stapled peptides to inhibit autophagy add to the growing literature showing that interfering with the protein-protein interactions of LC3/GABARAP proteins is a promising avenue for anti-cancer therapeutics.<sup>21,30</sup> Inhibiting autophagy can also subvert immune system evasion by solid tumors. For example, Yamamoto and co-workers found that in pancreatic ductal adenocarcinoma cells, MHC-I is degraded by NBR1-mediated autophagy, resulting in a lower antigen presentation and decreased CD8+ T cell activation compared to autophagy-inhibited cells.<sup>47</sup> Inhibiting autophagy has also been found to promote an antitumor immune response in high mutational burden tumors and can improve response to PD-1/PD-L1 therapy.<sup>48–51</sup> This may explain why a prior LC3B ligand showed unusually potent antitumor effects in mice compared to its *in vitro* activity.<sup>30</sup> In this work, we developed several stapled peptides with selectivity for GABARAP, including Pen3.2-*ortho*, MP3-*meta*, and MP3.2-*meta*, as well as one stapled peptide that inhibited both LC3 and GABARAP proteins, Pen8-*ortho*. These ligands all inhibited autophagy and potentiated cisplatin toxicity in OVCAR8 cells with similar potency. These results imply that blocking GABARAP may be at least as critical as blocking LC3B for efficient autophagy inhibition. Prior work which tested the effects of LC3B ligands and inhibitors did not examine their binding to GABARAP, leaving open the possibility that their biological effects were mediated in part (or perhaps even in full) by GABARAP inhibition.<sup>8,30,52</sup> Moving forward, we expect that GABARAP-selective ligands and ligands that bind both LC3 and GABARAP proteins will be useful classes of ligands for exploring potential combination therapies with DNA-damaging agents and potentially with checkpoint inhibitors as well.<sup>47</sup>

Autophagy, and specifically the LC3/GABARAP family of proteins, is also an emerging avenue for targeted protein degradation.<sup>53</sup> Autophagy-targeting chimeras (called AUTACs, among other acronyms)<sup>52–55</sup> link a compound that binds a protein-of-interest to another compound that promotes



recruitment to the autophagosome. AUTACs could have several advantages over proteolysis-targeting chimeras (PRO-TACs) because autophagy components such as LC3/GABARAP are broadly expressed in all tissue types and because autophagosome recruitment requires only physical tethering, not catalysis within a ternary complex. While peptides would likely get degraded in the lysosome, the stapled peptides reported here represent promising starting points for this exciting modality. Further, our data directly inform efforts to develop small-molecule AUTACs. For example, while LC3B is the more well-studied mammalian paralog, our data suggest GABARAP may be a better target for continued work in AUTAC development. GABARAP's central hydrophobic pocket can widen to accommodate a larger hydrophobic ligand (Figure 3c), which is not seen in structures of LC3B, and it has several adjacent hydrophobic pockets that can be exploited to improve binding affinity (Figure 3a,b). Thus, we expect GABARAP to be a key target for recruiting proteins-of-interest for degradation via autophagy.

## ■ ASSOCIATED CONTENT

### Supporting Information

The Supporting Information is available free of charge at <https://pubs.acs.org/doi/10.1021/jacs.2c04699>.

Materials and methods, chemical structures, compound characterization, additional data on binding, degradation, cell penetration, and effects in cell culture, full data sets for binding assays and cell penetration assay, and crystallographic data tables (PDF)

## ■ AUTHOR INFORMATION

### Corresponding Author

**Joshua A. Kritzer** – Department of Chemistry, Tufts University, Medford, Massachusetts 02155, United States; [orcid.org/0000-0003-2878-6781](https://orcid.org/0000-0003-2878-6781); Email: [joshua.kritzer@tufts.edu](mailto:joshua.kritzer@tufts.edu)

### Authors

**Howley Brown** – Department of Chemistry, Tufts University, Medford, Massachusetts 02155, United States  
**Mia Chung** – Department of Chemistry, Tufts University, Medford, Massachusetts 02155, United States  
**Alina Uffing** – Institute of Biological Information Processing, Structural Biochemistry (IBI-7), Forschungszentrum Jülich, S2425 Jülich, Germany; Institut für Physikalische Biologie, Heinrich-Heine-Universität Düsseldorf, 40225 Düsseldorf, Germany  
**Nefeli Batistatou** – Department of Chemistry, Tufts University, Medford, Massachusetts 02155, United States  
**Tiffany Tsang** – Department of Chemistry, Tufts University, Medford, Massachusetts 02155, United States; [orcid.org/0000-0002-0398-8590](https://orcid.org/0000-0002-0398-8590)  
**Samantha Daskocil** – Department of Experimental Therapeutics, The University of Texas MD Anderson Cancer Center, Houston, Texas 77030, United States  
**Weiqun Mao** – Department of Experimental Therapeutics, The University of Texas MD Anderson Cancer Center, Houston, Texas 77030, United States  
**Dieter Willbold** – Institute of Biological Information Processing, Structural Biochemistry (IBI-7), Forschungszentrum Jülich, S2425 Jülich, Germany; Institut

für Physikalische Biologie, Heinrich-Heine-Universität Düsseldorf, 40225 Düsseldorf, Germany

**Robert C. Bast, Jr.** – Department of Experimental Therapeutics, The University of Texas MD Anderson Cancer Center, Houston, Texas 77030, United States

**Zhen Lu** – Department of Experimental Therapeutics, The University of Texas MD Anderson Cancer Center, Houston, Texas 77030, United States

**Oliver H. Weiergräber** – Institute of Biological Information Processing, Structural Biochemistry (IBI-7), Forschungszentrum Jülich, S2425 Jülich, Germany

Complete contact information is available at:

<https://pubs.acs.org/doi/10.1021/jacs.2c04699>

### Notes

The authors declare no competing financial interest.

## ■ ACKNOWLEDGMENTS

This work was funded in part by NIH GM125856 and NSF 2003010 for J.A.K., a Beckman Scholars award from the Arnold O. and Mabel Beckman Foundation for M.C., Emerson Collective and MD Anderson Specialized Program of Research Excellence in Ovarian Cancer (P50 CA 217685, NCI) and NCI R01 CA 135354 for R.C.B. Jr. and Z.L., and the Deutsche Forschungsgemeinschaft (DFG, German Research Foundation) – Project-ID 267205415-SFB 1208, project B02 for D.W. The authors acknowledge the European Synchrotron Radiation Facility for provision of synchrotron radiation facilities, and they would like to thank Antoine Royant and Estelle Mossou for assistance in using beamlines ID23-2 and ID30B, respectively.

## ■ REFERENCES

- (1) Levine, B.; Kroemer, G. Autophagy in the Pathogenesis of Disease. *Cell* **2008**, *132*, 27–42.
- (2) White, E. The Role for Autophagy in Cancer. *J. Clin. Invest.* **2015**, *125*, 42–46.
- (3) Karsli-Uzunbas, G.; Guo, J. Y.; Price, S.; Teng, X.; Laddha, S. V.; Khor, S.; Kalaany, N. Y.; Jacks, T.; Chan, C. S.; Rabinowitz, J. D.; White, E. Autophagy Is Required for Glucose Homeostasis and Lung Tumor Maintenance. *Cancer Discovery* **2014**, *4*, 914–927.
- (4) Xie, X.; Koh, J. Y.; Price, S.; White, E.; Mehnert, J. M. Atg7 Overcomes Senescence and Promotes Growth of BrafV600E-Driven Melanoma. *Cancer Discovery* **2015**, *5*, 410–423.
- (5) Yang, S.; Wang, X.; Contino, G.; Liesa, M.; Sahin, E.; Ying, H.; Bause, A.; Li, Y.; Stommel, J. M.; Dell'antonio, G.; Mautner, J.; Tonon, G.; Haigis, M.; Shirihai, O. S.; Doglioni, C.; Bardeesy, N.; Kimmelman, A. C. Pancreatic Cancers Require Autophagy for Tumor Growth. *Genes Dev.* **2011**, *25*, 717–729.
- (6) Jiang, Y.; Ji, F.; Liu, Y.; He, M.; Zhang, Z.; Yang, J.; Wang, N.; Zhong, C.; Jin, Q.; Ye, X.; Chen, T. Cisplatin-Induced Autophagy Protects Breast Cancer Cells from Apoptosis by Regulating Yes-Associated Protein. *Oncol. Rep.* **2017**, *38*, 3668–3676.
- (7) Wang, J.; Wu, G. S. Role of Autophagy in Cisplatin Resistance in Ovarian Cancer Cells. *J. Biol. Chem.* **2014**, *289*, 17163–17173.
- (8) AlMasri, S. S.; Zenati, M. S.; Desilva, A.; Nassour, I.; Boone, B. A.; Singhi, A. D.; Bartlett, D. L.; Liotta, L. A.; Espina, V.; Loughran, P.; Lotze, M. T.; Paniccia, A.; Zeh, H. J., III; Zureikat, A. H.; Bahary, N. Encouraging Long-Term Survival Following Autophagy Inhibition Using Neoadjuvant Hydroxychloroquine and Gemcitabine for High-Risk Patients with Resectable Pancreatic Carcinoma. *Cancer Med.* **2021**, *10*, 7233–7241.
- (9) Anand, K.; Niravath, P.; Patel, T.; Ensor, J.; Rodriguez, A.; Boone, T.; Wong, S. T.; Chang, J. C. A Phase II Study of the Efficacy and Safety of Chloroquine in Combination With Taxanes in the

- Treatment of Patients With Advanced or Metastatic Anthracycline-Refractory Breast Cancer. *Clin. Breast Cancer* **2021**, *21*, 199–204.
- (10) Compter, I.; Eekers, D. B. P.; Hoebe, A.; Rouschop, K. M. A.; Reymen, B.; Ackermans, L.; Beckervordersantfort, J.; Bauer, N. J. C.; Anten, M. M.; Wesseling, P.; Postma, A. A.; De Ruyscher, D.; Lambin, P. Chloroquine Combined with Concurrent Radiotherapy and Temozolomide for Newly Diagnosed Glioblastoma: A Phase IB Trial. *Autophagy* **2021**, *17*, 2604–2612.
- (11) Xu, R.; Ji, Z.; Xu, C.; Zhu, J. The Clinical Value of Using Chloroquine or Hydroxychloroquine as Autophagy Inhibitors in the Treatment of Cancers. *Medicine* **2018**, *97*, No. e12912.
- (12) Leung, L.-S. B.; Neal, J. W.; Wakelee, H. A.; Sequist, L. V.; Marmor, M. F. Rapid Onset of Retinal Toxicity From High-Dose Hydroxychloroquine Given for Cancer Therapy. *Am. J. Ophthalmol.* **2015**, *160*, 799–805.
- (13) Mauthe, M.; Orhon, I.; Rocchi, C.; Zhou, X.; Luhr, M.; Hijlkema, K.-J.; Coppes, R. P.; Engedal, N.; Mari, M.; Reggiori, F. Chloroquine Inhibits Autophagic Flux by Decreasing Autophagosome-Lysosome Fusion. *Autophagy* **2018**, *14*, 1435–1455.
- (14) Kocak, M.; Erdi, S. E.; Jorba, G.; Maestro, I.; Farrés, J.; Kirkin, V.; Martinez, A.; Pless, O. Targeting Autophagy in Disease: Established and New Strategies. *Autophagy* **2022**, *18*, 473–495.
- (15) Lee, Y.-K.; Lee, J.-A. Role of the Mammalian ATG8/LC3 Family in Autophagy: Differential and Compensatory Roles in the Spatiotemporal Regulation of Autophagy. *BMB Rep.* **2016**, *49*, 424–430.
- (16) Birgisdottir, Á. B.; Lamark, T.; Johansen, T. The LIR Motif – Crucial for Selective Autophagy. *J. Cell Sci.* **2013**, *126*, 3237–3247.
- (17) Noda, N. N.; Ohsumi, Y.; Inagaki, F. Atg8-Family Interacting Motif Crucial for Selective Autophagy. *FEBS Lett.* **2010**, *584*, 1379–1385.
- (18) Weidberg, H.; Shvets, E.; Shpilka, T.; Shimron, F.; Shinder, V.; Elazar, Z. LC3 and GATE-16/GABARAP Subfamilies Are Both Essential yet Act Differently in Autophagosome Biogenesis. *EMBO J.* **2010**, *29*, 1792–1802.
- (19) Nguyen, T. N.; Padman, B. S.; Usher, J.; Oorschot, V.; Ramm, G.; Lazarou, M. Atg8 Family LC3/GABARAP Proteins Are Crucial for Autophagosome–Lysosome Fusion but Not Autophagosome Formation during PINK1/Parkin Mitophagy and Starvation. *J. Cell Biol.* **2016**, *215*, 857–874.
- (20) Johansen, T.; Lamark, T. Selective Autophagy: ATG8 Family Proteins, LIR Motifs and Cargo Receptors. *J. Mol. Biol.* **2020**, *432*, 80–103.
- (21) Putyrski, M.; Vakhrusheva, O.; Bonn, F.; Guntur, S.; Vorobyov, A.; Brandts, C.; Dikic, I.; Ernst, A. Disrupting the LC3 Interaction Region (LIR) Binding of Selective Autophagy Receptors Sensitizes AML Cell Lines to Cytarabine. *Front. Cell Dev. Biol.* **2020**, *8*, 208.
- (22) Jacquet, M.; Guittaut, M.; Fraichard, A.; Despouy, G. The Functions of Atg8-Family Proteins in Autophagy and Cancer: Linked or Unrelated? *Autophagy* **2021**, *17*, 599–611.
- (23) Wirth, M.; Zhang, W.; Razi, M.; Nyoni, L.; Joshi, D.; O'Reilly, N.; Johansen, T.; Tooze, S. A.; Mouilleron, S. Molecular Determinants Regulating Selective Binding of Autophagy Adapters and Receptors to ATG8 Proteins. *Nat. Commun.* **2019**, *10*, No. 2055.
- (24) Rogov, V. V.; Stolz, A.; Ravichandran, A. C.; Rios-Szwed, D. O.; Suzuki, H.; Kniss, A.; Löhr, F.; Wakatsuki, S.; Dötsch, V.; Dikic, I.; Dobson, R. C.; McEwan, D. G. Structural and Functional Analysis of the GABARAP Interaction Motif (GIM). *EMBO Rep.* **2017**, *18*, 1382–1396.
- (25) Huber, J.; Obata, M.; Gruber, J.; Akutsu, M.; Löhr, F.; Rogova, N.; Güntert, P.; Dikic, I.; Kirkin, V.; Komatsu, M.; Dötsch, V.; Rogov, V. V. An Atypical LIR Motif within UBA5 (Ubiquitin like Modifier Activating Enzyme 5) Interacts with GABARAP Proteins and Mediates Membrane Localization of UBA5. *Autophagy* **2020**, *16*, 256–270.
- (26) Cerulli, R. A.; Shehaj, L.; Brown, H.; Pace, J.; Mei, Y.; Kritzer, J. A. Stapled Peptide Inhibitors of Autophagy Adapter LC3B. *ChemBioChem* **2020**, *21*, 2777–2785.
- (27) Walensky, L. D.; Bird, G. H. Hydrocarbon-Stapled Peptides: Principles, Practice, and Progress. *J. Med. Chem.* **2014**, *57*, 6275–6288.
- (28) Weiergräber, O. H.; Stangler, T.; Thielmann, Y.; Mohrlüder, J.; Wiesehan, K.; Willbold, D. Ligand Binding Mode of GABAA Receptor-Associated Protein. *J. Mol. Biol.* **2008**, *381*, 1320–1331.
- (29) Li, J.; Zhu, R.; Chen, K.; Zheng, H.; Zhao, H.; Yuan, C.; Zhang, H.; Wang, C.; Zhang, M. Potent and Specific Atg8-Targeting Autophagy Inhibitory Peptides from Giant Ankyrins. *Nat. Chem. Biol.* **2018**, *14*, 778–787.
- (30) Gray, J. P.; Uddin, M. N.; Chaudhari, R.; Sutton, M. N.; Yang, H.; Rask, P.; Locke, H.; Engel, B. J.; Batistatou, N.; Wang, J.; Grindel, B. J.; Bhattacharya, P.; Gammon, S. T.; Zhang, S.; Piwnicka-Worms, D.; Kritzer, J. A.; Lu, Z.; Bast, R. C.; Millward, S. W. Directed Evolution of Cyclic Peptides for Inhibition of Autophagy. *Chem. Sci.* **2021**, *12*, 3526–3543.
- (31) Peraro, L.; Zou, Z.; Makwana, K. M.; Cummings, A. E.; Ball, H. L.; Yu, H.; Lin, Y.-S.; Levine, B.; Kritzer, J. A. Diversity-Oriented Stapling Yields Intrinsically Cell-Penetrant Inducers of Autophagy. *J. Am. Chem. Soc.* **2017**, *139*, 7792–7802.
- (32) Pace, J. R.; Lampkin, B. J.; Abakah, C.; Moyer, A.; Miao, J.; Deprey, K.; Cerulli, R. A.; Lin, Y.-S.; Baleja, J. D.; Baker, D.; Kritzer, J. A. Stapled  $\beta$ -Hairpins Featuring 4-Mercaptoproline. *J. Am. Chem. Soc.* **2021**, *143*, 15039–15044.
- (33) Sawyer, N.; Arora, P. S. Hydrogen Bond Surrogate Stabilization of  $\beta$ -Hairpins. *ACS Chem. Biol.* **2018**, *13*, 2027–2032.
- (34) Timmerman, P.; Beld, J.; Puijk, W. C.; Meloan, R. H. Rapid and Quantitative Cyclization of Multiple Peptide Loops onto Synthetic Scaffolds for Structural Mimicry of Protein Surfaces. *ChemBioChem* **2005**, *6*, 821–824.
- (35) Siegert, T. R.; Bird, M. J.; Makwana, K. M.; Kritzer, J. A. Analysis of Loops That Mediate Protein–Protein Interactions and Translation into Submicromolar Inhibitors. *J. Am. Chem. Soc.* **2016**, *138*, 12876–12884.
- (36) Peraro, L.; Siegert, T. R.; Kritzer, J. A. Conformational Restriction of Peptides Using Dithiol Bis-Alkylation. *Methods Enzymol.* **2016**, *580*, 303–332.
- (37) Heinis, C.; Rutherford, T.; Freund, S.; Winter, G. Phage-Encoded Combinatorial Chemical Libraries Based on Bicyclic Peptides. *Nat. Chem. Biol.* **2009**, *5*, 502–507.
- (38) Li, Y.; Cheng, X.; Li, M.; Wang, Y.; Fu, T.; Zhou, Z.; Wang, Y.; Gong, X.; Xu, X.; Liu, J.; Pan, L. Decoding Three Distinct States of the Syntaxin17 SNARE Motif in Mediating Autophagosome–Lysosome Fusion. *Proc. Natl. Acad. Sci. U.S.A.* **2020**, *117*, 21391–21402.
- (39) Zhao, J.; Li, Z.; Li, J. The Crystal Structure of the FAM134B–GABARAP Complex Provides Mechanistic Insights into the Selective Binding of FAM134 to the GABARAP Subfamily. *FEBS Open Bio* **2022**, *12*, 320–331.
- (40) Mochida, K.; Yamasaki, A.; Matoba, K.; Kirisako, H.; Noda, N. N.; Nakatogawa, H. Super-Assembly of ER-Phagy Receptor Atg40 Induces Local ER Remodeling at Contacts with Forming Autophagosomal Membranes. *Nat. Commun.* **2020**, *11*, No. 3306.
- (41) Ho, B. K.; Brasseur, R. The Ramachandran Plots of Glycine and Pre-Proline. *BMC Struct. Biol.* **2005**, *5*, 14.
- (42) MacArthur, M. W.; Thornton, J. M. Influence of Proline Residues on Protein Conformation. *J. Mol. Biol.* **1991**, *218*, 397–412.
- (43) Partridge, A. W.; Kaan, H. Y. K.; Juang, Y.-C.; Sadruddin, A.; Lim, S.; Brown, C. J.; Ng, S.; Thean, D.; Ferrer, F.; Johannes, C.; Yuen, T. Y.; Kannan, S.; Aronica, P.; Tan, Y. S.; Pradhan, M. R.; Verma, C. S.; Hochman, J.; Chen, S.; Wan, H.; Ha, S.; Sherborne, B.; Lane, D. P.; Sawyer, T. K. Incorporation of Putative Helix-Breaking Amino Acids in the Design of Novel Stapled Peptides: Exploring Biophysical and Cellular Permeability Properties. *Molecules* **2019**, *24*, 2292.
- (44) Peraro, L.; Deprey, K. L.; Moser, M. K.; Zou, Z.; Ball, H. L.; Levine, B.; Kritzer, J. A. Cell Penetration Profiling Using the Chloroalkane Penetration Assay. *J. Am. Chem. Soc.* **2018**, *140*, 11360–11369.

- (45) Deprey, K.; Kritzer, J. A. Quantitative Measurement of Cytosolic Penetration Using the Chloroalkane Penetration Assay. *Methods Enzymol.* **2020**, *641*, 277–309.
- (46) Deprey, K.; Batistatou, N.; Debets, M. F.; Godfrey, J.; VanderWall, K. B.; Miles, R. R.; Shehaj, L.; Guo, J.; Andreucci, A.; Kandasamy, P.; Lu, G.; Shimizu, M.; Vargeese, C.; Kritzer, J. A. Quantitative Measurement of Cytosolic and Nuclear Penetration of Oligonucleotide Therapeutics. *ACS Chem. Biol.* **2022**, *17*, 348–360.
- (47) Yamamoto, K.; Venida, A.; Yano, J.; Biancur, D. E.; Kakiuchi, M.; Gupta, S.; Sohn, A. S. W.; Mukhopadhyay, S.; Lin, E. Y.; Parker, S. J.; Banh, R. S.; Paulo, J. A.; Wen, K. W.; Debnath, J.; Kim, G. E.; Mancias, J. D.; Fearon, D. T.; Perera, R. M.; Kimmelman, A. C. Autophagy Promotes Immune Evasion of Pancreatic Cancer by Degrading MHC-I. *Nature* **2020**, *581*, 100–105.
- (48) Deng, J.; Thennavan, A.; Dolgalev, L.; Chen, T.; Li, J.; Marzio, A.; Poirier, J. T.; Peng, D. H.; Bulatovic, M.; Mukhopadhyay, S.; Silver, H.; Papadopoulos, E.; Pyon, V.; Thakurdin, C.; Han, H.; Li, F.; Li, S.; Ding, H.; Hu, H.; Pan, Y.; Weerasekara, V.; Jiang, B.; Wang, E. S.; Ahearn, I.; Philips, M.; Papagiannakopoulos, T.; Tsirogas, A.; Rothenberg, E.; Gainer, J.; Freeman, G. J.; Rudin, C. M.; Gray, N. S.; Hammerman, P. S.; Pagano, M.; Heymach, J. V.; Perou, C. M.; Bardeesy, N.; Wong, K.-K. ULK1 Inhibition Overcomes Compromised Antigen Presentation and Restores Antitumor Immunity in LKB1-Mutant Lung Cancer. *Nat. Cancer* **2021**, *2*, 503–514.
- (49) Poillet-Perez, L.; Sharp, D. W.; Yang, Y.; Laddha, S. V.; Ibrahim, M.; Bommarreddy, P. K.; Hu, Z. S.; Vieth, J.; Haas, M.; Rosenberg, M. W.; Rabinowitz, J. D.; Cao, J.; Guan, J.-L.; Ganesan, S.; Chan, C. S.; Mehnert, J. M.; Lattime, E. C.; White, E. Autophagy Promotes Growth of Tumors with High Mutational Burden by Inhibiting a T-Cell Immune Response. *Nat. Cancer* **2020**, *1*, 923–934.
- (50) Noman, M. Z.; Parpal, S.; Van Moer, K.; Moer, K. V.; Xiao, M.; Yu, Y.; Arakelian, T.; Viklund, J.; Viklund, J.; Milito, A. D.; De Milito, A.; Hasmim, M.; Hasmim, M.; Andersson, M.; Andersson, M.; Amaravadi, R. K.; Amaravadi, R. K.; Martinsson, J.; Martinsson, J.; Berchem, G.; Berchem, G.; Janji, B. Inhibition of Vps34 Reprograms Cold into Hot Inflamed Tumors and Improves Anti-PD-1/PD-L1 Immunotherapy. *Sci. Adv.* **2020**, *6*, No. eaax7881.
- (51) Wang, X.; Wu, W. K. K.; Gao, J.; Li, Z.; Dong, B.; Lin, X.; Li, Y.; Li, Y.; Gong, J.; Qi, C.; Peng, Z.; Yu, J.; Shen, L. Autophagy Inhibition Enhances PD-L1 Expression in Gastric Cancer. *J. Exp. Clin. Cancer Res.* **2019**, *38*, 140.
- (52) Li, Z.; Wang, C.; Wang, Z.; Zhu, C.; Li, J.; Sha, T.; Ma, L.; Gao, C.; Yang, Y.; Sun, Y.; Wang, J.; Sun, X.; Lu, C.; Difiglia, M.; Mei, Y.; Ding, C.; Luo, S.; Dang, Y.; Ding, Y.; Fei, Y.; Lu, B. Allele-Selective Lowering of Mutant HTT Protein by HTT-LC3 Linker Compounds. *Nature* **2019**, *575*, 203–209.
- (53) Alabi, S. B.; Crews, C. M. Major Advances in Targeted Protein Degradation: PROTACs, LYTACs, and MADTACs. *J. Biol. Chem.* **2021**, *296*, No. 100647.
- (54) Takahashi, D.; Moriyama, J.; Nakamura, T.; Miki, E.; Takahashi, E.; Sato, A.; Akaike, T.; Itto-Nakama, K.; Arimoto, H. AUTACs: Cargo-Specific Degradation Using Selective Autophagy. *Mol. Cell* **2019**, *76*, 797–810.
- (55) Pei, J.; Pan, X.; Wang, A.; Shuai, W.; Bu, F.; Tang, P.; Zhang, S.; Zhang, Y.; Wang, G.; Ouyang, L. Developing Potent LC3-Targeting AUTAC Tools for Protein Degradation with Selective Autophagy. *Chem. Commun.* **2021**, *57*, 13194–13197.

## Recommended by ACS

### Stretching Peptides to Generate Small Molecule $\beta$ -Strand Mimics

Zoë C. Adams, Philip E. Dawson, *et al.*

MARCH 15, 2023

ACS CENTRAL SCIENCE

READ 

### Biochemical and Structural Characterization of a Peptidic Inhibitor of the YAP:TEAD Interaction That Binds to the $\alpha$ -Helix Pocket on TEAD

Yannick Mesrouze, Patrick Chène, *et al.*

FEBRUARY 24, 2023

ACS CHEMICAL BIOLOGY

READ 

### Stretching Peptides' Potential to Target Protein–Protein Interactions

Naresh M. Venneti and Jennifer L. Stockdill

APRIL 12, 2023

ACS CENTRAL SCIENCE

READ 

### Reversible Dual-Covalent Molecular Locking of the 14-3-3/ERR $\gamma$ Protein–Protein Interaction as a Molecular Glue Drug Discovery Approach

Bente A. Somsen, Luc Brunsveld, *et al.*

MARCH 16, 2023

JOURNAL OF THE AMERICAN CHEMICAL SOCIETY

READ 

Get More Suggestions >





### 3.2. Exploring arylidene-indolinone ligands of autophagy proteins LC3B and GABARAP

<b>Authors</b>	Alexandria N. Leveille, Hawley Brown, Thomas Schwarzrock, Bennett True, Joanet Plasencia, Philipp Neudecker, <u>Alina Üffing</u> , Oliver H. Weiergräber, Dieter Willbold, Joshua A. Kritzer
<b>Journal</b>	BioRxiv (Preprint)
<b>Year of Publication</b>	2024 (Preprint)
<b>DOI</b>	10.1101/2024.02.25.581879
<b>Impact Factor</b>	-
<b>Contribution</b>	Expression and Purification of <sup>15</sup> N-GABARAP, HSQC NMR experiment (together with Philipp Neudecker), preparation of respective manuscript figure.
<b>Reprint Permission</b>	This article is made available under a CC-BY-NC-ND 4.0 license ( <a href="https://creativecommons.org/licenses/by-nc-nd/4.0/">https://creativecommons.org/licenses/by-nc-nd/4.0/</a> )

Note that only the main text is included in this dissertation, SI material can be found here:

<https://www.biorxiv.org/content/10.1101/2024.02.25.581879v1>



bioRxiv preprint doi: <https://doi.org/10.1101/2024.02.25.581879>; this version posted February 25, 2024. The copyright holder for this preprint (which was not certified by peer review) is the author/funder, who has granted bioRxiv a license to display the preprint in perpetuity. It is made available under aCC-BY-NC-ND 4.0 International license.

## Exploring Arylidene-Indolinone Ligands of Autophagy Proteins LC3B and GABARAP

Alexandria N. Leveille<sup>1</sup>, Hawley Brown<sup>1</sup>, Thomas Schwarzrock<sup>1</sup>, Bennett True<sup>1</sup>, Joanet Plasencia<sup>1</sup>, Philipp Neudecker<sup>2,3,4</sup>, Alina Üffing<sup>2,3,4</sup>, Oliver H. Weiergräber<sup>2,3,4</sup>, Dieter Willbold<sup>2,3,4</sup>, Joshua A. Kritzer<sup>1,\*</sup>

<sup>1</sup>Department of Chemistry, Tufts University, 62 Talbot Avenue, Medford MA

<sup>2</sup>Heinrich-Heine-Universität Düsseldorf, Mathematisch-Naturwissenschaftliche Fakultät, Institut für Physikalische Biologie, 40225 Düsseldorf, Germany.

<sup>3</sup>Forschungszentrum Jülich, Institut für Biologische Informationsprozesse: Strukturbiochemie (IBI-7), 52425 Jülich, Germany.

<sup>4</sup>Forschungszentrum Jülich, Jülich Centre for Structural Biology (JuStruct), 52425 Jülich, Germany

**Keywords:** autophagy · protein-protein interactions · small-molecule inhibitors · structure-activity relationships

**ABSTRACT:** Herein we report the first structure-activity studies of compound GW5074 which has demonstrated binding affinity to autophagy-related proteins LC3B and GABARAP. The literature has conflicting information on the binding affinities of this compound to LC3B and GABARAP, and there is some debate regarding its use as a component of autophagy-targeting chimeras (AUTACs) or autophagosome-tethering chimeras (ATTECs). We developed an AlphaScreen binding assay to compare the potencies of these compounds for inhibiting binding of known peptide ligands to LC3B and GABARAP. 38 analogs were synthesized and tested against both proteins. Inhibitory potencies were found to be mid to high micromolar, and 2D-NMR data revealed the binding site as hydrophobic pocket 1, where the native peptide ligands bind with an aromatic side chain. Our results suggest that GW5074 does bind LC3B and GABARAP in the micromolar range, but it may not be a good candidate for potent autophagy inhibition. These affinities could support further exploration in targeted protein degradation, but only if off-target effects can be appropriately controlled for.

Macroautophagy is a process by which intracellular cargo, including proteins, protein aggregates, and organelles, is recruited to and degraded by the lysosome. Macroautophagy (referred to here as simply “autophagy”) is essential for maintaining cellular homeostasis. In advanced cancers, autophagy contributes to disease progression through multiple mechanisms including immune evasion,<sup>1,2</sup> metabolic adaptation,<sup>3</sup> and accelerated metastasis.<sup>4,5</sup> Additionally, autophagy is typically upregulated in response to DNA-damaging agents and genetic studies have shown that inhibiting autophagy re-sensitizes late-stage cancers to cisplatin treatment.<sup>6–8</sup> Therefore, autophagy inhibitors are a promising area for novel combination therapies.<sup>9</sup> Unfortunately, commonly used autophagy inhibitors such as hydroxychloroquine are not specific to autophagy, they have many side effects, and they can have dose-limiting toxicity.<sup>10,11</sup> Targeting protein-protein interactions involved in autophagy is a good strategy for developing selective inhibitors.<sup>9</sup> Specifically, LC3/GABARAP family proteins mediate protein-protein interactions at every step of the autophagy pathway.<sup>12</sup> Genetic knockdowns and knockouts of LC3/GABARAP

proteins inhibit autophagy selectively, demonstrating that this family of autophagy proteins is a promising drug target.<sup>13–16</sup> At high concentrations, ligands for LC3/GABARAP proteins should be effective autophagy inhibitors, but at lower concentrations they could also be used as components of targeted degrader compounds. Such degrader compounds have been termed autophagy-targeted chimeras (AUTACs) or autophagosome-tethering chimeras (ATTECs), among other terms. These compounds tether proteins or cellular components of interest to the autophagosome, leading to the degradation of the liganded protein, organelle, or cellular component.<sup>17–29</sup>

GW5074 (Fig. 1, hereafter called compound 1) was one of the earliest small molecules reported to bind LC3B, the most well-studied LC3/GABARAP protein. It was discovered in 2019 by Li and coworkers as a compound that induced degradation of aggregated 72Q-huntingtin.<sup>19</sup> Since that report, 1 has been used for several applications. For example, in 2021, Li and coworkers attached 1 to a lipid droplet-binding compound to produce a chimeric compound that degraded lipid droplets.<sup>20</sup> Also in 2021, Fu et. al attached 1 to the BRD4 ligand JQ1,

bioRxiv preprint doi: <https://doi.org/10.1101/2024.02.25.581879>; this version posted February 25, 2024. The copyright holder for this preprint (which was not certified by peer review) is the author/funder, who has granted bioRxiv a license to display the preprint in perpetuity. It is made available under aCC-BY-NC-ND 4.0 International license.

producing a chimeric compound that degraded BRD4.<sup>17</sup> More recently, Gu and coworkers reported an ATTEC that incorporated **1** to degrade the protein PCSK9 as a potential atherosclerosis therapy.<sup>22</sup> Similarly, Dong and coworkers recently described an ATTEC using **1** to degrade PDE $\delta$ , an emerging target for pancreatic cancer therapy.<sup>29</sup>

These findings suggested that **1** could be used in selective and modular fashion to bind LC3/GABARAP proteins and induce the degradation of other proteins and cellular components via autophagy. However, other work has questioned the mechanism of degradation for ATTECs incorporating **1**. Recent findings by Winter, Waldmann, and coworkers found that **1** is a selective, covalent ligand of the E3 ligase DCAF11.<sup>30</sup> They further showed that its ability to direct targeted protein degradation is dependent on the proteasome and not lysosomal function, consistent with DCAF11 engagement in cells. Similarly, a recent preprint by Hong, Wang, Tian, Li, and coworkers found that a heterobifunctional molecule of JQ1 and a **1** derivative degraded BRD4 through recruitment of the E3 complex CRL4 which contains DCAF11.<sup>31</sup> Thus, degradation by chimeric compounds incorporating **1** may not occur via an autophagy-dependent mechanism. Notably, while the report from Winter, Waldmann, and coworkers tested many analogs of **1** for DCAF11 engagement, none were tested for LC3/GABARAP binding.

Compound **1** was derived from a screen of known bioactive compounds and it has not undergone any reported optimization or structure-activity relationship studies for LC3/GABARAP binding. This lack of information contributes to the questions surrounding the ability of **1** to bind LC3/GABARAP proteins. Even the published data on **1** binding to LC3/GABARAP proteins have been contradictory (Fig. 1). The binding affinity of **1** for recombinant LC3B was reported in different papers as 0.468  $\mu$ M (measured by small molecule microarray with a scanning oblique-incidence reflectivity difference microscope),<sup>19</sup> 8.9  $\mu$ M (measured by surface plasmon resonance),<sup>17</sup> and greater than 200  $\mu$ M (measured by 2D-NMR titration).<sup>32</sup> Overall, these contradictory findings called into question the actual binding affinity of **1** for LC3B and other family members. A recent report by Knapp, Rogov, and coworkers more directly addressed this question using competition fluorescence polarization, NMR titration, and NanoBRET assays. They found that **1** binds weakly to GABARAP-L2 and has weak, if any, binding to LC3B.<sup>32</sup> In that work, the authors suggested that these activities were too weak to account for the compound's ability to mediate targeted degradation.

Concurrently with these more recent studies, we took up the question of whether **1** binds to recombinant LC3B and GABARAP and whether it inhibits their interactions with representative ligands derived from native binding partners. We also sought to uncover structure-activity relationships for these inhibitory activities. We began by developing more reliable binding assays for recombinantly expressed LC3B and GABARAP. We first tried to test **1** in competitive fluorescence polarization assays that were previously developed in the Kritzer lab.<sup>33</sup> However, the compounds had background fluorescence which interfered with the assay. As a convenient alternative to biolayer interferometry assays developed by us and others,<sup>33–35</sup> we developed a solution-phase competition assay using AlphaScreen. The AlphaScreen assay (Fig. 2) reports on the inhibitor's ability to block binding of known

peptide ligands of LC3B or GABARAP which bind in the canonical protein-protein interaction site responsible for these proteins' functions. For GABARAP, the ligand was biotin-labeled K1 peptide, which has a  $K_d$  of  $55 \pm 8$  nM as measured by biolayer interferometry.<sup>34,36</sup> For LC3B, the ligand was a modified, biotin-labeled FYCO1 peptide, FYCO1S which has a  $K_d$  of  $330 \pm 30$  nM as measured by biolayer interferometry.<sup>33</sup> Using untagged versions of these tracer peptides as positive controls, we measured dose dependent inhibition in AlphaScreen with IC<sub>50</sub> values of  $55 \pm 3$  nM for K1 binding to GABARAP and inhibiting its interaction with biotinylated K1, and  $56 \pm 4$  nM for FYCO1S binding to LC3B and inhibiting its interaction with biotinylated FYCO1S. These controls demonstrate that this assay measures the dose-dependent inhibition of the protein-peptide interactions relevant for LC3/GABARAP functions in autophagy. These new assays are similar to the AlphaScreen assay reported in 2021 by Proschak and coworkers, who measured the disruption of binding between GST-LC3B and biotin-LIRtide, a short peptide derived from LC3-Interacting Region (LIR) of p62.<sup>37</sup>

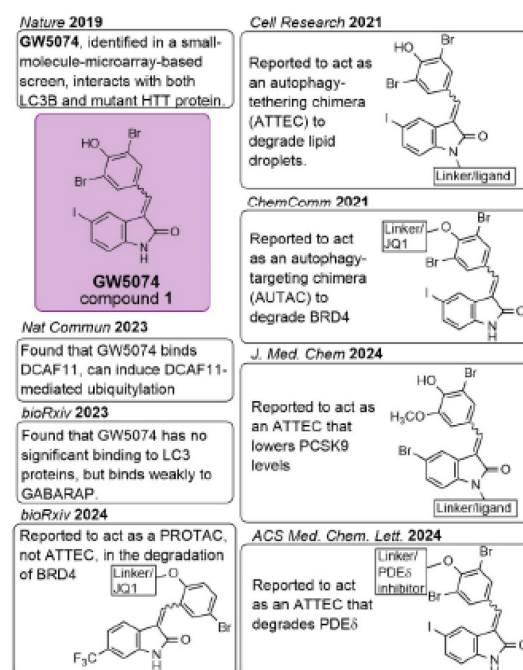


**Figure 1.** Summary of findings related to compound **1**, also known as GW5074, in prior literature. Most arylidene-indolinones analogous to compound **1** are interconverting diastereomers with respect to the double bond in the arylidene.



bioRxiv preprint doi: <https://doi.org/10.1101/2024.02.25.581879>; this version posted February 25, 2024. The copyright holder for this preprint (which was not certified by peer review) is the author/funder, who has granted bioRxiv a license to display the preprint in perpetuity. It is made available under aCC-BY-NC-ND 4.0 International license.

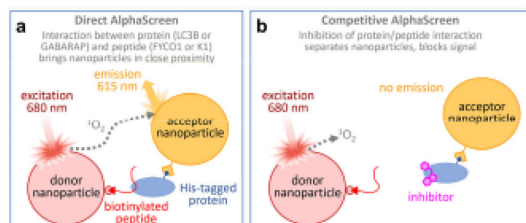
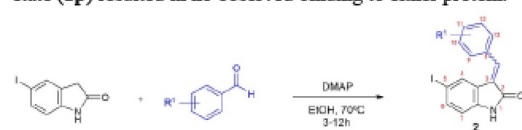


**Figure 2.** Newly developed AlphaScreen assays. One assay was used to measure inhibitory potency for inhibition of LC3B binding to the dye-labeled peptide ligand FYCO1S, and a similar assay was used to measure inhibitory potency for inhibition of GABARAP binding to the dye-labeled peptide ligand K1. Peptide ligands were immobilized on streptavidin-functionalized donor beads and recombinant LC3B or GABARAP was immobilized on Ni-NTA-functionalized acceptor beads. Additional assay details provided in Supporting Information.

Using the AlphaScreen assays, we measured the  $IC_{50}$  of **1** at  $4.75 \mu\text{M}$  for GABARAP and  $4.52 \mu\text{M}$  for LC3B. These results encouraged us to develop structure-activity relationships by altering one functional group at a time on **1** (Fig. 3). Commercially available oxindoles and aldehydes readily underwent an aldol condensation in the presence of a base and ethanol, allowing us to produce a library of 38 analogs in total. Considering alterations of the arylidene portion of **1**, we observed that removal of all functional groups from the arylidene resulted in complete loss of binding to both proteins (**2a**). Removal of just the phenolic hydroxyl group at C11 (**2b**) resulted in similar binding to GABARAP but five-fold poorer binding to LC3B. By contrast, removing the bromo groups at C10 and C12 while retaining the hydroxyl group at C11 (**2c**) resulted in only mild decrease in binding to LC3B, but nearly 10-fold poorer binding to GABARAP. Methylation of the phenolic hydroxyl group (**2d**) resulted in complete loss of binding to both proteins. Retaining one bromo group *ortho* to the hydroxy (**2e**) resulted in a decrease in binding to both proteins while moving the hydroxy group to the C9/C13 position (**2f**) resulted in decreased binding to GABARAP but comparable binding to LC3B compared to **1**.

Another series of compounds explored substitutions on the oxindole portion of **1** (Fig. 4). Methylation of the amide (**2g**) led to a loss of detectable binding to both proteins. Removal of iodine from oxindole position C5 (**2h**) also led to a loss of detectable binding to both proteins. Movement of the iodine from the C5 to the C6 position of the oxindole (**2i**) resulted in a slight decrease in binding to LC3B, but roughly 3-fold poorer binding to GABARAP. Replacement of iodine with fluorine at C6 (**2j**) resulted in complete loss of binding to both proteins, while replacement with a methyl group at C6 (**2k**) decreased binding to LC3B but increased binding to GABARAP relative to iodine at this position (**2i**). Moving the substituent back to the C5 position on the oxindole, replacement of the iodine with bromine (**2l**) resulted in slightly decreased binding to both proteins, while replacement with a tri-fluoromethyl group (**2m**) resulted in no detectable binding to either protein. A methyl group at the C5 position (**2n**) also resulted in slight decreases in binding to GABARAP and LC3B. Substituting a chlorine at C6 and a choroethyl at C5 position (**2o**) also resulted in a slight decrease in binding to both

proteins relative to **1**. Replacement at the C6 with a methyl acetate (**2p**) resulted in no observed binding to either protein.



	$IC_{50}$ ( $\mu\text{M}$ )			$IC_{50}$ ( $\mu\text{M}$ )	
	GABARAP	LC3B		GABARAP	LC3B
<b>1</b>	$4.75 \pm 0.83$	$4.52 \pm 1.7$	<b>2c</b>	$34.6 \pm 3.9$	$8.33 \pm 0.29$
<b>2a</b>	> 100	> 100	<b>2d</b>	> 100	> 100
<b>2b</b>	$4.96 \pm 0.93$	$23.1 \pm 1.1$	<b>2e</b>	$18.3 \pm 1.0$	$22.9 \pm 2.3$
			<b>2f</b>	$23.3 \pm 1.1$	$5.60 \pm 0.31$

**Figure 3.** Series 1, exploring alterations to the arylidene portion of compound **1**. Complete compound characterization and assay data are provided in Supporting Information.

	$IC_{50}$ ( $\mu\text{M}$ )			$IC_{50}$ ( $\mu\text{M}$ )	
	GABARAP	LC3B		GABARAP	LC3B
<b>1</b>	$4.75 \pm 0.83$	$4.52 \pm 1.7$	<b>2k</b>	$11.0 \pm 0.83$	$23.1 \pm 2.6$
<b>2g</b>	> 100	> 100	<b>2l</b>	$7.66 \pm 1.4$	$15.0 \pm 1.5$
<b>2h</b>	> 100	> 100	<b>2m</b>	> 100	> 100
<b>2i</b>	$15.8 \pm 2.3$	$8.19 \pm 1.0$	<b>2n</b>	$8.87 \pm 1.2$	$11.8 \pm 0.27$
<b>2j</b>	> 100	> 100	<b>2o</b>	$8.00 \pm 0.40$	$9.70 \pm 1.0$
			<b>2p</b>	> 100	> 100

**Figure 4.** Series 2, exploring alterations to the oxindole portion of compound **1**.

After acquiring these initial structure-activity relationships, we next sought to alter the scaffold of **1** starting with substituting the arylidene with various heterocycles (Fig. 5). Replacement of the phenyl group with a benzofuran (**2q**) or pyrrole (**2s**) resulted in no binding for either protein. However, replacement of the phenyl group with a *para*-trifluoro-biphenyl (**2r**), imidazole (**2t**), oxazole (**2u**), or a thiazole (**2v**) resulted in decreased binding relative to **1**, but still measurable binding to both proteins. Shifting the position of the nitrogen within the

bioRxiv preprint doi: <https://doi.org/10.1101/2024.02.25.581879>; this version posted February 25, 2024. The copyright holder for this preprint (which was not certified by peer review) is the author/funder, who has granted bioRxiv a license to display the preprint in perpetuity. It is made available under aCC-BY-NC-ND 4.0 International license.

thiazole ring (**2w**) resulted in a slight decrease in binding to GABARAP, but a large decrease in binding to LC3B relative to **2v**. Adding a methyl to the C4 position of the thiazole (**2x**) resulted in an improved binding to GABARAP and LC3 relative to the thiazole without the methyl group (**2x**), potencies similar to the oxazole (**2u**).

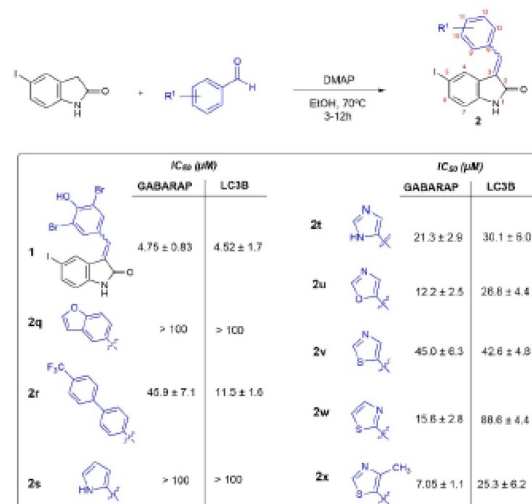


**Figure 5.** Series 3, exploring substitutions of heterocycles within the arylidene group.

The selectivity determinants of peptide and protein binding to LC3B and GABARAP have been extensively explored,<sup>33–35,38–41</sup> but few studies have explored selectivity of small molecule binding.<sup>32,37,42</sup> Compound **1** has similar apparent affinity for both proteins, but several analogs had selectivity for either LC3B or GABARAP (Fig. 6).

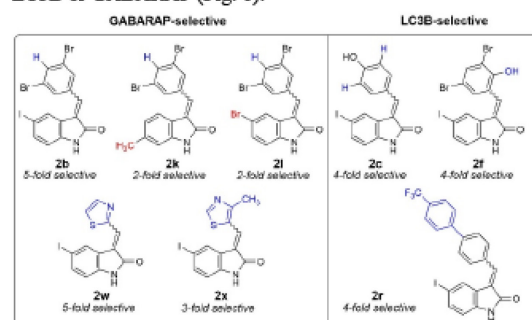


**Figure 6.** Summary of compounds with selectivity for GABARAP over LC3B, or selectivity for LC3B over GABARAP.

In recent findings, Winter, Waldmann, and coworkers demonstrated that **1** covalently reacts with the E3 ligase DCAF11.<sup>30</sup> Saturation of the arylidene double bond was shown to prevent reaction with DCAF11, consistent with a cysteine of DCAF11 reacting with the Michael acceptor on **1**. Guided by this SAR for DCAF11, we produced saturated versions of selected analogs to explore whether they would still bind LC3B or GABARAP. Saturation was achieved via reduction with

sodium borohydride (Fig. 7). Unfortunately, binding was diminished for all compounds after saturation with only a few still exhibiting any detectable binding (Fig. 7). Compounds **3a** and **3c** showed relatively similar, weak IC<sub>50</sub> values for both GABARAP (46.7 and 49.8 μM, respectively) and LC3B (28.9 and 34.8 μM, respectively). Weak binding was detected for both proteins for the saturated *para*-hydroxyl analog as well (**3b**). Very weak binding was detected for LC3B for the C4 methyl-thiazole (**3e**) but no binding was detected for GABARAP. Binding was lost to both proteins when the nitrogen position was moved within the thiazole (**3d**) and when *para*-trifluoro-biphenyl was substituted (**3f**) within the saturated scaffold.

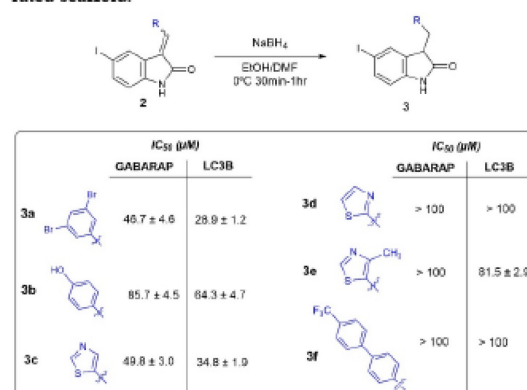


**Figure 7.** Series 4, selected compounds with a saturated arylidene.

To rule out an entirely nonspecific mode of action, we also tested selected analogs in an orthogonal assay for inhibition of beta-lactamase activity. If the mode of inhibition for LC3/GABARAP proteins was nonspecific, for instance via colloidal aggregation of the compounds leading to protein denaturation,<sup>43,44</sup> we would expect to see inhibition of an unrelated protein at similar concentrations. We observed no effect on beta-lactamase activity for compounds **1**, **2b**, and **3a** at concentrations up to 25 μM (Fig. S1). These results, along with the differential selectivity for LC3B versus GABARAP among different analogs (Fig. 6) and the SAR gathered to date (Fig. 8), provide additional evidence that these compounds inhibit LC3/GABARAP via selective binding to the LIR-domain-binding pocket.

bioRxiv preprint doi: <https://doi.org/10.1101/2024.02.25.581879>; this version posted February 25, 2024. The copyright holder for this preprint (which was not certified by peer review) is the author/funder, who has granted bioRxiv a license to display the preprint in perpetuity. It is made available under aCC-BY-NC-ND 4.0 International license.

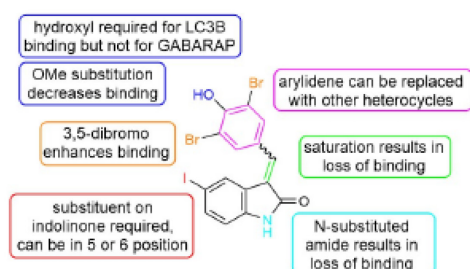


**Figure 8.** Summary of Structure-Activity Relationships of **1**.

To date, all compounds using **1** for targeted protein degradation (AUTACs and ATTECs) have attached a linker either to the C11 hydroxyl<sup>17,29</sup> or the oxindole amide,<sup>20,22</sup> suggesting that LC3/GABARAP binding is relatively insensitive to modifications at these positions. Additionally, **1** was first discovered to bind LC3B in a microarray in which it was linked to the array by the C11 hydroxyl.<sup>19</sup> These prior results contrast to our present work, which finds that methylation of the C11 hydroxyl (**2d**) results in loss of binding to both LC3B and GABARAP, removing the C11 hydroxyl (**2b**) results in loss of binding to LC3B but not GABARAP, and that N-methylating the amide amide on the oxindole (**2h**) results in a loss of binding to both proteins. No other group has directly reported on the effect of these conservative substitutions on the binding of **1** to LC3/GABARAP proteins. Within the context of a heterobifunctional ATTEC, it is clear from previous reports that the linker affects LC3/GABARAP binding. For example, Wang, Ouyang, and coworkers measured **1** binding LC3B with a  $K_d$  of 8.9  $\mu\text{M}$ , but when attached to JQ1 by linkers of various lengths and structures, binding to LC3B varied from 1.3  $\mu\text{M}$  to 73.2  $\mu\text{M}$ .<sup>17</sup> Similarly, Zhao, Guo, Gu, and coworkers found that changes in the linker structure within their PCSK9 ATTEC compounds resulted in an increase in binding to LC3B from 9.88  $\mu\text{M}$  to 5.69  $\mu\text{M}$ .<sup>22</sup> Given our results, it is possible that positive contributions to binding by the linker attached to the C11 hydroxyl or oxindole amide compensates for the decrease in binding to LC3/GABARAP proteins caused by substitution at these positions.

The binding site of compound **1** on GABARAP was investigated in more detail by titrating [ $^{15}\text{N}$ ] GABARAP with increasing amounts of **1** and monitoring GABARAP using 2D [ $^1\text{H}$ ,  $^{15}\text{N}$ ] HSQC NMR (Fig. 9a-b). Ligand binding led to sizeable chemical shift perturbations (CSPs), several of which (E8,

E17, E19, R22, K23, Y25, V29, V31, I32, V33, K48, Y49, L50, V51, S53, H70, F103, F104, Y106) systematically exceeded twice the root-mean-square CSP (Fig. 9a). Y49 was affected by strong line broadening in addition to a particularly large CSP. Mapping the chemical shift perturbations onto the molecular surface of GABARAP clearly shows that **1** binds to the N-terminal hydrophobic pocket of the two-pocket LIR binding site (Fig. 9c). This hydrophobic pocket, commonly referred to as HP1, is where aromatic residues from peptide ligands bind. This finding makes sense since the scaffold of **1** is made up of two aromatic ring systems. Also, this binding site may explain our SAR that the double bond of the arylidene must be unsaturated for low-micromolar binding, if both unsaturated rings must be coplanar to fit in the pocket. Given that residues lining HP1 are highly conserved across LC3/GABARAP subfamily members,<sup>40</sup> the binding of **1** in this pocket is consistent with the mild selectivity for LC3B or GABARAP found for the majority of compounds tested (Fig. 6).

Despite the growing interest in autophagy inhibitors for cancer therapy and for autophagy-mediated degradation, few small molecules with potent and selective LC3/GABARAP binding have been reported. Here, we further investigated the structure-activity relationships of compound **1** against both LC3B and GABARAP. The best compounds have low micromolar  $\text{IC}_{50}$  values for inhibiting the interactions of these proteins with known peptide ligands. Because LC3/GABARAP proteins are highly conserved and expressed in every tissue at moderate to high levels,<sup>45–47</sup> we anticipate that these compounds are likely not potent enough to make good candidates for autophagy inhibitors. Still, at micromolar potency they would be usable for autophagy-mediated targeted protein degradation if not for the reported off-target covalent binding of DCAF11, which was not directly explored in this work. While the double bond of the arylidene was required for low micromolar affinity for LC3B and GABARAP, the mechanism for the LC3B/GABARAP binding is unlikely to be covalent because these proteins lack cysteines. Instead, we infer that the planarity or other feature of the double bond is likely required for higher-affinity binding within the established binding pocket HP1. Overall, the structure-activity relationships uncovered here suggest that the LC3/GABARAP binding may yet be separable from the Michael acceptor, either by substituting the Michael acceptor with a planar isostere or by scaffold hopping to remove the Michael acceptor.



bioRxiv preprint doi: <https://doi.org/10.1101/2024.02.25.581879>; this version posted February 25, 2024. The copyright holder for this preprint (which was not certified by peer review) is the author/funder, who has granted bioRxiv a license to display the preprint in perpetuity. It is made available under aCC-BY-NC-ND 4.0 International license.

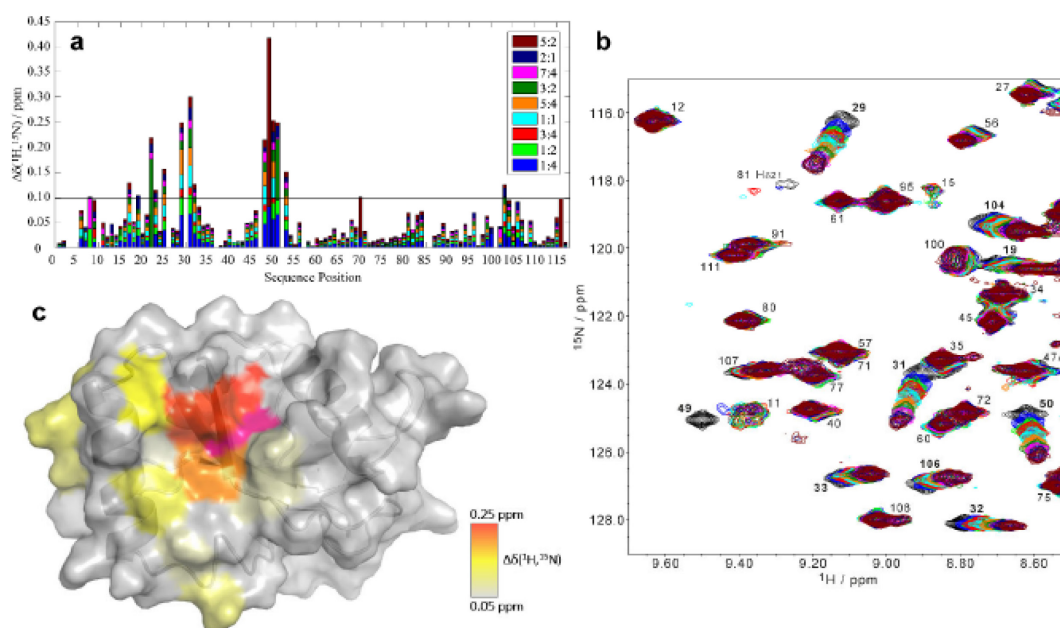


**Figure 9.** Titration of GABARAP with compound **1** as monitored by NMR spectroscopy. a) Chemical shift perturbations (CSP) for backbone amide resonances of GABARAP incubated with the indicated stoichiometric ratios of **1**:GABARAP. The horizontal line indicates the position of twice the root-mean-square CSP variation (0.0972 ppm at 5:2 excess of **1**). b) Section of the  $[^1\text{H}, ^{15}\text{N}]$  HSQC showing chemical shift perturbations with increasing concentrations of **1**. Spectra are color-coded to match the ratios shown in panel a, and the spectrum for GABARAP in the absence of **1** is shown in black. c) Molecular surface of GABARAP (PDB 1KOT)<sup>48</sup> with the residues with CSPs observed at 5:2 **1**:GABARAP shown in color. Y49, which is affected by strong line broadening in addition to a particularly large CSP, is highlighted in magenta.

Overall, we provide definitive evidence that **1** binds LC3B and GABARAP and inhibits their interactions with peptide ligands. We also provide the first structure-activity relationships which provide some insight into the selective recognition of LC3B and GABARAP by these compounds. Despite the ongoing controversy surrounding these compounds, our work suggests that compounds with similar scaffolds or similar pharmacophores could be viable LC3/GABARAP ligands for applications in cancer chemotherapy and targeted degradation of proteins, organelles, and protein aggregates. The similarity of compound **1**-induced CSP patterns observed for GABARAPL2 (ref. 32) and GABARAP (this study) attests to the high conservation of the core LIR docking site and to the challenges of devising small-molecule ligands targeting individual family members. More broadly, this work adds to the growing evidence that these protein-protein interactions are highly likely to be druggable using orally bioavailable small molecules.

## ASSOCIATED CONTENT

### Supporting Information

The Supporting Information is available free of charge on the ACS Publications website.

Full experimental details, full compound characterization, complete binding assay data, and additional supporting data, PDF

## AUTHOR INFORMATION

### Corresponding Author

\* Joshua A. Kritzer, Department of Chemistry, Tufts University, Medford Massachusetts 02155, United States  
<https://orcid.org/0000-0003-2878-6781>  
 Email: [joshua.kritzer@tufts.edu](mailto:joshua.kritzer@tufts.edu)

### Authors

Alexandria N. Leveille – Department of Chemistry, Tufts University, Medford Massachusetts 02155, United States, <https://orcid.org/0000-0002-0534-4828>  
 Hawley Brown - Department of Chemistry, Tufts University, Medford Massachusetts 02155, United States  
 Joaet Plasencia - Department of Chemistry, Tufts University, Medford Massachusetts 02155, United States  
 Thomas Schwarzrock - Department of Chemistry, Tufts University, Medford Massachusetts 02155, United States  
 Bennett True - Department of Chemistry, Tufts University, Medford Massachusetts 02155, United States  
 Philipp Neudecker - Institut für Biologische Informationsprozesse, Forschungszentrum Jülich, Jülich, Germany



bioRxiv preprint doi: <https://doi.org/10.1101/2024.02.25.581879>; this version posted February 25, 2024. The copyright holder for this preprint (which was not certified by peer review) is the author/funder, who has granted bioRxiv a license to display the preprint in perpetuity. It is made available under aCC-BY-NC-ND 4.0 International license.

52425. <https://orcid.org/0000-0002-0557-966X>

Alina Üffing - Institut für Biologische Informationsprozesse, Forschungszentrum Jülich, Jülich, Germany 52425

Oliver H. Weiergraber - Institut für Biologische Informationsprozesse, Forschungszentrum Jülich, Jülich, Germany 52425

Dieter Willbold - Institut für Biologische Informationsprozesse, Forschungszentrum Jülich, Jülich, Germany 52425

#### Author Contributions

A. L., H. B., and J.A.K. designed experiments. A.L., J.P., T.S., and B.T. prepared and characterized compounds. A. L. and H. B. measured binding affinities. P.N., A.Ü., O. H. W. and D. W. produced and interpreted NMR data and wrote the summary of the NMR results. A.L., H.B., and J.A.K. wrote the rest of the manuscript.

#### Funding Sources

This work was funded by NIH GM148407 to J.A.K., and the Deutsche Forschungsgemeinschaft (DFG, German Research Foundation)–Project-ID 267205415–SFB 1208, project B02 (D.W.)

#### ACKNOWLEDGMENT

The authors acknowledge access to the Jülich-Düsseldorf Biomolecular NMR Center.

#### ABBREVIATIONS

SPR, surface plasmon resonance; DMAP, 4-dimethylaminopyridine; EtOH, ethanol; NaBH<sub>4</sub>, sodium borohydride; DMF, dimethylformamide; LIR, LC3-interacting region.

#### REFERENCES

- Yamamoto K, Venida A, Yano J, et al. Autophagy promotes immune evasion of pancreatic cancer by degrading MHC-I. *Nature*. 2020;581(7806):100-105. doi:10.1038/s41586-020-2229-5
- Poillet-Perez L, Sharp DW, Yang Y, et al. Autophagy promotes growth of tumors with high mutational burden by inhibiting a T-cell immune response. *Nat Cancer*. 2020;1(9):923-934. doi:10.1038/s43018-020-00110-7
- White E, Lattime EC, Guo JY. Autophagy Regulates Stress Responses, Metabolism, and Anticancer Immunity. *Trends in Cancer*. 2021;7(8):778-789. doi:10.1016/j.trecan.2021.05.003
- Marsh T, Tolani B, Debnath J. The pleiotropic functions of autophagy in metastasis. *Journal of Cell Science*. 2021;134(2):jcs247056. doi:10.1242/jcs.247056
- Debnath J, Gammoh N, Ryan KM. Autophagy and autophagy-related pathways in cancer. *Nat Rev Mol Cell Biol*. Published online March 2, 2023:1-16. doi:10.1038/s41580-023-00585-z
- Gąsioriewicz BM, Koczurkiewicz-Adamczyk P, Piska K, Pękala E. Autophagy modulating agents as chemosensitizers for cisplatin therapy in cancer. *Invest New Drugs*. 2021;39(2):538-563. doi:10.1007/s10637-020-01032-y
- Lin JF, Lin YC, Tsai TF, Chen HE, Chou KY, Hwang TIS. Cisplatin induces protective autophagy through activation of BECN1 in human bladder cancer cells. *Drug Des Devel Ther*. 2017;11:1517-1533. doi:10.2147/DDDT.S126464
- Wang J, Wu GS. Role of Autophagy in Cisplatin Resistance in Ovarian Cancer Cells \*. *Journal of Biological Chemistry*. 2014;289(24):17163-17173. doi:10.1074/jbc.M114.558288
- Kocak M, Ezazi Erdi S, Jorba G, et al. Targeting autophagy in disease: established and new strategies. *Autophagy*. 2022;18(3):473-495. doi:10.1080/15548627.2021.1936359
- Leung LSB, Neal JW, Wakelee HA, Sequist LV, Marmor MF. Rapid Onset of Retinal Toxicity From High-Dose Hydroxychloroquine Given for Cancer Therapy. *American Journal of Ophthalmology*. 2015;160(4):799-805.e1. doi:10.1016/j.ajo.2015.07.012
- Mauthe M, Orhon I, Rocchi C, et al. Chloroquine inhibits autophagic flux by decreasing autophagosome-lysosome fusion. *Autophagy*. 2018;14(8):1435-1455. doi:10.1080/15548627.2018.1474314
- Nguyen TN, Lazarou M. A unifying model for the role of the ATG8 system in autophagy. *Journal of Cell Science*. 2022;135(11):jcs258997. doi:10.1242/jcs.258997
- Nguyen TN, Padman BS, Usher J, Oorschot V, Ramm G, Lazarou M. Atg8 family LC3/GABARAP proteins are crucial for autophagosome-lysosome fusion but not autophagosome formation during PINK1/Parkin mitophagy and starvation. *J Cell Biol*. 2016;215(6):857-874. doi:10.1083/jcb.201607039
- Maruyama Y, Sou YS, Kageyama S, et al. LC3B is indispensable for selective autophagy of p62 but not basal autophagy. *Biochemical and Biophysical Research Communications*. 2014;446(1):309-315. doi:10.1016/j.bbrc.2014.02.093
- Weidberg H, Shvets E, Shpilka T, Shimron F, Shinder V, Elazar Z. LC3 and GATE-16/GABARAP subfamilies are both essential yet act differently in autophagosome biogenesis. *EMBO J*. 2010;29(11):1792-1802. doi:10.1038/emboj.2010.74
- Bozic M, van den Bekerom L, Milne BA, et al. A conserved ATG2-GABARAP family interaction is critical for phagophore formation. *EMBO reports*. 2020;21(3):e48412. doi:10.15252/embr.201948412
- Pei J, Pan X, Wang A, et al. Developing potent LC3-targeting AUTAC tools for protein degradation with selective autophagy. *Chem Commun*. 2021;57(97):13194-13197. doi:10.1039/D1CC04661F

bioRxiv preprint doi: <https://doi.org/10.1101/2024.02.25.581879>; this version posted February 25, 2024. The copyright holder for this preprint (which was not certified by peer review) is the author/funder, who has granted bioRxiv a license to display the preprint in perpetuity. It is made available under aCC-BY-NC-ND 4.0 International license.

18. Takahashi D, Moriyama J, Nakamura T, et al. AUTACs: Cargo-Specific Degraders Using Selective Autophagy. *Molecular Cell*. 2019;76(5):797-810.e10. doi:10.1016/j.molcel.2019.09.009
19. Li Z, Wang C, Wang Z, et al. Allele-selective lowering of mutant HTT protein by HTT-LC3 linker compounds. *Nature*. 2019;575(7781):203-209. doi:10.1038/s41586-019-1722-1
20. Fu Y, Chen N, Wang Z, Luo S, Ding Y, Lu B. Degradation of lipid droplets by chimeric autophagy-tethering compounds. *Cell Res*. 2021;31(9):965-979. doi:10.1038/s41422-021-00532-7
21. Liu Z, Qin G, Yang J, et al. Targeting mitochondrial degradation by chimeric autophagy-tethering compounds. *Chem Sci*. Published online September 26, 2023. doi:10.1039/D3SC03600F
22. Ouyang Z, Ma M, Zhang Z, et al. Targeted Degradation of PCSK9 In Vivo by Autophagy-Tethering Compounds. *J Med Chem*. Published online December 19, 2023. doi:10.1021/acs.jmedchem.3c01634
23. Tong Y, Zhu W, Chen J, Zhang W, Xu F, Pang J. Targeted Degradation of Alpha-Synuclein by Autophagosome-Anchoring Chimera Peptides. *J Med Chem*. 2023;66(17):12614-12628. doi:10.1021/acs.jmedchem.3c01303
24. Dong G, Wu Y, Cheng J, et al. Ispinesib as an Effective Warhead for the Design of Autophagosome-Tethering Chimeras: Discovery of Potent Degraders of Nicotinamide Phosphoribosyltransferase (NAMPT). *J Med Chem*. 2022;65(11):7619-7628. doi:10.1021/acs.jmedchem.1c02001
25. Zeng Y, Xiao J, Xu Y, et al. Degradation of Cyclin-Dependent Kinase 9/Cyclin T1 by Optimized Microtubule-Associated Protein 1 Light Chain 3 Beta-Recruiting Coumarin Analogs. *J Med Chem*. 2023;66(18):12877-12893. doi:10.1021/acs.jmedchem.3c00828
26. Zhang Y, Huang J, Liang Y, et al. Clearance of lipid droplets by chimeric autophagy-tethering compound ameliorates the age-related macular degeneration phenotype in mice lacking APOE. *Autophagy*. 2023;0(0):1-14. doi:10.1080/15548627.2023.2220540
27. Liu M, Liu Z, Qin G, Ren J, Qu X. Bioorthogonally Activatable Autophagy-Tethering Compounds for Aptamer-Guided Mitochondrial Degradation. *Nano Lett*. 2023;23(11):4965-4973. doi:10.1021/acs.nanolett.3c00798
28. Liao X, Qin G, Liu Z, Ren J, Qu X. Bioorthogonal Aptamer-ATTEC Conjugates for Degradation of Alpha-Synuclein via Autophagy-Lysosomal Pathway. *Small*. n/a(n/a):2306760. doi:10.1002/smll.202306760
29. Bao J, Chen Z, Li Y, et al. Discovery of Novel PDE5 Autophagic Degraders: A Case Study of Autophagy-Tethering Compound (ATTEC). *ACS Med Chem Lett*. 2024;15(1):29-35. doi:10.1021/acsmedchemlett.3c00161
30. Xue G, Xie J, Hinterndorfer M, et al. Discovery of a Drug-like, Natural Product-Inspired DCAF11 Ligand Chemotype. *Nat Commun*. 2023;14(1):7908. doi:10.1038/s41467-023-43657-6
31. Wang Y, Wei T, Zhao M, et al. Discovery of Alkynyl Oxindole as a Novel PROTAC Moiety for Targeted Protein Degradation via CRL4DCAF11 Recruitment. *Biochemistry*. 2024. doi:10.1101/2024.02.15.580430
32. Schwalm MP, Dopfer J, Kumar A, et al. Targeting LC3/GABARAP for degrader development and autophagy modulation. Published online October 5, 2023. doi:10.1101/2023.10.05.560930
33. Cerulli RA, Shehaj L, Brown H, Pace J, Mei Y, Kritzer JA. Stapled Peptide Inhibitors of Autophagy Adapter LC3B. *ChemBioChem*. 2020;21(19):2777-2785. doi:10.1002/cbic.202000212
34. Brown H, Chung M, Üffing A, et al. Structure-Based Design of Stapled Peptides That Bind GABARAP and Inhibit Autophagy. *J Am Chem Soc*. 2022;144(32):14687-14697. doi:10.1021/jacs.2c04699
35. Wirth M, Zhang W, Razi M, et al. Molecular determinants regulating selective binding of autophagy adapters and receptors to ATG8 proteins. *Nature Communications*. 2019;10(1):2055. doi:10.1038/s41467-019-10059-6
36. Weiergräber OH, Stangler T, Thielmann Y, Mohrlüder J, Wiesehan K, Willbold D. Ligand Binding Mode of GABAA Receptor-Associated Protein. *Journal of Molecular Biology*. 2008;381(5):1320-1331. doi:10.1016/j.jmb.2008.06.086
37. Hartmann M, Huber J, Kramer JS, et al. Demonstrating Ligandability of the LC3A and LC3B Adapter Interface. *J Med Chem*. 2021;64(7):3720-3746. doi:10.1021/acs.jmedchem.0c01564
38. Gray JP, Uddin MN, Chaudhari R, et al. Directed evolution of cyclic peptides for inhibition of autophagy. *Chem Sci*. 2021;12(10):3526-3543. doi:10.1039/D0SC03603J
39. Putyrski M, Vakhrusheva O, Bonn F, et al. Disrupting the LC3 Interaction Region (LIR) Binding of Selective Autophagy Receptors Sensitizes AML Cell Lines to Cytarabine. *Frontiers in Cell and Developmental Biology*. 2020;8. Accessed December 24, 2023. <https://www.frontiersin.org/articles/10.3389/fcell.2020.00208>
40. Jatana N, Ascher DB, Pires DEV, Gokhale RS, Thukral L. Human LC3 and GABARAP subfamily members achieve functional specificity via specific structural modulations.

bioRxiv preprint doi: <https://doi.org/10.1101/2024.02.25.581879>; this version posted February 25, 2024. The copyright holder for this preprint (which was not certified by peer review) is the author/funder, who has granted bioRxiv a license to display the preprint in perpetuity. It is made available under aCC-BY-NC-ND 4.0 International license.

- Autophagy*. 2020;16(2):239-255. doi:10.1080/15548627.2019.1606636
41. Li J, Zhu R, Chen K, et al. Potent and specific Atg8-targeting autophagy inhibitory peptides from giant ankyrins. *Nature Chemical Biology*. 2018;14(8):778. doi:10.1038/s41589-018-0082-8
  42. Fan S, Yue L, Wan W, et al. Inhibition of Autophagy by a Small Molecule through Covalent Modification of the LC3 Protein. *Angewandte Chemie International Edition*. 2021;60(50):26105-26114. doi:10.1002/anie.202109464
  43. McGovern SL, Caselli E, Grigorieff N, Shoichet BK. A common mechanism underlying promiscuous inhibitors from virtual and high-throughput screening. *Journal of Medicinal Chemistry*. 2002;45(8):1712-1722.
  44. Aldrich C, Bertozzi C, Georg GI, et al. The Ecstasy and Agony of Assay Interference Compounds. *J Med Chem*. 2017;60(6):2165-2168. doi:10.1021/acs.jmedchem.7b00229
  45. Uhlen M, Fagerberg L, Hallström BM, et al. Tissue-based map of the human proteome. *Science*. 2015;347(6220):1260419. doi:10.1126/science.1260419
  46. Tissue expression of MAP1LC3B - Summary - The Human Protein Atlas. Accessed February 13, 2024. <https://www.proteinatlas.org/ENSG00000140941-MAP1LC3B/tissue>
  47. Tissue expression of GABARAP - Summary - The Human Protein Atlas. Accessed February 13, 2024. <https://www.proteinatlas.org/ENSG00000170296-GABARAP/tissue>
  48. Stangler T, Mayr LM, Willbold D. Solution Structure of Human GABAA Receptor-associated Protein GABARAP: IMPLICATIONS FOR BIOLOGICAL FUNCTION AND ITS REGULATION \*. *Journal of Biological Chemistry*. 2002;277(16):13363-13366. doi:10.1074/jbc.C200050200



### 3.3. GABARAP interacts with EGFR — supporting the unique role of this hAtg8 protein during receptor trafficking

<b>Authors</b>	<b><u>Alina Üffing</u></b> , Oliver H. Weiergräber, Melanie Schwarten, Silke Hoffmann, Dieter Willbold
<b>Journal</b>	FEBS Letters
<b>Year of Publication</b>	2024
<b>DOI</b>	<a href="https://doi.org/10.1002/1873-3468.14997">doi.org/10.1002/1873-3468.14997</a>
<b>Impact Factor</b>	3.0 (2023)
<b>Contribution</b>	Project conceptualization, protein purification, BLI experiments, screening for crystallization conditions, diffraction data collection (remote at ESRF), data processing, structure refinement and validation, NMR (together with Melanie Schwarten), cellular assays, data analysis and curation, visualization, writing and editing of the manuscript.
<b>Reprint Permission</b>	This article is made available under a CC-BY 4.0 license ( <a href="https://creativecommons.org/licenses/by/4.0/">https://creativecommons.org/licenses/by/4.0/</a> )

Additional SI material (BLI experiment data) can be found here:

<https://febs.onlinelibrary.wiley.com/doi/10.1002/1873-3468.14997>



## RESEARCH LETTER

# GABARAP interacts with EGFR — supporting the unique role of this hAtg8 protein during receptor trafficking

Alina Üffing<sup>1,2</sup> , Oliver H. Weiergräber<sup>1,2</sup> , Melanie Schwarten<sup>2</sup> , Silke Hoffmann<sup>2</sup>  and Dieter Willbold<sup>1,2</sup> 

<sup>1</sup> Heinrich-Heine-Universität Düsseldorf, Mathematisch-Naturwissenschaftliche Fakultät, Institut für Physikalische Biologie, Düsseldorf, Germany

<sup>2</sup> Forschungszentrum Jülich, Institut für Biologische Informationsprozesse: Strukturbiochemie (IBI-7), Jülich, Germany

## Correspondence

S. Hoffmann, Forschungszentrum Jülich,  
 Institut für Biologische  
 Informationsprozesse: Strukturbiochemie  
 (IBI-7), 52425 Jülich, Germany  
 Tel: +49 2461/61-9389  
 E-mail: [s.hoffmann@fz-juelich.de](mailto:s.hoffmann@fz-juelich.de)  
 O. H. Weiergräber, Heinrich-Heine-  
 Universität Düsseldorf, Mathematisch-  
 Naturwissenschaftliche Fakultät, Institut für  
 Physikalische Biologie, 40225 Düsseldorf,  
 Germany  
 Tel: +49 2461/61-2028  
 E-mail: [o.h.weiergraeber@fz-juelich.de](mailto:o.h.weiergraeber@fz-juelich.de)

[Correction added on 19 August 2024, after first online publication: The title is corrected from 'The hAtg8 protein GABARAP interacts with EGFR and supports its unique role during receptor trafficking' to 'GABARAP interacts with EGFR — supporting the unique role of this hAtg8 protein during receptor trafficking' in this version.]

(Received 14 May 2024, revised 2 July 2024, accepted 24 July 2024)

doi:10.1002/1873-3468.14997

Edited by Christian Griesinger

The human Atg8 family member GABARAP is involved in numerous autophagy-related and -unrelated processes. We recently observed that specifically the deficiency of GABARAP enhances epidermal growth factor receptor (EGFR) degradation upon ligand stimulation. Here, we report on two putative LC3-interacting regions (LIRs) within EGFR, the first of which (LIR1) is selected as a GABARAP binding site *in silico*. Indeed, *in vitro* interaction studies reveal preferential binding of LIR1 to GABARAP and GABARAPL1. Our X-ray data demonstrate interaction of core LIR1 residues FLPV with both hydrophobic pockets of GABARAP suggesting canonical binding. Although LIR1 occupies the LIR docking site, GABARAP Y49 and L50 appear dispensable in this case. Our data support the hypothesis that GABARAP affects the fate of EGFR at least in part through direct binding.

**Keywords:** AlphaFold; canonical binding; complex structure; LC3-interacting region; NMR; paralog-specificity; surface receptor; X-ray

## Abbreviations

AF2, AlphaFold 2; AP2, adaptor protein complex 2; BLI, biolayer interferometry; CASM, conjugation of Atg8 to single membranes; CBL, E3 ubiquitin-protein ligase CBL; CD36, platelet glycoprotein 4; CSP, chemical shift perturbation; CTD, carboxy-terminal domain; DHHC20, palmitoyltransferase ZDHHC20; DVL2, segment polarity protein disheveled homolog DVL-2; EGF, epidermal growth factor; EGFR, epidermal growth factor receptor; GABA<sub>A</sub>R,  $\gamma$ -aminobutyric acid type A receptor; GABARAP,  $\gamma$ -aminobutyric acid type A receptor-associated protein; GABARAPL,  $\gamma$ -aminobutyric acid type A receptor-associated protein-like; GRB2, growth factor receptor-bound protein 2; GST, glutathione S-transferase; hAtg8, human autophagy-related protein 8; HSQC, heteronuclear single quantum coherence; LC3/MAP1LC3, microtubule-associated protein 1 light chain 3; LDELS, LC3-dependent extracellular vesicle loading and secretion; LDS, LIR docking site; LIR, LC3-interacting region; MAPK/ERK, mitogen-activated protein kinase/extracellular signal-regulated kinases; PCM1, pericentriolar material 1 protein; p66SHC, p66 isoform of Src homology 2 domain-containing transforming protein 1 (SHC1); PIK3C3/PS34, phosphatidylinositol 3-kinase catalytic subunit type 3; SCOC, short coiled-coil protein; SQSTM1, sequestosome-1; TLR4, toll-like receptor 4; TREM2, triggering receptor expressed on myeloid cells 2; ULK1, unc-51-like kinase 1.



The human autophagy-related protein 8 (hAtg8) family consists of seven members, which can be divided into the GABARAP (GABARAP, GABARAPL1 and GABARAPL2) and LC3 (LC3A, LC3B, LC3B2 and LC3C) subfamilies. They are ubiquitin-like modifiers which can be conjugated to membranes in a E1-E2-E3 like enzyme cascade [1–3]. In the past, hAtg8s have been most extensively studied for their role in the conserved catabolic process of macroautophagy, hereafter referred to as autophagy [4,5]. While they are involved during the different steps of autophagy, from phagophore formation and extension to cargo sequestration and fusion with the lysosome [6–9], it still remains to be elucidated whether and for which steps they are essential and where alternative mechanisms take place [10]. Additionally, conjugation of hAtg8 to single endolysosomal membranes (CASM) has been reported as a key function in a variety of processes related to inflammation, cancer, and neurodegeneration [11–14]. Differential binding of ATG16L1, a component of the E3-ligase complex for membrane conjugation of hAtg8s, appears to be decisive for whether conjugation occurs on single or double membranes [15]. Interestingly, CASM has been shown to be important for receptor recycling of TREM2, CD36, and TLR4 in the context of cellular uptake of amyloid  $\beta$  [16] as well as secretion of the transferrin receptor in a process called LC3-dependent extracellular vesicle loading and secretion (LDELS) [17]. The trafficking of the  $\gamma$ -aminobutyric acid type A (GABA<sub>A</sub>) receptor, the eponymous GABARAP binding partner, to the plasma membrane is another example of a non-conventional role of a hAtg8 [18,19]. In addition to membrane conjugation, the versatile functions of hAtg8 proteins are facilitated through interactions with a conserved LC3-interacting region (LIR) [20], with its core consisting of four amino acids ( $\Theta_0$ -X<sub>1</sub>-X<sub>2</sub>-I<sub>3</sub>) with  $\Theta$  being an aromatic residue (W/F/Y) and I an aliphatic residue (L/I/V). Both the residues of the core LIR as well as surrounding residues regulate selective binding to the GABARAP or LC3 subfamily proteins, with Unc-51-like kinase 1 (ULK1) being an example of a LIR-containing protein with high preference for GABARAP and GABARAPL1 (30-fold affinity compared to the LC3 subfamily proteins) [20,21]. Moreover, binding to hAtg8s can be altered towards higher or lower affinities by phosphorylation [22]. Phosphorylation of the Golgi protein SCOC increases its affinity for the LC3 subfamily [23], and OPTN phosphorylation and subsequent increase in affinity has been shown to be important for autophagic clearance of *Salmonella* [24]. In contrast, tyrosine phosphorylation of the  $\Theta_0$  residue of the mitophagy receptor FUNDC1 has been

reported to weaken its interaction with LC3 [25]. Recently, we observed enhanced degradation of the epidermal growth factor (EGF)-receptor (EGFR) in response to EGF stimulation in cells deficient in GABARAP but not its paralogs, which was accompanied by decreased MAPK/ERK signaling as well as altered target gene expression [26]. Consistently, continuous live-cell imaging revealed lower EGF-647 levels in Huh-7.5 GABARAP single knockout cells compared to Huh-7.5 wildtype cells over time (Fig. S1A). Owing to two putative LIRs present in the regulatory C-terminal domain of the EGFR, we sought to investigate this phenotype from a biophysical and structural perspective, analyzing the specific binding mode shaping this putative interaction.

## Materials and methods

### DNA constructs

Genes encoding proteins for purification were expressed from pGEX-4-T2 vectors previously described [27,28], which can be found at Addgene for GABARAP (#73948), GABARAPL1 (#73945), GABARAPL2 (#73518) and LC3A (#73946). pGEX-4-T2-LC3B was cloned by restriction-ligation using BamHI and NotI. Point mutations substituting Y49 and L50 to alanines were introduced by site-directed mutagenesis for GABARAP and GABARAPL1. All constructs encoded full-length (unprocessed) versions of human Atg8 proteins. EGFR LIR1<sub>1076–1099</sub> fused to GABARAP by a glycine-serine linker (hereafter only EGFR LIR1-GABARAP) was ordered as a codon-optimized, synthetic construct in pGEX-4-T2 from GeneArt (Thermo Fisher Scientific, GeneArt, Regensburg, Germany). Please note that our EGFR numbering refers to the full-length receptor including the signal peptide (first 24 aa).

### Protein expression and purification

GABARAP, GABARAP<sub>Y49A/L50A</sub>, GABARAPL1, GABARAPL1<sub>Y49A/L59A</sub>, GABARAPL2, LC3A, and LC3B used for biolayer interferometry (BLI) experiments were expressed and purified from *E. coli* BL21(DE3) transformed with respective pGEX-4-T2 plasmids as previously described [29]. In short, glutathione S-transferase (GST) fusion proteins were first purified from soluble extracts by affinity chromatography using Glutathione Sepharose 4B (GE Healthcare now Cytiva, Marlborough, MA, US). After cleavage of the GST tag with thrombin, further purification was carried out by size exclusion chromatography using either a Hiload 26/60 Superdex 75 or a Hiload Superdex 16/600 75 preparatory grade column, which were equilibrated with 25 mM Tris, 150 mM NaCl (pH 7.5) and 0.5 mM tris(2-carboxyethyl)phosphine (TCEP), if proteins contained



Cysteine, and eluted in the same buffer. GST-EGFR-LIR1-GABARAP protein for X-ray crystallography was purified analogously from *E. coli* BL21(DE3) transformed with pGEX-4-T2-EGFR LIR1-GABARAP grown in LB medium. Gene expression was induced with 1 mM isopropyl  $\beta$ -D-thiogalactopyranoside (IPTG) at an OD<sub>600nm</sub> of 0.7 and for 22 h at 25 °C. Afterwards, cells were harvested by centrifugation at 3000 *g* for 30 min at 4 °C and washed once with PBS. The GST fusion protein was purified from the soluble extract by affinity chromatography using Glutathione Sepharose 4B (GE Healthcare). The GST tag was cleaved off using thrombin, yielding a 145 aa EGFR LIR1-GABARAP fusion, which was further purified by size exclusion chromatography using a Hiload 26/60 Superdex 75 preparatory grade column equilibrated with 10 mM Tris-HCl, 150 mM sodium chloride, pH 7 and eluted in the same buffer. <sup>15</sup>N-GABARAP for Heteronuclear Single Quantum Coherence (HSQC)-titration experiments was purified from *E. coli* BL21(DE3) transformed with pGEX-4-T2-GABARAP grown in M9 minimal medium with 1 g·L<sup>-1</sup> <sup>15</sup>NH<sub>4</sub>Cl. Gene expression was induced with 1 mM IPTG at an OD<sub>600nm</sub> of 0.7 and for 20 h at 25 °C. Cells were harvested and <sup>15</sup>N-GST-GABARAP was purified by affinity chromatography as described above. After thrombin cleavage, <sup>15</sup>N-GABARAP was further purified by size exclusion chromatography using a Hiload 26/60 Superdex 75 preparatory grade column equilibrated with 25 mM NaH<sub>2</sub>PO<sub>4</sub>/Na<sub>2</sub>HPO<sub>4</sub>, 100 mM KCl, 100 mM NaCl, 50  $\mu$ M ethylenediaminetetraacetic acid (EDTA), pH 6.9 and eluted in the same buffer.

### Biolayer interferometry

BLI experiments were performed on an Octet Red 96 (FORTÉBIO) as previously described [26]. In short, peptides with N-terminal biotinylation were ordered from CASLO ( $\geq 95\%$  purity, Table S1) and immobilized on High Precision Streptavidin (SAX) biosensors (FORTÉBIO/Sartorius). Purified hAtg8 proteins were used as analyte in increasing concentrations (Data S1). For dissociation constant ( $K_D$ ) calculation, respective reference sensor response levels were subtracted and baselines aligned followed by steady-state evaluation by plotting the respective response levels against the applied protein concentration. Curves were fitted by non-linear regression according to the One-site binding model using GraphPad Prism version 9 for Windows (GraphPad Software, Boston, MA, USA). Only fitted  $K_D$  values corresponding to a saturation level of at least 0.25 nm and *R*-square above 0.985 are shown. Quality of each hAtg8 as an analyte was assessed by also determining its binding to the PCM1 LIR peptide, for which published reference data are available w.r.t. all hAtg8s [20]. Owing to the many different ligand-analyte combinations, we report the results of individual measurements, unless stated otherwise (refer to Data S1 related to Figs 1B,C, 4B, C, Fig. S1C).

### X-ray crystallography and data processing

EGFR LIR1-GABARAP in 10 mM Tris-HCl and 150 mM NaCl, pH 7, was concentrated to approximately 17 mg·mL<sup>-1</sup> using Vivaspin 20/2 centrifugal filter units (3 kDa cutoff). Crystallization was performed by the sitting-drop vapor diffusion method, using a Freedom Evo robotic device (Tecan) with commercially available screening sets and combining 0.5  $\mu$ L of protein solution and 0.5  $\mu$ L of reservoir solution for each drop. Several conditions yielded crystals. The crystal which was used for structure determination developed in 0.17 M ammonium acetate, 0.085 M sodium citrate, pH 5.6, 25.5% (w/v) PEG 4000 and 15% (v/v) glycerol. X-ray diffraction data was collected at 100 K on beamline ID30A-3/MASSIF-3 of the European Synchrotron Radiation Facility (ESRF; Grenoble, France; doi: 10.1515/ESRF-DC-1524662410). XDS and XSCALE [30] were used for data processing and reflections to a  $d_{\min}$  of 2.05 Å were included in the final dataset. The structure of GABARAP was determined by molecular replacement with MOLREP [31] using the structure of GABARAP from its K1 peptide complex (PDB ID: 3D32) as template. Coordinates of the EGFR LIR1 peptide were generated using COOT [32], and the model was improved by reciprocal-space refinement with phenix.refine [33] alternating with interactive rebuilding in COOT. According to validation using the wwPDB validation pipeline, the model features good geometry with no outliers in the Ramachandran plot and <1% of unusual side chain rotamers. Coordinates and structure factor amplitudes were deposited in the PDB ([www.ebi.ac.uk/pdbe](http://www.ebi.ac.uk/pdbe)) with accession number 8S1M (doi: 10.2210/pdb8S1M/pdb). For statistics of data collection and refinement, refer to Table S2. Figures were created using the PyMOL Molecular Graphics System, Version 3.0, Schrödinger, LLC.

### NMR titrations and data analysis

Titration of GABARAP with EGFR LIR1 and PCM1 LIR peptides spanning residues 1076–1099 and 1954–1968, respectively, were monitored by recording 2D [<sup>1</sup>H, <sup>15</sup>N] HSQC spectra at a temperature of 25.0 °C on a Bruker 900 MHz Avance Neo spectrometer equipped with a triple resonance <sup>1</sup>H, <sup>13</sup>C, <sup>15</sup>N TCI cryoprobe. <sup>15</sup>N-GABARAP was concentrated to 200  $\mu$ M in 25 mM NaH<sub>2</sub>PO<sub>4</sub>/Na<sub>2</sub>HPO<sub>4</sub>, 100 mM KCl, 100 mM NaCl, 50  $\mu$ M EDTA, and 5% (v/v) D<sub>2</sub>O. 2D [<sup>1</sup>H, <sup>15</sup>N] HSQC spectra were recorded after stepwise addition of peptide up to a two-fold molar excess. For chemical shift perturbation (CSP) analysis, <sup>1</sup>H chemical shift changes,  $\Delta\delta(^1\text{H})$ , and <sup>15</sup>N chemical shift changes,  $\Delta\delta(^{15}\text{N})$ , in units of ppm were combined according to the following equation:

$$\Delta\delta(^1\text{H}, ^{15}\text{N}) = \sqrt{(\Delta\delta(^1\text{H}))^2 + (0.2 \times \Delta\delta(^{15}\text{N}))^2}$$

For mapping on GABARAP (PDB ID: 1KOT), residues were colored according to  $\Delta\delta(^1\text{H}, ^{15}\text{N})$  values at two-fold

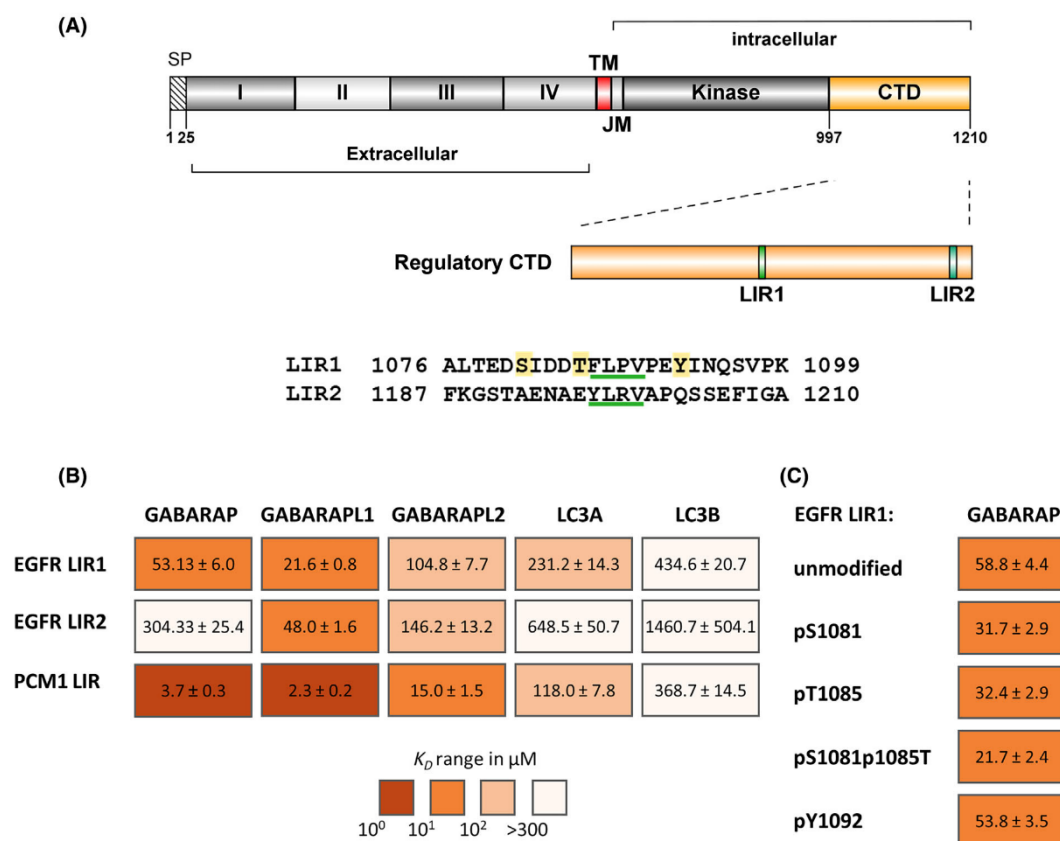


**Fig. 1.** EGFR LIR1 preferentially interacts with GABARAP/L1 with only moderate influence of phosphorylation (A) Schematic representation of the EGFR domain structure with LIR1 and LIR2 indicated in the C-terminal domain as well as the respective amino acid sequences. Core LIRs are underlined in green. For LIR1, phosphorylation sites investigated in (C) are shown in yellow. (B)  $K_D$  values [ $\mu$ M] of human Atg8 paralogs GABARAP, GABARAPL1, GABARAPL2, LC3A and LC3B with EGFR peptides. (C)  $K_D$  values [ $\mu$ M] of phosphorylated (p) EGFR LIR1 variants with GABARAP. Color scaled according to affinity as determined by biolayer interferometry.  $K_D$  values are shown with standard error calculated from non-linear regression. SP, signal peptide; TM, transmembrane; JM, juxtamembrane. EGFR was illustrated using IBS 2.0 [35].

molar excess using the PyMOL Molecular Graphics System, Version 3.0 Schrödinger, LLC (New York, NY, US).

## Results

### EGFR LIR1 preferentially interacts with GABARAP and GABARAPL1 with minor impact of phosphorylation

The previously reported enhanced EGFR degradation after EGF stimulation, specifically in GABARAP single knockout cells included a first hypothesis regarding a direct interaction between GABARAP and EGFR, including the observation of a putative extended LIR motif (positions 1086–1089) in the regulatory carboxy-

terminal domain (CTD) of EGFR [26]. Interestingly, the regulatory C-terminal domain (CTD) of EGFR, exogenously expressed as a fusion protein with green fluorescent protein (EGFR CTD-GFP) in HEK293 cells, can be enriched from whole cell lysates by purified GST-GABARAP (Fig. S1B). Moreover, by the iLIR prediction tool [34] another putative LIR motif located adjacent to the very end of the CTD is predicted (Fig. 1A). While the first putative core LIR comprises the amino acids FLPV, the second (position 1197 to 1200) consists of YLRV. Considering the EGFR sequences of different mammals, segments corresponding to LIR1 and LIR2 appear to range among the more conserved regions within the CTD, with frequently identical core sequences (Fig. S2); this suggests

that an activity of these regions is preserved during evolution, a fact that often applies to functional LIRs [36]. We next tested whether these two LIRs are also selected as GABARAP binding sites within EGFR CTD-derived sequences by the artificial intelligence-based structure prediction tool AlphaFold 2 (AF2)-multimer [37,38], which can predict binding sites of Atg8s with high accuracy especially in intrinsically disordered protein regions [36]. While we found FLPV-related binding in many of the resulting models, not a single model involved YLRV (Fig. S3A,B). In the following, we used synthetic peptides, representing residues 1076–1099 (LIR1) and 1190–1210 (LIR2) of EGFR for *in vitro* binding experiments with GABARAP applying biolayer interferometry (BLI, for peptide sequences refer to Table S1). To investigate whether the observed GABARAP-specific phenotype previously observed in HEK293 and Huh-7.5 cells might be mirrored by a direct and paralog-specific interaction, we included all paralogs with notable mRNA expression levels (cutoff: nTPM >10, for values and details refer to Table S3) in at least one of the two cell lines, these being GABARAP, GABARAPL1, GABARAPL2, LC3A, and LC3B, in our analysis. A peptide comprising the LIR motif (residues 1954–1968) of the well-described GABARAP interactor pericentriolar material 1 protein (PCM1) was included as control, with our  $K_D$  values largely matching those published [20]. When comparing LIR1 and LIR2 binding, a clear difference was found especially for GABARAP, with an about 6-fold higher affinity for LIR1 ( $K_D$  of  $54.7 \pm 3.6 \mu\text{M}$  (mean/SD from three independent experiments)) over LIR2, while for the other investigated paralogs affinity differences were more modest (about 1.4 to 3.4-fold higher for LIR1), with LIR2 binding usually still appearing weaker. Importantly, LIR1 showed a particular specificity for GABARAP and its closest relative, GABARAPL1, with approximately 2-fold (5-fold), 4-fold (11-fold), and 8-fold (20-fold) stronger binding of GABARAP (GABARAPL1) to LIR1 relative to the respective affinities obtained for the paralogs GABARAPL2, LC3A and LC3B. For both LIR peptides, the lowest affinities were measured for LC3B with 3-digit  $\mu\text{M}$  to mM  $K_D$  values (Fig. 1B). Interestingly, both LIR peptides contain phosphorylation sites, of which Y1092 and Y1197 have been extensively described for their role in EGFR signaling [39–44] while the roles of S1081 and T1085 remain more elusive [45–47]. Phosphorylation of either S1081 or T1085, both located upstream of the core LIR1, slightly enhanced GABARAP's affinity (~1.8-fold), while phosphorylation of both sites simultaneously enhanced its binding

to above two-fold change (2.7-fold, Fig. 1C). Our *in-vitro* interaction studies revealed virtually unchanged binding of EGFR LIR1 to GABARAP when phosphorylated at residue Y1092 located downstream of the core LIR1, which also applies for the paralogs (Fig. S4, top). Curiously, phosphorylation of  $\Theta_0$  residue Y1197 within the core (YLRV) of LIR2 did not show the expected detrimental effect on the interaction of LIR2 with GABARAP or with its paralogs (Fig. S4, bottom).

As GABARAPL1 exhibits by far lower expression levels than GABARAP ([www.proteinatlas.org](http://www.proteinatlas.org), v23; [48]) within the cell lines analyzed in Dobner (2020), our structural investigations focused on the interaction of EGFR LIR1 with GABARAP.

### X-ray complex structure reveals canonical binding of EGFR LIR1 to GABARAP

To further investigate the interaction mode between the putative LIR1 of the EGFR and GABARAP, a chimeric protein consisting of EGFR residues 1076–1099 fused to GABARAP (EGFR LIR1-GABARAP) was expressed, purified and used for crystallization. We were able to obtain crystals and determine the structure, resolving GABARAP together with residues 1082–1099 of the EGFR LIR1 peptide (Fig. 2A, Table S1), which were found to interact with the GABARAP moiety of a symmetry-equivalent molecule. While the two N-terminal helices and the ubiquitin-like core of GABARAP as well as the core LIR1 of EGFR (FLPV), which contacts the hydrophobic pockets of GABARAP, featured well defined electron density, EGFR residues surrounding the core LIR were less clearly defined. Together with elevated B factors obtained during refinement, this points towards enhanced dynamics of both segments flanking the core LIR (Fig. 2B). Consequently, the following structural analysis of the inter-molecular interface between GABARAP and EGFR LIR1 focusses on the core LIR. Residue F1086 of the EGFR, representing position  $\Theta_0$  of the core LIR motif, is inserted into hydrophobic pocket 1 (HP1), supported by hydrophobic interactions with residues I21, P30, L50, K48 and F104 of GABARAP. The side chain of core LIR residue X<sub>1</sub> (L1087) is within van der Waals distance of Y49 and K46, possibly involved in hydrophobic interactions, as well as R67. Additionally, the amide nitrogen and carbonyl oxygen of EGFR L1087 are oriented towards strand  $\beta_2$  of GABARAP and placed within hydrogen bonding distance of its K48 carbonyl oxygen and its L50 amide, respectively. In contrast, EGFR residue P1088 (X<sub>2</sub>) does not appear to be involved in

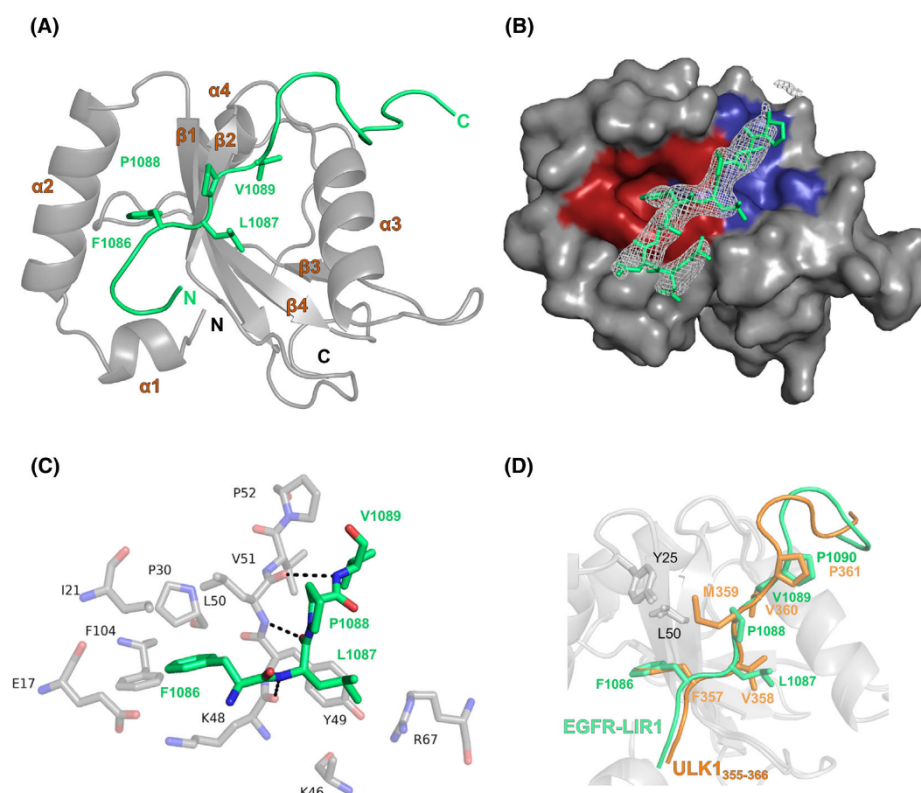


**Fig. 2.** X-ray structure of EGFR LIR1-GABARAP. (A) Overall structure of the EGFR LIR1 in complex with GABARAP presented as cartoon. GABARAP is shown in gray and the EGFR peptide in green. Coordinates and structure factors have been deposited in the Protein Data Bank with accession number 8S1M. (B) Surface representation of GABARAP with HP1 (red) and HP2 (blue) indicated. The  $2mF_o - DF_c$  map covering the EGFR peptide is colored white and contoured at 0.8 sigma and the EGFR peptide model is shown in green. (C) Core LIR residues (FLPV, in green) together with respective GABARAP residues at a distance lower than 4 Å. Hydrogen bonds are displayed as dashed lines. (D) Comparison of EGFR LIR1 and ULK1 extended core LIR (PDB: 6HYO, [20]) with GABARAP.

the interaction with GABARAP. The second hydrophobic pocket of GABARAP is occupied by V1089 of EGFR, representing  $\Gamma_3$  of the core LIR motif, which is involved in hydrophobic interactions with V51 and P52 (Fig. 2C). Superposition with the complex structure of the ULK1 LIR with GABARAP [20] reveals a similar binding interface of ULK1 residues 355 to 366 and EGFR residues 1084 to 1095 with GABARAP (Fig. 2D). While  $\Theta_0$  and  $\Gamma_3$  as well as the  $X_4$  position are represented by the same amino acids (F, V, and P, respectively),  $X_1$  and  $X_2$  differ between the two peptides. The ULK1 LIR possesses a valine at the  $X_1$  position, which likely allows for similar hydrophobic interactions with Y49 as L1087 in the EGFR LIR1. However, while P1088 in  $X_2$  shows no direct contact with GABARAP, the corresponding M359 in the ULK1 LIR is positioned in close proximity to

GABARAP residues Y25 and L50 and thus interacts with HP1. This could partially explain the much stronger ( $\sim 1000$ -fold, [20]) binding affinity of the ULK1 peptide, despite the similarity of the LIRs. We also superimposed our complex structure with the *in silico* structural models and found a high degree of agreement between the relevant binding interfaces regardless of whether the complete cytoplasmic domain of the EGFR or shorter fragments thereof served as input (Fig. S3B), confirming the previously described accurate predictability of Atg8-ligand complexes by AF2 [36].

#### EGFR and PCM1 LIR peptides impact the same region of GABARAP in solution

In order to gain more precise information on the contribution of individual GABARAP residues, we next

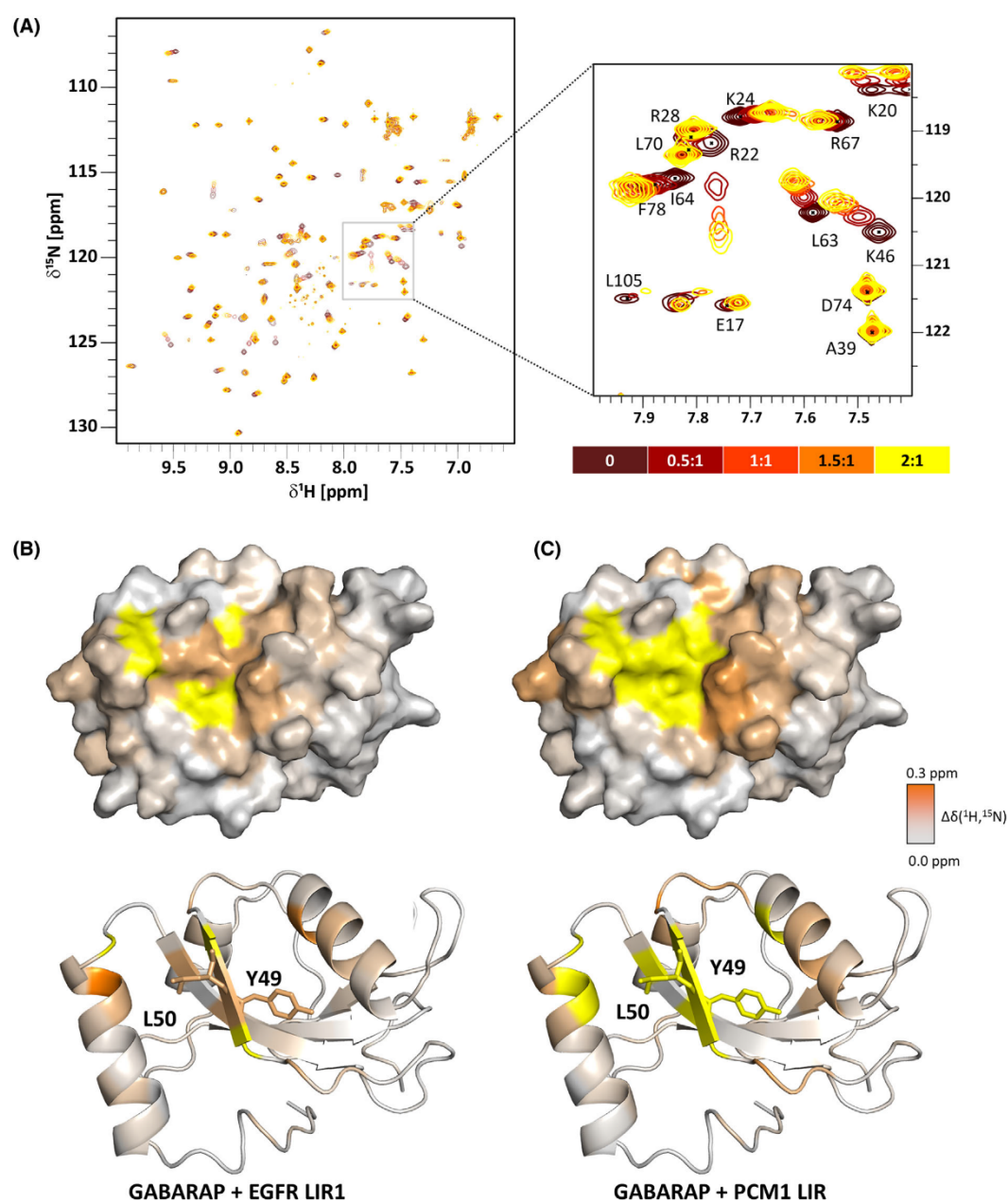


**Fig. 3.** Interaction between GABARAP and LIR peptides in solution. (A) 2D NMR spectrum ( $^1\text{H}$ - $^{15}\text{N}$ -HSQC) of GABARAP incubated with increasing amounts of EGFR LIR1 and exemplary zoom-in of peaks representing affected residues. (B, C) Chemical shift perturbations during titrations of  $^{15}\text{N}$ -GABARAP with LIR peptides from EGFR and PCM1 (2:1) mapped on the GABARAP structure (PDB ID: [1K01](#)) displayed as surface (top) and ribbon (bottom). Residues corresponding to disappearing HSQC peaks are presented in yellow.



mapped the GABARAP binding interface of a free EGFR LIR peptide using NMR chemical shift perturbation (CSP) data, and in addition compared it with that of the PCM1 LIR. As seen in the 2D  $^1\text{H}$ - $^{15}\text{N}$  HSQC spectrum (Fig. 3A), GABARAP without ligand exhibited the known resonances for natively folded GABARAP. Upon stepwise addition of the EGFR LIR1 ligand, several peaks displayed changes in chemical shift or line broadening beyond detection. At two-fold molar excess of EGFR LIR1 peptide, residues surrounding the hydrophobic pockets, HP1 and HP2 of GABARAP, specifically I21, R22, V29, V31, K46, Y49, L50, S53, F60 and L63 showed chemical shift perturbations above 0.1 ppm. Additionally, the peaks for Y25, K48 and V51 had disappeared, indicating intermediate exchange and thus a defining character of these residues for EGFR LIR1 binding (Fig. 3B, Fig. S5). In comparison, more residues were affected with the PCM1 LIR peptide as ligand at two-fold excess, with more residue peaks showing line broadening beyond detection (Fig. 3C, Fig. S5). This included the LDS residues Y49 and L50 of GABARAP, which have been previously described to be crucial for many LIR-LDS interactions [49]. Overall, the mapping of the CSP data on the GABARAP surface shows that binding of both ligands, EGFR LIR1 and PCM1 LIR, affect the same region, namely the LDS of GABARAP in a canonical manner, however, Y49 and L50 appeared to be less defining for binding of EGFR LIR1.

#### The interaction of EGFR LIR1 with GABARAP is independent of Y49A and L50A but is hindered by Pen8-ortho

To further verify the mode of binding, in particular the involvement of residues Y49 and L50 located in HP2 and HP1, respectively (see Fig. 4A), additional *in vitro* binding experiments were carried out. GABARAP<sub>Y49A/L50A</sub> and GABARAPL1<sub>Y49A/L50A</sub> were purified and subjected to BLI with immobilized PCM1 LIR and EGFR LIR1 respectively. In accordance with previous reports, PCM1 LIR binding was more than 20-fold reduced for GABARAP<sub>Y49A/L50A</sub> ( $99.2 \pm 6.7 \mu\text{M}$ ) and GABARAPL1<sub>Y49A/L50A</sub> ( $273.3 \pm 21.8 \mu\text{M}$ ) compared to the wildtype proteins ( $4.2 \pm 0.6$  and  $4.9 \pm 0.5 \mu\text{M}$ ). In contrast, EGFR LIR1 binding was not influenced by the two mutations, neither for GABARAP/GABARAP<sub>Y49A/L50A</sub> ( $52.0 \pm 3.0$  and  $39.0 \pm 2.6 \mu\text{M}$ ), nor GABARAPL1/GABARAPL1<sub>Y49A/L50A</sub> ( $29.7 \pm 1.1$  and  $19.1 \pm 1.2 \mu\text{M}$ , Fig. 4B). The ability of both GST-GABARAP and GST-GABARAP<sub>Y49A/L50A</sub> to enrich endogenous EGFR from cell lysates, while within the same sample

SQSTM1, described to depend on Y49 and L50 [49], showed a decrease with GST-GABARAP<sub>Y49A/L50A</sub> (Fig. S6), notably supports the dispensability of these two GABARAP residues for EGFR (LIR1) binding. Finally, additional interaction studies were carried out using the stapled peptide Pen8-ortho, which has been described to bind to the GABARAP LDS with high affinity ( $K_D$ : 14 nM) [29]. As expected, when preincubating GABARAP with a 1.5-fold molar excess of Pen8-ortho, 10-fold reduced binding to the immobilized EGFR LIR1 was observed (Fig. 4C). In conclusion, EGFR LIR1 appears to interact with GABARAP in a canonical, LDS-dependent manner, however, without relying on GABARAP residues Y49 and L50.

## Discussion

Receptor tyrosine kinase signaling, endocytic trafficking and autophagy are pathways important for cellular metabolism, which not only intersect at multiple stages, but also share several molecular components [50–53]. Following the observation of altered EGFR degradation and signaling, specifically in GABARAP single knockout cells [26], we sought to investigate a putative direct interaction between the hAtg8 protein GABARAP and the EGFR. Interestingly, the core EGFR-LIR1'FLPV' possesses the same  $\Theta_0$  and  $\Gamma_3$  residues as known hAtg8 interactors preferentially binding the GABARAP subfamily, namely PCM1, ULK1, ULK2 and PIK3C3/VPS34 [20,21,54]. The  $X_1$  residue is occupied by a leucine, which shows van der Waals distance with hydrophobic amino acids of GABARAP in our X-ray structure. While being atypical for a GABARAP interaction motif (GIM), examples for non-selective hAtg8 interactors with leucine in the  $X_1$  position, e.g. DVL2 have been described [21]. Notably, the  $X_2$  position, the least conserved residue of the consensus core LIR [55] and often not defining for GABARAP binding [56,57], is occupied by proline, a rather uncommon amino acid in this position. This P1088 does not appear to be involved in the interaction with GABARAP, possibly explaining the lower binding affinity of the EGFR LIR1 compared to related LIRs (e.g. in PCM1 and ULK1 [20]). Mutation studies have shown that proline residues in the  $X_2$  position are disruptive to the LIR-LDS binding [20,21]; however, in case of the PLEKHM1 LIR, this effect was milder for GABARAP than LC3B [21]. Additionally, proline as  $X_2$  residues has been reported for functional LIRs of the valosin-containing protein (p97) as well as the pro-oxidant adaptor p66SHC [58,59]. Beyond the core, the EGFR LIR1 shares a proline as  $X_4$  residue (i.e. C-terminal to the core LIR)

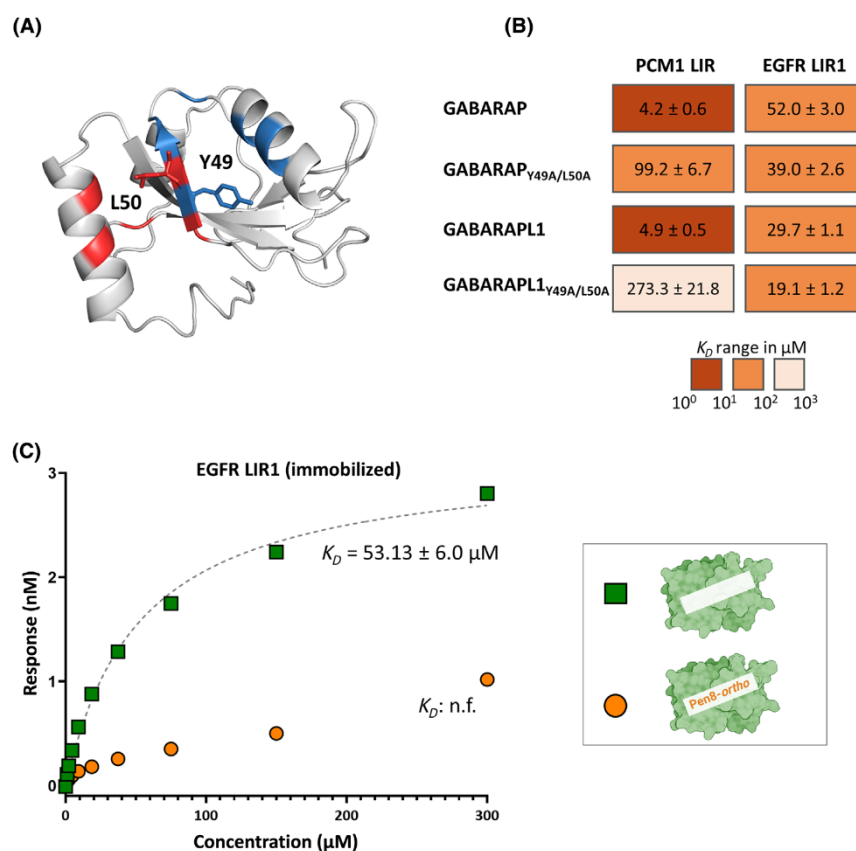


**Fig. 4.** (A) Ribbon model of GABARAP with residues forming hydrophobic pockets HP1 and HP2 in red and blue, respectively. Residues Y49 and L50 are presented as sticks (B)  $K_D$  values [ $\mu\text{M}$ ] of immobilized PCM1 and EGFR peptides with GABARAP/L1 and their Y49A/L50A variants as determined by biolayer interferometry. (C) Biolayer interferometry data for immobilized EGFR LIR1 peptide with either free GABARAP or GABARAP preincubated with the high-affinity binder Pen8-ortho. Effects of corresponding DMSO concentrations on binding were excluded (see Data S1 for details).  $K_D$  values are shown with standard error calculated from non-linear regression. (n.f., not fitable).

with ULK1, which has been suggested to inhibit LC3s binding [20], possibly explaining the lower EGFR LIR1 affinities for LC3A and LC3B. The N-terminal region preceding the core LIR ( $X_{-3}$ – $X_{-1}$ ) has also frequently been reported to influence binding affinity and specificity, and acidic (D, E) as well as phosphorylatable residues (S, T) appear to be common in these positions [55,60,61]. Indeed, N-terminal to the core LIR, the EGFR LIR1 has several acidic amino acids as well as serine and threonine, with  $X_{-3}$ – $X_{-1}$  being DDT, in fact,  $X_{-3}$  is located in proximity to H9 of GABARAP, possibly engaging in electrostatic interactions. Our investigation of the putative N-terminal phosphorylation sites, S1081 and T1085, revealed only slight increase in affinity. Interestingly, SCOC LIR

phosphorylation did also only lead to slightly enhanced affinity for GABARAP [23], whereas in other cases, drastic effects of phosphorylation have been reported, e.g.  $\sim 100$ -fold increase in affinity of LC3B to Nix upon phosphorylation of S34 and S35 in  $X_{-1}$  and  $X_{-2}$  [62].

EGFR internalization following EGF stimulation is regulated by parallel processes, namely clathrin-mediated endocytosis (CME), which itself can be categorized into AP2-dependent and AP2-independent CME, and non-clathrin endocytosis (NCE) which subsequently influence, degradation, recycling and signaling through multiple redundant and cooperative mechanisms [63–65]. Owing to the fact that neither these processes, nor the versatile roles of

hAtg8 proteins or possible compensatory effects resulting from GABARAP knockout are fully understood, pinpointing the molecular mechanism by which GABARAP influences the fate of the EGFR after EGF stimulation remains a challenge. While Dobner *et al.* [26] extensively discussed potential indirect mechanisms by which GABARAP could influence EGFR fate after stimulation, our data prompt us to also speculate on a direct interaction of the EGFR LIR1 with GABARAP. EGFR endocytosis and signaling is regulated by several binding sites within the CTD which are in proximity to the EGFR LIR1. This includes sites targeted by AP2 (positions 998–1001 (YLRA), 1034–1035 (LL) [65]), the palmitoyltransferase DHHC20 (cysteines at positions 1049, 1058, 1146 [66,67]) and the E3-ubiquitin ligase CBL (Y1069 [68,69]). Strikingly, the core LIR1 is located in the immediate vicinity of Y1092, a GRB2-binding site when phosphorylated [69,70]. Thus, LIR1-associated GABARAP could be suggested to hamper Y1092 phosphorylation itself and/or hamper GRB2 binding at pY1092, thus mitigating E3 ubiquitin-protein ligase CBL recruitment, EGFR ubiquitination and its lysosomal re-routing [69,70]. This provides a rationale for both the initially reduced pY1092 levels and the persistently higher levels of phosphorylated ERK observed in the presence of GABARAP compared to its absence [26]. Due to limited knowledge regarding the timeline of binding events following EGF stimulation in presence and absence of GABARAP, obtaining solid experimental evidence remains challenging. Despite the scarcity of examples, LIR-LDS interactions between receptors and hAtg8 have been proposed to be functionally relevant during diverse processes of receptor routing including their autophagic degradation (“signalophagy”) [71,72], anterograde trafficking [18] and secretion [17]. With our data, including the first X-ray structure of GABARAP with a surface receptor fragment, we propose the EGFR to be another of the yet few examples [73,74] of a receptor whose fate is influenced by an individual hAtg8. Since receptor trafficking upon EGF treatment is altered in cells lacking GABARAP, direct hAtg8-receptor interactions appear to not solely serve the autophagic degradation of RTKs in stressed cells, as shown for MET [71,72], but may alternatively play a general role during endosomal RTK transport in cells, possibly in a paralog-specific manner. Future studies designed to enrich our sparse understanding of RTK trafficking and associated LIR-dependencies will have to show whether this scenario proposed on the basis of *in vitro* binding data and the EGFR LIR1-GABARAP complex structure is indeed biologically relevant.

## Acknowledgement

This work was funded by the Deutsche Forschungsgemeinschaft (DFG, German Research Foundation)—Project-ID 267205415—SFB 1208 to D.W. Pen8-ortho was kindly supplied by Joshua Kritzer (Tufts University). We would like to thank the staff of the ESRF and EMBL Grenoble for assistance and support in using beamline ID30A-3 under proposal number MX-2399.

## Author contributions

Conceptualization: SH, AÜ; investigation: AÜ (protein purification, BLI, X-ray, NMR; SI material), MS (NMR), OHW (X-ray); formal analysis: AÜ; validation: SH, AÜ, OHW resources: DW; data curation: AÜ, OHW; visualization: AÜ; writing & original draft preparation: AÜ, SH; review and editing: all authors; supervision: SH, OHW; project administration: DW; funding acquisition: DW.

## Data accessibility

The X-ray data described in the main text has been deposited to the PDB (doi: [10.2210/pdb8S1M/pdb](https://doi.org/10.2210/pdb8S1M/pdb), accession number 8S1M). Individual BLI measurement data are available in the supplementary data of this article. All other data are available from the corresponding author upon reasonable request.

## References

- 1 Tanida I, Tanida-Miyake E, Komatsu M, Ueno T and Kominami E (2002) Human Apg3p/Aut1p homologue is an authentic E2 enzyme for multiple substrates, GATE-16, GABARAP, and MAP-LC3, and facilitates the conjugation of hApg12p to hApg5p. *J Biol Chem* **277**, 13739–13744.
- 2 Hanada T, Noda NN, Satomi Y, Ichimura Y, Fujioka Y, Takao T, Inagaki F and Ohsumi Y (2007) The Atg12-Atg5 conjugate has a novel E3-like activity for protein lipidation in autophagy. *J Biol Chem* **282**, 37298–37302.
- 3 Tanida I, Ueno T and Kominami E (2004) LC3 conjugation system in mammalian autophagy. *Int J Biochem Cell Biol* **36**, 2503–2518.
- 4 Gatica D, Lahiri V and Klionsky DJ (2018) Cargo recognition and degradation by selective autophagy. *Nat Cell Biol* **20**, 233–242.
- 5 Mizushima N (2020) The ATG conjugation systems in autophagy. *Curr Opin Cell Biol* **63**, 1–10.
- 6 Zhang W, Nishimura T, Gahlot D, Saito C, Davis C, Jefferies HBJ, Schreiber A, Thukral L, Tooze SA. Cis-membrane association of human ATG8 proteins



- N-terminus mediates autophagy. *BioRxiv* [preprint] 2022. doi: [10.1101/2022.06.10.495627](https://doi.org/10.1101/2022.06.10.495627)
- 7 Nguyen TN, Padman BS, Usher J, Oorschot V, Ramm G and Lazarou M (2016) Atg8 family LC3/GABARAP proteins are crucial for autophagosome-lysosome fusion but not autophagosome formation during PINK1/parkin mitophagy and starvation. *J Cell Biol* **215**, 857–874.
  - 8 Weidberg H, Shvets E, Shpilka T, Shimron F, Shinder V and Elazar Z (2010) LC3 and GATE-16/GABARAP subfamilies are both essential yet act differently in autophagosome biogenesis. *EMBO J* **29**, 1792–1802.
  - 9 Szalai P, Hagen LK, Saetre F, Luhr M, Sponheim M, Øverbye A, Mills IG, Seglen PO and Engedal N (2015) Autophagic bulk sequestration of cytosolic cargo is independent of LC3, but requires GABARAPs. *Exp Cell Res* **333**, 21–38.
  - 10 Nguyen TN and Lazarou M (2022) A unifying model for the role of the ATG8 system in autophagy. *J Cell Sci* **135**, jcs258997.
  - 11 Durgan J and Florey O (2022) Many roads lead to CASM: diverse stimuli of noncanonical autophagy share a unifying molecular mechanism. *Sci Adv* **8**, eabo1274.
  - 12 Fischer TD, Wang C, Padman BS, Lazarou M and Youle RJ (2020) STING induces LC3B lipidation onto single-membrane vesicles via the V-ATPase and ATG16L1-WD40 domain. *J Cell Biol* **219**, e202009128.
  - 13 Cunha LD, Yang M, Carter R, Guy C, Harris L, Crawford JC, Quarato G, Boada-Romero E, Kalkavan H, Johnson MDL *et al.* (2018) LC3-associated phagocytosis in myeloid cells promotes tumor immune tolerance. *Cell* **175**, 429–441.e16.
  - 14 Heckmann BL, Teubner BJW, Tummers B, Boada-Romero E, Harris L, Yang M, Guy CS, Zakharenko SS and Green DR (2019) LC3-associated endocytosis facilitates beta-amyloid clearance and mitigates neurodegeneration in murine Alzheimer's disease. *Cell* **178**, 536–551. e14.
  - 15 Fletcher K, Ulferts R, Jacquin E, Veith T, Gammoh N, Arasteh JM, Mayer U, Carding SR, Wileman T, Beale R *et al.* (2018) The WD40 domain of ATG16L1 is required for its non-canonical role in lipidation of LC3 at single membranes. *EMBO J* **37**, e97840.
  - 16 Heckmann BL, Teubner BJW, Boada-Romero E, Tummers B, Guy C, Fitzgerald P, Mayer U, Carding S, Zakharenko SS, Wileman T *et al.* (2020) Noncanonical function of an autophagy protein prevents spontaneous Alzheimer's disease. *Sci Adv* **6**, eabb9036.
  - 17 Gardner JO, Leidal AM, Nguyen TA and Debnath J (2023) LC3-dependent EV loading and secretion (LDELS) promotes TFRC (transferrin receptor) secretion via extracellular vesicles. *Autophagy* **19**, 1551–1561.
  - 18 Ye J, Zou G, Zhu R, Kong C, Miao C, Zhang M, Li J, Xiong W and Wang C (2021) Structural basis of GABARAP-mediated GABAA receptor trafficking and functions on GABAergic synaptic transmission. *Nat Commun* **12**, 297.
  - 19 Leil TA, Chen ZW, Chang CS and Olsen CS (2004) GABAA receptor-associated protein traffics GABAA receptors to the plasma membrane in neurons. *J Neurosci* **24**, 11429–11438.
  - 20 Wirth M, Zhang W, Razi M, Nyoni L, Joshi D, O'Reilly N, Johansen T, Tooze SA and Moulleron S (2019) Molecular determinants regulating selective binding of autophagy adapters and receptors to ATG8 proteins. *Nat Commun* **10**, 2055.
  - 21 Rogov VV, Stolz A, Ravichandran AC, Rios-Szwed DO, Suzuki H, Kniss A, Löhr F, Wakatsuki S, Dötsch V, Dikic I *et al.* (2017) Structural and functional analysis of the GABARAP interaction motif (GIM). *EMBO Rep* **18**, 1382–1396.
  - 22 Rogov VV, Nezis IP, Tsapras P, Zhang H, Dagdas Y, Noda NN, Nakatogawa H, Wirth M, Moulleron S, McEwan DG *et al.* (2023) Atg8 family proteins, LIR/AIM motifs and other interaction modes. *Autophagy Reports* **2**, doi: [10.1080/27694127.2023.2188523](https://doi.org/10.1080/27694127.2023.2188523)
  - 23 Wirth M, Moulleron S, Zhang W, Sjøttem E, Princely Abudu Y, Jain A, Lauritz Olsvik H, Bruun JA, Razi M, Jefferies HBJ *et al.* (2021) Phosphorylation of the LIR domain of SCOC modulates ATG8 binding affinity and specificity. *J Mol Biol* **433**, 166987.
  - 24 Wild PF, McEwan DG, Wagner S, Rogov VV, Brady NR, Richter B, Korac J, Waidmann O, Choudhary C, Dötsch V *et al.* (2011) Phosphorylation of the autophagy receptor optineurin Restricts Salmonella Growth. *Science* **333**, 233.
  - 25 Kuang Y, Ma K, Zhou C, Ding P, Zhu Y, Chen Q and Xia B (2016) Structural basis for the phosphorylation of FUNDC1 LIR as a molecular switch of mitophagy. *Autophagy* **12**, 2363–2373.
  - 26 Dobner J, Simons IM, Rufinatscha K, Hänsch S, Schwarten M, Weiergräber OH, Abdollahzadeh I, Gensch T, Bode JG, Hoffmann S *et al.* (2020) Deficiency of GABARAP but not its paralogs causes enhanced EGF-induced EGFR degradation. *Cells* **9**, 1296.
  - 27 Stangler T, Mayr LM and Willbold D (2002) Solution structure of human GABA(a) receptor-associated protein GABARAP – implications for biological function and its regulation. *J Biol Chem* **277**, 13363–13366.
  - 28 Ma P, Schwarten M, Schneider L, Boeske A, Henke N, Lisak D, Weber S, Mohrlüder J, Stoldt M, Strodel B *et al.* (2013) Interaction of Bcl-2 with the autophagy-related GABAA receptor-associated protein

- (GABARAP): biophysical characterization and functional implications. *J Biol Chem* **288**, 37204–37215.
- 29 Brown H, Chung M, Üffing A, Batistatou N, Tsang T, Doskocil S, Mao W, Willbold D, Bast RC Jr, Lu Z *et al.* (2022) Structure-based Design of Stapled Peptides that Bind GABARAP and inhibit autophagy. *J Am Chem Soc* **144**, 14687–14697.
  - 30 Kabsch W (2010) XDS. *Acta Crystallogr D Biol Crystallogr* **66**, 125–132.
  - 31 Vagin A and Teplyakov A (2010) Molecular replacement with MOLREP. *Acta Crystallogr D Biol Crystallogr* **66**, 22–25.
  - 32 Emsley P, Lohkamp B, Scott WG and Cowtan K (2010) Features and development of Coot. *Acta Crystallogr D Biol Crystallogr* **66**, 486–501.
  - 33 Liebschner D, Afonine PV, Baker ML, Bunkóczi G, Chen VB, Croll TI, Hintze B, Hung LW, Jain S, McCoy AJ *et al.* (2019) Macromolecular structure determination using X-rays, neutrons and electrons: recent developments in phenix. *Acta Crystallogr D Struct Biol* **75**, 861–877.
  - 34 Kalvari I, Tsompanis S, Mulakkal NC, Osgood R, Johansen T, Nezis IP and Promponas VJ (2014) iLIR: a web resource for prediction of Atg8-family interacting proteins. *Autophagy* **10**, 913–925.
  - 35 Xie Y, Li H, Luo X, Li H, Gao Q, Zhang L, Teng Y, Zhao Q, Zuo Z and Ren J (2022) IBS 2.0: an upgraded illustrator for the visualization of biological sequences. *Nucleic Acids Res* **50**, W420–W426.
  - 36 Ibrahim T, Khandare V, Mirkin FG, Tumas Y, Bubeck D and Bozkurt TO (2023) AlphaFold2-multimer guided high-accuracy prediction of typical and atypical ATG8-binding motifs. *PLoS Biol* **21**, e3001962.
  - 37 Evans R, O'Neill M, Pritzel A, Antropova N, Senior A, Green T, Židek A, Bates R, Blackwell S, Yim J *et al.* (2022) Protein complex prediction with AlphaFold-multimer. *BioRxiv [preprint]* doi: [10.1101/2021.10.04.463034](https://doi.org/10.1101/2021.10.04.463034)
  - 38 Mirdita M, Schütze K, Moriwaki Y, Heo L, Ovchinnikov S and Steinegger M (2022) ColabFold: making protein folding accessible to all. *Nat Methods* **19**, 679–682.
  - 39 Batzer AG, Rotin D, Ureña JM, Skolnik EY and Schlessinger J (1994) Hierarchy of binding sites for Grb2 and Shc on the epidermal growth factor receptor. *Mol Cell Biol* **14**, 5192–5201.
  - 40 Sorkin A, Waters C, Overholser KA and Carpenter G (1991) Multiple autophosphorylation site mutations of the epidermal growth factor receptor. Analysis of kinase activity and endocytosis. *J Biol Chem* **266**, 8355–8362.
  - 41 Okutani T, Okabayashi Y, Kido Y, Sugimoto Y, Sakaguchi K, Matuoka K, Takenawa T and Kasuga M (1994) Grb2/ash binds directly to tyrosines 1068 and 1086 and indirectly to tyrosine 1148 of activated human epidermal growth factor receptors in intact cells. *J Biol Chem* **269**, 31310–31314.
  - 42 Wirth D, Ozdemir E and Hristova K (2023) Quantification of ligand and mutation-induced bias in EGFR phosphorylation in direct response to ligand binding. *Nat Commun* **14**, 7579.
  - 43 Jura N, Endres NF, Engel K, Deindl S, das R, Lamers MH, Wemmer DE, Zhang X and Kuriyan J (2009) Mechanism for activation of the EGF receptor catalytic domain by the juxtamembrane segment. *Cell* **137**, 1293–1307.
  - 44 Tarcic G, Boguslavsky SK, Wakim J, Kiuchi T, Liu A, Reinitz F, Nathanson D, Takahashi T, Mischel PS, Ng T *et al.* (2009) An unbiased screen identifies DEP-1 tumor suppressor as a phosphatase controlling EGFR endocytosis. *Curr Biol* **19**, 1788–1798.
  - 45 Tong J, Taylor P, Peterman SM, Prakash A and Moran MF (2009) Epidermal growth factor receptor phosphorylation sites Ser991 and Tyr998 are implicated in the regulation of receptor endocytosis and phosphorylations at Ser1039 and Thr1041. *Mol Cell Proteomics* **8**, 2131–2144.
  - 46 Zhang G, Fang B, Liu RZ, Lin H, Kinose F, Bai Y, Oguz U, Remily-Wood ER, Li J, Altiok S *et al.* (2011) Mass spectrometry mapping of epidermal growth factor receptor phosphorylation related to oncogenic mutations and tyrosine kinase inhibitor sensitivity. *J Proteome Res* **10**, 305–319.
  - 47 Wu SL, Kim J, Bandle RW, Liotta L, Petricoin E and Karger BL (2006) Dynamic profiling of the post-translational modifications and interaction partners of epidermal growth factor receptor signaling after stimulation by epidermal growth factor using extended range proteomic analysis (ERPA). *Mol Cell Proteomics* **5**, 1610–1627.
  - 48 Uhlen M, Oksvold P, Fagerberg L, Lundberg E, Jonasson K, Forsberg M, Zwahlen M, Kampf C, Wester K, Hober S *et al.* (2010) Towards a knowledge-based human protein atlas. *Nat Biotechnol* **28**, 1248–1250.
  - 49 Behrends C, Sowa ME, Gygi SP and Harper JW (2010) Network organization of the human autophagy system. *Nature* **466**, 68–76.
  - 50 Birgisdottir AB and Johansen T (2020) Autophagy and endocytosis – interconnections and interdependencies. *J Cell Sci* **133**, jcs228114.
  - 51 Fraser J, Cabodevilla AG, Simpson J and Gammoh N (2017) Interplay of autophagy, receptor tyrosine kinase signalling and endocytic trafficking. *Essays Biochem* **61**, 597–607.
  - 52 Montero-Vergara J, Plachetta K, Kinch L, Bernhardt S, Kashyap K, Levine B, Thukral L, Vetter M, Thomsen C, Wiemann S *et al.* (2024) GRB2 is a BECN1 interacting protein that regulates autophagy. *Cell Death Dis* **15**, 14.

- 53 Coelho PP, Hesketh GG, Pedersen A, Kuzmin E, Fortier AMN, Bell ES, Ratcliffe CDH, Gingras AC and Park M (2022) Endosomal LC3C-pathway selectively targets plasma membrane cargo for autophagic degradation. *Nat Commun* **13**, 3812.
- 54 Birgisdottir AB, Mouilleron S, Bhujabal Z, Wirth M, Sjøttem E, Evjen G, Zhang W, Lee R, O'Reilly N, Tooze SA *et al.* (2019) Members of the autophagy class III phosphatidylinositol 3-kinase complex I interact with GABARAP and GABARAPL1 via LIR motifs. *Autophagy* **15**, 1333–1355.
- 55 Johansen T and Lamark T (2020) Selective autophagy: ATG8 family proteins, LIR motifs and cargo receptors. *J Mol Biol* **432**, 80–103.
- 56 Alemu EA, Lamark T, Torgersen KM, Birgisdottir AB, Larsen KB, Jain A, Olsvik H, Øvervatn A, Kirkin V and Johansen T (2012) ATG8 family proteins act as scaffolds for assembly of the ULK complex: sequence requirements for LC3-interacting region (LIR) motifs. *J Biol Chem* **287**, 39275–39290.
- 57 Skytte Rasmussen M, Mouilleron S, Kumar Shrestha B, Wirth M, Lee R, Bowitz Larsen K, Abudu Princely Y, O'Reilly N, Sjøttem E, Tooze SA *et al.* (2017) ATG4B contains a C-terminal LIR motif important for binding and efficient cleavage of mammalian orthologs of yeast Atg8. *Autophagy* **13**, 834–853.
- 58 Guo X, Sun X, Hu D, Fujioka H, Vyas R, Chakrapani S, Joshi AU, Luo Y, Mochly-Rosen D and Qi X (2016) VCP recruitment to mitochondria causes mitophagy impairment and neurodegeneration in models of Huntington's disease. *Nat Commun* **7**, 12646.
- 59 Onnis A, Cianfanelli V, Cassioli C, Samardzic D, Pelicci PG, Cecconi F and Baldari CT (2018) The pro-oxidant adaptor p66SHC promotes B cell mitophagy by disrupting mitochondrial integrity and recruiting LC3-II. *Autophagy* **14**, 2117–2138.
- 60 Pankiv S, Clausen TH, Lamark T, Brech A, Bruun JA, Outzen H, Øvervatn A, Bjørkøy G and Johansen T (2007) p62/SQSTM1 binds directly to Atg8/LC3 to facilitate degradation of ubiquitinated protein aggregates by autophagy. *J Biol Chem* **282**, 24131–24145.
- 61 Noda NN, Ohsumi Y and Inagaki F (2010) Atg8-family interacting motif crucial for selective autophagy. *FEBS Lett* **584**, 1379–1385.
- 62 Rogov VV, Suzuki H, Marinković M, Lang V, Kato R, Kawasaki M, Buljubašić M, Šprung M, Rogova N, Wakatsuki S *et al.* (2017) Phosphorylation of the mitochondrial autophagy receptor nix enhances its interaction with LC3 proteins. *Sci Rep* **7**, 1131.
- 63 Sigismund S, Argenzio E, Tosoni D, Cavallaro E, Polo S and di Fiore PP (2008) Clathrin-mediated internalization is essential for sustained EGFR signaling but dispensable for degradation. *Dev Cell* **15**, 209–219.
- 64 Pascolutti R, Algisi V, Conte A, Raimondi A, Pasham M, Upadhyayula S, Gaudin R, Maritzen T, Barbieri E, Caldieri G *et al.* (2019) Molecularly distinct Clathrin-coated pits differentially impact EGFR fate and signaling. *Cell Rep* **27**, 3049–3061 e6.
- 65 Goh LK, Huang F, Kim W, Gygi S and Sorkin A (2010) Multiple mechanisms collectively regulate clathrin-mediated endocytosis of the epidermal growth factor receptor. *J Cell Biol* **189**, 871–883.
- 66 Runkle KB, Kharbanda A, Stypulkowski E, Cao XJ, Wang W, Garcia BA and Witze ES (2016) Inhibition of DHHC20-mediated EGFR palmitoylation creates a dependence on EGFR signaling. *Mol Cell* **62**, 385–396.
- 67 Kadry YA, Lee JY and Witze ES (2021) Regulation of EGFR signalling by palmitoylation and its role in tumorigenesis. *Open Biol* **11**, 210033.
- 68 Levkowitz G, Waterman H, Ettenberg SA, Katz M, Tsygankov AY, Alroy I, Lavi S, Iwai K, Reiss Y, Ciechanover A *et al.* (1999) Ubiquitin ligase activity and tyrosine phosphorylation underlie suppression of growth factor signaling by c-Cbl/Sli-1. *Mol Cell* **4**, 1029–1040.
- 69 Waterman H, Katz M, Rubin C, Shtiegman K, Lavi S, Elson A, Jovin T and Yarden Y (2002) A mutant EGF-receptor defective in ubiquitylation and endocytosis unveils a role for Grb2 in negative signaling. *EMBO J* **21**, 303–313.
- 70 Jiang X, Huang F, Marusyk A and Sorkin A (2003) Grb2 regulates internalization of EGF receptors through clathrin-coated pits. *Mol Biol Cell* **14**, 858–870.
- 71 Bell ES, Coelho PP, Ratcliffe CDH, Rajadurai CV, Peschard P, Vaillancourt R, Zuo D and Park M (2019) LC3C-mediated autophagy selectively regulates the met RTK and HGF-stimulated migration and invasion. *Cell Rep* **29**, 4053–4068 e6.
- 72 Huang X, Gan G, Wang X, Xu T and Xie W (2019) The HGF-MET axis coordinates liver cancer metabolism and autophagy for chemotherapeutic resistance. *Autophagy* **15**, 1258–1279.
- 73 Sandilands E, Serrels B, Wilkinson S and Frame MC (2012) Src-dependent autophagic degradation of ret in FAK-signalling-defective cancer cells. *EMBO Rep* **13**, 733–740.
- 74 Sandilands E, Serrels B, McEwan DG, Morton JP, Macagno JP, McLeod K, Stevens C, Brunton VG, Langdon WY, Vidal M *et al.* (2011) Autophagic targeting of Src promotes cancer cell survival following reduced FAK signalling. *Nat Cell Biol* **14**, 51–60.

## Supporting information

Additional supporting information may be found online in the Supporting Information section at the end of the article.

**Fig. S1.** EGF-647 levels in wildtype and GABARAP KO cells over time and affinity enrichment of EGFR.

**Fig. S2.** Conservation of LIR1 and LIR2 surrounding regions within mammals.

**Fig. S3.** Prediction of GABARAP binding site selection within the EGFR cytoplasmic region.

**Fig. S4.**  $K_D$  values of pY1092 EGFR-LIR1 and pY1197 EGFR-LIR2 and hAtg8 paralogs.

**Fig. S5.** CSP for backbone amide resonances of GABARAP with LIR peptides.

**Fig. S6.** Affinity enrichment of endogenous EGFR and SQSTM1 from cells.

**Table S1.** Peptides used for BLI affinity measurements.

**Table S2.** RNA expression profile of hAtg8.

**Table S3.** Data collection and refinement statistics.

**Data S1.** BLI measurement data related to Figs 1B,C, 4B,C, Fig. S1C.

SI Figures

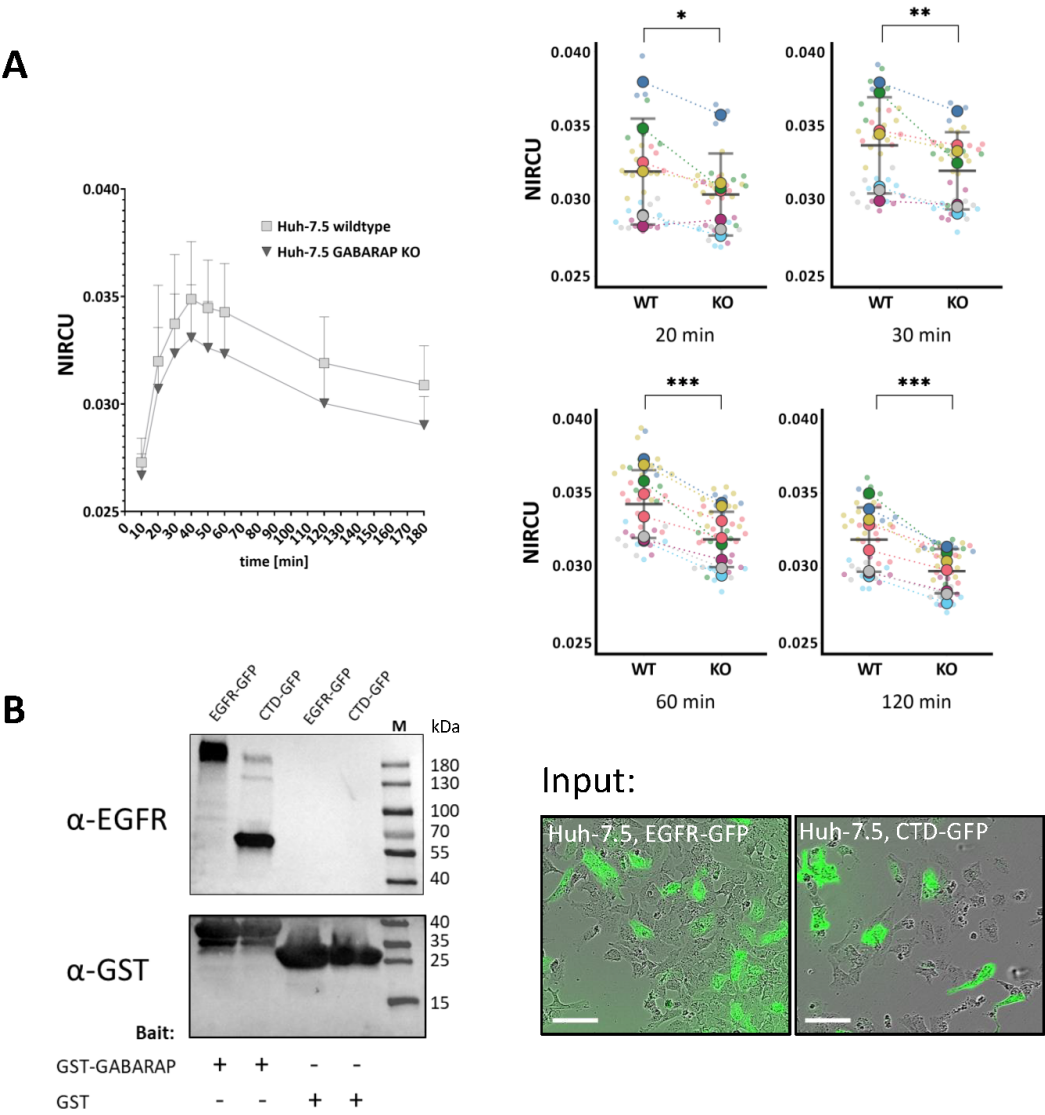


**Figure S1.** (A) EGF-647 levels in Huh-7.5 wildtype (WT) and GABARAP KO (KO) cells over time (left) measured in near infrared calibrated units (NIRCU), and selected time points with technical (small circles) and biological replicates (big circles) depicted (right). Mean value and standard deviation are indicated. \*  $P=0.12$ , \*\*  $P=0.003$ , \*\*\*  $P<0.001$ , paired t-test. (B) Huh-7.5 cells were transfected with plasmids encoding EGFR-GFP and CTD-GFP respectively. Lysates were used for affinity enrichment with GST-GABARAP. GST only was used as control. The respective western blot was stained with antibodies against EGFR and GST. Scale bars: 100  $\mu\text{m}$ .

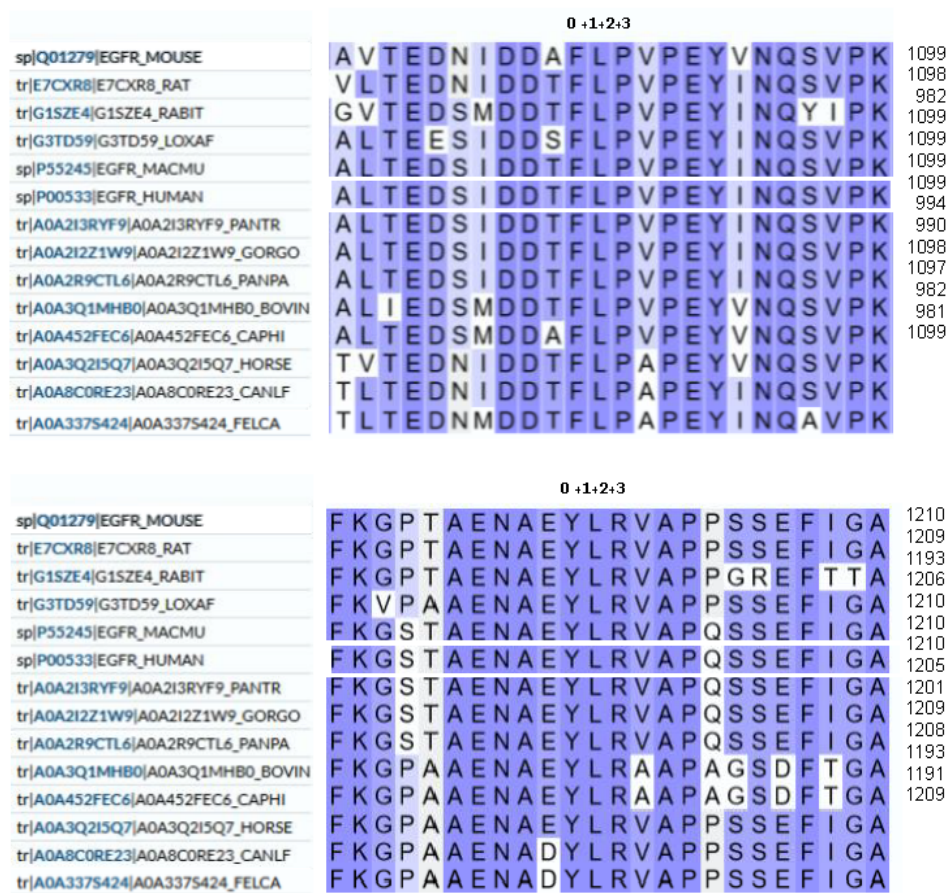


**Figure S2.** Conservation of LIR1 and LIR2 surrounding regions within mammals. The multiple sequence alignment for the selected EGFR protein sequences (full-length) was obtained using the Align function of the UniProt Consortium [4] according to described protocols [5]. The human EGFR sequence is highlighted by a white box. Only the two relevant sequence segments (top: LIR1, bottom: LIR2) are shown with the corresponding LIR-core positions numbered from 0 to +3. Interestingly, if divergent, position +3 in both core LIRs appears to be preferentially occupied by alanine.



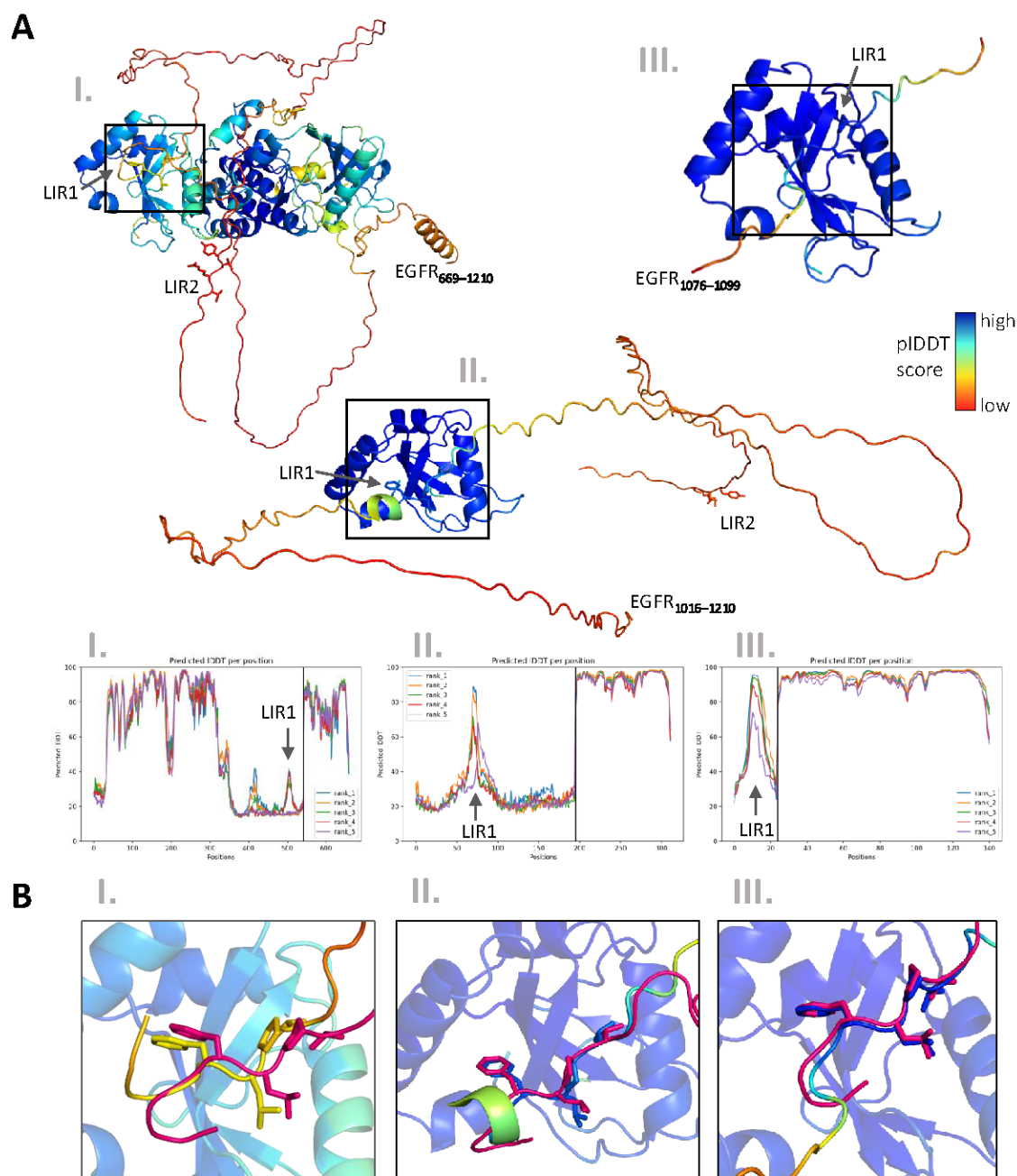


**Figure S3.** Prediction of GABARAP binding site selection within the EGFR cytoplasmic region (**A**). AF2-multimer prediction of complex structures of GABARAP and the EGFR cytoplasmic domain (I.) or fragments thereof (II. and III.). Models (colored according to their respective IDDT scores) along with their predicted IDDT plots are shown. As both LIR1 and LIR2 are located within intrinsically disordered protein regions of EGFR, an AF2-related bias (lower selection probability for LIRs in more structured regions [6]) for either of them is not expected. PTMs are neglected as they cannot be processed by AF2. Although a canonical LIR2-GABARAP LDS interaction was predicted for the short EGFR fragment (1190–1210) as input, LIR2 was not selected with any of the larger EGFR CTD fragments tested, their LIR1-mutated (FLPV to ALPA) versions or when offering two GABARAP molecules as input (not shown). (**B**) Superposition of the X-ray structure (8S1M) with AF2 rank 1 models of GABARAP in complex with LIR1 in the context of the entire cytoplasmic domain (I.), the EGFR fragment 1016–1210 (II.) and the 24mer peptide (III.), used for BLI. Only respective core LIR residues are depicted with those from 8S1M colored in pink. IDDT: Local Distance Difference Test

	GABARAP	GABARAPL1	GABARAPL2	LC3A	LC3B
pY1092 EGFR LIR1	46.23 ± 4.45	19.5 ± 0.6	98.0 ± 10.8	135.7 ± 6.9	337.9 ± 20.9
pY1197 EGFR LIR2	302.31 ± 26.61	30.9 ± 1.4	199.2 ± 15.8	229.7 ± 12.3	511.2 ± 39.0

K<sub>D</sub> range in  $\mu\text{M}$

10<sup>0</sup>   10<sup>1</sup>   10<sup>2</sup>   >300

**Figure S4.** K<sub>D</sub> values [ $\mu\text{M}$ ] with standard error calculated from non-linear regression of pY1092 EGFR-LIR1 and pY1197 EGFR-LIR2 (phosphorylated core LIR tyrosine) and human Atg8 paralogs.

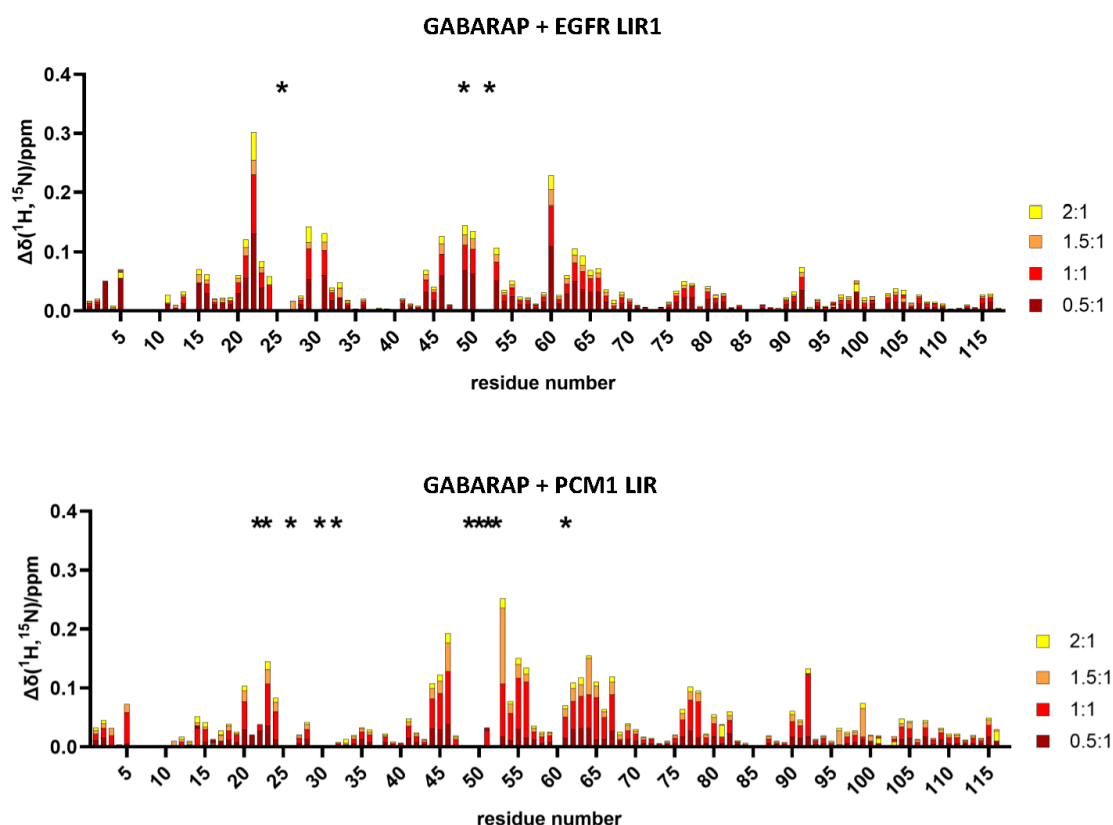


**Figure S5.** CSP for backbone amide resonances of GABARAP incubated with the indicated stoichiometric ratios of EGFR LIR1 (top) and PCM1 LIR (bottom) peptides. Asterisks represent residues affected by strong line broadening beyond detection - Y25, K48 and V51 in case of EGFR LIR1 and I21, R22, Y24, K48, Y49, L50, V51, F60 in case of PCM1 LIR.



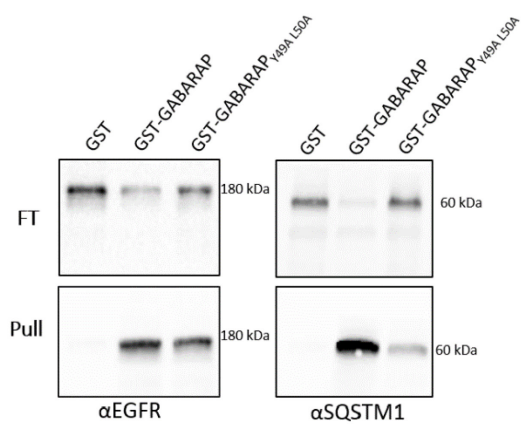


**Figure S6.** Affinity enrichment of endogenous EGFR (left) and SQSTM1 (right) from Huh-7.5 cells with GST-GABARAP and GST-GABARAP<sub>Y49A/L50A</sub> affinity purified from bacterial lysate.

## SI Tables

**Table S1. Peptides used for BLI affinity measurements:** (phosphorylation is indicated by p).

Peptide	Sequence
EGFR LIR1	Biotin-Ahx-ALTEDSIDDTFLPVPEYINQSVPK-NH <sub>2</sub>
(pS)EGFR LIR1	Biotin-Ahx-ALTED(pS)IDDTFLPVPEYINQSVPK-NH <sub>2</sub>
(pT)EGFR LIR1	Biotin-Ahx-ALTEDSIDD(pT)FLPVPEYINQSVPK-NH <sub>2</sub>
(pSpT)EGFR LIR1	Biotin-Ahx-ALTED(pS)IDD(pT)FLPVPEYINQSVPK-NH <sub>2</sub>
(pY)EGFR LIR1	Biotin-Ahx-ALTEDSIDDTFLPVPE(pY)INQSVPK-NH <sub>2</sub>
EGFR LIR2	Biotin-Ahx-STAENAEYLRVAPQSSEFIGA-NH <sub>2</sub>
(pY)EGFR LIR2	Biotin-Ahx-STAENAEYLRVAPQSSEFIGA-NH <sub>2</sub>
PCMI LIR (1954–1968)	Biotin-Ahx-SQKSDEEDFVKVEDLPLKLT-NH <sub>2</sub>

Ahx: Amino-hexanoic acid linker

**Table S2. RNA expression profile of hATG8.** Data are extracted from the Cell Lines section of the Human Protein Atlas (<https://www.proteinatlas.org/humanproteome/cell+line>; v23). nTPM: normalized transcripts per million.

hATG8	nTPM	
	HEK293	Huh7
GABARAP	445.0	496.4
GABARAPL1	28.0	43.3
GABARAPL2	195.8	112.1
LC3A	1.9	13.4
LC3B	76.0	79.2
LC3B2	1.8	2.1
LC3C	1.0	0

**Table S3. Data collection and refinement statistics.**

EGFR LIR1-GABARAP	
<b>Data collection</b>	
Space group	I23
Cell dimensions	
a, b, c (Å)	101.28, 101.28, 101.28
α, β, γ (°)	90, 90, 90
Resolution (Å)	41.35–2.05 (2.10–2.05) *
R <sub>measure</sub>	0.076 (3.308)
CC1/2	1 (0.365)
Mean I/σ(I)	21.91 (1.08)
Completeness (%)	99.95 (100.00)
Multiplicity	20.09 (20.10)
<b>Refinement</b>	
Resolution (Å)	41.35–2.05
No. reflections	11007 (1081)
R <sub>work</sub> / R <sub>free</sub>	0.2019 / 0.2286
No. atoms	1134
Protein	1101
Ligand/ion	7
Water	26
Mean B-factors (Å <sup>2</sup> )	72.05
Protein	72.13
Ligand/ion	84.31
Water	65.20
R.m.s. deviations	
Bond lengths (Å)	0.005
Bond angles (°)	0.67

\*Values in parentheses are for the highest-resolution shell.

## SI Methods

### Cell culture

Human hepatoma Huh-7.5 wildtype and GABARAP KO cells [1] were grown in Dulbecco's Modified Eagle Medium (DMEM) high glucose (Sigma Aldrich, D5796), supplemented with 10% heat inactivated fetal bovine serum (Sigma Aldrich, F9665) and 1% penicillin/streptomycin (Sigma Aldrich, P4333) at 37°C and 5% CO<sub>2</sub>. Cells were passaged at approximately 80% confluency. For transfection, cells were grown in 6-well plates to at least 70% confluency and transfected with 3 µg plasmid DNA per well, using 9 µl Lipofectamine 2000 (Thermo Fisher Scientific, 11668019).

### Continuous live-cell microscopy

For continuously monitoring the levels of EGF-Alexa647 in Huh-7.5 wildtype and GABARAP KO cells, real-time live cell microscopy (Incucyte SX5, Sartorius) was applied. The day prior to the experiment, 10,000 cells per well were seeded into 96 well plates. The following day, cells were cooled on ice for 10 min and 40 ng/ml EGF Alexa Fluor 647 (EGF-647; Thermo Fisher Scientific, E35351) in cold medium was added to the cells, which were incubated for one hour at 4°C on ice protected from light to allow ligand binding to the receptor. Afterwards, the medium was exchanged to remove free EGF-647 and cells were transferred into the Incucyte SX5, where images were recorded every 10 min for one hour and subsequently every hour using the 'adherent cell-by-cell' mode and the Phase and near infrared (NIR) channels. For analysis, the Incucyte cell-by-cell software (version 2021C; Sartorius) was applied to analyze the fluorescence intensity per cell over time. Cells with exceptionally high fluorescence intensity (above 145 NIR calibrated units (NIRCU), less than 2% of all cells) were excluded.

### Affinity enrichment and immunoblotting

Huh-7.5 (either untransfected or transfected with pEGFR-GFP/pCTD-GFP, coding for full-length EGFR or for residues 971 to 1210 comprising the regulatory C-terminal domain of the receptor) cells were harvested by trypsinization, washed once in PBS and lysed with NP40 buffer (20 mM Tris HCl, 200 mM NaCl, 1 mM EDTA, 0.5% NP40, 1 mM phenylmethylsulfonylfluoride (PMSF) and 1x Halt protease and phosphatase inhibitor [Thermo Fisher Scientific, 78442]) by incubation on ice for 30 min and vigorous pipetting every 10 min. Insoluble cell parts were sedimented by centrifugation for 10 min at 17,000 x g. GSH Sepharose beads (GE Healthcare, 17075605) were loaded with respective proteins by incubation with bacterial lysate containing GST-GABARAP, GST-GABARAP<sub>Y49A/L50A</sub> (refer to main text for details on expression) or purified GST, respectively and thoroughly washed. The cell lysates were precleared (GST loaded beads for 2 hours at 4°C) and subsequently incubated overnight at 4°C with GST-GABARAP, GST-GABARAP<sub>Y49A/L50A</sub> or GST loaded GSH beads, respectively. Beads were washed four times with cell lysis buffer, combined with Lämmli buffer and heated to 95°C for 10 minutes. Subsequently, samples were separated by SDS-PAGE using precast stain-free gels (Bio-Rad Laboratories, 4568124), transferred to 0.2 µm PVDF membranes (Bio-Rad Laboratories, 1704156) and blocked in 5% BSA (AppliChem, A1391) in TBS-T (136 mM NaCl, 2.7 mM KCl, 24.7 mM Tris-HCl, pH 7.4, 0.05% Tween-20 [AppliChem, A4974]) for 1 h. Membrane was incubated with primary antibody



### 3.4. Highlighting the hidden: monitoring the avidity-driven association of a fluorescent GABARAP tandem with microtubules in living cells

<b>Authors</b>	<u>Alina Üffing</u> , Lisa Gold, Thomas Gensch, Oliver H. Weiergräber, Silke Hoffmann, Dieter Willbold
<b>Journal</b>	Autophagy Reports
<b>Year of Publication</b>	2024
<b>DOI</b>	10.1080/27694127.2024.2348899
<b>Impact Factor</b>	-
<b>Contribution</b>	Project conceptualization, plasmid construction, cell culture & transfection, confocal microscopy (live-cell and Immunofluorescence) data analysis and curation, visualization, writing and editing of the manuscript.
<b>Reprint Permission</b>	<p>This is an Open Access article distributed under the terms of the Creative Commons Attribution License</p> <p>(<a href="http://creativecommons.org/licenses/by/4.0/">http://creativecommons.org/licenses/by/4.0/</a>), which permits unrestricted use, distribution, and reproduction in any medium, provided the original work is properly cited.</p>



## Highlighting the hidden: monitoring the avidity-driven association of a fluorescent GABARAP tandem with microtubules in living cells

Alina Üffing<sup>a,b</sup>, Lisa Gold<sup>b</sup>, Thomas Gensch<sup>c</sup>, Oliver H. Weiergräber<sup>a</sup>,  
Silke Hoffmann<sup>b</sup> and Dieter Willbold<sup>a,b</sup>


<sup>a</sup>Heinrich-Heine-Universität Düsseldorf, Mathematisch-Naturwissenschaftliche Fakultät, Institut für Physikalische Biologie, Düsseldorf, Germany; <sup>b</sup>Forschungszentrum Jülich, Institut für Biologische Informationsprozesse: Strukturbiochemie (IBI-7), Jülich, Germany; <sup>c</sup>Forschungszentrum Jülich, Institut für Biologische Informationsprozesse: Molekulare und Zelluläre Physiologie (IBI-1), Jülich, Germany

### ABSTRACT

GABARAP, like other ATG8 proteins, is a ubiquitin-like modifier and its C-terminal lipid conjugation enables association with cellular membranes. To prevent interference with the lipidation process, N-terminal fluorescent protein (FP) tagging strategies have become the standard for studying ATG8 localization and function in living cells, significantly contributing to our understanding of this protein family's multifaceted roles. We employed live cell imaging with particular emphasis on a GABARAP split-tandem construct, GABARAP(G116A)-mTagBFP2-GABARAP (G-B-G), which retains both a free N-terminus and a lipidation-competent c-terminus, while bivalence creates a gain in affinity conferred by avidity. Notably, reminiscent of early *in vitro* studies demonstrating an interaction of GABARAP and tubulin, our results revealed a robust association of G-B-G with the microtubule network in living cells. We show that the presence of several basic residues in the amino-terminal helical subdomain of GABARAP and avidity emerged as essential for robust MT association, whereas lipidation ability was not decisive. Interestingly, while the position of the FP-tag had little influence on the result, the nature of the FP itself was crucial, with mTagBFP2 being required for tracking GABARAP tandems in the vicinity of MTs. Though artificial effects cannot be excluded, we assume that G-B-G, with its increased avidity, can give visibility to processes that are based on inherently weak interactions, and thus can help elucidate potential roles of GABARAP e.g. in microtubule-associated processes that are integral to autophagy-related and -unrelated cellular transport.

**CONTACT** Silke Hoffmann  [si.hoffmann@fz-juelich.de](mailto:si.hoffmann@fz-juelich.de)  Forschungszentrum Jülich, Institut für Biologische Informationsprozesse: Strukturbiochemie (IBI-7), 52425, Jülich, Germany

This article has been republished with minor changes. These changes do not impact the academic content of the article.

 Supplemental data for this article can be accessed online at <https://doi.org/10.1080/27694127.2024.2348899>

© 2024 The Author(s). Published by Informa UK Limited, trading as Taylor & Francis Group.

This is an Open Access article distributed under the terms of the Creative Commons Attribution License (<http://creativecommons.org/licenses/by/4.0/>), which permits unrestricted use, distribution, and reproduction in any medium, provided the original work is properly cited. The terms on which this article has been published allow the posting of the Accepted Manuscript in a repository by the author(s) or with their consent.

**ARTICLE HISTORY** Received 13 Dec 2023; Revised 22 Apr 2024; Accepted 22 Apr 2024

**KEYWORDS** ATG8; bivalence; live-cell imaging; tubulin; mTagBFP2; tagging

## Introduction

The  $\gamma$ -aminobutyric acid type A receptor associated protein GABARAP belongs to the autophagy related protein 8 (ATG8) family, which in humans comprises a total of seven proteins. Human ATG8s are commonly split into two subfamilies, one containing the microtubule-associated protein 1 light chain 3 (MAP1LC3, hereafter referred to as LC3) isoforms LC3A, LC3B, LC3B2, LC3C, and one containing GABARAP, GABARAPL1, GABARAPL2. Like all ATG8 proteins, GABARAP consists of two N-terminal alpha-helices followed by a ubiquitin-like fold, and can similarly to ubiquitin be covalently conjugated to a substrate by an E1-E2-E3-like enzyme cascade [1–5]. Prior to substrate conjugation, ATG8s' C-termini require processing by an ATG4 cysteine protease resulting in the exposure of a terminal glycine residue (e.g. G116 in GABARAP or G120 in LC3B). Deconjugation is also mediated by ATG4 proteases, making the process reversible [6–8]. Unlike ubiquitin, which is conjugated to amino groups in proteins, ATG8s usually exploit phosphatidylethanolamine (PE) or -serine (PS) as substrates, localizing them to membranes when lipidated [9]. However, exceptions have recently been described for both types of modifiers [10–12].

To avoid conflict with the cellular lipidation process, N-terminal tagging strategies have been highly recommended for all ATG8s in the past [13], because C-terminal tagging would either result in loss of the tag or, in case of ATG4 processing-resistant ATG8 mutants like GABARAP(G116A), prevent membrane conjugation [13,14]. ATG8s with N-terminal FP tags are for instance widely used to monitor autophagy [15–17], and in conjunction with other techniques, have helped to elucidate the versatile roles of ATG8 proteins and shaped the current understanding of this multi-faceted protein family, which has been associated with a, still growing, plethora of autophagy-related and -unrelated functions [18–21].

Interestingly, most of the underlying mechanisms have in common that they involve direct interactions of the ATG8s with other proteins. In the majority these interactions rely on a conserved motif in the interaction partner (LC3-interacting region, LIR; ATG8/GABARAP-interacting motif, AIM/GIM) and its corresponding docking site (often termed LDS for LIR-docking site) spanning two hydrophobic pockets on the ATG8 protein surface [22,23].

While it appears that both the lipidation machinery and many LIR-LDS-mediated ATG8-associated processes can tolerate the presence of bulky, and even multiple, N-terminal tags [24], a growing body of evidence



demonstrates that common ATG8 constructs, with bulky FP tags at least twice their size, can be functionally compromised and/or mislocalized. One example are studies on mitophagy, where N-terminal FP-tags were detrimental to GABARAP's localization to mitochondria [25,26], while the smaller haemagglutinin-tag (HA-tag) did not inhibit mitochondrial targeting [26]. The unique N-terminal region of ATG8 proteins distinguishes them from other ubiquitin-like proteins and its primary structure also varies remarkably among the different GABARAPs/LC3s. Notably, structural biology studies indicate that, contrary to the conserved and rather rigid ubiquitin-like cores, the N-termini of several human ATG8s, like the yeast Atg8 ancestor, exhibit high flexibility [1,27-29]. The N-terminal region of GABARAP, for instance, is known to adopt multiple conformations [1,30] and has been described to be involved in its self-association [31,32], in the regulation of its proteasomal degradation through MIB1-mediated ubiquitination of K13 and K23 [33], and in its membrane association [34]. Historically, one of the first described functional features of the GABARAP N-terminal region was its tubulin and microtubule (MT) binding activity *in vitro* [35,36], albeit affinities between GABARAP and tubulin-derived peptides spanning the tubulin C-termini have been considered low [30]. As appropriate data in the cellular context are sparse [36], further investigation of GABARAP's MT association in living cells is still pending. Since systematic studies on ATG8-tagging strategies in general have received little attention in the past, we sought to fill this gap by employing a live cell imaging approach using cells expressing different FP arrangements of GABARAP. In contrast to the popular FP-GABARAP orientation, the presented work focuses on a so-called GABARAP split-tandem construct, GABARAP(G116A)-mTagBFP2-GABARAP (G-B-G). In G-B-G, an ATG4-resistant GABARAP with G116A substitution is joined to a central FP (mTagBFP2) followed by another GABARAP. In addition, its bivalence creates a gain in affinity conferred by avidity, potentially visualizing localizations of GABARAP which otherwise, presumably due to low-affinity interactions, might be hidden.

## Material & methods

### DNA constructs

Plasmids used throughout this study are listed in Table 1. All newly introduced vectors were generated by restriction-ligation cloning into pcDNA5/FRT/TO. Synthetic DNA fragments encoding GABARAP(G116A)-mTagBFP2-GABARAP (G-B-G), GABARAP(5X/G116A)-mCherry-GABARAP ( $G^{5X}$ -mCh-G), GABARAP(G116A)-mTagBFP2-GABARAP(5X) (G-B- $G^{5X}$ ) and GABARAP(G116A)-mTagBFP2 (G-B) were obtained from Geneart and BioCat. All used constructs were sequence

**Table 1.** List of constructs used in this work, together with short names, vector backbone, protein encoded, details (e.g. position-specific amino acid substitutions), and reference or source. Abbreviations: G: GABARAP; B: mTagBFP2; mCh: mCherry; Y: eYFP; \*: G116A or G120A.

Short names	Vector	Encoding	Details	Reference/Source
G-B-G	pcDNA5/ FRT/TO	GABARAP(G116A)-mTagBFP2- GABARAP		Addgene #212106
G <sup>5X</sup> -B-G	pcDNA5/ FRT/TO	GABARAP(5X/G116A)-mTagBFP2- GABARAP	5X: K2, K13, R15, K20, K23 to A	Addgene #212107
G-B-G <sup>5X</sup>	pcDNA5/ FRT/TO	GABARAP(G116A)-mTagBFP2- GABARAP(5X)	5X: K2, K13, R15, K20, K23 to A	Addgene #218425
G <sup>5X</sup> -B-G <sup>5X</sup>	pcDNA5/ FRT/TO	GABARAP(5X/G116A)-mTagBFP2- GABARAP(5X)	5X: K2, K13, R15, K20, K23 to A	Addgene #218426
G-B-G*	pcDNA5/ FRT/TO	GABARAP(G116A)-mTagBFP2- GABARAP(G116A)	lipidation-deficient	Addgene #212108
B-G-G	pcDNA5/ FRT/TO	mTagBFP2-GABARAP(G116A)- GABARAP		Addgene #212109
B-G	pcDNA5/ FRT/TO	mTagBFP2-GABARAP		Addgene #212110
Y-G	pcDNA5/ FRT/TO	eYFP-GABARAP		Addgene #212111
G-B	pcDNA5/ FRT/TO	GABARAP(G116A)-mTagBFP2		Addgene #212112
G	pcDNA5/ FRT/TO	GABARAP	tag-less	Addgene #218427
G-mCh-G	pcDNA5/ FRT/TO	GABARAP(G116A)-mCherry- GABARAP		Addgene #212113
mEos- tubulin	mEos3.2-C1	mEos3.2-Tubulin-C-18		Addgene #57484

verified (Microsynth SeqLab). The respective plasmid DNAs have been deposited at the Addgene plasmid repository, where more detailed information for each construct can be accessed.

### Cell culture and transfection

Human hepatoma Huh-7.5 GABARAP KO cells, HEK293 Flp in TRex GABARAP KO cells [37] and HeLa cells were cultured in Dulbecco's Modified Eagle Medium (DMEM) high glucose (Sigma Aldrich, D5796), supplemented with 10% heat inactivated fetal bovine serum (Sigma Aldrich, F9665) and 1% penicillin/streptomycin (Sigma Aldrich, P4333) at 37°C and 5% CO<sub>2</sub>. Cells were passaged at 80% confluency and routinely checked for mycoplasma contamination.

For transfection, cells were grown in 6- or 12- well plates to at least 70% confluency and transfected with 3 or 1.5 µg plasmid DNA per well, using 9 or 4.5 µl Lipofectamine 2000 (Thermo Fisher Scientific, 11668019) respectively. Cells were seeded into fibronectin (Sigma Aldrich, F1141) coated 35 mm glass-bottom IBIDI dishes 1.5-3 h post transfection and either imaged after 24-42 h or fixed for immunocytochemistry.

### ***Immunocytochemistry***

Transfected Huh-7.5 *GABARAP* SKO cells were fixed for 10 min with precooled methanol and subsequently for 1 minute with precooled acetone, both at  $-20^{\circ}\text{C}$ . After two washes with PBS (137 mM NaCl, 2.7 mM KCl, 1.8 mM  $\text{KH}_2\text{PO}_4$ , 10 mM  $\text{Na}_2\text{HPO}_4$ , pH 7.4), non-specific binding sites were blocked with 5% (w/v) BSA (AppliChem, A1391) in PBS for 1–2 h. Cells were incubated with primary antibody (anti-*GABARAP* rabbit polyclonal [Proteintech, 18723-I-AP] diluted 1:100 in PBS containing 1% (w/v) BSA and 0.3% (v/v) Triton X-100 (AppliChem, A4975) for 2 h or overnight and afterwards washed twice with PBS. Cells were stained with secondary antibody (anti-rabbit-Alexa647 [abcam, ab150083]) diluted 1:200 in the abovementioned solution for 1 h. Following two washes with PBS, cells were imaged and stored in PBS containing 0.05% (w/v) sodium azide.

### ***Confocal Laser Scanning Microscopy***

Cells were imaged using a LSM 710 confocal laser scanning system (Zeiss), operated with ZEN black 2009 software and a Plan-Apochromat 63x/1.40 Oil DIC M27 objective. For live-cell imaging at  $37^{\circ}\text{C}$ , a temperature-controlled microscopy stage was used. For staining of actin and microtubules, medium was supplemented with 500 nM SiR-tubulin (Spirochrome, SC002) or 1  $\mu\text{M}$  SiR-actin (Spirochrome, SC001) and cells were incubated for 4 to 8 h prior to imaging. In the case of Huh-7.5 *GABARAP* KO and HEK293 Flp in TRex *GABARAP* KO, cells were additionally treated with 10  $\mu\text{M}$  verapamil. The laser excitation wavelength and emission filters for the cells expressing fusion protein constructs were 405 nm and 410–509/530 nm for mTagBFP2, 514 nm and 519–621 nm for eYFP, 543 nm and 578–696 nm for mCherry and 633 nm and 638–759 nm for cells stained with SiR-probes.

### ***Colocalization colormap***

To obtain a spatial representation of the colocalization of *G-B-G* with SiR-tubulin or SiR-actin we used the “colocalization colormap” Plugin for ImageJ [38], which is based on the Jaskolski algorithm [39]. This method creates a pseudo-color map of correlations between pairs of corresponding pixels in two input images. As input for the analysis we used smoothed images (3x3 mean filter) of *G-B-G*-expressing Huh-7.5 *GABARAP* KO cells counter-stained either with SiR-tubulin or SiR-actin. Per analysed cell, five regions of interest (ROIs) of 40x40 pixels were split into their corresponding mTagBFP2- and SiR-channels. For each ROI the normalized mean deviation product (nMDP) was calculated for all corresponding pixels in the two channels, mathematically representing correlation between

intensities of each pixel pair. The distribution of the calculated nMDP values was plotted, resulting in a colocalization colormap for each ROI. Such maps display the spatial correlation between the two fluorescent signals (mTagBFP2 and SiR), and because a jet colormap is implemented in the plugin by default, hot colours indicate colocalization and cold colours indicate separation. As a quantitative measure, the plugin also calculates the index of correlation (Icorr), which represents the fraction of positively colocalized pixels in each analyzed ROI. Finally, in order to compare the results, the distribution of Icorr values obtained for either G-B-G and SiR-tubulin or G-B-G and SiR-actin were plotted separately, and were subjected to statistical evaluation.

### ***Quantitative analysis of N:C, Nu:N and F:C ratios***

To quantify the nucleocytoplasmic (N:C) ratio, five randomly ROIs ( $\varnothing$  10 px) were manually drawn in the nucleus as well as in the puncta-devoid cytoplasmic region of each cell using ImageJ. Mean intensities of nuclear and cytoplasmic ROIs from mTagBFP2 and eYFP channels were measured and divided. Likewise, mean intensities from 2-3 nucleoli ROIs were measured and divided by the mean nuclear intensity for both channels to determine the nucleolar to nucleoplasm (Nu:N) ratio of each cell. Filament to cytoplasm (F:C) ratios were determined by selecting 2-3 regions surrounding filaments using the polygon selection tool in ImageJ. For each filament ROI, a corresponding ROI of the same shape and size was placed in a nearby cytoplasmic region without filaments. Mean intensities were measured and F:C ratios calculated per ROI pair and cell. In case of co-transfected cells, this was done for both the mTagBFP2 and the eYFP channel. In case of single construct transfection and co-staining with SiR-tubulin, ROI pairs were selected according to most intense signals in the SiR channel and mean intensities were measured from the mTagBFP2 channel. N:C, Nu:N and F:C ratios were plotted and subjected to statistical evaluation.

### ***Microtubule organization analysis***

For analysis of the microtubule cytoskeleton, images showing a G-B-G expressing and an un-transfected control cell (co-)stained with SiR-tubulin were selected. The areas of both individual cells were manually traced according to the transmission image and saved as ROIs. SiR channels were skeletonized using the ImageJ LPX filter2D plugin (filter = lineFilters, linemode = lineExtract, giwsiter = 5, mdnmsLen = 15, pickup = otsu, shaveLen = 5, delLen = 5) [40]. Afterwards, the skeleton image type was set to 8 bit, duplicated, ROIs selected and background set to black (0,0,0) to obtain a skeletonized microtubule image per cell (ROI). Subsequently, the skeleton of each cell was analysed using ImageJ (Analyze >

Skeleton) to tag endpoint, junction and slab pixels (the pixels between junctions and endpoints). Length of branches above 3 pixels was plotted for each cell in  $\mu\text{m}$ .

Additionally, cytoskeleton bundling parameters (Skewness and coefficient of variation [CV]) were obtained from the skeleton images of each cell according to an ImageJ macro published by [41], modified for analysis of single plane images.

### **Prediction of complex structures**

Potential modes of interaction of human GABARAP or its mTagBFP2 tandem constructs with microtubules were investigated *in silico* with AlphaFold2 [42], using the ColabFold implementation [43]. Complexes of GABARAP and a TBA1A-TBB5 (Uniprot accession Q71U36, P07437) dimer were predicted using a local installation (github.com/YoshitakaMo/localcolabfold) running on a Linux workstation equipped with an nVidia GPU, while data for the larger complexes of G-B-G or B-G-G with a tetrameric tubulin chain (TBA1A-TBB5-TBA1A-TBB5) were uploaded to the COSMIC<sup>2</sup> platform [44] for processing by ColabFold. For each subject, five models were generated with inclusion of template information, using multiple sequence alignment mode *mmseqs2\_uniref\_env*, model type *alphafold2\_multimer\_v3*, a maximum of 20 recycle steps, and recycling controlled by *recycle\_early\_stop\_tolerance:0.5* and *stop\_at\_score:90* for the local and remote installations, respectively. All models were subjected to relaxation using Amber as implemented in the ColabFold pipeline. The highest ranked model without steric clashes, according to predicted IDDT statistics, is used for further evaluation; the complete list of models along with predicted IDDT and PAE plots is shown as supplemental information (Fig. S5). Figures were created using the PyMOL Molecular Graphics System, Version 2.7 Schrödinger, LLC.

### **Statistical analysis**

Mean N:C and Nu:N values per cell as well as resulting statistics from paired t-tests were plotted using GraphPad Prism version 9. Mean F:C values per cell were analyzed by paired t-test in case of co-transfected cells and one-way Anova with Tukey's multiple comparison test for single transfections with different constructs using GraphPad Prism version 9, and mean values as well as individual values were plotted using SuperPlot (<https://huygens.science.uva.nl/SuperPlotsOfData/>). Mean Icorr values per cell were analyzed by unpaired t-test, and individual values as well as means were plotted using GraphPad Prism 9 and SuperPlot, respectively. Branch length was analyzed for each cell pair using Mann-Whitney test, and individual values were plotted with GraphPad Prism 9.

## Results

### G-B-G exhibits subcellular localization distinct from Y-G

Due to Atg8-like proteins being C-terminally conjugated to lipids, their N-terminal fusions with fluorescent proteins (FP-ATG8s), such as the yellow fluorescent protein-tagged GABARAP (Y-G) used in this study, have a long tradition in the study of their function in living cells. Macroautophagy/autophagy induction typically triggers FP-ATG8s to localize to punctate structures, interpreted as their lipidated forms associated with autophagic membranes. Under basal conditions, being the focus here, FP-ATG8s are known for their diffuse cytoplasmic and nuclear distribution - commonly interpreted as their free, unlipidated forms. To restrict GABARAP functionalities to the transfected constructs, excluding any contribution from an endogenous GABARAP background, Huh-7.5 *GABARAP* knockout cells, hereafter abbreviated as Huh KO cells, were used throughout this study unless otherwise stated. In order to be able to directly compare the behavior of the novel split tandem construct G-B-G with that of Y-G under basal conditions, cells were co-transfected with the corresponding expression plasmids (Table 1). Overexpressed Y-G showed, as expected, a diffuse cytoplasmic distribution and high intensities in the nucleoplasm, however, co-expressed G-B-G emerged at a variety of intracellular structures, resulting in a more heterogenous staining pattern (Figure 1A). Even though the mean nucleocytoplasmic (N:C) ratio of Y-G ( $1.69 \pm 0.34$ ) was significantly higher than for G-B-G ( $1.03 \pm 0.45$ ), the latter showed relatively high intensities at diverse nuclear subcompartments including the nucleolus, with a higher mean nucleoli-to-nucleoplasm (Nu:N) ratio ( $2.27 \pm 0.49$ ) compared to Y-G ( $1.09 \pm 0.11$ ; Figure 1B-D).

Most strikingly, G-B-G intensity was frequently high at filamental structures while those were barely visible in the yellow channel (Y-G) in the respective cells (Figure 1E). This is also reflected in the corresponding F:C ratios, which were significantly higher in the case of G-B-G (Y-G:  $1.05 \pm 0.05$ , G-B-G:  $1.57 \pm 0.2$ ; Figure 1F). To assess whether the discrepancies in signal distribution between G-B-G and Y-G arose from bivalence of G-B-G, the different FPs used, and/or their position in the fusion proteins, Huh KO cells were transfected with additional constructs expressing N- or C-terminal fusions of mTagBFP2 with GABARAP (B-G or G-B) as well as tandem GABARAP with N-terminal mTagBFP2 (B-G-G). For high nucleolar signal intensities, the FP seems to be decisive as cells expressing Y-G did not but B-G did highlight nucleoli in a manner seen in G-B-G expressing cells (Fig. S1B-D). In contrast to G-B-G, B-G transfected cells showed no apparent filamentous pattern. In addition, in cells expressing a C-terminally tagged, lipidation-deficient GABARAP with a free and unaltered N-terminus (G-B) no robust filamentous pattern could be monitored either (Fig. S1E), suggesting that the mere

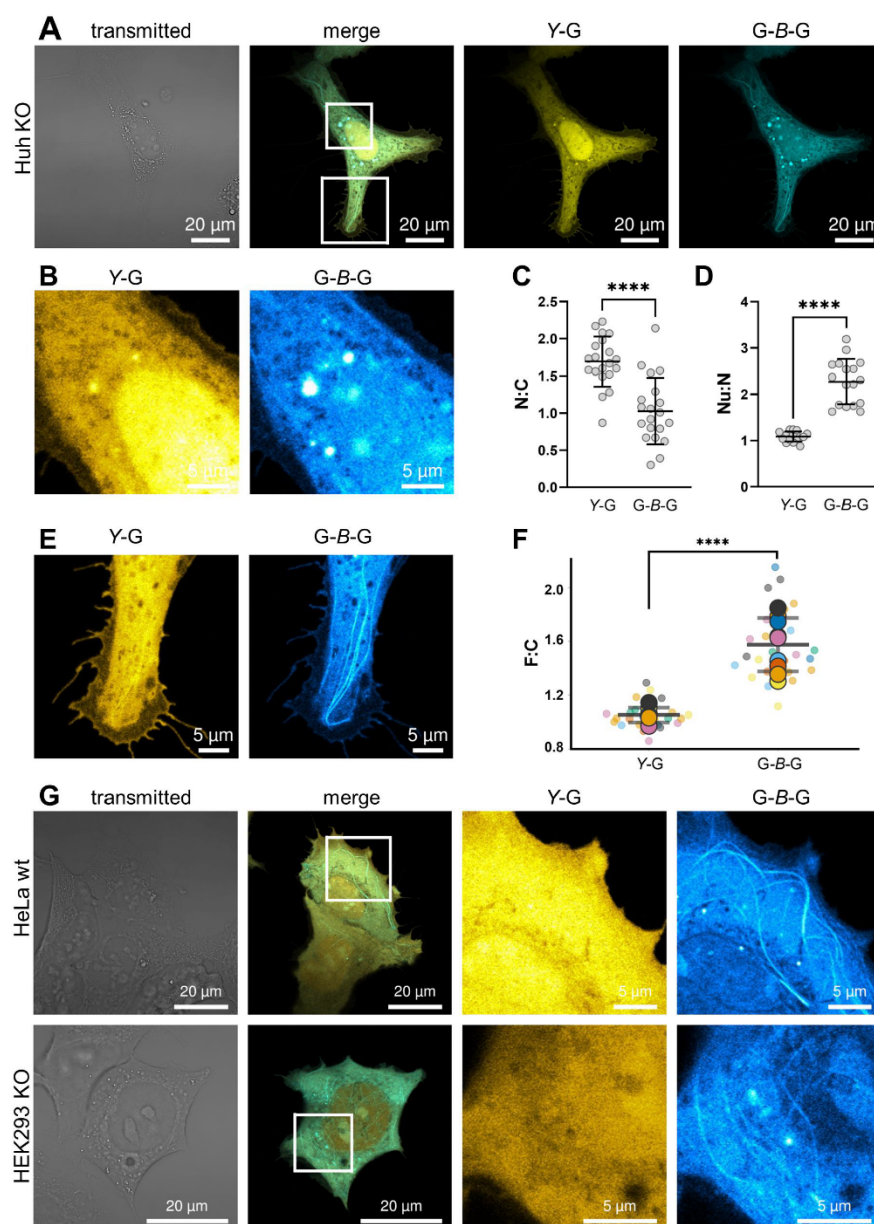


**Figure 1** Distinct subcellular distribution of Y-G and G-B-G. **(A)** Exemplary image of a Huh-7.5 GABARAP KO cell expressing G-B-G and Y-G. Distinct signals are visible at different subcellular locations including **(B)** nucleus and nucleoli and **(E)** filaments. Quantification of **(C)** nucleocytoplasmic ratio (N:C), Mean:  $1.03 \pm 0.45$  for G-B-G and  $1.69 \pm 0.34$  for Y-G; **(D)** Nucleoli to nucleoplasm (Nu:N) ratio, Mean:  $2.27 \pm 0.49$  for G-B-G and  $1.09 \pm 0.11$  for Y-G and **(F)** filament to cytoplasm ratios (F:C), Mean:  $1.57 \pm 0.2$  for G-B-G and  $1.05 \pm 0.05$  for Y-G measured by mean fluorescence intensity. \*\*\*\*  $P < 0.0001$ , paired t-test. Values are represented as means  $\pm$  SD ( $n=20$  (N:C), 17 (S:N), 9 (F:C)) from two independent experiments). See Fig. S1A for a detailed description of the quantification procedure applied. All cells and ROIs that went into the quantification can be reviewed on Bioline Archive. **(G)** In HEK293 GABARAP SKO and HeLa wildtype cells, distinct features can also be observed for overexpressed G-B-G compared to Y-G.



presence of an unmodified N-terminus is not sufficient to establish filament association of a single, FP-linked GABARAP or at least fails to achieve the degree of association sufficient for a robust microscopic detection. Notably, N-terminal FP-tagging of two consecutive GABARAPs, as shown for *B-G-G* transfected cells (Fig. S1F), resulted in the appearance of filaments reminiscent in extent of those in *G-B-G* transfected cells. Thus, enhancing affinity through bivalence by combining two GABARAP moieties in a single FP-fusion appears to be critical for highlighting filaments in living cells.

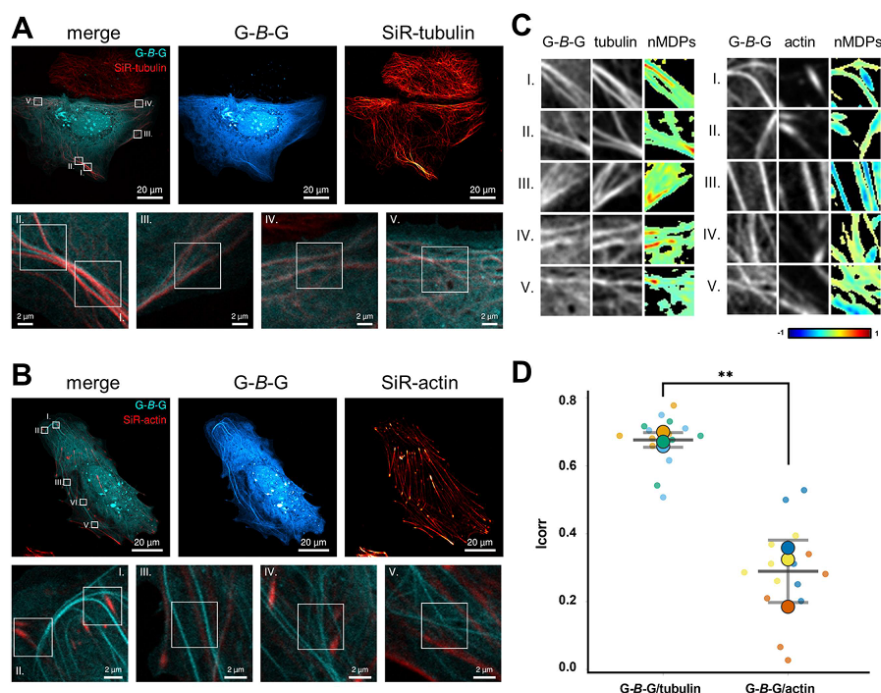
Notably, this phenomenon and the other distinct features of *G-B-G* and *Y-G* described above were also evident in other lines as illustrated for HEK293 cells in a GABARAP single-KO background, and for wildtype HeLa cells (Figure 1G). However, since we observed pronounced *G-B-G*-decorated filaments particularly frequently in Huh KO cells, this line was used for all further experiments.

### **G-B-G-decorated filamental structures correspond to microtubules**

To investigate the identity of the *G-B-G* enriched filamental structures, Huh KO cells expressing *G-B-G* were co-stained with SiR-tubulin and SiR-actin. Representative images showed a broad match of the fluorescence signals for *G-B-G* with SiR-tubulin (Figure 2A, Fig. S2A), whereas *G-B-G* and SiR-actin signals overlapped poorly, at best appearing with a parallel offset or crossing each other (Figure 2B, Fig. S2B). Spatial correlation of *G-B-G* with SiR-tubulin and SiR-actin signals was quantitated as outlined in the Methods section; *I*corr values determined for *G-B-G* and tubulin ( $0.68 \pm 0.02$ ) were significantly higher than those for *G-B-G* and actin ( $0.29 \pm 0.09$ ), confirming the above-mentioned observation (Figure 2C–D). In most cases the enrichment of *G-B-G* along MTs was uniform, but in some cells *G-B-G* positive puncta, possibly *G-B-G* decorated transport vesicles, were observed in proximity to MTs (Fig. S2C, D), raising the idea of a connection between vesicle-associated GABARAP and MTs.

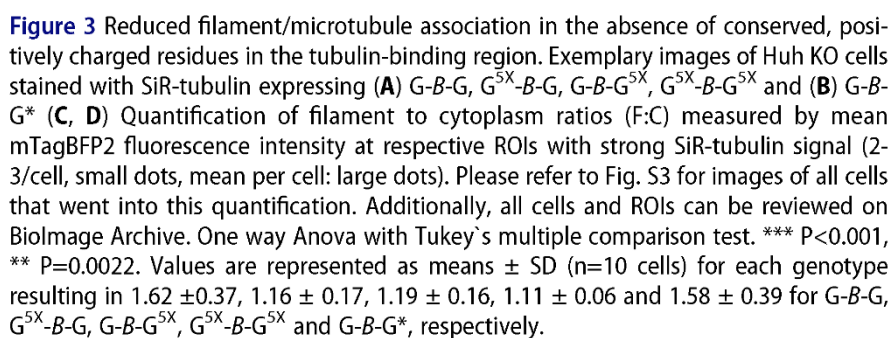
### **Enrichment of G-B-G at microtubules relies on two intact GABARAP N-termini while lipidation capability is dispensable**

Having shown that *G-B-G* associates preferentially with MTs, we then asked which regions in GABARAP, or in *G-B-G*, might be involved. For this purpose, Huh KO cells expressing *G<sup>5X</sup>-B-G* or *G-B-G<sup>5X</sup>* with a total of five alanine substitutions of N-terminal basic residues (K2A, K13A, R15A, K20A, K23A) either in the first or second GABARAP moiety of the split tandem construct were investigated, as basic residues have been



**Figure 2** Filamental G-B-G structures correlate with SiR-tubulin signal. Representative live-cell images of G-B-G expressing Huh KO cells stained with (A) SiR-tubulin or (B) SiR-actin. Bottom panels show magnifications around five selected ROIs per cell. (C) Grey-scale images of the ROIs depicted in (A) and (B) highlighting the distribution pattern of G-B-G and tubulin (left) or actin (right). The corresponding colocalization colormaps (nMDPs, 40x40 pixel) show the spatial correlation between the two fluorescent signals (mTagBFP2 and SiR), with hot colors indicating colocalization and cold color indicating separation (n=3; refer to Fig. S3 for replicates). (D) Graphical representation of the corresponding Icorr values representing the fraction of positively correlated pixels for G-B-G and tubulin or actin. Values are plotted both for each ROI (small dots; Icorr of the same cell have the same color) and as mean Icorr for all ROIs of a single cell (large dots). From the latter the overall Icorr mean and SD for G-B-G and tubulin ( $0.68 \pm 0.02$ ) and G-B-G and actin ( $0.29 \pm 0.09$ ) were calculated. \*\* P=0.0021; unpaired t-test.

suggested to be part of GABARAP's tubulin binding motif in former *in vitro* studies. Compared to control cells expressing G-B-G,  $G^{5X}$ -B-G or G-B-G $^{5X}$  transfected cells expressing constructs with a single intact tubulin-binding motif mostly showed little to no enrichment at MTs as visualized by co-staining with SiR-tubulin (Figure 3A & Fig. S3A-C). Indeed,  $G^{5X}$ -B-G and G-B-G $^{5X}$  transfected cells were not distinguishable from  $G^{5X}$ -B-G $^{5X}$  expressing cells, indicating that substituting the basic amino acids in the second GABARAP molecule had no further influence on the result (Figure 3A, C & Fig. S3A-D). Additionally, Huh KO cells expressing G-B-G\* and co-stained with SiR-tubulin were imaged,



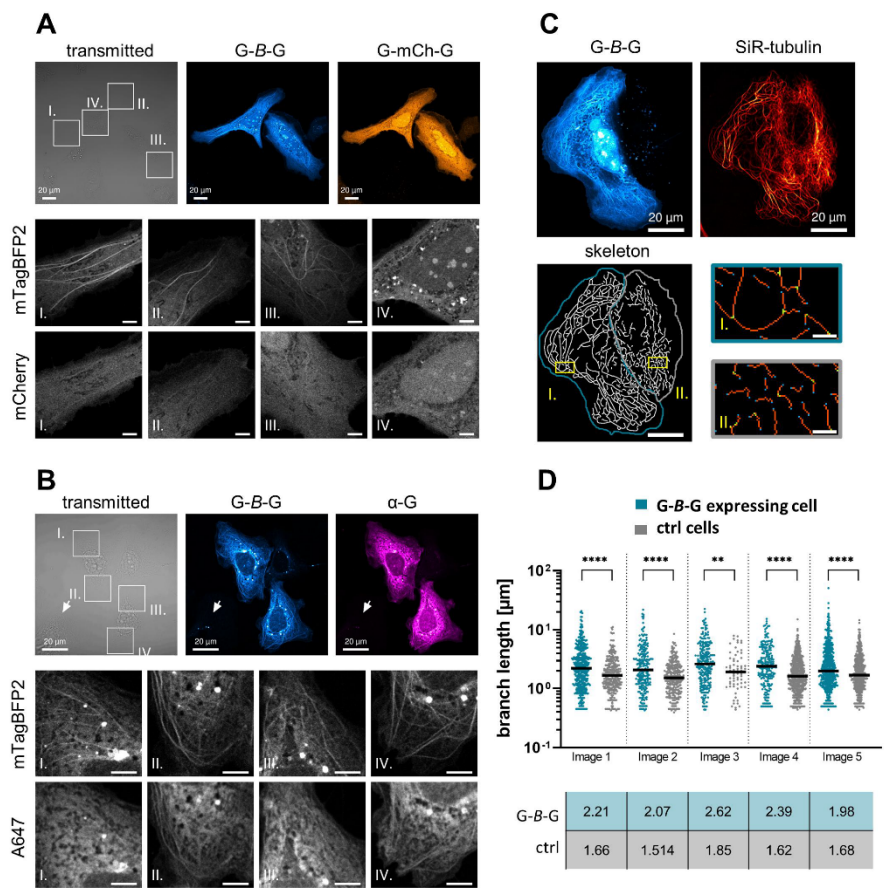


**Figure 4** FPs appear sensitive to the MT environment, while G-B-G can alter microtubule network organization (A) Exemplary image of G-B-G and G-mCh-G expressing Huh KO cells. The bottom panels show magnifications of four selected ROIs. Scale bars = 5  $\mu$ m (B) Exemplary image of G-B-G expressing cells fixed and immunostained with anti-GABARAP polyclonal primary antibody. Arrows indicates exemplary non-transfected control cell. The bottom panels show magnifications of four selected ROIs. Scalebars = 5  $\mu$ m (C) Altered microtubule organization in G-B-G expressing Huh KO cells. Top images show exemplary G-B-G expressing cell and control cell, both stained with SiR-tubulin (Image 1). Bottom images show skeleton of SiR-tubulin stain in Image 1. The G-B-G expressing cell is marked in blue, the control cell in gray. Skeleton was thresholded and dilated for visualization purposes. Exemplary regions are marked in yellow and shown as magnified ROIs (Scale bar = 2  $\mu$ m) from skeletonized image after tagging of endpoint (blue), junction (green) and slab (orange) pixels for each cell. (D) Quantification of branch length from 5 images (see Fig. S4D) each displaying a G-B-G expressing and control cell. \*\*\*\* P < 0.0001, \*\* P=0.0021, Mann-Whitney test. Individual branches are represented including medians, with values in table below the graph.

permitting investigation of whether lipidation is required for MT association, as the corresponding G-B-G\* fusion protein is devoid of C-terminal glycine residues suitable for lipidation in both GABARAPs. Interestingly, lipidation deficiency did not appear to inhibit enrichment of G-B-G\* at MTs, as cells expressing this construct presented themselves indistinguishable from cells expressing the unmodified G-B-G (Figure 3B, D & Fig. S3E).

These observations were again substantiated by quantitative analysis. While mean F:C ratios of G-B-G and G-B-G\* expressing cells showed no significant difference ( $1.62 \pm 0.37$  and  $1.58 \pm 0.39$ ), enrichment at filaments compared to adjacent cytoplasm was significantly lower for both G<sup>5X</sup>-B-G, G-B-G<sup>5X</sup> ( $1.16 \pm 0.17$ ,  $1.19 \pm 0.16$ ) and G<sup>5X</sup>-B-G<sup>5X</sup> ( $1.11 \pm 0.06$ ). These findings thus reinforce the conclusion already drawn from the monovalent constructs B-G and G-B (Fig. S1D, E) and support the idea of avidity-mediated affinity enhancement.

### ***Tandem GABARAP requires mTagBFP2 for visualization of its microtubule association and cytoskeletal remodeling***

To our surprise, when changing the FP from mTagBFP2 to mCherry (*mCh*) within the split-tandem construct, no highlighting of filamentous structures occurred in cells expressing G-*mCh*-G (Fig. S4A). As full-length translation and a good expression level of G-*mCh*-G, just as for any other tandem construct, was confirmed (Fig. S4B), we concluded that the behaviour of the GABARAP tandem was influenced by the type of FP selected. Therefore, we also inspected G-B-G and G-*mCh*-G co-expressing cells, and selected for those cells that showed a filamentous staining pattern in the blue channel. In such cells, filaments were also faintly visible in the red channel in some regions, though they were hard to distinguish from background (Figure 4A). To better understand this phenomenon, we next made some efforts to visualize MT-associated G-B-G independently of mTagBFP2's intrinsic fluorescence, using immunofluorescence. Fluorescence from mTagBFP2, even following fixation, was suitable to select for cells with a pronounced MT-like G-B-G pattern. Counterstaining the same cells with a polyclonal anti-GABARAP antibody in combination with an Alexa647-conjugated secondary antibody resulted in a prominent cytoplasmic staining pattern with very limited obvious filament staining particularly in the cell center (Figure 4B, I./III.). However, if one focuses on regions of the flattened cell periphery where less background from freely diffusing G-B-G is expected, a filamentous pattern was frequently evident also in the IF-stain (Figure 4B, II./IV.). Since the IF staining pattern obtained was reminiscent of the G-*mCh*-G staining pattern of cells cotransfected with G-B-G, we envision the vicinity of MTs as a preferable environment specifically for mTagBFP2 (see discussion for more details).



We finally used the same antibody in an immunofluorescence staining together with an anti-tubulin antibody to investigate what happens when GABARAP is overexpressed without any fusion partner (Fig. S4C). With this setup, no enrichment of GABARAP at MTs occurred, again in accordance with the idea of avidity-based affinity enhancement.

During investigation of G-B-G expressing cells, it became apparent that G-B-G decorated MTs often appeared strikingly long and curved, with a tendency to even build loops. To analyze this prominent alteration of the MT network, Huh KO cells expressing G-B-G were co-stained with SiR-tubulin. Pairs of untransfected cells and cells strongly expressing G-B-G were selected and analyzed regarding their MT network organization; we observed clear differences in the network throughout the analyzed cells, with G-B-G expressing cells presenting prominently long and curved MTs (Figure 4C). Skeletonization of filamental structures in the SiR channel and subsequent determination of branch length, defined as distance between endpoint and/or junction pixels, showed significantly longer branches for all analyzed G-B-G expressing cells (extending up to 50  $\mu\text{m}$ ) compared to control cells (Figure 4D, Fig. S4D). Additionally, cytoskeleton bundling parameters, namely coefficient of variance (CV) and skewness, were examined for pairs of G-B-G expressing and control cells with similar mean intensities in the SiR-channel (less than 1.6-fold difference, Image 1,2,5). Higher CV and Skewness values for G-B-G expressing cells compared to control cells supported the frequent visual observation of high SiR-tubulin intensities associated with pronounced, long MTs (Figure S4E). It is important to note that the altered MT network organization in G-B-G expressing cells was not only observable with SiR-tubulin staining, which is known to stabilize MTs, but also in fixed cells stained with an antibody against  $\beta$ -tubulin (Fig. S4F).

### ***AlphaFold predictions suggest charge-mediated GABARAP enrichment at microtubules rather than a distinct binding mode***

The presence of two GABARAP molecules in the fusion protein construct G-B-G appeared to be the critical factor for MT association. Using ColabFold to predict the structural arrangement of G-B-G with a protofilament composed of two tubulin dimers (TBA1A-TBB5), we sought to address the question whether this interaction is sterically plausible. First, orientation of the two GABARAP moieties towards the tubulin chain and of mTagBFP2 away from it was consistently observed, with the GABARAPs typically aligning with the tubulin protofilament in such a way that one protomer is skipped (Figure 5A, Fig. S5A). Despite significant variance among individual models regarding details of the predicted contacts, GABARAP was frequently suggested to associate with the negatively charged C-terminal tail present in both  $\alpha$ - and  $\beta$ -tubulin. Due to the inherent disorder of this segment, GABARAP is unlikely to

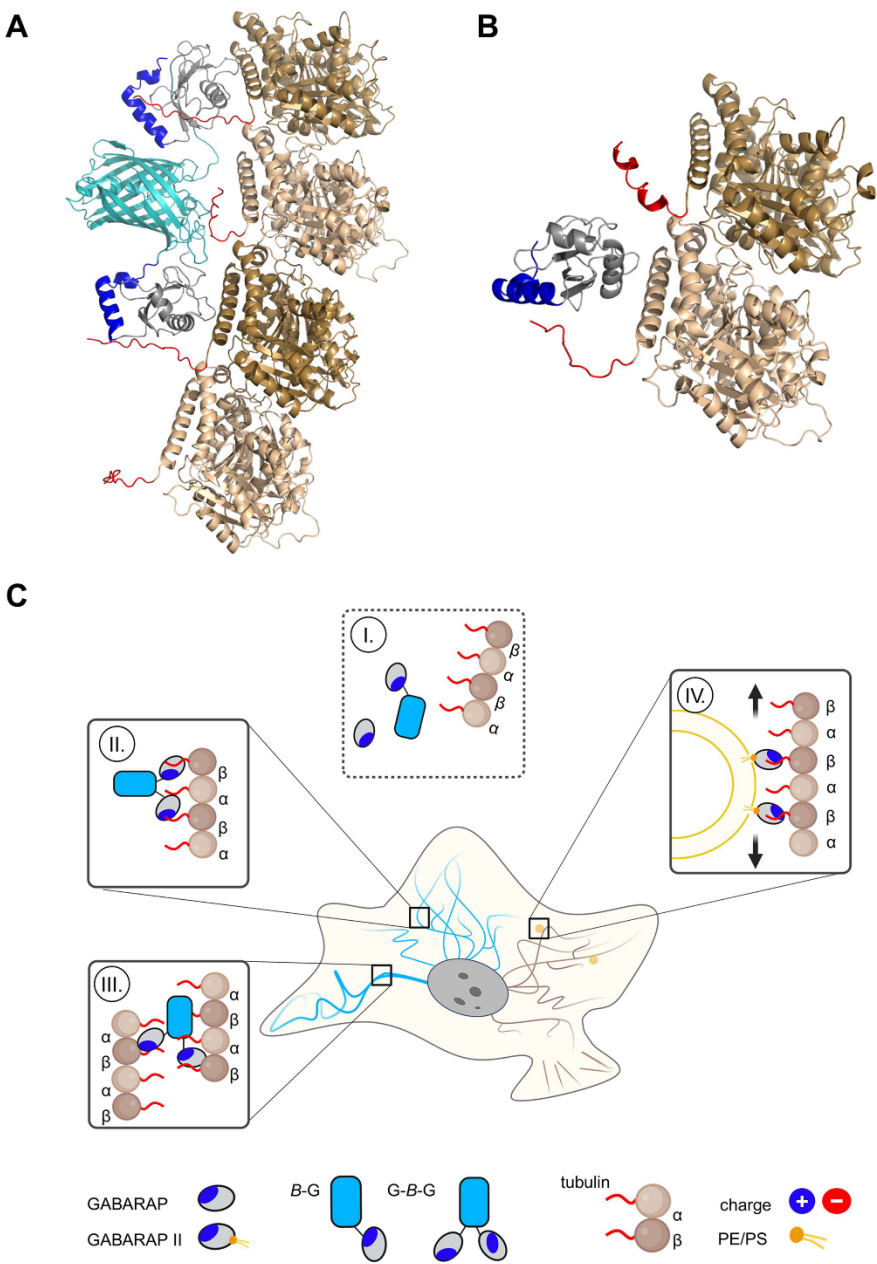


**Figure 5** Predictions support a GABARAP-tubulin interaction, although FP and valency of GABARAP likely influence the biological outcome. Complex models of tubulin oligomers with G-B-G (**A**) and GABARAP (**B**). This study's observations along with their possible biological consequences are summarized schematically in (**C**), with more details being explained in the main text. Created with BioRender.com



adopt a well-defined orientation relative to the globular tubulin core, as reflected by high PAE scores for intermolecular pairs of residues. With due caution owing to the complexity of the system, these predictions support the idea of electrostatic interactions between G-B-G and microtubules. Predictions of untagged GABARAP with a TBA1A-TBB5 dimer also hint at an attraction of GABARAP toward the exposed C-terminal tails of the tubulin monomers (Figure 5B, Fig. S5B). In accordance with the observation in cells, where B-G-G showed enrichment at MTs comparable to G-B-G, ColabFold predicted a similar charge-dominated tubulin interaction of GABARAP moieties, despite their shorter separation in B-G-G (Fig. S5C). However, predictions with untagged GABARAP and tetrameric tubulin did not yield consistent results, possibly indicating a lower interaction propensity. Notably, these calculations do not include the various post-translational modifications described for both GABARAP and tubulin and only represent tubulin dimers and tetramers of specific isotypes, TBB5 and TBA1A. However, both post-translational modifications and isotypes are important for structure and functions of MTs, as well as for interactions with other proteins, possibly including the proposed interaction with GABARAP.

## Discussion

The aim of this work was to exploit novel FP-based tagging strategies to microscopically track GABARAP, a member of the hATG8 family, in living cells, thereby identifying new options for visualizing its functionalities. We propose that in particular GABARAP tandem constructs may expand the scope of current strategies, such as the use of conventional N-terminal FP tags [45,46], or the use of LIR-based sensors [15,47-49]. While particularly N-terminal FP tags provide plenty of options to follow autophagic processes [14], smaller tags (such as HA) or tagless strategies are mandatory in certain situations [26,34]. Taking advantage of avidity through the combination of two GABARAP molecules in one construct, our strategy particularly targets GABARAP activities featuring only moderate interaction strengths for individual binding events.

In detail, we observed differences in the nucleocytoplasmic intensity ratios between G-B-G and the conventionally labeled Y-G (expressed simultaneously or separately) with an overall higher ratio for Y-G. Little is known about the role of GABARAP in the nucleus yet, and pronounced nuclear localization of ATG8s has been interpreted as an artefact in some settings [14]. For LC3B, which is characterized better in this respect, its nuclear pool [50], its differing levels across nuclear compartments [51], and its contribution to nuclear surveillance mechanisms are well described [52-54]; in part these findings may also apply for GABARAP. For instance, GABARAP binds, like LC3B, to lamin B1 [52] and is reported to be sensitive to deacetylase inhibitors [55], which is reminiscent of

acetylation-dependent shuttling of LC3B between nucleus and cytoplasm [50]. Notably, in *C. elegans* the GABARAP homolog LGG-1 is involved in modulating lifespan by regulating nuclear dynamics [56]. Higher intensities in the nucleoli compared to the nucleoplasm were observed for G-B-G and B-G compared to Y-G, suggesting that the FP choice and not the number of GABARAPs in the construct is decisive here. B-G might be an excellent choice to address GABARAP shuttling between nuclear compartments, technically even in a more direct way than previously reported for LC3B fusions with Venus, a close relative of YFP [53].

The most striking feature of G-B-G is its ability to highlight filamentous structures, namely MTs, in the cytoplasm, a behavior hitherto undocumented for conventional FP-tagged GABARAP/ATG8s. Notably, the FP itself significantly influenced the result, as demonstrated for G-mCh-G. As we do not have in-depth experimental data on this, we can only speculate on the reasons why mTagBFP2 appears to have a particular effect on the system studied here. In principle, the identity of the FP may influence the preferred relative orientation of the GABARAP moieties in the tandem construct and hence their MT interaction propensity, but this does not seem very likely given the insensitivity to the position of mTagBFP2 (G-B-G vs. B-G-G). Under certain conditions individual FPs themselves may exhibit an as yet uncharacterized intrinsic tubulin-binding capacity or may interact with certain MT-associated proteins, however, we are not aware of any described MT-binding of free mTagBFP2. In addition, we show that using mTagBFP2 within tubulin-binding incompetent GABARAP tandem constructs does not lead to association with MTs either. Besides a positive contribution of mTagBFP2 to MT association, an absence of negative effects (such as repulsion) compared to other FPs (e.g. mCherry) would also explain the differences observed. Fluorescent proteins are inherently sensitive to solution conditions, and certain environments are known to affect chromophore functionality and ultimately the measurable fluorescence intensity of some FPs [57-59]. It should be noted, that MTs have highly unusual electrical properties due to the exceptionally negatively charged C-termini of tubulin subunits giving rise to a length-dependent net dipole moment of the entire MT [60]. As one conceptual possibility the vicinity of an MT is suggested to be a confined zone of the cytoplasm with very special characteristics [60,61]. Thus, an alteration of the properties of the FP, locally restricted to the MT zone and maybe differently pronounced depending on the FP used, could also serve as a possible, albeit speculative explanation for our observations. Interestingly, G-B-G fluorescence retained a pronounced MT-like pattern even following fixation, while counterstaining with a polyclonal anti-GABARAP antibody resulted in a prominent cytoplasmic stain with only some filaments

visible in the flattened cell periphery. Curiously, a recent independent study also revealed different behaviors of mTagBFP (a close relative of mTagBFP2 [62,63]) and mCherry, interestingly in the context of a sensor for tyrosinated MTs [64]. Overall, the question why mTagBFP2 has this peculiar effect on the system studied here is awaiting a definite answer. Nonetheless, our results are significant because they show a striking example of what can in principle apply to any binding study with FP-target protein (e.g. GABARAP) fusion proteins: individual FPs may modulate the degree of visibility of the binding event of interest to different extents, either by differential “interference” with the binding itself (including both positive and negative contributions) or by different modulation of the fluorescence strength (enhancement or attenuation) by the environment of the FP in the bound state.

Nevertheless, there is abundant evidence for a seemingly robust interaction of GABARAP both with tubulin and assembled MTs *in vitro*. GST-GABARAP associates with purified tubulin but not actin, and heterologously expressed GABARAP interacted with *in-vitro* assembled MTs [36], supporting our observation that lipidation is not a prerequisite for G-B-G enrichment at MTs in cells. The tubulin-binding region was narrowed down to the first 35 residues of GABARAP [36], and positively charged residues promote GABARAP’s association with MTs through ionic interactions with the negatively charged C-terminal tails of the tubulin monomers [31,36]. This is consistent with our observation of significantly reduced MT association for  $G^{5X}$ -B-G, G-B- $G^{5X}$  and  $G^{5X}$ -B- $G^{5X}$ , which lack the basic residues K2, K13, R15, K20 and K23 in the first, the second or both GABARAP(s) of the split tandem. While colocalization of GABARAP with MTs has been demonstrated by immunofluorescence under endogenous conditions in Chinese hamster ovary cells more than 20 years ago, utilizing an in-house polyclonal anti-GABARAP antibody [36], this has not been consistently observed by other groups, presumably due to specific properties of the antibodies used. For instance, the epitope of the monoclonal antibody 8H5 developed in our lab [65] overlaps with the proposed tubulin-binding region of GABARAP, preventing detection of the MT-associated fraction. A commercially available polyclonal GABARAP antibody can visualize GABARAP at MTs, though staining is faint and restricted to cells overexpressing G-B-G. Notably, NMR experiments probing GABARAP with short peptides derived from the  $\alpha$ - or  $\beta$ -tubulin C-terminal tails revealed only moderate affinities (dissociation constants in the 0.1–0.2 mM range) with low specificity [30]. In agreement with these data, in our study constructs with a single GABARAP molecule (B-G, G-B) did not arrange in filamentous patterns within living cells, while two GABARAPs combined in a tandem reporter (G-B-G, B-G-G) were required and sufficient to robustly colocalise with MTs in living cells.

It is known that GABARAP can promote MT polymerization *in vitro* and that the first 22 N-terminal residues are sufficient for this purpose [31,35]. In addition, an MT-bundling activity was suspected for GABARAP [66] and for its close relative GABARAPL1 [67]. Shielding of the negatively charged C-terminal tails of tubulin protomers by positively charged patches on MT-associated proteins, as described for the cytoskeleton-associated protein glycine-rich (CAP-Gly) domain of p150<sup>glued</sup> [68], offers one possible mechanism for these *in-vitro* observations. Likewise, the basic N-termini of GABARAP and GABARAPL1 may neutralize the repulsive negative surface charge of MTs. Interestingly, we repeatedly observed an altered MT network organization including cytoskeleton bundling in G-B-G expressing cells, indicating that this GABARAP activity may indeed have significance *in vivo*. Since the G-B-G construct offers two tubulin binding sites, it also could bridge individual MTs to form bundles. The bundling promoting properties of the MT associated protein tau have been suggested to be based on a similar mechanism [69]. Remarkably, Nymann-Andersen et al. (2002) already discussed MT binding of GABARAP dimers [70]. How the observed MT network alterations are facilitated in detail, and to what extent the effects observed with the split tandem construct can be translated to wild-type cells expressing GABARAP at endogenous levels remains to be elucidated in future investigations. However, we hypothesize that, if GABARAP-mediated MT changes are relevant at all under endogenous GABARAP levels, they should be confined to well-defined patches of locally high GABARAP density, but are unlikely to produce such global changes in MT organization as observed under G-B-G overexpression.

Compared to the relatively controlled conditions *in vitro*, factors influencing MT dynamics and stability in living cells are much more complex. Stability determining factors include the prevalence of tubulin isoforms [71], different post-translational modifications [72-76], and the presence or absence of diverse MT associated proteins (MAPs, [77,78]), which often regulate transport along MTs [79,80]. Kinesin family member 5B (KIF5B), for instance, has been connected to lysosome transport in autophagy, and its depletion led to perinuclear accumulation of autophagosomes in cancer cells [81,82]. In the context of insulin vesicle transport a connection between KIF5B and GABARAP has been proposed, as GABARAP appears to promote vesicle trafficking by KIF5B [83]. Considering our results, it is conceivable that GABARAP not only presents transport vesicles to KIF5B by connecting vesicles and MTs and thereby stabilizing the kinesin-cargo complex, but at high local concentrations additionally stabilizes MTs and thereby supports KIF5B binding and corresponding anterograde vesicular transport.

Given that members of the LC3 subfamily of ATG8 proteins have been first described as light chains of the MT interacting proteins MAP1A and MAP1B [84,85], further connections between ATG8s and MTs do not seem far-fetched. Accordingly, the connection between autophagy and the

cytoskeleton has been extensively studied and reviewed [86-89]. Regarding autophagy-unrelated functions, an interplay between GABARAP and MTs has been suggested for the anterograde transport of e.g. the GABA<sub>A</sub>, angiotensin II type 1 and  $\kappa$  opioid receptors [46,90,91]. The LC3B-mediated transport of melanosomes along MTs and their detachment from MTs by ATG4B-mediated delipidation is another example of this connection [92].

In summary, while untagged and conventionally tagged GABARAP, e.g. *B-G*, do not visibly associate with MTs even under overexpression (Figure 5C-I), *G-B-G* accumulates on MTs (Figure 5C-II) owing to the bivalent nature of the construct and the yet to be defined role of mTagBFP2 in this process. Drechsler et al (2019) recently reported that multivalence is a critical property of MAPs, conferring MT-bundling abilities, optionally by bridging individual MTs which can lead to bundling [93]. However, as bundling could be an artificial activity of GABARAP tandems (Figure 5C-III), this aspect should be viewed with caution. GABARAP-decorated vesicles such as autophagosomes and endolysosomal vesicles [94], however, could present multiple GABARAPs in proximity to MTs, resulting in significant avidity through multivalence. Such multiple GABARAP-MT interactions might therefore assist in keeping those vesicles on the MT track, possibly promoting their transport (Figure 5C-IV).

As both impaired MT dynamics and defective autophagy as well as their interplay have been linked to human disease [95-97], understanding how GABARAP and other ATG8 proteins influence MT stability and related processes may also provide novel insights into pathophysiology and suggest improved strategies of intervention. While our results employing a GABARAP split tandem construct within living cells are not necessarily transferrable to the functionalities of endogenous GABARAP, our results may serve as a motivation to re-visit the GABARAP-microtubule interaction described more than 20 years ago using today's techniques.

## Abbreviation

ATG8: autophagy related protein 8  
 FP: fluorescent protein  
 GABARAP:  $\gamma$ -aminobutyric acid type A receptor-associated protein  
 Icorr: Index of correlation  
 KO: knockout  
 LDS: LIR docking site  
 LIR: LC3-interacting region  
 MAP1LC3/LC3: microtubule associated protein 1 light chain 3  
 MAP: microtubule associated protein  
 MT: microtubule  
 nMDP: normalized mean deviation product  
 ROI: region of interest  
 SiR: Silicon rhodamine

## Acknowledgment

We thank Tom Boissonnet and Vanessa Fuchs (Center for Advanced Imaging (CAI), Heinrich Heine University Düsseldorf, Germany) for their kind assistance in using OMERO and in submitting the data to the Bioline Archive. We are grateful to Bernd Hoffmann (IBI-2) supporting us with anti-tubulin antibody and the cytoskeleton fixation protocol.

## Data and material availability

Original imaging data is available on Bioline Archive at <https://www.ebi.ac.uk/biosciences/bioimages/studies/S-BIAD952>. All described plasmids are deposited at Addgene.

## Competing interests

The authors declare that they have no conflicts of interest with the contents of this article.

## Author contributions

Conceptualization: S.H., O.H.W., A.Ü., T.G.; validation: S.H., O.H.W., A.Ü.; formal analysis: A.Ü.; investigation: A.Ü., L.G., O.H.W.; resources: D.W.; data curation: A.Ü.; writing—original draft preparation: A.Ü., S.H.; writing – review and editing: S.H., O.H.W., A.Ü., T. G., L.G., D.W.; visualization: A.Ü.; supervision: S.H., O.H.W.; project administration: D.W.; funding acquisition: D.W.

## Funding

This work was funded by the Deutsche Forschungsgemeinschaft (DFG, German Research Foundation)—Project-ID 267205415—SFB 1208 to D.W.

## ORCID

Alina Üffing  <http://orcid.org/0000-0001-8808-1033>  
 Thomas Gensch  <http://orcid.org/0000-0002-3903-4705>  
 Oliver H. Weiergräber  <http://orcid.org/0000-0002-2410-3691>  
 Silke Hoffmann  <http://orcid.org/0000-0003-1414-8957>  
 Dieter Willbold  <http://orcid.org/0000-0002-0065-7366>

## References

1. Stangler T, Mayr LM, Willbold D. Solution structure of human GABA(A) receptor-associated protein GABARAP – Implications for biological function and its regulation. *J Biol Chem.* 2002 Apr 19;277(16):13363–13366. doi: [10.1074/jbc.C200050200](https://doi.org/10.1074/jbc.C200050200)

2. Komatsu M, Tanida I, Ueno T, et al. The C-terminal region of an Apg7p/Cvt2p is required for homodimerization and is essential for its E1 activity and E1-E2 complex formation. *J Biol Chem*. 2001 Mar 30;276(13):9846–54.
3. Tanida I, Tanida-Miyake E, Komatsu M, et al. Human Apg3p/Aut1p homologue is an authentic E2 enzyme for multiple substrates, GATE-16, GABARAP, and MAP-LC3, and facilitates the conjugation of hApg12p to hApg5p. *J Biol Chem*. 2002 Apr 19;277(16):13739–44.
4. Lystad AH, Carlsson SR, Simonsen A. Toward the function of mammalian ATG12-ATG5-ATG16L1 complex in autophagy and related processes. *Autophagy*. 2019 Aug;15(8):1485–1486.
5. Fracchiolla D, Chang C, Hurley JH, et al. A PI3K-WIP1 positive feedback loop allosterically activates LC3 lipidation in autophagy. *J Cell Biol*. 2020 Jul 6;219(7).
6. Li M, Hou Y, Wang J, et al. Kinetics comparisons of mammalian Atg4 homologues indicate selective preferences toward diverse Atg8 substrates. *J Biol Chem*. 2011 Mar 4;286(9):7327–38.
7. Fujita N, Itoh T, Omori H, et al. The Atg16L complex specifies the site of LC3 lipidation for membrane biogenesis in autophagy. *Mol Biol Cell*. 2008 May;19(5):2092–100.
8. Tamargo-Gomez I, Martinez-Garcia GG, Suarez MF, et al. ATG4D is the main ATG8 delipidating enzyme in mammalian cells and protects against cerebellar neurodegeneration. *Cell Death Differ*. 2021 Sep;28(9):2651–2672.
9. Ichimura Y, Kirisako T, Takao T, et al. A ubiquitin-like system mediates protein lipidation. *Nature*. 2000 Nov 23;408(6811):488–92.
10. Agrotis A, Pengo N, Burden JJ, et al. Redundancy of human ATG4 protease isoforms in autophagy and LC3/GABARAP processing revealed in cells. *Autophagy*. 2019 Jun;15(6):976–997.
11. Carosi JM, Nguyen TN, Lazarou M, et al. ATG8ylation of proteins: A way to cope with cell stress? *J Cell Biol*. 2021 Nov 1;220(11).
12. Sakamaki JI, Ode KL, Kurikawa Y, et al. Ubiquitination of phosphatidylethanolamine in organellar membranes. *Molecular Cell*. 2022;82(19):3677–3692.
13. Klionsky DJ. For the last time, it is GFP-Atg8, not Atg8-GFP (and the same goes for LC3). *Autophagy*. 2011 Oct;7(10):1093–4.
14. Klionsky DJ, Abdel-Aziz AK, Abdelfatah S, et al. Guidelines for the use and interpretation of assays for monitoring autophagy (4th edition). *Autophagy*. 2021 Jan;17(1):1–382.
15. Park SW, Jeon P, Jun YW, et al. Monitoring LC3- or GABARAP-positive autophagic membranes using modified RavZ-based probes. *Sci Rep*. 2019 Nov 12;9(1):16593.
16. Tanida I, Wakabayashi M, Kanematsu T, et al. Lysosomal turnover of GABARAP-phospholipid conjugate is activated during differentiation of C2C12 cells to myotubes without inactivation of the mTor kinase-signaling pathway. *Autophagy*. 2006 Oct-Dec;2(4):264–71.
17. Kabeya Y, Mizushima N, Yamamoto A, et al. LC3, GABARAP and GATE16 localize to autophagosomal membrane depending on form-II formation. *J Cell Sci*. 2004 Jun 1;117(13):2805–2812.
18. Martinez J, Almendinger J, Oberst A, et al. Microtubule-associated protein 1 light chain 3 alpha (LC3)-associated phagocytosis is required for the efficient clearance of dead cells. *Proc Natl Acad Sci USA*. 2011 Oct 18;108(42):17396–401.

19. Leidal AM, Huang HH, Marsh T, et al. The LC3-conjugation machinery specifies the loading of RNA-binding proteins into extracellular vesicles. *Nat Cell Biol.* 2020 Feb;22(2):187–199.
20. Heckmann BL, Teubner BJW, Tummers B, et al. LC3-associated endocytosis facilitates beta-amyloid clearance and mitigates neurodegeneration in murine alzheimer's disease. *Cell.* 2019 Jul 25;178(3):536–551 e14.
21. Solvik TA, Nguyen TA, Tony Lin YH, et al. Secretory autophagy maintains proteostasis upon lysosome inhibition. *J Cell Biol.* 2022 Jun 6;221(6):e202110151.
22. Wirth M, Zhang W, Razi M, et al. Molecular determinants regulating selective binding of autophagy adapters and receptors to ATG8 proteins. *Nat Commun.* 2019 May 3;10(1):2055.
23. Behrends C, Sowa ME, Gygi SP, et al. Network organization of the human autophagy system. *Nature.* 2010 Jul 1;466(7302):68–76.
24. Kim H, Kim H, Choi J, et al. visualization of autophagy progression by a red-green-blue autophagy sensor. *ACS Sens.* 2020 Dec 24;5(12):3850–3861.
25. Lazarou M, Sliter DA, Kane LA, et al. The ubiquitin kinase PINK1 recruits autophagy receptors to induce mitophagy. *Nature.* 2015 Aug 20;524(7565):309–314.
26. Nguyen TN, Padman BS, Usher J, et al. Atg8 family LC3/GABARAP proteins are crucial for autophagosome-lysosome fusion but not autophagosome formation during PINK1/Parkin mitophagy and starvation. *J Cell Biol.* 2016 Dec 19;215(6):857–874.
27. Krichel C, Möckel C, Schillinger O, et al. Solution structure of the autophagy-related protein LC3C reveals a polyproline II motif on a mobile tether with phosphorylation site. *Sci Rep.* 2019 Oct 2;9(1):14167.
28. Schwarten M, Stoldt M, Mohrlüder J, et al. Solution structure of Atg8 reveals conformational polymorphism of the N-terminal domain. *Biochem Biophys Res Commun.* 2010 May 7;395(3):426–31.
29. Möckel C, Kubiak J, Schillinger O, et al. Integrated NMR, fluorescence, and molecular dynamics benchmark study of protein mechanics and hydrodynamics. *J Phys Chem B.* 2019 Feb 21;123(7):1453–1480.
30. Knight D, Harris R, McAlister MSB, et al. The X-ray crystal structure and putative ligand-derived peptide binding properties of gamma-aminobutyric acid receptor type A receptor-associated protein. *J Biol Chem.* 2002 Feb 15;277(7):5556–5561.
31. Coyle JE, Qamar S, Rajashankar KR, et al. Structure of GABARAP in two conformations: Implications for GABA(A) receptor localization and tubulin binding. *Neuron.* 2002 Jan 3;33(1):63–74.
32. Pacheco V, Ma P, Thielmann Y, et al. Assessment of GABARAP self-association by its diffusion properties. *J Biomol NMR.* 2010 Sep;48(1):49–58.
33. Joachim J, Razi M, Judith D, et al. Centriolar Satellites Control GABARAP Ubiquitination and GABARAP-Mediated Autophagy. *Curr Biol.* 2017 Jul 24;27(14):2123–2136 e7.
34. Zhang W, Nishimura T, Gahlot D, et al. Autophagosome membrane expansion is mediated by the N-terminus and cis-membrane association of human ATG8s. *Elife.* 2023 Jun 8;12:e89185.
35. Wang HB, Bedford FK, Brandon NJ, et al. GABA(A)-receptor-associated protein links GABA(A) receptors and the cytoskeleton. *Nature.* 1999 Jan 7;397(6714):69–72.



36. Wang H, Olsen RW. Binding of the GABA(A) receptor-associated protein (GABARAP) to microtubules and microfilaments suggests involvement of the cytoskeleton in GABARAPGABA(A) receptor interaction. *J Neurochem.* 2000 Aug;75(2):644–55.
37. Dobner J, Simons IM, Rufinatscha K, et al. Deficiency of GABARAP but not its Paralogs Causes Enhanced EGF-induced EGFR Degradation. *Cells.* 2020 May 22;9(5):1296.
38. Gorlewicz A, Krawczyk K, Szczepankiewicz AA, et al. Colocalization colormap -an imageJ plugin for the quantification and visualization of colocalized signals. *Neuroinformatics.* 2020 Oct;18(4):661–664.
39. Jaskolski F, Mülle C, Manzoni OJ. An automated method to quantify and visualize colocalized fluorescent signals. *J Neurosci Methods.* 2005 Jul 15;146(1):42–9.
40. Ueda H, Yokota E, Kutsuna N, et al. Myosin-dependent endoplasmic reticulum motility and F-actin organization in plant cells. *Proc Natl Acad Sci USA.* 2010 Apr 13;107(15):6894–9.
41. Higaki T, Akita K, Katoh K. Coefficient of variation as an image-intensity metric for cytoskeleton bundling. *Sci Rep.* 2020 Dec 21;10(1):22187.
42. Evans R, O'Neill M, Pritzel A, et al. Protein complex prediction with AlphaFold-Multimer. *BioRxiv.* 2022. doi: [10.1101/2021.10.04.463034](https://doi.org/10.1101/2021.10.04.463034)
43. Mirdita M, Schütze K, Moriwaki Y, et al. ColabFold: making protein folding accessible to all. *Nat Methods.* 2022 Jun;19(6):679–682.
44. Cianfrocco MA, Wong-Barnum M, Youn C, et al. COSMIC2: A science gateway for cryo-electron microscopy structure determination. *Proceedings of the Practice and Experience in Advanced Research Computing 2017 on Sustainability, Success and Impact 2017.* New York, NY, USA: Association for Computing Machinery. p. 1–5.
45. Kabeya Y, Mizushima N, Ueno T, et al. LC3, a mammalian homologue of yeast Apg8p, is localized in autophagosome membranes after processing. *EMBO J.* 2000 Nov 1;19(21):5720–8.
46. Leil TA, Chen ZW, Chang CS, et al. GABAA receptor-associated protein traffics GABAA receptors to the plasma membrane in neurons. *J Neurosci.* 2004 Dec 15;24(50):11429–38.
47. Park SW, Jeon P, Yamasaki A, et al. Development of new tools to study membrane-anchored mammalian Atg8 proteins. *Autophagy.* 2023 May;19(5):1424–1443.
48. Stolz A, Putyrski M, Kutle I, et al. Fluorescence-based ATG8 sensors monitor localization and function of LC3/GABARAP proteins. *EMBO J.* 2017 Feb 15;36(4):549–564.
49. Lee YK, Jun YW, Choi HE, et al. Development of LC3/GABARAP sensors containing a LIR and a hydrophobic domain to monitor autophagy. *EMBO J.* 2017 Apr 13;36(8):1100–1116.
50. Huang R, Xu Y, Wan W, et al. Deacetylation of nuclear LC3 drives autophagy initiation under starvation. *Mol Cell.* 2015 Feb 5;57(3):456–66.
51. Koukourakis MI, Kalamida D, Giatromanolaki A, et al. Autophagosome proteins LC3A, LC3B and LC3C have distinct subcellular distribution kinetics and expression in cancer cell lines. *PLOS One.* 2015;10(9):e0137675.
52. Dou Z, Xu C, Donahue G, et al. Autophagy mediates degradation of nuclear lamina. *Nature.* 2015 Nov 5;527(7576):105–9.

53. Kraft LJ, Manral P, Dowler J, et al. Nuclear LC3 associates with slowly diffusing complexes that survey the nucleolus. *Traffic*. 2016 Apr;17(4):369–99.
54. Shim MS, Nettesheim A, Hirt J, et al. The autophagic protein LC3 translocates to the nucleus and localizes in the nucleolus associated to NUFIP1 in response to cyclic mechanical stress. *Autophagy*. 2020 Jul;16(7):1248–1261.
55. Baeken MW, Weckmann K, Diefenthaler P, et al. Novel insights into the cellular localization and regulation of the autophagosomal proteins LC3A, LC3B and LC3C. *Cells*. 2020 Oct 18;9(10):2315.
56. Kumar AV, Kang T, Thakurta TG, et al. Exportin 1 modulates life span by regulating nucleolar dynamics via the autophagy protein LGG-1/GABARAP. *Sci Adv*. 2022 Apr;8(13):eabj1604.
57. Kneen M, Farinas J, Li Y, et al. Green fluorescent protein as a noninvasive intracellular pH indicator. *Biophys J*. 1998 Mar;74(3):1591–9.
58. Roberts TM, Rudolf F, Meyer A, et al. Identification and characterisation of a pH-stable GFP. *Sci Rep*. 2016 Jun 21;6:28166.
59. Zhong S, Navaratnam D, Santos-Sacchi J. A genetically-encoded YFP sensor with enhanced chloride sensitivity, photostability and reduced pH interference demonstrates augmented transmembrane chloride movement by gerbil prestin (SLC26a5). *PLOS One*. 2014;9(6):e99095.
60. Kalra AP, Eakins BB, Patel SD, et al. All wired up: an exploration of the electrical properties of microtubules and tubulin. *ACS Nano*. 2020 Dec 22;14(12):16301–16320.
61. Kalra AP, Benny A, Travis SM, et al. Electronic energy migration in microtubules. *ACS Cent Sci*. 2023 Mar 22;9(3):352–361.
62. Subach OM, Cranfill PJ, Davidson MW, et al. An enhanced monomeric blue fluorescent protein with the high chemical stability of the chromophore. *PLOS One*. 2011;6(12):e28674.
63. Subach OM, Gundorov IS, Yoshimura M, et al. Conversion of red fluorescent protein into a bright blue probe. *Chem Biol*. 2008 Oct 20;15(10):1116–24.
64. Kesarwani S, Lama P, Chandra A, et al. Genetically encoded live-cell sensor for tyrosinated microtubules. *J Cell Biol*. 2020 Oct 5;219(10):e201912107.
65. Simons IM, Mohrlüder J, Feederle R, et al. The highly GABARAP specific rat monoclonal antibody 8H5 visualizes GABARAP in immunofluorescence imaging at endogenous levels. *Sci Rep*. 2019 Jan 24;9(1):526.
66. Yoon Y, Oakley BR. Purification and characterization of assembly-competent tubulin from *Aspergillus nidulans*. *Biochemistry*. 1995 May 16;34(19):6373–81.
67. Mansuy V, Boireau W, Fraichard A, et al. GEC1, a protein related to GABARAP, interacts with tubulin and GABA(A) receptor. *Biochem Biophys Res Commun*. 2004 Dec 10;325(2):639–48.
68. Wang Q, Crevenna AH, Kunze I, et al. Structural basis for the extended CAP-Gly domains of p150(glued) binding to microtubules and the implication for tubulin dynamics. *Proc Natl Acad Sci USA*. 2014 Aug 5;111(31):11347–52.
69. Feinstein HE, Benbow SJ, LaPointe NE, et al. Oligomerization of the microtubule-associated protein tau is mediated by its N-terminal sequences: implications for normal and pathological tau action. *J Neurochem*. 2016 Jun;137(6):939–54.
70. Nymann-Andersen J, Wang HB, Olsen RW. Biochemical identification of the binding domain in the GABA(A) receptor-associated protein (GABARAP) mediating dimer formation. *Neuropharmacology*. 2002 Sep;43(4):476–481.

71. Fu G, Yan S, Khoo CJ, et al. Integrated regulation of tubulin tyrosination and microtubule stability by human alpha-tubulin isoforms. *Cell Rep.* 2023 Jun 21;42(6):112653.
72. Portran D, Schaedel L, Xu Z, et al. Tubulin acetylation protects long-lived microtubules against mechanical ageing. *Nat Cell Biol.* 2017 Apr;19(4):391–398.
73. Eshun-Wilson L, Zhang R, Portran D, et al. Effects of alpha-tubulin acetylation on microtubule structure and stability. *Proc Natl Acad Sci USA.* 2019 May 21;116(21):10366–10371.
74. Tas RP, Chazeau A, Cloin BMC, et al. Differentiation between oppositely oriented microtubules controls polarized neuronal transport. *Neuron.* 2017 Dec 20;96(6):1264–1271 e5.
75. Konno A, Ikegami K, Konishi Y, et al. *Ttll9*<sup>-/-</sup> mice sperm flagella show shortening of doublet 7, reduction of doublet 5 polyglutamylation and a stall in beating. *J Cell Sci.* 2016 Jul 15;129(14):2757–66.
76. Bonnet C, Boucher D, Lazereg S, et al. Differential binding regulation of microtubule-associated proteins MAP1A, MAP1B, and MAP2 by tubulin polyglutamylation. *J Biol Chem.* 2001 Apr 20;276(16):12839–48.
77. Shigematsu H, Imasaki T, Doki C, et al. Structural insight into microtubule stabilization and kinesin inhibition by Tau family MAPs. *J Cell Biol.* 2018 Dec 3;217(12):4155–4163.
78. Cuveillier C, Delaroche J, Seggio M, et al. MAP6 is an intraluminal protein that induces neuronal microtubules to coil. *Science Advances.* 2020;6:eaaz4344.
79. Konishi Y, Setou M. Tubulin tyrosination navigates the kinesin-1 motor domain to axons. *Nat Neurosci.* 2009 May;12(5):559–67.
80. Kapitein LC, Schlager MA, Kuijpers M, et al. Mixed microtubules steer dynein-driven cargo transport into dendrites. *Curr Biol.* 2010 Feb 23;20(4):290–9.
81. Guardia CM, Farias GG, Jia R, et al. BORC functions upstream of kinesins 1 and 3 to coordinate regional movement of lysosomes along different microtubule Tracks. *Cell Rep.* 2016 Nov 15;17(8):1950–1961.
82. Cardoso CM, Groth-Pedersen L, Hoyer-Hansen M, et al. Depletion of kinesin 5B affects lysosomal distribution and stability and induces peri-nuclear accumulation of autophagosomes in cancer cells. *PLOS One.* 2009;4(2):e4424.
83. Asano S, Nemoto T, Kitayama T, et al. Phospholipase C-related catalytically inactive protein (PRIP) controls KIF5B-mediated insulin secretion. *Biol Open.* 2014 May 8;3(6):463–74.
84. Mann SS, Hammarback JA. Molecular characterization of light chain 3. A microtubule binding subunit of MAP1A and MAP1B. *Journal of Biological Chemistry.* 1994;269(15):11492–11497.
85. Kouno T, Mizuguchi M, Tanida I, et al. Solution structure of microtubule-associated protein light chain 3 and identification of its functional subdomains. *J Biol Chem.* 2005 Jul 1;280(26):24610–7.
86. Monastyrsky I, Rieter E, Klionsky DJ, et al. Multiple roles of the cytoskeleton in autophagy. *Biol Rev Camb Philos Soc.* 2009 Aug;84(3):431–48.
87. Mackeh R, Perdiz D, Lorin S, et al. Autophagy and microtubules – new story, old players. *J Cell Sci.* 2013 Mar 1;126(Pt 5):1071–80.
88. Kast DJ, Dominguez R. The cytoskeleton-autophagy connection. *Curr Biol.* 2017 Apr 24;27(8):R318–R326.
89. Kimura S, Noda T, Yoshimori T. Dynein-dependent movement of autophagosomes mediates efficient encounters with lysosomes. *Cell Struct Funct.* 2008;33.

90. Cook JL, Re RN, deHaro DL, et al. The trafficking protein GABARAP binds to and enhances plasma membrane expression and function of the angiotensin II type 1 receptor. *Circ Res*. 2008 Jun 20;102(12):1539–47.
91. Chen C, Wang Y, Huang P, et al. Effects of C-terminal modifications of GEC1 protein and gamma-aminobutyric acid type A (GABA(A)) receptor-associated protein (GABARAP), two microtubule-associated proteins, on kappa opioid receptor expression. *J Biol Chem*. 2011 Apr 29;286(17):15106–15.
92. Ramkumar A, Murthy D, Raja DA, et al. Classical autophagy proteins LC3B and ATG4B facilitate melanosome movement on cytoskeletal tracks. *Autophagy*. 2017 Aug 3;13(8):1331–1347.
93. Drechsler H, Xu Y, Geyer VF, et al. Multivalent electrostatic microtubule interactions of synthetic peptides are sufficient to mimic advanced MAP-like behavior. *Mol Biol Cell*. 2019 Nov 15;30(24):2953–2968.
94. Durgan J, Florey O. Many roads lead to CASM: Diverse stimuli of noncanonical autophagy share a unifying molecular mechanism. *Sci Adv*. 2022 Oct 28;8(43):eabo1274.
95. Naren P, Samim KS, Tryphena KP, et al. Microtubule acetylation dyshomeostasis in Parkinson's disease. *Transl Neurodegener*. 2023 May 8;12(1):20.
96. Guo F, Liu X, Cai H, et al. Autophagy in neurodegenerative diseases: pathogenesis and therapy. *Brain Pathol*. 2018 Jan;28(1):3–13.
97. Arduino DM, Esteves AR, Cortes L, et al. Mitochondrial metabolism in Parkinson's disease impairs quality control autophagy by hampering microtubule-dependent traffic. *Hum Mol Genet*. 2012 Nov 1;21(21):4680–702.

## Supplementary information (SI)

### SI Methods

#### Immunocytochemistry

Transfected Huh-7.5 *GABARAP* SKO cells shown in Fig.S4C were washed in Cytoskeleton buffer (CB, 150 mM NaCl, 5 mM MgCl<sub>2</sub>, 5 mM EGTA, 5 mM glucose, 10 mM MES, 1 g/L streptomycin) and fixed in 3.7% PFA in CB for 20 min at 37°C. The reaction was stopped with 30 mM glycine in CB for 5 min, like all following steps, if not indicated otherwise, at room temperature. The cells were permeabilized with 2% Triton-X-100 for 2 min, washed thrice for 5 min with CB and non-specific binding sites were blocked with 5% (w/v) milk powder in CB for 30-45 min. Afterwards, cells were incubated with primary antibodies against GABARAP (anti-GABARAP rabbit polyclonal [Proteintech, 18723-I-AP] diluted 1:100 in CB containing 1% (w/v) milk powder and against  $\alpha$ -tubulin (anti- $\alpha$ -tubulin, rat monoclonal clone YL1/2, [Sigma-Aldrich, MAB1864]) diluted 1:200 in CB containing 1% (w/v) milk powder for 1 h at 37°C. Next, cells were washed thrice in CB and stained with secondary antibodies (anti-rabbit-Alexa647 [abcam, ab150083] and anti-rat-CY3 [Jackson ImmunoResearch, 112-165-006]) diluted 1:200 in CB containing 1% (w/v) milk powder for 45 min at 37°C. After 2 washes in CB, and one in PBS (137 mM NaCl, 2.7 mM KCl, 1.8 mM KH<sub>2</sub>PO<sub>4</sub>, 10 mM Na<sub>2</sub>HPO<sub>4</sub>, pH 7.4), cells were imaged and stored in PBS containing 0.05% (w/v) sodium azide. Transfected Huh-7.5 *GABARAP* SKO cells shown in Fig.S4F were fixed for 10 min with precooled methanol and subsequently for 1 minute with precooled acetone, both at -20°C. After two washes with PBS, non-specific binding sites were blocked with 5% (w/v) BSA in PBS for 1 h. Cells were incubated with anti- $\beta$ -tubulin-CY3 mouse monoclonal [Sigma Aldrich, C4585]) diluted 1:100 in PBS containing 1% (w/v) BSA (AppliChem, A1391) and 0.3% (v/v) Triton X-100 (AppliChem, A4975) for 2 h or overnight and afterwards washed twice with PBS. Finally, cells were imaged and stored in PBS containing 0.05% (w/v) sodium azide.

#### Immunoblotting

Transfected Huh-7.5 *GABARAP* SKO cells were harvested by trypsinization, washed once in PBS and lysed with NP40 buffer (20 mM Tris HCl, 200 mM NaCl, 1 mM EDTA, 0.5% NP40, 1 mM PMSF and 1x Halt Protease and Phosphatase inhibitor [Thermo Fisher Scientific, 78442]) by incubation on ice for 30 min and vigorous pipetting every 10 min. Insoluble cell parts were sedimented by centrifugation for 10 min at 17,000 x g. Total protein concentration of supernatant was determined by BCA assay (Thermo Scientific, 23225). Samples were separated by SDS-PAGE using precast stain-free gels (Bio-Rad Laboratories, 4568124), transferred to 0.2  $\mu$ M PVDF membranes (Bio-Rad Laboratories, 1704156) and blocked in 5% BSA (AppliChem, A1391) in TBS-T (136 mM NaCl, 2.7 mM KCl, 24.7 mM Tris-HCl, pH 7.4, 0.05% Tween-20 [AppliChem, A4974]) for 1 h. Membrane was incubated with primary anti GABARAP antibody (Cell Signaling Technology, 13733) overnight at 4°C, washed 3 times with TBS-T, incubated with secondary antibody (goat anti-rabbit, HRP-conjugated [Dako, P0448]) for 1 h at room temperature and again washed thrice with TBS-T. Signals were visualized with Clarity western ECL substrate (Bio-Rad Laboratories, 1705061).

## SI Figures

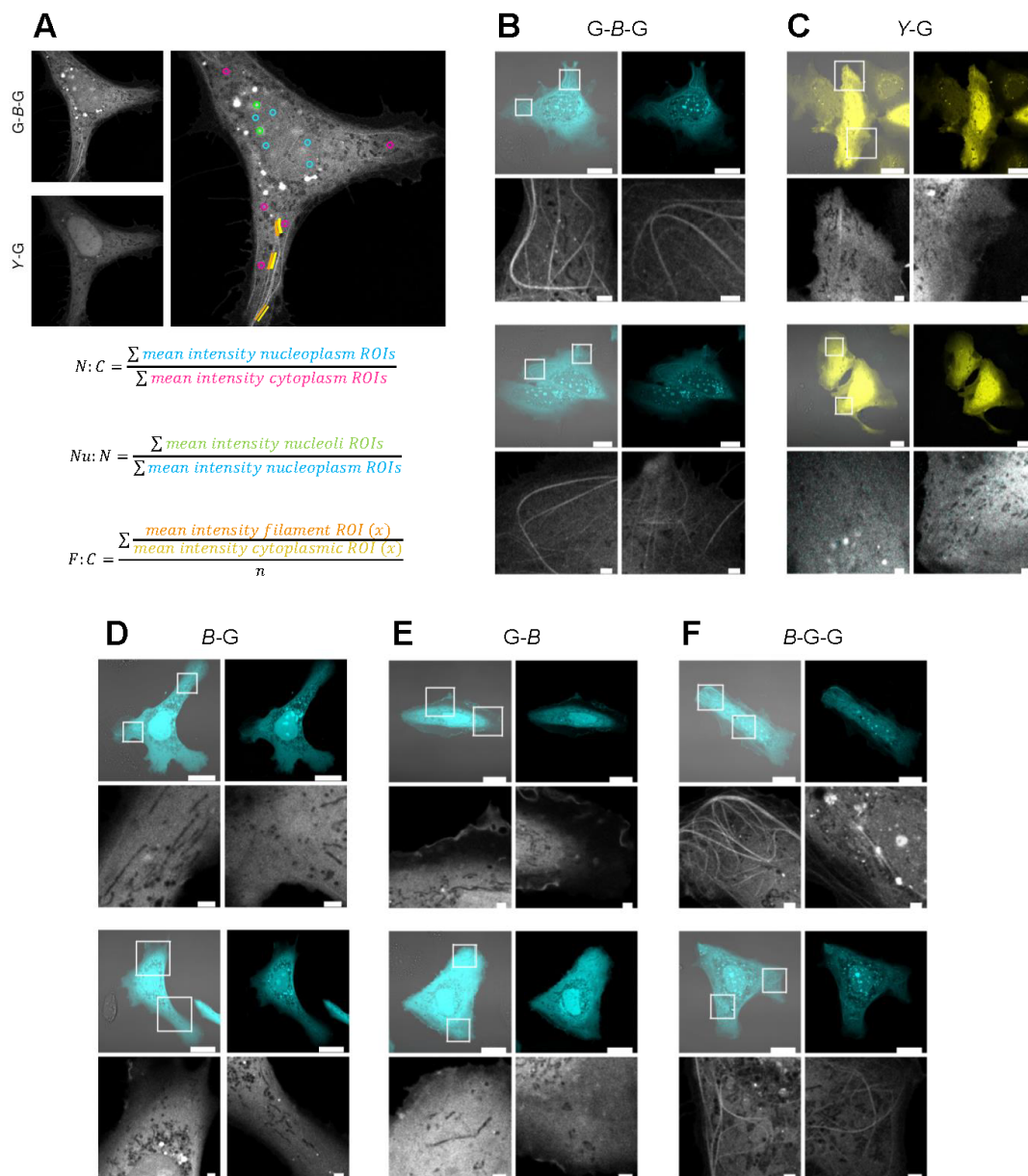


**Figure S1.** (A) Example of cytoplasmic, nucleoplasmic, nucleoli and filament ROIs in a Huh KO cell expressing G-B-G and Y-G as well as the formulas used for calculation of N:C, Nu:N and F:C ratios. All images and ROIs of cells analyzed accordingly can be found on BioImageArchive. (B-F) Live cell images of Huh KO cells expressing G-B-G (B), Y-G (C), B-G (D), G-B (E) B-G-G (F). Whole cells (merge with transmitted and G-B-G channel) as well as detailed ROIs are shown for two cells per construct. Scale bars represent 20  $\mu\text{m}$  for whole cells and 2  $\mu\text{m}$  for zoom ins.



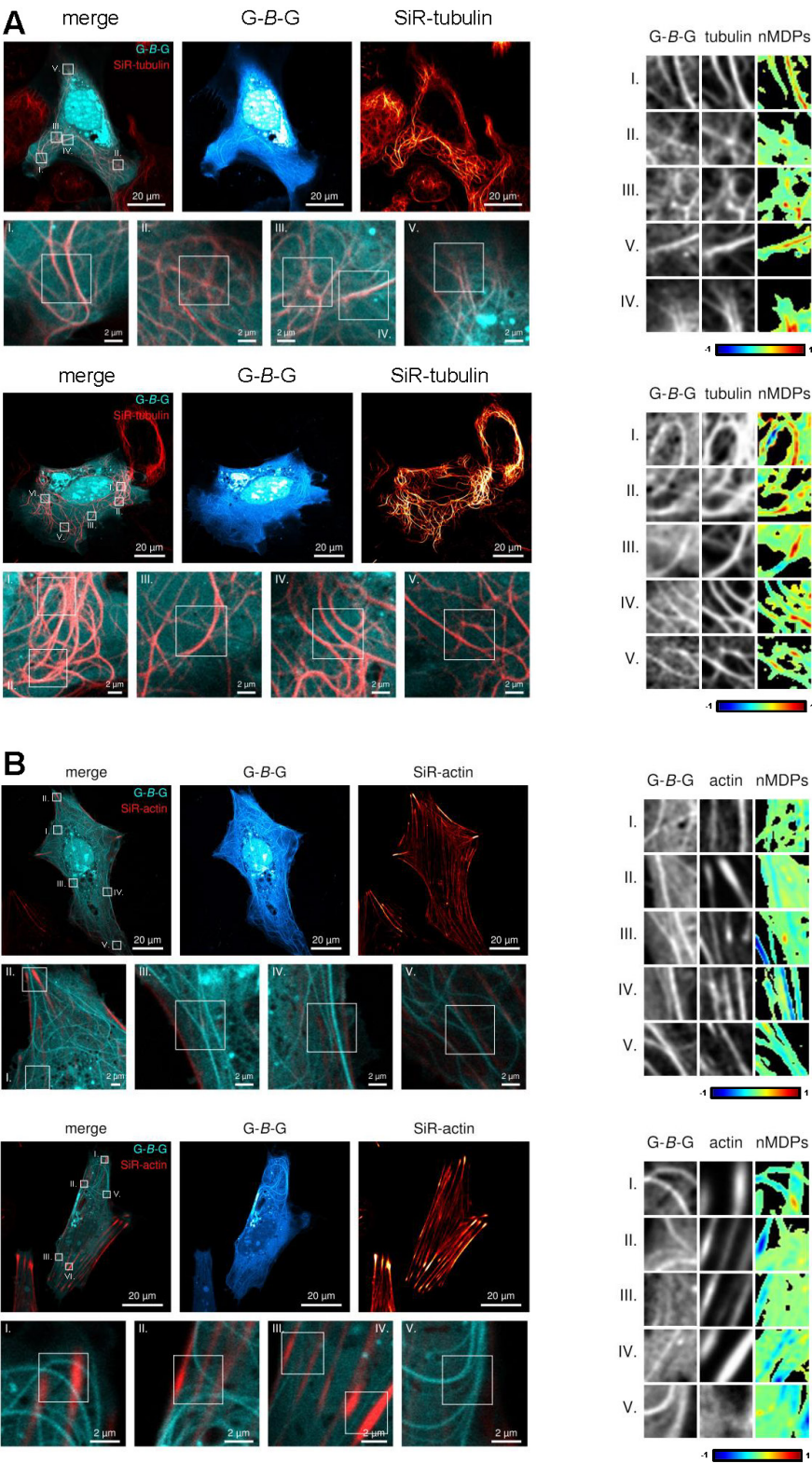
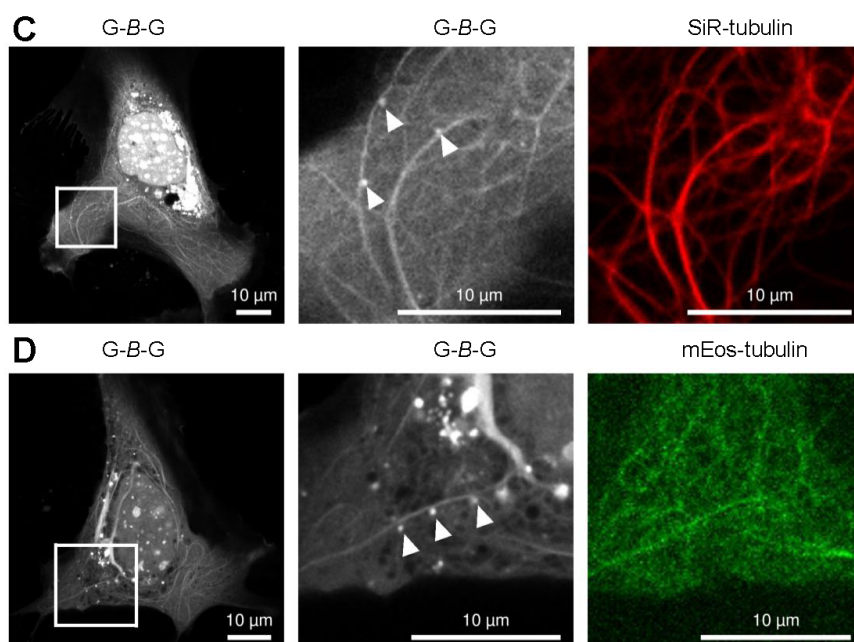
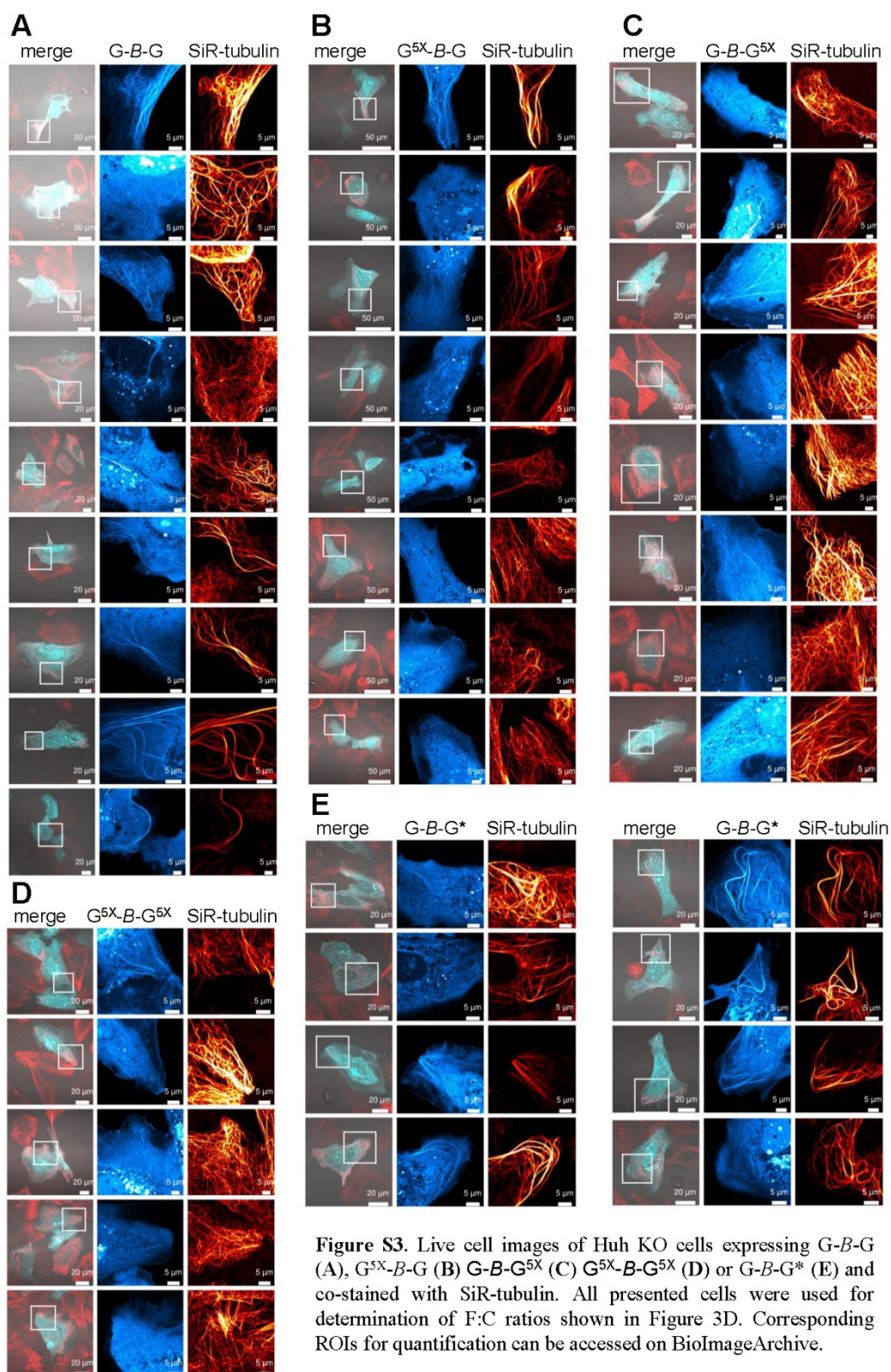


Figure S2. Continued on the following page.



**Figure S2.** Live cell images of Huh KO cells expressing G-B-G and stained either with SiR-tubulin (A) or SiR-actin (B) together with their colocalization colormaps. The corresponding Icorr values are included within the graph given in Fig. 2D. (C-D) Live cell images of Huh KO cells expressing G-B-G and either co-stained with SiR-tubulin (C) or co-transfected with a plasmid encoding mEos-tubulin (D) Zoom in images show microtubules decorated with G-B-G positive puncta, likely transport vesicles.





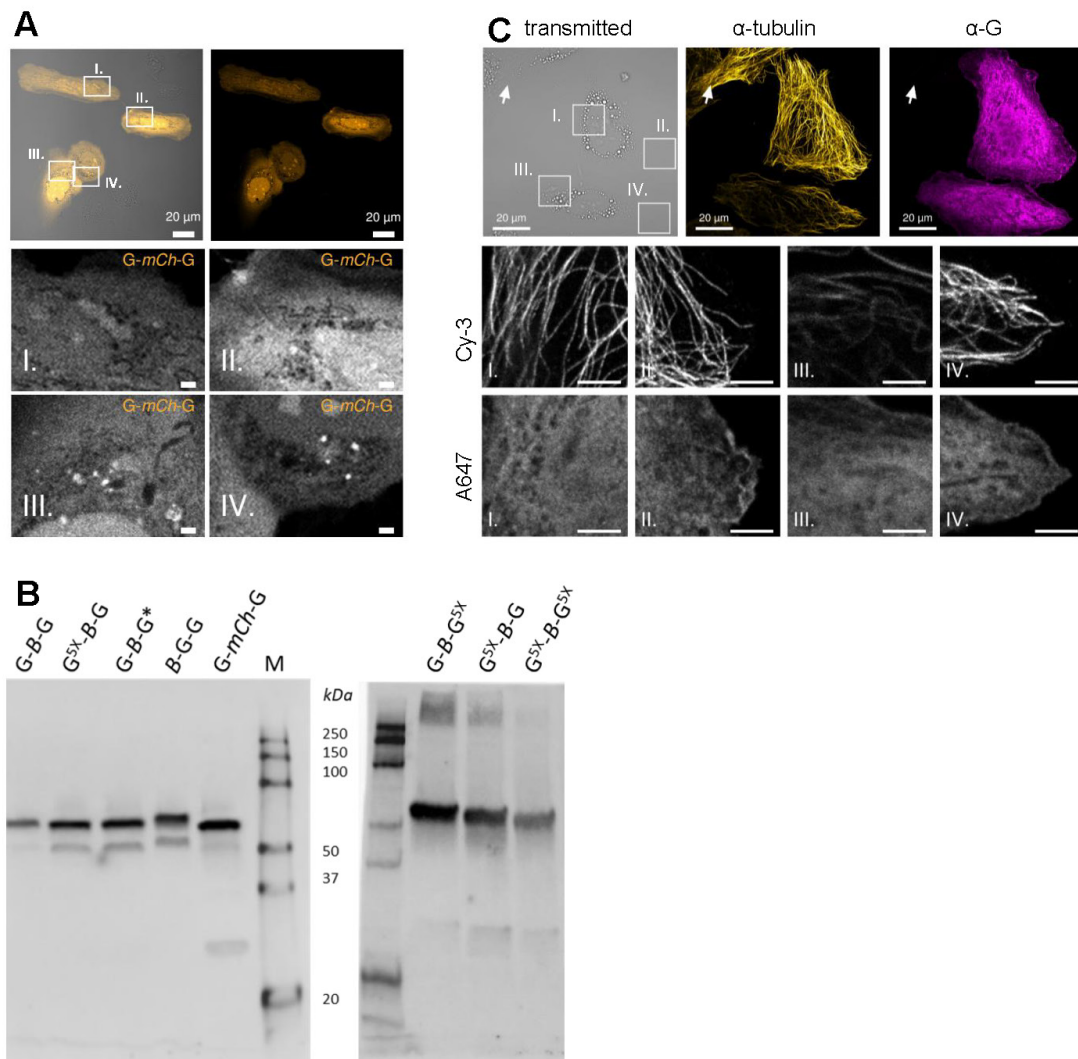


**Figure S4.** Continued on the following page.

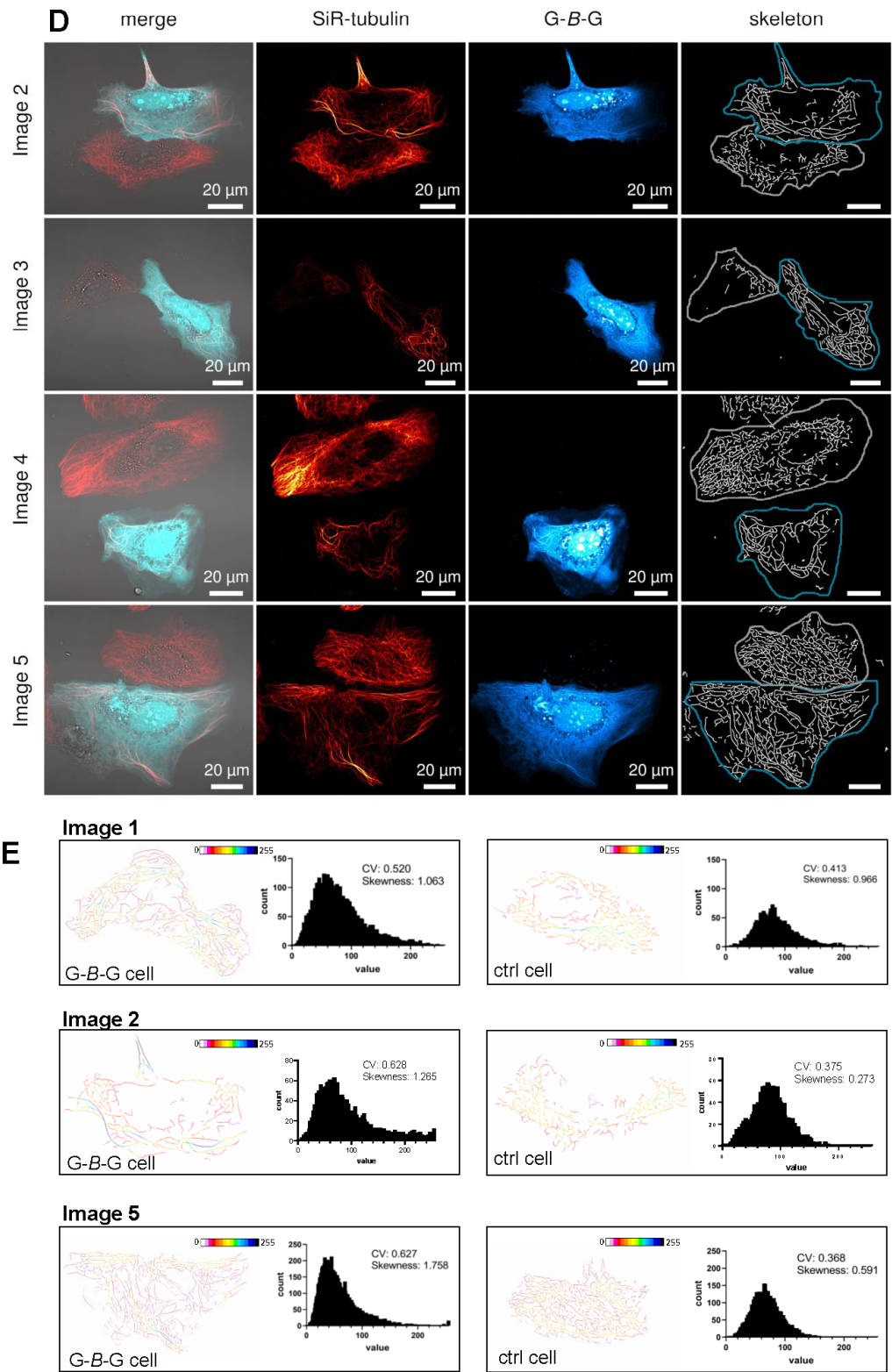
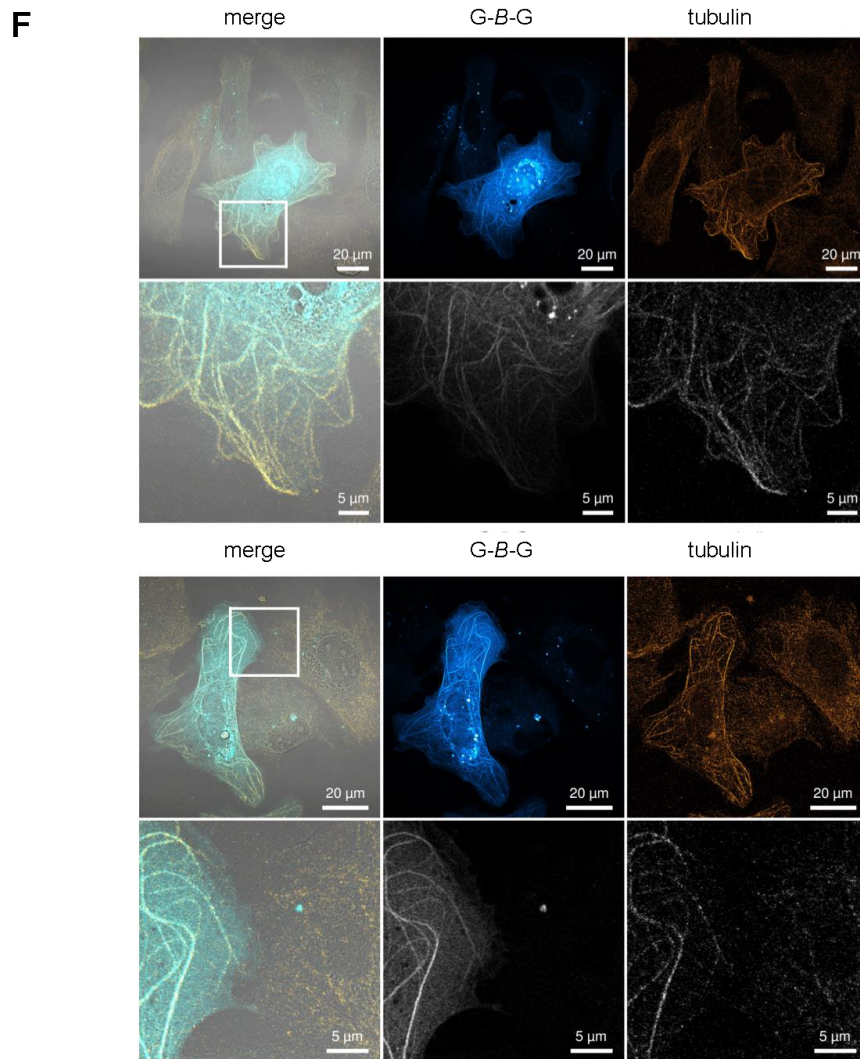
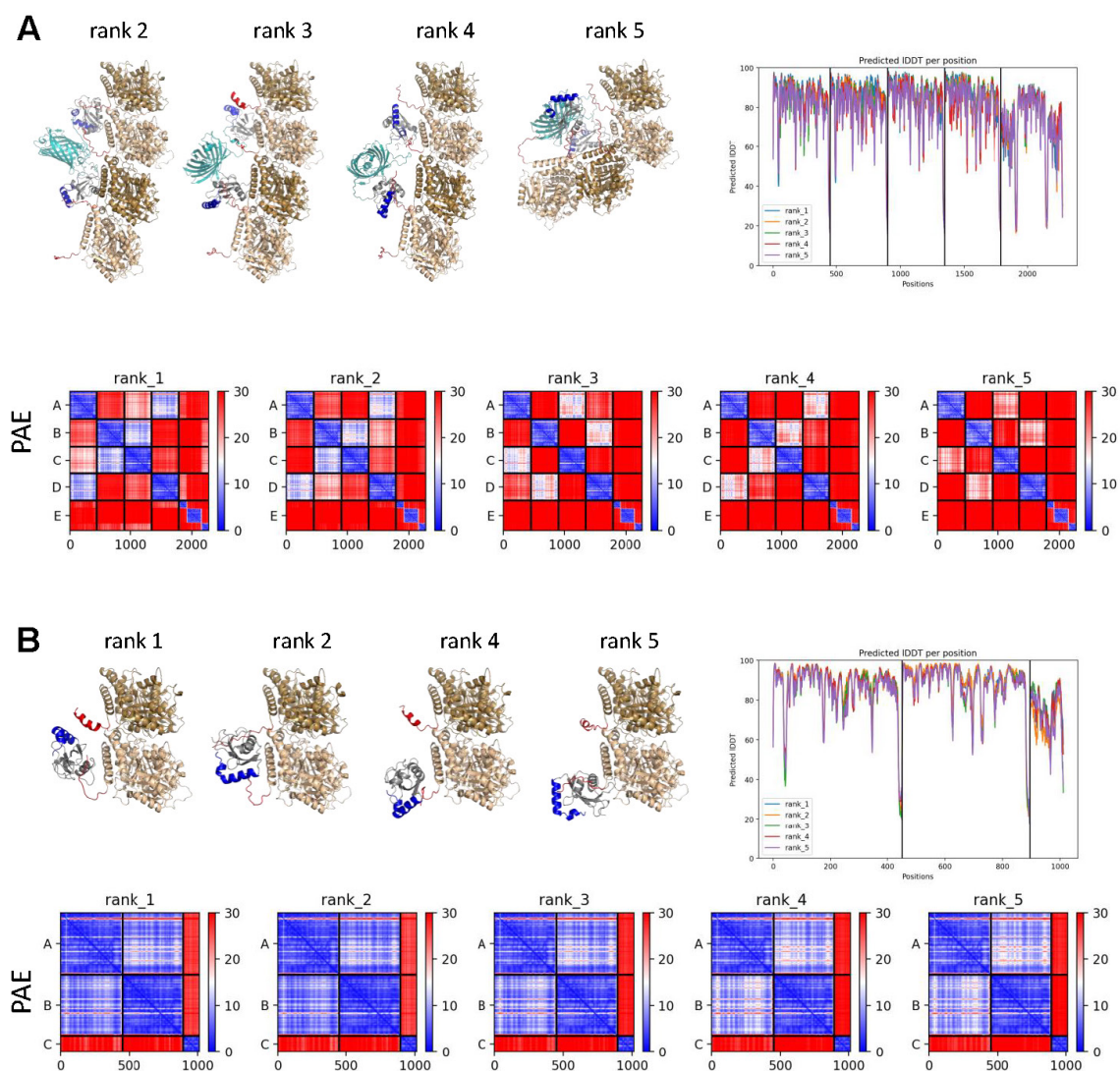


Figure S4. Continued on the following page.





**Figure S4.** (A) Huh KO cells expressing split tandem construct *G-mCh-G*. The bottom panels show magnifications (Scale bars = 2  $\mu$ m) of four selected ROIs. (B) Full length expression of different split tandem constructs (*G-B-G*, *G<sup>5X</sup>-B-G*, *G-B-G\**, *B-G-G*, *G-mCh-G* and *G-B-G<sup>5X</sup>*, *G<sup>5X</sup>-B-G* (shown on both membranes), *G<sup>5X</sup>-B-G<sup>5X</sup>*) was confirmed by Immunoblot from whole cell lysates of Huh KO cells transfected with the respective plasmids and staining with GABARAP antibody (Cell Signaling Technology, 13733). The most intense bands were detected at the expected size of the construct at approximately 55 kDa. The signal at about 25 kDa is unlikely to contribute to fluorescence signal in cells. Ladder: BioRad, #1610375. (C) Huh KO cells expressing GABARAP (without tag), fixed and stained with primary antibodies against tubulin and GABARAP (Sigma-Aldrich, MAB1864 & Proteintech, 18723-I-AP). Arrows indicate exemplary non-transfected control cell. The bottom panels show magnifications (Scale bars = 5  $\mu$ m) of four selected ROIs for both channels. (D) Images of Huh KO cell pairs, one expressing *G-B-G* and a second untransfected control cell, stained with SiR-tubulin. Skeletons, thresholded and dilated for visualization, for analysis of branch length as shown in Figure 4C are displayed. (E) For image 1, 2 and 5, color coded skeletons according to tubulin intensity values and corresponding cytoskeleton bundling parameters are displayed (F) Images of fixed Huh cells transiently transfected with plasmid encoding *G-B-G* and stained with an antibody against tubulin. Cells showing strong *G-B-G* expression present an altered tubulin staining pattern.



**Figure S5.** Continued on the following page.

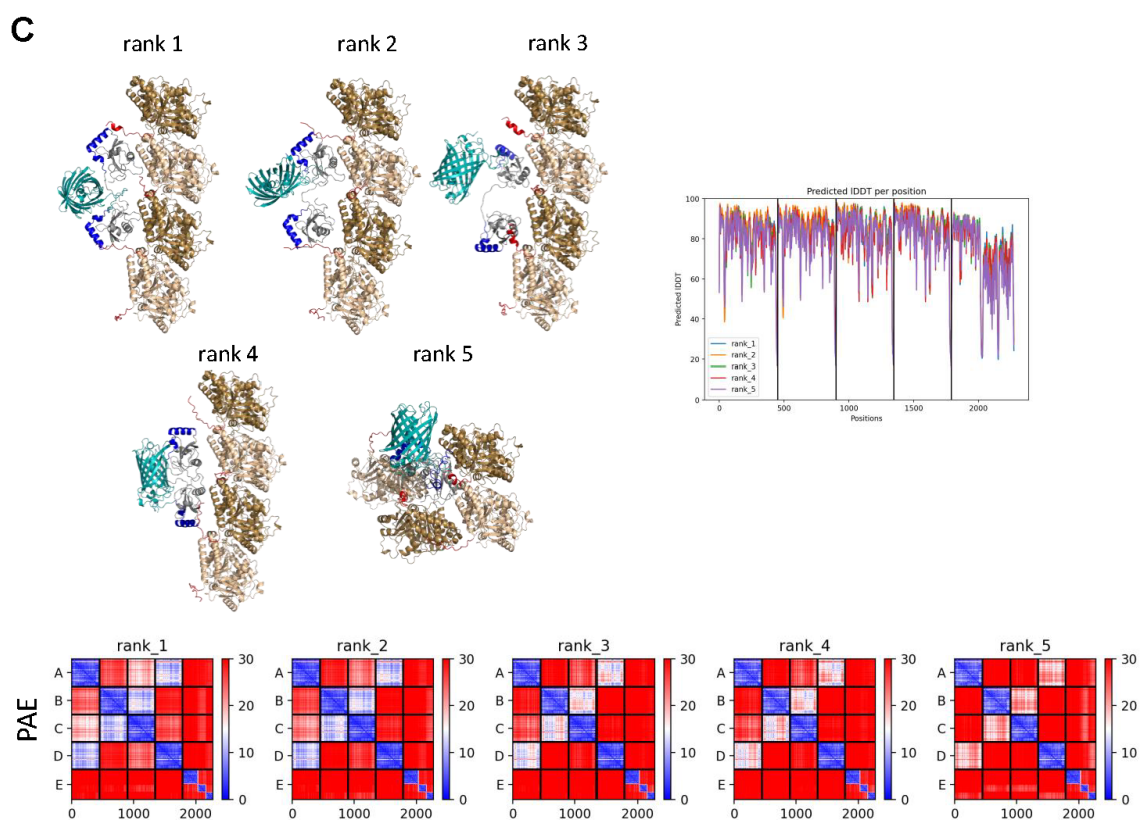
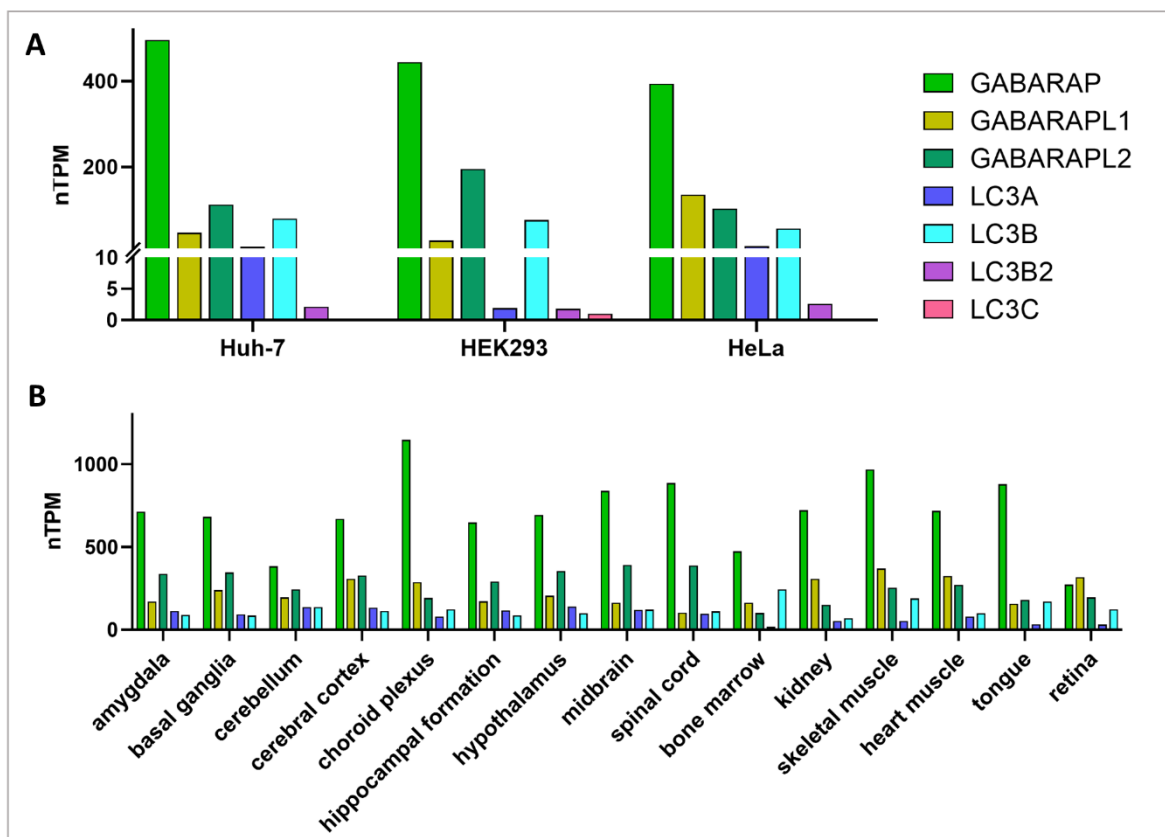


**Figure S5.** Additional Colabfold models and their corresponding ranks as well as well as per residue confidence values, namely predicted local difference distance test (pLDDT) and predicted aligned error (PAE) for models presented in Figure 5, namely G-B-G with a TBB5 and TBA1A tetramer (A) and GABARAP with TBB5 and TBA1A (B). Additionally, models for B-G-G with a TBB5 and TBA1A tetramer is shown (C).

## 4 Summary and Conclusion

Since mammalian and human homologs of yeast Atg8 were first mentioned (Kirisako et al., 1999, Lang et al., 1998), these proteins and their functions have been extensively studied. The manuscripts presented in this thesis focus on interactions of GABARAP, which is the human ATG8 paralog with the highest mRNA expression levels under basal conditions in many cell lines, including the ones used here (Figure 6A). Interestingly, this pattern can also be observed on a tissue level, with GABARAP being the paralog with highest mRNA expression in most of the tissues listed in the Human Protein Atlas (Uhlen et al., 2015, Uhlen et al., 2010; Figure 6B). Although protein levels cannot be directly inferred from mRNA expression levels, a positive correlation between the two has been reported (Buccitelli and Selbach, 2020). It is noteworthy that, while ATG8 proteins in general have been the subject of an increasing number of publications, with a peak in 2021 (Figure 6C), LC3B and the LC3 subfamily have received substantially more attention than GABARAP and the GABARAP subfamily, respectively (Figure 6D).



\*Figure 6, continued on next page

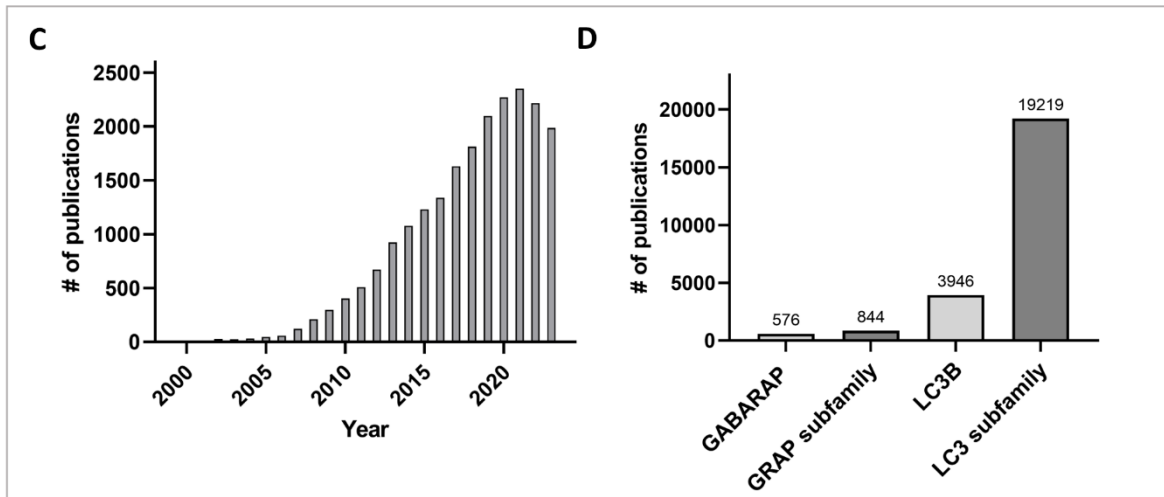


**Figure 6. Overview of ATG8 related publications.** mRNA expression levels of ATG8 paralogs in cell lines applied in this work (A) and in selected tissues (B) according to the Human Protein Atlas (Uhlen et al., 2015, Uhlen et al., 2010). Tissues exhibiting mRNA expression in the top 10% for any one of the paralogs were included. LC3C and LC3B2 are not shown in (B) due to expression levels below 10 nTPM for all tissues documented. nTPM: normalized transcripts per million. (C) Publications on human ATG8 paralogs listed on PubMed (<http://www.ncbi.nlm.nih.gov/pubmed>; Sayers et al., 2011, Sayers et al., 2024), search term: LC3A[Title/Abstract] OR LC3B[Title/Abstract] OR LC3C[Title/Abstract] OR LC3[Title/Abstract] OR LC3B2[Title/Abstract] OR MAP1LC3A[Title/Abstract] OR MAP1LC3B[Title/Abstract] OR MAP1LC3C[Title/Abstract] OR MAP1LC3[Title/Abstract] OR MAP1ALC3[Title/Abstract] OR MAP1ALC3A[Title/Abstract] OR MAP1ALC3B[Title/Abstract] OR MAP1ALC3C[Title/Abstract] OR GABARAP[Title/Abstract] OR GABARAPL1[Title/Abstract] OR GEC-1[Title/Abstract] OR GEC1[Title/Abstract] OR GABARAPL2[Title/Abstract] OR GATE16[Title/Abstract] OR GATE-16[Title/Abstract] over time (1998–2023). (D) Number of publications retrieved by PubMed search for GABARAP, the GABARAP subfamily, LC3B and the LC3 subfamily as of 06/07/2024. Graphs were created using GraphPad Prism 9.

Nevertheless, it has become clear that the GABARAPs fulfill non-redundant functions and play a prominent role during autophagy, e.g. in autophagosome-lysosome fusion (Nguyen et al., 2016, Vaites et al., 2018). The fact that GABARAP appears to play a specific role in certain pathologies (Gulla et al., 2024, Salah et al., 2016) provides an additional rationale for putting GABARAP more into the spotlight. The studies included in this work contribute to this task by providing new insights into GABARAP function from different perspectives, applying a broad range of methods.

In the following paragraphs, the key findings of these studies are summarized (Figure 7) and limitations and future perspectives are described. More detailed discussions on each study can be found in the respective sections of the included manuscripts.

The interactions of the stapled peptides Pen3-*ortho* and Pen8-*ortho*, respectively, with GABARAP, described in chapter 3.1. (Brown et al., 2022), were investigated by x-ray crystallography. Purified GABARAP was co-crystallized with the stapled peptides (provided by collaboration partners: Kritzer Group, Tufts University, MA, USA), and diffraction data were collected (ESFR, Grenoble, France). The resolved structural models (PDB IDs: 7ZKR & 7ZL7) revealed binding of the stapled peptides to the hydrophobic pockets of GABARAP in different orientations, which correlates with distinct paralog selectivity. This is likely facilitated through GABARAPs ability to undergo induced fit to support binding of an additional large hydrophobic residue to HP2 in case of antiparallel binding as



seen for Pen3-*ortho*. Notably, these peptides can penetrate cells, inhibit autophagy and synergize with cisplatin to inhibit proliferation of ovarian cancer cells (chapter 3.1., Brown et al., 2022).

The small-molecule compound GW5074 (also provided by the Kritzer Group, Tufts University, MA, USA) has been previously described as the LC3 binding component of an ATTEC (Li et al 2019). However, subsequent reports showed that this compound can also covalently interact with the E3 ligase DCAF11, thereby directing at least some of its targets to the proteasome (Xue et al., 2023). Addressing contradictory reports on interactions between GW5074 and ATG8 proteins (Pei et al., 2021, Li et al., 2019, Schwalm et al., Preprint 2023a), chapter 3.2. reports binding of GW5074 to LC3B and GABARAP (Leveille et al., Preprint 2024). While within this project, co-crystallization efforts with GW5074 and GABARAP did not yield diffracting crystals, HSQC titration experiments with <sup>15</sup>N-labelled GABARAP revealed engagement of GW5074 with GABARAPs HP1. Furthermore, the study describes the binding determinants of arylidene-indolinone ligands in regulating selectivity and affinity, thereby laying the groundwork for further development of improved (selective) small-molecule interactors of ATG8 proteins.

In order to evaluate the applicability of both stapled peptides and small-molecule compounds as research tools and therapeutics, further research regarding their functions in cells and organisms will be required. This includes investigations on how different processes including canonical and non-canonical autophagy, as well as receptor trafficking processes are affected. Considering that GABARAP can have both tumor-promoting and tumor-suppressing functions (Gulla et al., 2024, Jacquet et al., 2021, Salah et al., 2016), it will be crucial to define suitable indications for the administration of artificial GABARAP/ATG8 ligands to human subjects.

Chapter 3.3. explores a previously reported EGFR degradation phenotype, specifically in GABARAP knockout cells, from a biophysical and structural perspective (Üffing et al., 2024b). For this purpose, the ATG8 paralogs were purified and analyzed regarding their affinity towards EGFR-derived peptides, LIR1 and LIR2 as well as phosphorylated analogs, by biolayer interferometry (BLI). These experiments revealed selective binding of LIR1 to GABARAP/GABARAPL1, with moderate influence of phosphorylation in residues surrounding the core LIR. Subsequently, a chimeric EGFR LIR1-GABARAP protein was purified, crystallized and diffraction data collected, leading to a structural model (PDB ID: 8S1M) which showed binding of the EGFR LIR1 to GABARAP in a canonical LIR-LDS dependent fashion, while also confirming molecular determinants regulating selectivity in a broader sense. In addition, the EGFR LIR1 binding site on GABARAP was mapped by the use of chemical shift perturbation data gained from a <sup>15</sup>N-HSQC titration experiment, further confirming engagement of HP1 and HP2 residues of GABARAP in the interaction in solution. Overall, these results provide a plausible hypothesis for the observed phenotype of enhanced EGFR degradation, specifically in GABARAP knockout cells.

However, whether and to which degree this direct interaction influences EGFR's fate in a cellular context still remains to be determined. On the one hand, this question could be tackled by reintroducing wildtype and LIR binding-deficient GABARAP into GABARAP knockout cells, either at endogenous levels or through overexpression. However, as most of GABARAPs interactions are LIR-LDS based, this might not yield conclusive results. This approach additionally requires determination of mutations leading to disruption of the interaction between GABARAP and the EGFR LIR1 *in vitro*, as this was not achieved by exchanging Tyr49 and Leu50 (residues typically addressed) to alanine. On the other hand, the LIRs in the EGFR C-terminal domain could be mutated endogenously. While this could impede putative GABARAP binding, it could also influence EGFR signaling due to the presence of the regulatory tyrosine residues Tyr1092 (LIR1) and Tyr1197 (LIR2) in the vicinity of or within the LIRs, respectively. With the interplay between endocytic trafficking and autophagy in mind, it also seems likely that multiple mechanisms involving GABARAP, possibly including this direct interaction, affect EGFR trafficking after stimulation. These could potentially attenuate the phenotype in cells containing LIR-deficient EGFR. Another question for future investigations concerns the posttranslational modifications of the EGFR after stimulation. To elucidate whether GABARAP indeed reduces phosphorylation and/or growth factor receptor-bound protein 2 (GRB2) association to pTyr1092, EGFR phosphorylation and ubiquitylation patterns at different timepoints after stimulation in wildtype and GABARAP knockout cells could be analyzed by mass spectrometry.

Finally, intracellular GABARAP localization and corresponding interactions were investigated by live-cell microscopy applying novel fluorescent fusion proteins in chapter 3.4 (Üffing et al., 2024a; raw data on BioImage Archive, Accession: S-BIAD952). Typically, fusion of fluorescent proteins to the N-terminus of ATG8s (yielding, e.g., EYFP-GABARAP) is applied to monitor localization in cells. Here, a bivalent GABARAP-mTagBFP2-GABARAP tandem construct was introduced with the idea that it could potentially exhibit a localization distinct from conventionally tagged GABARAP, through increased avidity in case of inherently weak interactions and/or through the availability of two free termini. Indeed, GABARAP-mTagBFP2-GABARAP associates with microtubules, bringing their early reported interaction with GABARAP back into focus. Besides requiring specific fluorophore properties and two GABARAP moieties, the interaction between the GABARAP tandem construct and microtubules relies on positively charged amino acids in the N-terminus of GABARAP. Thereby, the study connects early *in-vitro* studies (Coyle et al., 2002, Wang and Olsen, 2000, Wang et al., 1999) with observations in cells. However, due to the artificial nature of the construct and transient overexpression, the biological relevance of this interaction remains to be determined. For this purpose, one could endogenously mutate the positively charged residues (Lys2, Lys13, Arg15, Lys20, Lys23) in the GABARAP N-terminus and analyze the localization of the respective GABARAP

mutant protein compared to wildtype GABARAP. On a functional level, effects on transport of endolysosomal vesicles and autophagosomes could be examined, by tracking Rab7- and LC3B-positive structures, respectively (Fu et al., 2014, Cason and Holzbaur, 2023). Another question for future investigation will be whether the observed behavior of the GABARAP tandem construct is paralog specific. Despite LC3s being initially described as microtubule associated proteins (Mann and Hammarback, 1994), preliminary data with an analogous LC3B tandem construct strikingly indicate less association with microtubules (not shown). Besides microtubule association, the GABARAP tandem construct showed additional differences in subcellular localization compared to conventionally tagged GABARAP. Further investigations of these differences under both basal and autophagy inducing conditions have the potential to highlight additional localizations and corresponding functions of ATG8 proteins, which are otherwise overlooked.

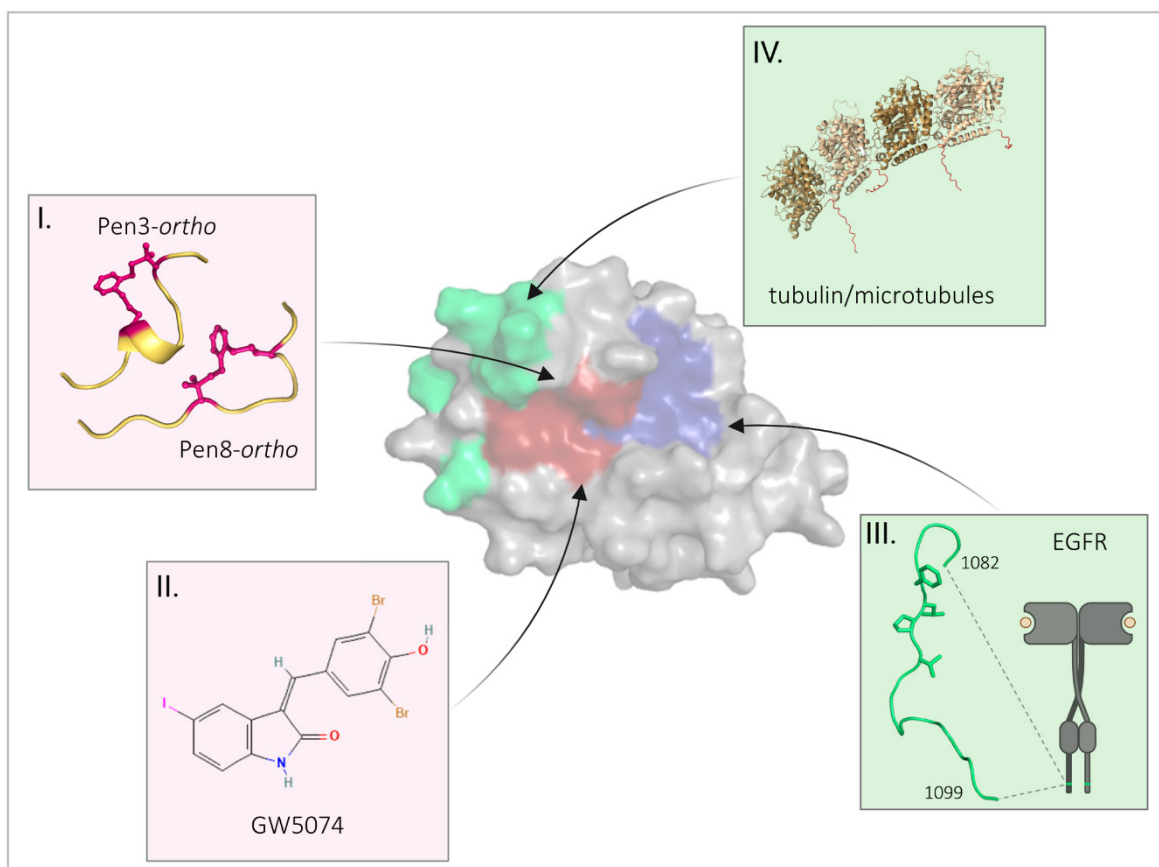


**Figure 7. Overview of artificial (pink background) and putative biological interactors of GABARAP (green background) investigated in this work.** The artificial GABARAP ligands Pen3-*ortho* and Pen8-*ortho* (stapled peptides) interact with both hydrophobic pockets of GABARAP via different binding modes, explaining paralog-selective binding of Pen3-*ortho* but not Pen8-*ortho* (I., chapter 3.1.). The small-molecule compound GW5074 primarily engages with HP1 of GABARAP (II., chapter 3.2.). The putative biological interactors include the EGFR, which interacts with GABARAP HP1 and HP2 via the LIR1 motif in its C-terminal domain (III., chapter 3.3.) and tubulin/microtubules, which associate with positively charged residues in the N-terminus of GABARAP (IV., Chapter 3.4.). Image was created with BioRender.com and PyMOL Molecular Graphics System, Version 3.0 Schrödinger, LLC. GW5074 2D structure reprinted from PubChem (CID 5924208, <https://pubchem.ncbi.nlm.nih.gov/compound/5924208#section=2D-Structure>) HP1: red, HP2: blue, basic N-terminal residues: green.

Despite being a small protein of only 14 kDa, the ATG8 protein GABARAP is involved in wide variety of processes, which are important for cellular homeostasis but can also contribute to disease. By revealing novel aspects of the versatile interactions of GABARAPs, this work contributes to balancing the knowledge of individual ATG8 paralogs and motivates further research on their non-redundant functions.

## 5 List of Publications and Presentations

### 5.1. Publications

Hawley Brown, Mia Chung, **Alina Üffing**, Nefeli Batistatou, Tiffany Tsang, Samantha Daskocil, Weiqun Mao, Dieter Willbold, Robert C. Bast Jr., Zhen Lu, Oliver H. Weiergräber, and Joshua A. Kritzer. Structure-Based Design of Stapled Peptides That Bind GABARAP and Inhibit Autophagy. *Journal of the American Chemical Society*, 2022 144 (32), 14687-14697. doi.org/10.1021/jacs.2c04699.

**Alina Üffing**, Lisa Gold, Thomas Gensch, Oliver H. Weiergräber, Silke Hoffmann, Dieter Willbold. Highlighting the hidden: monitoring the avidity-driven association of a fluorescent GABARAP tandem with microtubules in living cells. *Autophagy Reports*, 2024 3(1). doi.org/10.1080/27694127.2024.2348899.

**Alina Üffing**, Oliver H. Weiergräber, Melanie Schwarten, Silke Hoffmann, Dieter Willbold. GABARAP interacts with EGFR — supporting the unique role of this hAtg8 protein during receptor trafficking. *FEBS Letters*, 2024. doi.org/10.1002/1873-3468.14997.

Additional publication not included in this thesis:

Julia L. Sanwald, Jochen Dobner, Indra M. Simons, Gereon Poschmann, Kai Stühler, **Alina Üffing**, Silke Hoffmann, Dieter Willbold. Lack of GABARAP-Type Proteins Is Accompanied by Altered Golgi Morphology and Surfaceome Composition. *International Journal of Molecular Sciences*. 2021, 22, 85. Doi.org/ 10.3390/ijms22010085.

### 5.2. Preprints/submitted manuscripts

Alexandria N. Leveille, Hawley Brown, Thomas Schwarzrock, Bennett True, Joanet Plasencia, Philipp Neudecker, **Alina Üffing**, Oliver H. Weiergräber, Dieter Willbold, Joshua A. Kritzer. Exploring Arylidene-Indolinone Ligands of Autophagy Proteins LC3B and GABARAP. *BioRxiv*, 2024, doi.org/10.1101/2024.02.25.581879.

### 5.3. Poster Presentations

Alina Üffing, Silke Hoffmann, Oliver H. Weiergräber & Dieter Willbold. GABARAP meets EGFR – Structural clues to the GABARAP-specific phenotype during EGFR degradation.  
FOR2625 SYMPOSIUM “LYSOSOMES & AUTOPHAGY”, May 5-6, 2022, Berlin, Germany

Alina Üffing, Silke Hoffmann, Oliver H. Weiergräber & Dieter Willbold. GABARAP meets EGFR – Structural clues to the GABARAP-specific phenotype during EGFR degradation.  
EMBO Workshop “Integrating the molecular, mechanistic and physiological diversity of autophagy”, 27 June – 01 July 2022, Eger, Hungary

Alina Üffing, Lisa Gold, Thomas Gensch, Oliver H. Weiergräber, Silke Hoffmann, Dieter Willbold. Monitoring the association of hATG8s with microtubules in living cells.  
Gordon Research Conference “Autophagy in Stress, Development and Disease”, March 10 – 15, 2024, Barga (Lucca), Italy & associated Gordon Research Seminar, March 9 – 10, 2024, Barga (Lucca), Italy

## 5 References

- ALEMU, E. A., LAMARK, T., TORGERSEN, K. M., BIRGISDOTTIR, A. B., LARSEN, K. B., JAIN, A., OLSVIK, H., OVERVATN, A., KIRKIN, V. & JOHANSEN, T. 2012. ATG8 family proteins act as scaffolds for assembly of the ULK complex: sequence requirements for LC3-interacting region (LIR) motifs. *J Biol Chem*, 287, 39275-90.
- ALI, M. G., WAHBA, H. M., IGELMANN, S., CYR, N., FERBEYRE, G. & OMICHINSKI, J. G. 2024. Structural and functional characterization of the role of acetylation on the interactions of the human Atg8-family proteins with the autophagy receptor TP53INP2/DOR. *Autophagy*, 1-20.
- ARSTILA, A. U. & TRUMP, B. F. 1968. Studies on cellular autophagocytosis. The formation of autophagic vacuoles in the liver after glucagon administration. *Am J Pathol*, 53, 687-733.
- BAEKEN, M. W., WECKMANN, K., DIEFENTHALER, P., SCHULTE, J., YUSIFLI, K., MOOSMANN, B., BEHL, C. & HAJIEVA, P. 2020. Novel Insights into the Cellular Localization and Regulation of the Autophagosomal Proteins LC3A, LC3B and LC3C. *Cells*, 9.
- BAKER, R. W. & HUGHSON, F. M. 2016. Chaperoning SNARE assembly and disassembly. *Nat Rev Mol Cell Biol*, 17, 465-79.
- BARROW-MCGEE, R., KISHI, N., JOFFRE, C., MENARD, L., HERVIEU, A., BAKHOUCHE, B. A., NOVAL, A. J., MAI, A., GUZMAN, C., ROBBEZ-MASSON, L., ITURRIOZ, X., HULIT, J., BRENNAN, C. H., HART, I. R., PARKER, P. J., IVASKA, J. & KERMORGANT, S. 2016. Beta 1-integrin-c-Met cooperation reveals an inside-in survival signalling on autophagy-related endomembranes. *Nat Commun*, 7, 11942.
- BASKARAN, S., CARLSON, L. A., STJEPANOVIC, G., YOUNG, L. N., KIM, D. J., GROB, P., STANLEY, R. E., NOGALES, E. & HURLEY, J. H. 2014. Architecture and dynamics of the autophagic phosphatidylinositol 3-kinase complex. *Elife*, 3.
- BEHREND, C., SOWA, M. E., GYGI, S. P. & HARPER, J. W. 2010. Network organization of the human autophagy system. *Nature*, 466, 68-76.
- BELL, E. S., COELHO, P. P., RATCLIFFE, C. D. H., RAJADURAI, C. V., PESCHARD, P., VAILLANCOURT, R., ZUO, D. & PARK, M. 2019. LC3C-Mediated Autophagy Selectively Regulates the Met RTK and HGF-Stimulated Migration and Invasion. *Cell Rep*, 29, 4053-4068 e6.
- BIRGISDOTTIR, A. B. & JOHANSEN, T. 2020. Autophagy and endocytosis - interconnections and interdependencies. *J Cell Sci*, 133.
- BIRGISDOTTIR, A. B., LAMARK, T. & JOHANSEN, T. 2013. The LIR motif - crucial for selective autophagy. *J Cell Sci*, 126, 3237-47.
- BIRGISDOTTIR, A. B., MOUILLERON, S., BHUJABAL, Z., WIRTH, M., SJOTTEM, E., EVJEN, G., ZHANG, W., LEE, R., O'REILLY, N., TOOZE, S. A., LAMARK, T. & JOHANSEN, T. 2019. Members of the autophagy class III phosphatidylinositol 3-kinase complex I interact with GABARAP and GABARAPL1 via LIR motifs. *Autophagy*, 15, 1333-1355.
- BJORKOY, G., LAMARK, T., BRECH, A., OUTZEN, H., PERANDER, M., OVERVATN, A., STENMARK, H. & JOHANSEN, T. 2005. p62/SQSTM1 forms protein aggregates degraded by autophagy and has a protective effect on huntingtin-induced cell death. *J Cell Biol*, 171, 603-14.
- BOZIC, M., VAN DEN BEKEROM, L., MILNE, B. A., GOODMAN, N., ROBERSTON, L., PRESCOTT, A. R., MACARTNEY, T. J., DAWE, N. & MCEWAN, D. G. 2020. A conserved ATG2-GABARAP family interaction is critical for phagophore formation. *EMBO Rep*, 21, e48412.
- BROWN, H., CHUNG, M., ÜFFING, A., BATISTATOU, N., TSANG, T., DOSKOCIL, S., MAO, W., WILLBOLD, D., BAST, R. C., JR., LU, Z., WEIERGRÄBER, O. H. & KRITZER, J. A. 2022. Structure-Based Design of Stapled Peptides That Bind GABARAP and Inhibit Autophagy. *J Am Chem Soc*, 144, 14687-14697.
- BUCCITELLI, C. & SELBACH, M. 2020. mRNAs, proteins and the emerging principles of gene expression control. *Nat Rev Genet*, 21, 630-644.
- CACCAMO, A., MAJUMDER, S., RICHARDSON, A., STRONG, R. & ODDO, S. 2010. Molecular interplay between mammalian target of rapamycin (mTOR), amyloid-beta, and Tau: effects on cognitive impairments. *J Biol Chem*, 285, 13107-20.



- CAROSI, J. M., HEIN, L. K., SANDOW, J. J., DANG, L. V. P., HATTERSLEY, K., DENTON, D., KUMAR, S. & SARGEANT, T. J. 2024. Autophagy captures the retromer-TBC1D5 complex to inhibit receptor recycling. *Autophagy*, 20, 863-882.
- CASON, S. E. & HOLZBAUR, E. L. F. 2023. Axonal transport of autophagosomes is regulated by dynein activators JIP3/JIP4 and ARF/RAB GTPases. *J Cell Biol*, 222.
- CERULLI, R. A., SHEHAJ, L., BROWN, H., PACE, J., MEI, Y. & KRITZER, J. A. 2020. Stapled Peptide Inhibitors of Autophagy Adapter LC3B. *Chembiochem*, 21, 2777-2785.
- CHAN, E. Y., KIR, S. & TOOZE, S. A. 2007. siRNA screening of the kinome identifies ULK1 as a multidomain modulator of autophagy. *J Biol Chem*, 282, 25464-74.
- CHAUHAN, S., KUMAR, S., JAIN, A., PONPUAK, M., MUDD, M. H., KIMURA, T., CHOI, S. W., PETERS, R., MANDELL, M., BRUUN, J. A., JOHANSEN, T. & DERETIC, V. 2016. TRIMs and Galectins Globally Cooperate and TRIM16 and Galectin-3 Co-direct Autophagy in Endomembrane Damage Homeostasis. *Dev Cell*, 39, 13-27.
- CHEN, C., LI, J. G., CHEN, Y., HUANG, P., WANG, Y. & LIU-CHEN, L. Y. 2006. GEC1 interacts with the kappa opioid receptor and enhances expression of the receptor. *J Biol Chem*, 281, 7983-93.
- CHEN, C., WANG, Y., HUANG, P. & LIU-CHEN, L. Y. 2011. Effects of C-terminal modifications of GEC1 protein and gamma-aminobutyric acid type A (GABA<sub>A</sub>) receptor-associated protein (GABARAP), two microtubule-associated proteins, on kappa opioid receptor expression. *J Biol Chem*, 286, 15106-15.
- CHEN, L., WANG, H., VICINI, S. & OLSEN, R. W. 2000. The  $\gamma$ -aminobutyric acid type A (GABA<sub>A</sub>) receptor-associated protein (GABARAP) promotes GABA<sub>A</sub> receptor clustering and modulates the channel kinetics. *PNAS*, 97, 11557-11562.
- CHENG, X., WANG, Y., GONG, Y., LI, F., GUO, Y., HU, S., LIU, J. & PAN, L. 2016. Structural basis of FYCO1 and MAP1LC3A interaction reveals a novel binding mode for Atg8-family proteins. *Autophagy*, 12, 1330-9.
- CHINO, H., YAMASAKI, A., ODE, K. L., UEDA, H. R., NODA, N. N. & MIZUSHIMA, N. 2022. Phosphorylation by casein kinase 2 enhances the interaction between ER-phagy receptor TEX264 and ATG8 proteins. *EMBO Rep*, 23, e54801.
- CHOWDHURY, S., OTOMO, C., LEITNER, A., OHASHI, K., AEBERSOLD, R., LANDER, G. C. & OTOMO, T. 2018. Insights into autophagosome biogenesis from structural and biochemical analyses of the ATG2A-WIP1 complex. *Proceedings of the National Academy of Sciences of the United States of America*, 115, E9792-E9801.
- COELHO, P. P., HESKETH, G. G., PEDERSEN, A., KUZMIN, E., FORTIER, A. N., BELL, E. S., RATCLIFFE, C. D. H., GINGRAS, A. C. & PARK, M. 2022. Endosomal LC3C-pathway selectively targets plasma membrane cargo for autophagic degradation. *Nat Commun*, 13, 3812.
- COELHO, P. P. & PARK, M. 2023. LEAP: a novel LC3C-dependent pathway connects autophagy, endocytic trafficking and signaling. *Autophagy*, 19, 1354-1356.
- COLLIER, J. J., GUISSART, C., OLAHOVA, M., SASORITH, S., PIRON-PRUNIER, F., SUOMI, F., ZHANG, D., MARTINEZ-LOPEZ, N., LÉBOUCQ, N., BAHR, A., AZZARELLO-BURRI, S., REICH, S., SCHOLS, L., POLVIKOSKI, T. M., MEYER, P., LARRIEU, L., SCHAEFER, A. M., ALSAIF, H. S., ALYAMANI, S., ZUCHNER, S., BARBOSA, I. A., DESHPANDE, C., PYLE, A., RAUCH, A., SYNOFZIK, M., ALKURAYA, F. S., RIVIER, F., RYTEN, M., MCFARLAND, R., DELAHODDE, A., MCWILLIAMS, T. G., KOENIG, M. & TAYLOR, R. W. 2021. Developmental Consequences of Defective ATG7-Mediated Autophagy in Humans. *N Engl J Med*, 384, 2406-2417.
- COOK, J. L., RE, R. N., DEHARO, D. L., ABADIE, J. M., PETERS, M. & ALAM, J. 2008. The trafficking protein GABARAP binds to and enhances plasma membrane expression and function of the angiotensin II type 1 receptor. *Circ Res*, 102, 1539-47.
- COYLE, J. E., QAMAR, S., RAJASHANKAR, K. R. & NIKOLOV, D. B. 2002. Structure of GABARAP in two conformations: Implications for GABA<sub>A</sub> receptor localization and tubulin binding. *Neuron*, 33, 63-74.
- CRIGHTON, D., WILKINSON, S., O'PREY, J., SYED, N., SMITH, P., HARRISON, P. R., GASCO, M., GARRONE, O., CROOK, T. & RYAN, K. M. 2006. DRAM, a p53-induced modulator of autophagy, is critical for apoptosis. *Cell*, 126, 121-34.

- CUERVO, A. M., ELAZAR, Z., EVANS, C., GE, L., HANSEN, M., JAATTELA, M., LIANG, J. R. A., LOOS, B., MIZUSHIMA, N., SIMON, A. K., TOOZE, S., YOSHIMORI, T. & NAKAMURA, S. 2024. Next questions in autophagy. *Nat Cell Biol*, 26, 661-666.
- DE DUVE, C. 1963. The lysosome concept. In: DE REUCK, A. & CAMERON, M. (eds.) *Novartis Foundation Symposia*.
- DEBNATH, J., GAMMOH, N. & RYAN, K. M. 2023. Autophagy and autophagy-related pathways in cancer. *Nat Rev Mol Cell Biol*, 24, 560-575.
- DEOSARAN, E., LARSEN, K. B., HUA, R., SARGENT, G., WANG, Y., KIM, S., LAMARK, T., JAUREGUI, M., LAW, K., LIPPINCOTT-SCHWARTZ, J., BRECH, A., JOHANSEN, T. & KIM, P. K. 2013. NBR1 acts as an autophagy receptor for peroxisomes. *J Cell Sci*, 126, 939-52.
- DIAO, J., LIU, R., RONG, Y., ZHAO, M., ZHANG, J., LAI, Y., ZHOU, Q., WILZ, L. M., LI, J., VIVONA, S., PFUETZNER, R. A., BRUNGER, A. T. & ZHONG, Q. 2015. ATG14 promotes membrane tethering and fusion of autophagosomes to endolysosomes. *Nature*, 520, 563-6.
- DING, Y., FEI, Y. & LU, B. 2020. Emerging New Concepts of Degradation Technologies. *Trends Pharmacol Sci*, 41, 464-474.
- DOBNER, J., SIMONS, I. M., RUFINATSCHA, K., HÄNSCH, S., SCHWARTEN, M., WEIERGRÄBER, O. H., ABDOLLAHZADEH, I., GENSCHE, T., BODE, J. G., HOFFMANN, S. & WILLBOLD, D. 2020. Deficiency of GABARAP but not its Paralogs Causes Enhanced EGF-induced EGFR Degradation. *Cells*, 9.
- DOOLEY, H. C., RAZI, M., POLSON, H. E., GIRARDIN, S. E., WILSON, M. I. & TOOZE, S. A. 2014. WIPI2 links LC3 conjugation with PI3P, autophagosome formation, and pathogen clearance by recruiting Atg12-5-16L1. *Mol Cell*, 55, 238-52.
- DOUDNA, J. A. & CHARPENTIER, E. 2014. Genome editing. The new frontier of genome engineering with CRISPR-Cas9. *Science*, 346, 1258096.
- DURGAN, J. & FLOREY, O. 2021. A new flavor of cellular Atg8-family protein lipidation - alternative conjugation to phosphatidylserine during CASM. *Autophagy*, 17, 2642-2644.
- DURGAN, J. & FLOREY, O. 2022. Many roads lead to CASM: Diverse stimuli of noncanonical autophagy share a unifying molecular mechanism. *Sci Adv*, 8, eabo1274.
- DURGAN, J., LYSTAD, A. H., SLOAN, K., CARLSSON, S. R., WILSON, M. I., MARCASSA, E., ULFERTS, R., WEBSTER, J., LOPEZ-CLAVIJO, A. F., WAKELAM, M. J., BEALE, R., SIMONSEN, A., OXLEY, D. & FLOREY, O. 2021. Non-canonical autophagy drives alternative ATG8 conjugation to phosphatidylserine. *Mol Cell*, 81, 2031-2040 e8.
- ECK, F., PHUYAL, S., SMITH, M. D., KAULICH, M., WILKINSON, S., FARHAN, H. & BEHRENDT, C. 2020. ACSL3 is a novel GABARAPL2 interactor that links ubiquitylation and lipid droplet biogenesis. *J Cell Sci*, 133.
- ELBASHIR, S. M., HARBORTH, J., LENDECKEL, W., YALCIN, A., WEBER, K. & TUSCHL, T. 2001. Duplexes of 21-nucleotide RNAs mediate RNA interference in cultured mammalian cells. *Nature*, 411, 494-8.
- FANG, E. F., HOU, Y., PALIKARAS, K., ADRIAANSE, B. A., KERR, J. S., YANG, B., LAUTRUP, S., HASAN-OLIVE, M. M., CAPONIO, D., DAN, X., ROCKTASCHEL, P., CROTEAU, D. L., AKBARI, M., GREIG, N. H., FLADBY, T., NILSEN, H., CADER, M. Z., MATTSO, M. P., TAVERNARAKIS, N. & BOHR, V. A. 2019. Mitophagy inhibits amyloid-beta and tau pathology and reverses cognitive deficits in models of Alzheimer's disease. *Nat Neurosci*, 22, 401-412.
- FENG, Y., HE, D., YAO, Z. & KLIONSKY, D. J. 2014. The machinery of macroautophagy. *Cell Res*, 24, 24-41.
- FISCHER, T. D., WANG, C., PADMAN, B. S., LAZAROU, M. & YOUNG, R. J. 2020. STING induces LC3B lipidation onto single-membrane vesicles via the V-ATPase and ATG16L1-WD40 domain. *J Cell Biol*, 219, e202009128.
- FLETCHER, K., ULFERTS, R., JACQUIN, E., VEITH, T., GAMMOH, N., ARASTEH, J. M., MAYER, U., CARDING, S. R., WILEMAN, T., BEALE, R. & FLOREY, O. 2018. The WD40 domain of ATG16L1 is required for its non-canonical role in lipidation of LC3 at single membranes. *EMBO J*, 37.
- FLOREY, O., GAMMOH, N., KIM, S. E., JIANG, X. & OVERHOLTZER, M. 2015. V-ATPase and osmotic imbalances activate endolysosomal LC3 lipidation. *Autophagy*, 11, 88-99.

- FLOREY, O., KIM, S. E., SANDOVAL, C. P., HAYNES, C. M. & OVERHOLTZER, M. 2011. Autophagy machinery mediates macroendocytic processing and entotic cell death by targeting single membranes. *Nat Cell Biol*, 13, 1335-43.
- FLOREY, O. & OVERHOLTZER, M. 2012. Autophagy proteins in macroendocytic engulfment. *Trends Cell Biol*, 22, 374-80.
- FRACCHIOLLA, D., CHANG, C., HURLEY, J. H. & MARTENS, S. 2020. A PI3K-WIP1 positive feedback loop allosterically activates LC3 lipidation in autophagy. *J Cell Biol*, 219.
- FRACCHIOLLA, D. & MARTENS, S. 2018. Sorting out "non-canonical" autophagy. *EMBO J*, 37.
- FRASER, J., CABODEVILLA, A. G., SIMPSON, J. & GAMMOH, N. 2017. Interplay of autophagy, receptor tyrosine kinase signalling and endocytic trafficking. *Essays Biochem*, 61, 597-607.
- FRASER, J., SIMPSON, J., FONTANA, R., KISHI-ITAKURA, C., KTISTAKIS, N. T. & GAMMOH, N. 2019. Targeting of early endosomes by autophagy facilitates EGFR recycling and signalling. *EMBO Rep*, 20, e47734.
- FU, M. M., NIRSCHL, J. J. & HOLZBAUR, E. L. F. 2014. LC3 binding to the scaffolding protein JIP1 regulates processive dynein-driven transport of autophagosomes. *Dev Cell*, 29, 577-590.
- FUJITA, N., HAYASHI-NISHINO, M., FUKUMOTO, H., OMORI, H., YAMAMOTO, A., NODA, T. & YOSHIMORI, T. 2008a. An Atg4B mutant hampers the lipidation of LC3 paralogues and causes defects in autophagosome closure. *Mol Biol Cell*, 19, 4651-9.
- FUJITA, N., ITOH, T., OMORI, H., FUKUDA, M., NODA, T. & YOSHIMORI, T. 2008b. The Atg16L complex specifies the site of LC3 lipidation for membrane biogenesis in autophagy. *Mol Biol Cell*, 19, 2092-100.
- GALLUZZI, L., PIETROCOLA, F., BRAVO-SAN PEDRO, J. M., AMARAVADI, R. K., BAEHRECKE, E. H., CECCONI, F., CODOGNO, P., DEBNATH, J., GEWIRTZ, D. A., KARANTZA, V., KIMMELMAN, A., KUMAR, S., LEVINE, B., MAIURI, M. C., MARTIN, S. J., PENNINGER, J., PIACENTINI, M., RUBINSZTEIN, D. C., SIMON, H. U., SIMONSEN, A., THORBURN, A. M., VELASCO, G., RYAN, K. M. & KROEMER, G. 2015. Autophagy in malignant transformation and cancer progression. *EMBO J*, 34, 856-80.
- GAMMOH, N., FLOREY, O., OVERHOLTZER, M. & JIANG, X. 2013. Interaction between FIP200 and ATG16L1 distinguishes ULK1 complex-dependent and -independent autophagy. *Nat Struct Mol Biol*, 20, 144-9.
- GANLEY, I. G., LAM DU, H., WANG, J., DING, X., CHEN, S. & JIANG, X. 2009. ULK1.ATG13.FIP200 complex mediates mTOR signaling and is essential for autophagy. *J Biol Chem*, 284, 12297-305.
- GARDNER, J. O., LEIDAL, A. M., NGUYEN, T. A. & DEBNATH, J. 2023. LC3-dependent EV loading and secretion (LDELS) promotes TFRC (transferrin receptor) secretion via extracellular vesicles. *Autophagy*, 19, 1551-1561.
- GATICA, D., LAHIRI, V. & KLIONSKY, D. J. 2018. Cargo recognition and degradation by selective autophagy. *Nat Cell Biol*, 20, 233-242.
- GOMEZ-SANCHEZ, R., ROSE, J., GUIMARAES, R., MARI, M., PAPINSKI, D., RIETER, E., GEERTS, W. J., HARDENBERG, R., KRAFT, C., UNGERMANN, C. & REGGIORI, F. 2018. Atg9 establishes Atg2-dependent contact sites between the endoplasmic reticulum and phagophores. *J Cell Biol*, 217, 2743-2763.
- GONG, L., CULLINANE, M., TREERAT, P., RAMM, G., PRESCOTT, M., ADLER, B., BOYCE, J. D. & DEVENISH, R. J. 2011. The Burkholderia pseudomallei type III secretion system and BopA are required for evasion of LC3-associated phagocytosis. *PLoS One*, 6, e17852.
- GOODWIN, J. M., WALKUP, W. G., HOOPER, K., LI, T., KISHI-ITAKURA, C., NG, A., LEHMBERG, T., JHA, A., KOMMINENI, S., FLETCHER, K., GARCIA-FORTANET, J., FAN, Y., TANG, Q., WEI, M., AGRAWAL, A., BUDHE, S. R., ROUDURI, S. R., BAIRD, D., SAUNDERS, J., KISELAR, J., CHANCE, M. R., BALLABIO, A., APPLETON, B. A., BRUMELL, J. H., FLOREY, O. & MURPHY, L. O. 2021. GABARAP sequesters the FLCN-FNIP tumor suppressor complex to couple autophagy with lysosomal biogenesis. *Sci Adv*, 7, eabj2485.
- GORDON, P. B. & SEGLEN, P. O. 1988. Prelysosomal convergence of autophagic and endocytic pathways. *Biochem Biophys Res Commun*, 151, 40-7.

- GRAY, J. P., UDDIN, M. N., CHAUDHARI, R., SUTTON, M. N., YANG, H., RASK, P., LOCKE, H., ENGEL, B. J., BATISTATOU, N., WANG, J., GRINDEL, B. J., BHATTACHARYA, P., GAMMON, S. T., ZHANG, S., PIWNICA-WORMS, D., KRITZER, J. A., LU, Z., BAST, R. C., JR. & MILLWARD, S. W. 2021. Directed evolution of cyclic peptides for inhibition of autophagy. *Chem Sci*, 12, 3526-3543.
- GREEN, F., O'HARE, T., BLACKWELL, A. & ENNS, C. A. 2002. Association of human transferrin receptor with GABARAP. *FEBS LETT*, 518.
- GRUNWALD, D. S., OTTO, N. M., PARK, J. M., SONG, D. & KIM, D. H. 2020. GABARAPs and LC3s have opposite roles in regulating ULK1 for autophagy induction. *Autophagy*, 16, 600-614.
- GU, Y., PRINCELY ABUDU, Y., KUMAR, S., BISSA, B., CHOI, S. W., JIA, J., LAZAROU, M., ESKELINEN, E. L., JOHANSEN, T. & DERETIC, V. 2019. Mammalian Atg8 proteins regulate lysosome and autolysosome biogenesis through SNAREs. *EMBO J*, 38, e101994.
- GULLA, A., MORELLI, E., JOHNSTONE, M., TURI, M., SAMUR, M. K., BOTTA, C., CIFRIC, S., FOLINO, P., VINAIXA, D., BARELLO, F., CLERICUZIO, C., FAVASULI, V. K., MAISANO, D., TALLURI, S., PRABHALA, R., BIANCHI, G., FULCINITI, M., WEN, K., KURATA, K., LIU, J., PENAILILLO, J., BRAGONI, A., SAPINO, A., RICHARDSON, P. G., CHAUHAN, D., CARRASCO, R. D., HIDESHIMA, T., MUNSHI, N. C. & ANDERSON, K. C. 2024. Loss of GABARAP mediates resistance to immunogenic chemotherapy in multiple myeloma. *Blood*, 143, 2612-2626.
- GUO, H., CHITIPROLU, M., RONCEVIC, L., JAVALET, C., HEMMING, F. J., TRUNG, M. T., MENG, L., LATREILLE, E., TANESE DE SOUZA, C., MCCULLOCH, D., BALDWIN, R. M., AUER, R., COTE, J., RUSSELL, R. C., SADOUL, R. & GIBBINGS, D. 2017. Atg5 Disassociates the V(1)V(0)-ATPase to Promote Exosome Production and Tumor Metastasis Independent of Canonical Macroautophagy. *Dev Cell*, 43, 716-730 e7.
- HANADA, T., NODA, N. N., SATOMI, Y., ICHIMURA, Y., FUJIOKA, Y., TAKAO, T., INAGAKI, F. & OHSUMI, Y. 2007. The Atg12-Atg5 conjugate has a novel E3-like activity for protein lipidation in autophagy. *J Biol Chem*, 282, 37298-37302.
- HARA, T., NAKAMURA, K., MATSUI, M., YAMAMOTO, A., NAKAHARA, Y., SUZUKI-MIGISHIMA, R., YOKOYAMA, M., MISHIMA, K., SAITO, I., OKANO, H. & MIZUSHIMA, N. 2006. Suppression of basal autophagy in neural cells causes neurodegenerative disease in mice. *Nature*, 441, 885-9.
- HARDING, T. M., MORANO, K. A., SCOTT, S. V. & KLIONSKY, D. J. 1995. Isolation and characterization of yeast mutants in the cytoplasm to vacuole protein targeting pathway. *J Cell Biol*, 131, 591-602.
- HARTMANN, M., HUBER, J., KRAMER, J. S., HEERING, J., PIETSCH, L., STARK, H., ODADZIC, D., BISCHOFF, I., FURST, R., SCHRODER, M., AKUTSU, M., CHAIKUAD, A., DOTSCHE, V., KNAPP, S., BIONDI, R. M., ROGOV, V. V. & PROSCHAK, E. 2021. Demonstrating Ligandability of the LC3A and LC3B Adapter Interface. *J Med Chem*, 64, 3720-3746.
- HE, H., DANG, Y., DAI, F., GUO, Z., WU, J., SHE, X., PEI, Y., CHEN, Y., LING, W., WU, C., ZHAO, S., LIU, J. O. & YU, L. 2003. Post-translational modifications of three members of the human MAP1LC3 family and detection of a novel type of modification for MAP1LC3B. *J Biol Chem*, 278, 29278-87.
- HECKMANN, B. L., TEUBNER, B. J. W., BOADA-ROMERO, E., TUMMERS, B., GUY, C., FITZGERALD, P., MAYER, U., CARDING, S., ZAKHARENKO, S. S., WILEMAN, T. & GREEN, D. R. 2020. Noncanonical function of an autophagy protein prevents spontaneous Alzheimer's disease. *Sci Adv*, 6, eabb9036.
- HECKMANN, B. L., TEUBNER, B. J. W., TUMMERS, B., BOADA-ROMERO, E., HARRIS, L., YANG, M., GUY, C. S., ZAKHARENKO, S. S. & GREEN, D. R. 2019. LC3-Associated Endocytosis Facilitates beta-Amyloid Clearance and Mitigates Neurodegeneration in Murine Alzheimer's Disease. *Cell*, 178, 536-551 e14.
- HERHAUS, L., BHASKARA, R. M., LYSTAD, A. H., GESTAL-MATO, U., COVARRUBIAS-PINTO, A., BONN, F., SIMONSEN, A., HUMMER, G. & DIKIC, I. 2020. TBK1-mediated phosphorylation of LC3C and GABARAP-L2 controls autophagosome shedding by ATG4 protease. *EMBO Rep*, 21, e48317.

- HERVAS, J. H., LANDAJUELA, A., ANTON, Z., SHNYROVA, A. V., GONI, F. M. & ALONSO, A. 2017. Human ATG3 binding to lipid bilayers: role of lipid geometry, and electric charge. *Sci Rep*, 7, 15614.
- HONDA, S., ARAKAWA, S., NISHIDA, Y., YAMAGUCHI, H., ISHII, E. & SHIMIZU, S. 2014. Ulk1-mediated Atg5-independent macroautophagy mediates elimination of mitochondria from embryonic reticulocytes. *Nat Commun*, 5, 4004.
- HOOPER, K. M., JACQUIN, E., LI, T., GOODWIN, J. M., BRUMELL, J. H., DURGAN, J. & FLOREY, O. 2022. V-ATPase is a universal regulator of LC3-associated phagocytosis and non-canonical autophagy. *J Cell Biol*, 221.
- HUANG, P., ZHAO, C., CHEN, C., WHITEHEART, S. W. & LIU-CHEN, L. Y. 2022. Does GEC1 Enhance Expression and Forward Trafficking of the Kappa Opioid Receptor (KOR) via Its Ability to Interact with NSF Directly? *Handb Exp Pharmacol*, 271, 83-96.
- HUANG, X., GAN, G., WANG, X., XU, T. & XIE, W. 2019. The HGF-MET axis coordinates liver cancer metabolism and autophagy for chemotherapeutic resistance. *Autophagy*, 15, 1258-1279.
- ICHIMURA, Y., KIRISAKO, T., TAKAO, T., SATOMI, Y., SHIMONISHI, Y., ISHIHARA, N., MIZUSHIMA, N., TANIDA, I., KOMINAMI, E., OHSUMI, M., NODA, T. & OHSUMI, Y. 2000. A ubiquitin-like system mediates protein lipidation. *Nature*, 408, 488-92.
- ICHIMURA, Y., KUMANOMIDOU, T., SOU, Y. S., MIZUSHIMA, T., EZAKI, J., UENO, T., KOMINAMI, E., YAMANE, T., TANAKA, K. & KOMATSU, M. 2008. Structural basis for sorting mechanism of p62 in selective autophagy. *J Biol Chem*, 283, 22847-57.
- INOMATA, M., XU, S., CHANDRA, P., MEYDANI, S. N., TAKEMURA, G., PHILIPS, J. A. & LEONG, J. M. 2020. Macrophage LC3-associated phagocytosis is an immune defense against *Streptococcus pneumoniae* that diminishes with host aging. *Proc Natl Acad Sci U S A*, 117, 33561-33569.
- ITAKURA, E., KISHI-ITAKURA, C. & MIZUSHIMA, N. 2012. The hairpin-type tail-anchored SNARE syntaxin 17 targets to autophagosomes for fusion with endosomes/lysosomes. *Cell*, 151, 1256-69.
- ITAKURA, E. & MIZUSHIMA, N. 2010. Characterization of autophagosome formation site by a hierarchical analysis of mammalian Atg proteins. *Autophagy*, 6, 764-76.
- JACQUET, M., GUITTAUT, M., FRAICHARD, A. & DESPOUY, G. 2021. The functions of Atg8-family proteins in autophagy and cancer: linked or unrelated? *Autophagy*, 17, 599-611.
- JACQUIN, E., LECLERC-MERCIER, S., JUDON, C., BLANCHARD, E., FRAITAG, S. & FLOREY, O. 2017. Pharmacological modulators of autophagy activate a parallel noncanonical pathway driving unconventional LC3 lipidation. *Autophagy*, 13, 854-867.
- JATANA, N., ASCHER, D. B., PIRES, D. E. V., GOKHALE, R. S. & THUKRAL, L. 2020. Human LC3 and GABARAP subfamily members achieve functional specificity via specific structural modulations. *Autophagy*, 16, 239-255.
- JAVED, R., JAIN, A., DUQUE, T., HENDRIX, E., PADDAR, M. A., KHAN, S., CLAUDE-TAUPIN, A., JIA, J., ALLERS, L., WANG, F., MUDD, M., TIMMINS, G., LIDKE, K., RUSTEN, T. E., AKEPATI, P. R., HE, Y., REGGIORI, F., ESKELINEN, E. L. & DERETIC, V. 2023. Mammalian ATG8 proteins maintain autophagosomal membrane integrity through ESCRTs. *EMBO J*, 42, e112845.
- JIN, M., LIU, X. & KLIONSKY, D. J. 2013. SnapShot: Selective autophagy. *Cell*, 152, 368-368 e2.
- JOACHIM, J., RAZI, M., JUDITH, D., WIRTH, M., CALAMITA, E., ENCHEVA, V., DYNLACHT, B. D., SNIJDERS, A. P., O'REILLY, N., JEFFERIES, H. B. J. & TOOZE, S. A. 2017. Centriolar Satellites Control GABARAP Ubiquitination and GABARAP-Mediated Autophagy. *Curr Biol*, 27, 2123-2136 e7.
- JOHANSEN, T., BIRGISDOTTIR, Å. B., HUBER, J., KNISS, A., DÖTSCH, V., KIRKIN, V. & ROGOV, V. V. 2017. Methods for Studying Interactions Between Atg8/LC3/GABARAP and LIR-Containing Proteins. *Molecular Characterization of Autophagic Responses, Pt A*, 587, 143-169.
- JOHANSEN, T. & LAMARK, T. 2020. Selective Autophagy: ATG8 Family Proteins, LIR Motifs and Cargo Receptors. *J Mol Biol*, 432, 80-103.
- JUDITH, D., JEFFERIES, H. B. J., BOEING, S., FRITH, D., SNIJDERS, A. P. & TOOZE, S. A. 2019. ATG9A shapes the forming autophagosome through Arfaptin 2 and phosphatidylinositol 4-kinase IIIbeta. *J Cell Biol*, 218, 1634-1652.

- KABEYA, Y., MIZUSHIMA, N., UENO, T., YAMAMOTO, A., KIRISAKO, T., NODA, T., KOMINAMI, E., OHSUMI, Y. & YOSHIMORI, T. 2000. LC3, a mammalian homologue of yeast Apg8p, is localized in autophagosome membranes after processing. *EMBO J*, 19, 5720-8.
- KABEYA, Y., MIZUSHIMA, N., YAMAMOTO, A., OSHITANI-OKAMOTO, S., OHSUMI, Y. & YOSHIMORI, T. 2004. LC3, GABARAP and GATE16 localize to autophagosomal membrane depending on form-II formation. *J Cell Sci*, 117, 2805-2812.
- KALVARI, I., TSOMPANIS, S., MULAKKAL, N. C., OSGOOD, R., JOHANSEN, T., NEZIS, I. P. & PROMPONAS, V. J. 2014. iLIR: A web resource for prediction of Atg8-family interacting proteins. *Autophagy*, 10, 913-25.
- KARANASIOS, E., STAPLETON, E., MANIFAVA, M., KAIZUKA, T., MIZUSHIMA, N., WALKER, S. A. & KTISTAKIS, N. T. 2013. Dynamic association of the ULK1 complex with omegasomes during autophagy induction. *J Cell Sci*, 126, 5224-38.
- KARSLI-UZUNBAS, G., GUO, J. Y., PRICE, S., TENG, X., LADDHA, S. V., KHOR, S., KALAANY, N. Y., JACKS, T., CHAN, C. S., RABINOWITZ, J. D. & WHITE, E. 2014. Autophagy is required for glucose homeostasis and lung tumor maintenance. *Cancer Discov*, 4, 914-27.
- KAUFFMAN, K. J., YU, S., JIN, J., MUGO, B., NGUYEN, N., O'BRIEN, A., NAG, S., LYSTAD, A. H. & MELIA, T. J. 2018. Delipidation of mammalian Atg8-family proteins by each of the four ATG4 proteases. *Autophagy*, 14, 992-1010.
- KAUR, N., DE LA BALLINA, L. R., HAUKAAS, H. S., TORGERSEN, M. L., RADULOVIC, M., MUNSON, M. J., SABIRSH, A., STENMARK, H., SIMONSEN, A., CARLSSON, S. R. & LYSTAD, A. H. 2023. TECPR1 is activated by damage-induced sphingomyelin exposure to mediate noncanonical autophagy. *EMBO J*, 42, e113105.
- KELLNER, R., DE LA CONCEPCION, J. C., MAQBOOL, A., KAMOUN, S. & DAGDAS, Y. F. 2017. ATG8 Expansion: A Driver of Selective Autophagy Diversification? *Trends Plant Sci*, 22, 204-214.
- KENZELMANN BROZ, D., SPANO MELLO, S., BIEGING, K. T., JIANG, D., DUSEK, R. L., BRADY, C. A., SIDOW, A. & ATTARDI, L. D. 2013. Global genomic profiling reveals an extensive p53-regulated autophagy program contributing to key p53 responses. *Genes Dev*, 27, 1016-31.
- KHAMINETS, A., HEINRICH, T., MARI, M., GRUMATI, P., HUEBNER, A. K., AKUTSU, M., LIEBMANN, L., STOLZ, A., NIETZSCHE, S., KOCH, N., MAUTHE, M., KATONA, I., QUALMANN, B., WEIS, J., REGGIORI, F., KURTH, I., HUBNER, C. A. & DIKIC, I. 2015. Regulation of endoplasmic reticulum turnover by selective autophagy. *Nature*, 522, 354-8.
- KIMURA, S., NODA, T. & YOSHIMORI, T. 2007. Dissection of the autophagosome maturation process by a novel reporter protein, tandem fluorescent-tagged LC3. *Autophagy*, 3, 452-60.
- KIRISAKO, T., BABA, M., ISHIHARA, N., MIYAZAWA, K., OHSUMI, M., YOSHIMORI, T., NODA, T. & OHSUMI, Y. 1999. Formation process of autophagosome is traced with Apg8/Aut7p in yeast. *J Cell Biol*, 147, 435-446.
- KIRKIN, V., LAMARK, T., SOU, Y. S., BJORKOY, G., NUNN, J. L., BRUUN, J. A., SHVETS, E., MCEWAN, D. G., CLAUSEN, T. H., WILD, P., BILUSIC, I., THEURILLAT, J. P., OVERVATN, A., ISHII, T., ELAZAR, Z., KOMATSU, M., DIKIC, I. & JOHANSEN, T. 2009. A role for NBR1 in autophagosomal degradation of ubiquitinated substrates. *Mol Cell*, 33, 505-16.
- KIRKIN, V. & ROGOV, V. V. 2019. A Diversity of Selective Autophagy Receptors Determines the Specificity of the Autophagy Pathway. *Mol Cell*, 76, 268-285.
- KITTLER, J. T., ROSTAING, P., SCHIAVO, G., FRITSCHY, J. M., OLSEN, R., TRILLER, A. & MOSS, S. J. 2001. The subcellular distribution of GABARAP and its ability to interact with NSF suggest a role for this protein in the intracellular transport of GABA<sub>A</sub> receptors. *Mol Cell Neurosci*, 18, 13-25.
- KLIONSKY, D. J., ABDEL-AZIZ, A. K., ABDELFAHAH, S. & AL., E. 2021a. Guidelines for the use and interpretation of assays for monitoring autophagy (4th edition). *Autophagy*, 17, 1-382.
- KLIONSKY, D. J., PETRONI, G., AMARAVADI, R. K., BAEHRECKE, E. H., BALLABIO, A., BOYA, P., BRAVO-SAN PEDRO, J. M., CADWELL, K., CECCONI, F., CHOI, A. M. K., CHOI, M. E., CHU, C. T., CODOGNO, P., COLOMBO, M. I., CUERVO, A. M., DERETIC, V., DIKIC, I., ELAZAR, Z., ESKELINEN, E. L., FIMIA, G. M., GEWIRTZ, D. A., GREEN, D. R., HANSEN, M., JAATTELA, M., JOHANSEN, T., JUHASZ, G., KARANTZA, V., KRAFT, C., KROEMER, G., KTISTAKIS, N. T., KUMAR, S., LOPEZ-OTIN, C., MACLEOD, K. F., MADEO, F., MARTINEZ, J., MELENDEZ, A.,

- MIZUSHIMA, N., MUNZ, C., PENNINGER, J. M., PERERA, R. M., PIACENTINI, M., REGGIORI, F., RUBINSZTEIN, D. C., RYAN, K. M., SADOSHIMA, J., SANTAMBROGIO, L., SCORRANO, L., SIMON, H. U., SIMON, A. K., SIMONSEN, A., STOLZ, A., TAVERNARAKIS, N., TOOZE, S. A., YOSHIMORI, T., YUAN, J., YUE, Z., ZHONG, Q., GALLUZZI, L. & PIETROCOLA, F. 2021b. Autophagy in major human diseases. *EMBO J*, 40, e108863.
- KOCAK, M., EZAZI ERDI, S., JORBA, G., MAESTRO, I., FARRES, J., KIRKIN, V., MARTINEZ, A. & PLESS, O. 2021. Targeting autophagy in disease: established and new strategies. *Autophagy*, 1-23.
- KOCAK, M., EZAZI ERDI, S., JORBA, G., MAESTRO, I., FARRES, J., KIRKIN, V., MARTINEZ, A. & PLESS, O. 2022. Targeting autophagy in disease: established and new strategies. *Autophagy*, 18, 473-495.
- KOMATSU, M., WAGURI, S., CHIBA, T., MURATA, S., IWATA, J., TANIDA, I., UENO, T., KOIKE, M., UCHIYAMA, Y., KOMINAMI, E. & TANAKA, K. 2006. Loss of autophagy in the central nervous system causes neurodegeneration in mice. *Nature*, 441, 880-4.
- KOMATSU, M., WAGURI, S., UENO, T., IWATA, J., MURATA, S., TANIDA, I., EZAKI, J., MIZUSHIMA, N., OHSUMI, Y., UCHIYAMA, Y., KOMINAMI, E., TANAKA, K. & CHIBA, T. 2005. Impairment of starvation-induced and constitutive autophagy in Atg7-deficient mice. *J Cell Biol*, 169, 425-34.
- KORAC, J., SCHAEFFER, V., KOVACEVIC, I., CLEMENT, A. M., JUNGBLUT, B., BEHL, C., TERZIC, J. & DIKIC, I. 2013. Ubiquitin-independent function of optineurin in autophagic clearance of protein aggregates. *J Cell Sci*, 126, 580-92.
- KOUNO, T., MIZUGUCHI, M., TANIDA, I., UENO, T., KANEMATSU, T., MORI, Y., SHINODA, H., HIRATA, M., KOMINAMI, E. & KAWANO, K. 2005. Solution structure of microtubule-associated protein light chain 3 and identification of its functional subdomains. *J Biol Chem*, 280, 24610-7.
- KRAFT, C., KIJANSKA, M., KALIE, E., SIERGIEJUK, E., LEE, S. S., SEMPLICIO, G., STOFFEL, I., BREZOVICH, A., VERMA, M., HANSMANN, I., AMMERER, G., HOFMANN, K., TOOZE, S. & PETER, M. 2012. Binding of the Atg1/ULK1 kinase to the ubiquitin-like protein Atg8 regulates autophagy. *EMBO J*, 31, 3691-703.
- KRICHEL, C., MÖCKEL, C., SCHILLINGER, O., HUESGEN, P. F., STICHT, H., STRODEL, B., WEIERGRÄBER, O. H., WILLBOLD, D. & NEUDECKER, P. 2019. Solution structure of the autophagy-related protein LC3C reveals a polyproline II motif on a mobile tether with phosphorylation site. *Sci Rep*, 9, 14167.
- KTISTAKIS, N. & FLOREY, O. 2019. *Autophagy - Methods and Protocols*.
- KUANG, Y., MA, K., ZHOU, C., DING, P., ZHU, Y., CHEN, Q. & XIA, B. 2016. Structural basis for the phosphorylation of FUNDC1 LIR as a molecular switch of mitophagy. *Autophagy*, 12, 2363-2373.
- KUMAR, S., JAIN, A., FARZAM, F., JIA, J., GU, Y., CHOI, S. W., MUDD, M. H., CLAUDE-TAUPIN, A., WESTER, M. J., LIDKE, K. A., RUSTEN, T. E. & DERETIC, V. 2018. Mechanism of Stx17 recruitment to autophagosomes via IRGM and mammalian Atg8 proteins. *J Cell Biol*, 217, 997-1013.
- KUMAR, S., JIA, J. & DERETIC, V. 2021. Atg8ylation as a general membrane stress and remodeling response. *Cell Stress*, 5, 128-142.
- KUROKI, T., OSARI, S., NAGATA, K. & KAWAGUCHI, A. 2018. Influenza A Virus NS1 Protein Suppresses JNK1-Dependent Autophagosome Formation Mediated by Rab11a Recycling Endosomes. *Front Microbiol*, 9, 3120.
- KUWAHARA, T. & IWATSUBO, T. 2024. CASM mediates LRRK2 recruitment and activation under lysosomal stress. *Autophagy*.
- KUZNETSOV, S. A. & GELFAND, V. I. 1987. 18 kDa microtubule-associated protein: identification as a new light chain (LC-3) of microtubule-associated protein 1 (MAP-1). *FEBS LETT*, 212, 145-8.
- LAINEZ, S., VALENTE, P., ONTORIA-OVIEDO, I., ESTEVEZ-HERRERA, J., CAMPRUBI-ROBLES, M., FERRER-MONTIEL, A. & PLANELLAS-CASES, R. 2010. GABA<sub>A</sub> receptor associated protein (GABARAP) modulates TRPV1 expression and channel function and desensitization. *FASEB J*, 24, 1958-70.



- LANG, T., SCHAEFFELER, E., BERNREUTHER, D., BREDSCHNEIDER, M., WOLF, D. H. & THUMM, M. 1998. Aut2p and Aut7p, two novel microtubule-associated proteins are essential for delivery of autophagic vesicles to the vacuole. *EMBO J*, 17, 3597-607.
- LAZAROU, M., SLITER, D. A., KANE, L. A., SARRAF, S. A., WANG, C., BURMAN, J. L., SIDERIS, D. P., FOGEL, A. I. & YOULE, R. J. 2015. The ubiquitin kinase PINK1 recruits autophagy receptors to induce mitophagy. *Nature*, 524, 309-314.
- LEBOVITZ, C. B., ROBERTSON, A. G., GOYA, R., JONES, S. J., MORIN, R. D., MARRA, M. A. & GORSKI, S. M. 2015. Cross-cancer profiling of molecular alterations within the human autophagy interaction network. *Autophagy*, 11, 1668-87.
- LEE, Y. K. & LEE, J. A. 2016. Role of the mammalian ATG8/LC3 family in autophagy: differential and compensatory roles in the spatiotemporal regulation of autophagy. *BMB Rep*, 49, 424-30.
- LEIDAL, A. M. & DEBNATH, J. 2020. LC3-dependent extracellular vesicle loading and secretion (LDELS). *Autophagy*, 16, 1162-1163.
- LEIDAL, A. M., HUANG, H. H., MARSH, T., SOLVIK, T., ZHANG, D., YE, J., KAI, F., GOLDSMITH, J., LIU, J. Y., HUANG, Y. H., MONKKONEN, T., VLAHAKIS, A., HUANG, E. J., GOODARZI, H., YU, L., WIITA, A. P. & DEBNATH, J. 2020. The LC3-conjugation machinery specifies the loading of RNA-binding proteins into extracellular vesicles. *Nat Cell Biol*, 22, 187-199.
- LEIL, T. A., CHEN, Z. W., CHANG, C. S. & OLSEN, R. W. 2004. GABA<sub>A</sub> receptor-associated protein traffics GABA<sub>A</sub> receptors to the plasma membrane in neurons. *J Neurosci*, 24, 11429-38.
- LEUNG, L. S., NEAL, J. W., WAKELEE, H. A., SEQUIST, L. V. & MARMOR, M. F. 2015. Rapid Onset of Retinal Toxicity From High-Dose Hydroxychloroquine Given for Cancer Therapy. *Am J Ophthalmol*, 160, 799-805 e1.
- LEVEILLE, A. N., BROWN, H., SCHWARZROCK, T., TRUE, B., PLASENCIA, J., NEUDECKER, P., ÜFFING, A., WEIERGRÄBER, O. H., WILLBOLD, D. & KRITZER, J. A. 2024. Exploring Arylidene-Indolinone Ligands of Autophagy Proteins LC3B and GABARAP. *BioRxiv*.
- LI, J., ZHU, R., CHEN, K., ZHENG, H., ZHAO, H., YUAN, C., ZHANG, H., WANG, C. & ZHANG, M. 2018. Potent and specific Atg8-targeting autophagy inhibitory peptides from giant ankyrins. *Nat Chem Biol*, 14, 778-787.
- LI, Z., WANG, C., WANG, Z., ZHU, C., LI, J., SHA, T., MA, L., GAO, C., YANG, Y., SUN, Y., WANG, J., SUN, X., LU, C., DIFIGLIA, M., MEI, Y., DING, C., LUO, S., DANG, Y., DING, Y., FEI, Y. & LU, B. 2019. Allele-selective lowering of mutant HTT protein by HTT-LC3 linker compounds. *Nature*, 575, 203-209.
- LIANG, X. H., JACKSON, S., SEAMAN, M., BROWN, K., KEMPKE, B., HIBSHOOSH, H. & LEVINE, B. 1999. Induction of autophagy and inhibition of tumorigenesis by beclin 1. *Nature*, 402, 672-6.
- LYSTAD, A. H., CARLSSON, S. R. & SIMONSEN, A. 2019. Toward the function of mammalian ATG12-ATG5-ATG16L1 complex in autophagy and related processes. *Autophagy*, 15, 1485-1486.
- MA, J., BECKER, C., LOWELL, C. A. & UNDERHILL, D. M. 2012. Dectin-1-triggered Recruitment of Light Chain 3 Protein to Phagosomes Facilitates Major Histocompatibility Complex Class II Presentation of Fungal-derived Antigens. *J Biol Chem*, 287, 34149-34156.
- MA, P., SCHWARTEN, M., SCHNEIDER, L., BOESKE, A., HENKE, N., LISAK, D., WEBER, S., MOHRLÜDER, J., STOLDT, M., STRODEL, B., METHNER, A., HOFFMANN, S., WEIERGRÄBER, O. H. & WILLBOLD, D. 2013. Interaction of Bcl-2 with the autophagy-related GABA<sub>A</sub> receptor-associated protein (GABARAP): biophysical characterization and functional implications. *J Biol Chem*, 288, 37204-15.
- MA, X., LU, C., CHEN, Y., LI, S., MA, N., TAO, X., LI, Y., WANG, J., ZHOU, M., YAN, Y. B., LI, P., HEYDARI, K., DENG, H., ZHANG, M., YI, C. & GE, L. 2022. CCT2 is an aggrephagy receptor for clearance of solid protein aggregates. *Cell*, 185, 1325-1345 e22.
- MADEIRA, F., PEARCE, M., TIVEY, A. R. N., BASUTKAR, P., LEE, J., EDBALI, O., MADHUSOODANAN, N., KOLESNIKOV, A. & LOPEZ, R. 2022. Search and sequence analysis tools services from EMBL-EBI in 2022. *Nucleic Acids Res*, 50, W276-W279.
- MAEDA, S., OTOMO, C. & OTOMO, T. 2019. The autophagic membrane tether ATG2A transfers lipids between membranes. *Elife*, 8.

- MAEDA, S., YAMAMOTO, H., KINCH, L. N., GARZA, C. M., TAKAHASHI, S., OTOMO, C., GRISHIN, N. V., FORLI, S., MIZUSHIMA, N. & OTOMO, T. 2020. Structure, lipid scrambling activity and role in autophagosome formation of ATG9A. *Nat Struct Mol Biol*, 27, 1194-1201.
- MAEJIMA, I., TAKAHASHI, A., OMORI, H., KIMURA, T., TAKABATAKE, Y., SAITOH, T., YAMAMOTO, A., HAMASAKI, M., NODA, T., ISAKA, Y. & YOSHIMORI, T. 2013. Autophagy sequesters damaged lysosomes to control lysosomal biogenesis and kidney injury. *EMBO J*, 32, 2336-47.
- MANN, M. & HAMMARBACK, J. A. 1996. Gene Localization and Developmental Expression of Light Chain 3: A Common Subunit of Microtubule-Associated Protein 1A (MAP1A) and MAP1B. *J Neurosci Res*, 43.
- MANN, S. S. & HAMMARBACK, J. A. 1994. Molecular characterization of light chain 3. A microtubule binding subunit of MAP1A and MAP1B. *J Biol Chem*, 269, 11492-11497.
- MANSUY, V., BOIREAU, W., FRAICHARD, A., SCHLICK, J. L., JOUVENOT, M. & DELAGE-MOURROUX, R. 2004. GEC1, a protein related to GABARAP, interacts with tubulin and GABA<sub>A</sub> receptor. *Biochem Biophys Res Commun*, 325, 639-48.
- MARSHALL, R. S., HUA, Z., MALI, S., MCLOUGHLIN, F. & VIERSTRA, R. D. 2019. ATG8-Binding UIM Proteins Define a New Class of Autophagy Adaptors and Receptors. *Cell*, 177, 766-781 e24.
- MARTENS, S. & FRACCHIOLLA, D. 2020. Activation and targeting of ATG8 protein lipidation. *Cell Discov*, 6, 23.
- MARTINEZ-LOPEZ, N., ATHONVARANGKUL, D., MISHALL, P., SAHU, S. & SINGH, R. 2013. Autophagy proteins regulate ERK phosphorylation. *Nat Commun*, 4, 2799.
- MARTINEZ, J., ALMENDINGER, J., OBERST, A., NESS, R., DILLON, C. P., FITZGERALD, P., HENGARTNER, M. O. & GREEN, D. R. 2011. Microtubule-associated protein 1 light chain 3 alpha (LC3)-associated phagocytosis is required for the efficient clearance of dead cells. *Proc Natl Acad Sci U S A*, 108, 17396-401.
- MARUYAMA, T., ALAM, J. M., FUKUDA, T., KAGEYAMA, S., KIRISAKO, H., ISHII, Y., SHIMADA, I., OHSUMI, Y., KOMATSU, M., KANKI, T., NAKATOGAWA, H. & NODA, N. N. 2021. Membrane perturbation by lipidated Atg8 underlies autophagosome biogenesis. *Nat Struct Mol Biol*, 28, 583-593.
- MARWAHA, R., ARYA, S. B., JAGGA, D., KAUR, H., TULI, A. & SHARMA, M. 2017. The Rab7 effector PLEKHM1 binds Arl8b to promote cargo traffic to lysosomes. *J Cell Biol*, 216, 1051-1070.
- MASUELLI, L., GRANATO, M., BENVENUTO, M., MATTERA, R., BERNARDINI, R., MATTEI, M., D'AMATI, G., D'ORAZI, G., FAGGIONI, A., BEI, R. & CIRONE, M. 2017. Chloroquine supplementation increases the cytotoxic effect of curcumin against Her2/neu overexpressing breast cancer cells in vitro and in vivo in nude mice while counteracts it in immune competent mice. *Oncoimmunology*, 6, e1356151.
- MAUTHE, M., ORHON, I., ROCCHI, C., ZHOU, X., LUHR, M., HIJLKEMA, K. J., COPPES, R. P., ENGEDAL, N., MARI, M. & REGGIORI, F. 2018. Chloroquine inhibits autophagic flux by decreasing autophagosome-lysosome fusion. *Autophagy*, 14, 1435-1455.
- MCEWAN, D. G., POPOVIC, D., GUBAS, A., TERAWAKI, S., SUZUKI, H., STADEL, D., COXON, F. P., MIRANDA DE STEGMANN, D., BHOGARAJU, S., MADDI, K., KIRCHOF, A., GATTI, E., HELFRICH, M. H., WAKATSUKI, S., BEHREND, C., PIERRE, P. & DIKIC, I. 2015. PLEKHM1 regulates autophagosome-lysosome fusion through HOPS complex and LC3/GABARAP proteins. *Mol Cell*, 57, 39-54.
- MEI, L., CHEN, X., WEI, F., HUANG, X., LIU, L., YAO, J., CHEN, J., LUO, X., WANG, Z. & YANG, A. 2023. Tethering ATG16L1 or LC3 induces targeted autophagic degradation of protein aggregates and mitochondria. *Autophagy*, 19, 2997-3013.
- MELIA, T. J., LYSTAD, A. H. & SIMONSEN, A. 2020. Autophagosome biogenesis: From membrane growth to closure. *J Cell Biol*, 219.
- MENZIES, F. M., FLEMING, A. & RUBINSZTEIN, D. C. 2015. Compromised autophagy and neurodegenerative diseases. *Nat Rev Neurosci*, 16, 345-57.
- MICHAUD, M., MARTINS, I., SUKKURWALA, A. Q., ADJEMIAN, S., MA, Y., PELLEGATTI, P., SHEN, S., KEPP, O., SCOAZEC, M., MIGNOT, G., RELLO-VARONA, S., TAILLER, M., MENDER, L., VACCHELLI, E., GALLUZZI, L., GHIRINGHELLI, F., DI VIRGILIO, F., ZITVOGEL, L. & KROEMER, S.

- G. 2011. Autophagy-dependent anticancer immune responses induced by chemotherapeutic agents in mice. *Science*, 334, 1573-7.
- MIZUSHIMA, N. 2004. Methods for monitoring autophagy. *Int J Biochem Cell Biol*, 36, 2491-502.
- MIZUSHIMA, N. 2020. The ATG conjugation systems in autophagy. *Curr Opin Cell Biol*, 63, 1-10.
- MIZUSHIMA, N. & KOMATSU, M. 2011. Autophagy: renovation of cells and tissues. *Cell*, 147, 728-41.
- MIZUSHIMA, N., KUMA, A., KOBAYASHI, Y., YAMAMOTO, A., MATSUBAE, M., TAKAO, T., NATSUME, T., OHSUMI, Y. & YOSHIMORI, T. 2003. Mouse Apg16L, a novel WD-repeat protein, targets to the autophagic isolation membrane with the Apg12-Apg5 conjugate. *J Cell Sci*, 116, 1679-88.
- MIZUSHIMA, N., SUGITA, H., YOSHIMORI, T. & OHSUMI, Y. 1998. A new protein conjugation system in human - The counterpart of the yeast Apg12p conjugation system essential for autophagy. *J Biol Chem*, 273, 33889-33892.
- MIZUSHIMA, N., YOSHIMORI, T. & OHSUMI, Y. 2011. The role of Atg proteins in autophagosome formation. *Annu Rev Cell Dev Biol*, 27, 107-32.
- MOHRLÜDER, J., HOFFMANN, Y., STANGLER, T., HÄNEL, K. & WILLBOLD, D. 2007a. Identification of clathrin heavy chain as a direct interaction partner for the gamma-aminobutyric acid type A receptor associated protein. *Biochemistry*, 46, 14537-43.
- MOHRLÜDER, J., STANGLER, T., HOFFMANN, Y., WIESEHAN, K., MATARUGA, A. & WILLBOLD, D. 2007b. Identification of calreticulin as a ligand of GABARAP by phage display screening of a peptide library. *FEBS J*, 274, 5543-55.
- NALAWANSHA, D. A. & CREWS, C. M. 2020. PROTACs: An Emerging Therapeutic Modality in Precision Medicine. *Cell Chem Biol*, 27, 998-1014.
- NARENDRA, D., TANAKA, A., SUEN, D. F. & YOULE, R. J. 2008. Parkin is recruited selectively to impaired mitochondria and promotes their autophagy. *J Cell Biol*, 183, 795-803.
- NATH, S., DANCOURT, J., SHTEYN, V., PUENTE, G., FONG, W. M., NAG, S., BEWERSDORF, J., YAMAMOTO, A., ANTONNY, B. & MELIA, T. J. 2014. Lipidation of the LC3/GABARAP family of autophagy proteins relies on a membrane-curvature-sensing domain in Atg3. *Nat Cell Biol*, 16, 415-24.
- NGUYEN, T. N. & LAZAROU, M. 2022. A unifying model for the role of the ATG8 system in autophagy. *J Cell Sci*, 135.
- NGUYEN, T. N., PADMAN, B. S., USHER, J., OORSCHOT, V., RAMM, G. & LAZAROU, M. 2016. Atg8 family LC3/GABARAP proteins are crucial for autophagosome-lysosome fusion but not autophagosome formation during PINK1/Parkin mitophagy and starvation. *J Cell Biol*, 215, 857-874.
- NISHIMURA, T., TAMURA, N., KONO, N., SHIMANAKA, Y., ARAI, H., YAMAMOTO, H. & MIZUSHIMA, N. 2017. Autophagosome formation is initiated at phosphatidylinositol synthase-enriched ER subdomains. *EMBO J*, 36, 1719-1735.
- NISHIMURA, T. & TOOZE, S. A. 2020. Emerging roles of ATG proteins and membrane lipids in autophagosome formation. *Cell Discov*, 6, 32.
- NODA, N. N. 2021. Atg2 and Atg9: Intermembrane and interleaflet lipid transporters driving autophagy. *Biochim Biophys Acta Mol Cell Biol Lipids*, 1866, 158956.
- NODA, N. N., KUMETA, H., NAKATOGAWA, H., SATOO, K., ADACHI, W., ISHII, J., FUJIOKA, Y., OHSUMI, Y. & INAGAKI, F. 2008. Structural basis of target recognition by Atg8/LC3 during selective autophagy. *Genes Cells*, 13, 1211-8.
- NODA, N. N., OHSUMI, Y. & INAGAKI, F. 2010. Atg8-family interacting motif crucial for selective autophagy. *FEBS LETT*, 584, 1379-85.
- NODA, T. 2017. Autophagy in the context of the cellular membrane-trafficking system: the enigma of Atg9 vesicles. *Biochem Soc Trans*, 45, 1323-1331.
- NOVAK, I., KIRKIN, V., MCEWAN, D. G., ZHANG, J., WILD, P., ROZENKNOP, A., ROGOV, V., LOHR, F., POPOVIC, D., OCCHIPINTI, A., REICHERT, A. S., TERZIC, J., DOTSCH, V., NEY, P. A. & DIKIC, I. 2010. Nix is a selective autophagy receptor for mitochondrial clearance. *EMBO Rep*, 11, 45-51.

- OHNSTAD, A. E., DELGADO, J. M., NORTH, B. J., NASA, I., KETTENBACH, A. N., SCHULTZ, S. W. & SHOEMAKER, C. J. 2020. Receptor-mediated clustering of FIP200 bypasses the role of LC3 lipidation in autophagy. *EMBO J*, 39, e104948.
- OHSUMI, Y. 2014. Historical landmarks of autophagy research. *Cell Res*, 24, 9-23.
- ORVEDAHL, A., SUMPTER, R., JR., XIAO, G., NG, A., ZOU, Z., TANG, Y., NARIMATSU, M., GILPIN, C., SUN, Q., ROTH, M., FORST, C. V., WRANA, J. L., ZHANG, Y. E., LUBY-PHELPS, K., XAVIER, R. J., XIE, Y. & LEVINE, B. 2011. Image-based genome-wide siRNA screen identifies selective autophagy factors. *Nature*, 480, 113-7.
- OTOMO, C., METLAGEL, Z., TAKAESU, G. & OTOMO, T. 2013. Structure of the human ATG12~ATG5 conjugate required for LC3 lipidation in autophagy. *Nat Struct Mol Biol*, 20, 59-66.
- PANKIV, S., ALEMU, E. A., BRECH, A., BRUUN, J. A., LAMARK, T., OVERVATN, A., BJORKOY, G. & JOHANSEN, T. 2010. FYCO1 is a Rab7 effector that binds to LC3 and PI3P to mediate microtubule plus end-directed vesicle transport. *J Cell Biol*, 188, 253-69.
- PANKIV, S., CLAUSEN, T. H., LAMARK, T., BRECH, A., BRUUN, J. A., OUTZEN, H., OVERVATN, A., BJORKOY, G. & JOHANSEN, T. 2007. p62/SQSTM1 binds directly to Atg8/LC3 to facilitate degradation of ubiquitinated protein aggregates by autophagy. *J Biol Chem*, 282, 24131-45.
- PAZ, Y., ELAZAR, Z. & FASS, D. 2000. Structure of GATE-16, membrane transport modulator and mammalian ortholog of autophagocytosis factor Aut7p. *J Biol Chem*, 275, 25445-50.
- PEI, J., PAN, X., WANG, A., SHUAI, W., BU, F., TANG, P., ZHANG, S., ZHANG, Y., WANG, G. & OUYANG, L. 2021. Developing potent LC3-targeting AUTAC tools for protein degradation with selective autophagy. *Chem Commun (Camb)*, 57, 13194-13197.
- PELLERIN, I., VUILLERMOZ, C., JOUVENOT, M., ORDENER, C., ROYEZ, M. & ADESSI, G. L. 1993. Identification and characterization of an early estrogen-regulated RNA in cultured guinea-pig endometrial cells. *Mol Cell Endocrinol*, 90, R17-21.
- PENGO, N., AGROTIS, A., PRAK, K., JONES, J. & KETTELER, R. 2017. A reversible phospho-switch mediated by ULK1 regulates the activity of autophagy protease ATG4B. *Nat Commun*, 8, 294.
- POPOVIC, D., AKUTSU, M., NOVAK, I., HARPER, J. W., BEHREND, C. & DIKIC, I. 2012. Rab GTPase-activating proteins in autophagy: regulation of endocytic and autophagy pathways by direct binding to human ATG8 modifiers. *Mol Cell Biol*, 32, 1733-44.
- QU, X., YU, J., BHAGAT, G., FURUYA, N., HIBSHOOSH, H., TROXEL, A., ROSEN, J., ESKELINEN, E. L., MIZUSHIMA, N., OHSUMI, Y., CATTORETTI, G. & LEVINE, B. 2003. Promotion of tumorigenesis by heterozygous disruption of the beclin 1 autophagy gene. *J Clin Invest*, 112, 1809-20.
- RAVENHILL, B. J., BOYLE, K. B., VON MUHLINEN, N., ELLISON, C. J., MASSON, G. R., OTTEN, E. G., FOGLEIN, A., WILLIAMS, R. & RANDOW, F. 2019. The Cargo Receptor NDP52 Initiates Selective Autophagy by Recruiting the ULK Complex to Cytosol-Invasive Bacteria. *Mol Cell*, 74, 320-329 e6.
- RAVIKUMAR, B., DUDEN, R. & RUBINSZTEIN, D. C. 2002. Aggregate-prone proteins with polyglutamine and polyalanine expansions are degraded by autophagy. *Hum Mol Genet*, 11, 1107-17.
- RAVIKUMAR, B., VACHER, C., BERGER, Z., DAVIES, J. E., LUO, S., OROZ, L. G., SCARAVILLI, F., EASTON, D. F., DUDEN, R., O'KANE, C. J. & RUBINSZTEIN, D. C. 2004. Inhibition of mTOR induces autophagy and reduces toxicity of polyglutamine expansions in fly and mouse models of Huntington disease. *Nat Genet*, 36, 585-95.
- REBECCA, V. W. & AMARAVADI, R. K. 2016. Emerging strategies to effectively target autophagy in cancer. *Oncogene*, 35, 1-11.
- ROGOV, V. V., NEZIS, I. P., TSAPRAS, P., ZHANG, H., DAGDAS, Y., NODA, N. N., NAKATOGAWA, H., WIRTH, M., MOUILLERON, S., MCEWAN, D. G., BEHREND, C., DERETIC, V., ELAZAR, Z., TOOZE, S. A., DIKIC, I., LAMARK, T. & JOHANSEN, T. 2023. Atg8 family proteins, LIR/AIM motifs and other interaction modes. *Autophagy Reports*, 2.
- ROGOV, V. V., STOLZ, A., RAVICHANDRAN, A. C., RIOS-SZWED, D. O., SUZUKI, H., KNISS, A., LOHR, F., WAKATSUKI, S., DOTSCH, V., DIKIC, I., DOBSON, R. C. & MCEWAN, D. G. 2017a. Structural and functional analysis of the GABARAP interaction motif (GIM). *EMBO REP*, 18, 1382-1396.

- ROGOV, V. V., SUZUKI, H., FISKIN, E., WILD, P., KNISS, A., ROZENKNOP, A., KATO, R., KAWASAKI, M., MCEWAN, D. G., LOHR, F., GUNTERT, P., DIKIC, I., WAKATSUKI, S. & DOTSCHE, V. 2013. Structural basis for phosphorylation-triggered autophagic clearance of *Salmonella*. *Biochem J*, 454, 459-66.
- ROGOV, V. V., SUZUKI, H., MARINKOVIC, M., LANG, V., KATO, R., KAWASAKI, M., BULJUBASIC, M., SPRUNG, M., ROGOVA, N., WAKATSUKI, S., HAMACHER-BRADY, A., DOTSCHE, V., DIKIC, I., BRADY, N. R. & NOVAK, I. 2017b. Phosphorylation of the mitochondrial autophagy receptor Nix enhances its interaction with LC3 proteins. *Sci Rep*, 7, 1131.
- ROY, S., LEIDAL, A. M., YE, J., RONEN, S. M. & DEBNATH, J. 2017. Autophagy-Dependent Shuttling of TBC1D5 Controls Plasma Membrane Translocation of GLUT1 and Glucose Uptake. *Mol Cell*, 67, 84-95 e5.
- RUBINSZTEIN, D. C., CODOGNO, P. & LEVINE, B. 2012. Autophagy modulation as a potential therapeutic target for diverse diseases. *Nat Rev Drug Discov*, 11, 709-30.
- RUSSELL, R. C. & GUAN, K. L. 2022. The multifaceted role of autophagy in cancer. *EMBO J*, 41, e110031.
- RUSSELL, R. C., TIAN, Y., YUAN, H., PARK, H. W., CHANG, Y. Y., KIM, J., KIM, H., NEUFELD, T. P., DILLIN, A. & GUAN, K. L. 2013. ULK1 induces autophagy by phosphorylating Beclin-1 and activating VPS34 lipid kinase. *Nat Cell Biol*, 15, 741-50.
- SAGIV, Y., LEGESSE-MILLER, A., PORAT, A. & ELAZAR, Z. 2000. GATE-16, a membrane transport modulator, interacts with NSF and the Golgi v-SNARE GOS-28. *EMBO J*, 19, 1494-504.
- SAKUMA, C., SHIZUKUISHI, S., OGAWA, M., HONJO, Y., TAKEYAMA, H., GUAN, J.-L., WEISER, J., SASAI, M., YAMAMOTO, M., OHNISHI, M. & AKEDA, Y. 2024. Individual Atg8 paralogs and a bacterial metabolite sequentially promote hierarchical CSM-xenophagy induction and transition. *Cell Rep*, 43.
- SALAH, F. S., EBBINGHAUS, M., MULEY, V. Y., ZHOU, Z., AL-SAAD, K. R., PACYNA-GENGELBACH, M., O'SULLIVAN, G. A., BETZ, H., KONIG, R., WANG, Z. Q., BRAUER, R. & PETERSEN, I. 2016. Tumor suppression in mice lacking GABARAP, an Atg8/LC3 family member implicated in autophagy, is associated with alterations in cytokine secretion and cell death. *Cell Death Dis*, 7, e2205.
- SANCHEZ-WANDELMER, J., KRIEGENBURG, F., ROHRINGER, S., SCHUSCHNIG, M., GOMEZ-SANCHEZ, R., ZENS, B., ABREU, S., HARDENBERG, R., HOLLENSTEIN, D., GAO, J., UNGERMANN, C., MARTENS, S., KRAFT, C. & REGGIORI, F. 2017. Atg4 proteolytic activity can be inhibited by Atg1 phosphorylation. *Nat Commun*, 8, 295.
- SANJUAN, M. A., DILLON, C. P., TAIT, S. W., MOSHIACH, S., DORSEY, F., CONNELL, S., KOMATSU, M., TANAKA, K., CLEVELAND, J. L., WITHOFF, S. & GREEN, D. R. 2007. Toll-like receptor signalling in macrophages links the autophagy pathway to phagocytosis. *Nature*, 450, 1253-7.
- SANWALD, J. L., DOBNER, J., SIMONS, I. M., POSCHMANN, G., STUHLER, K., ÜFFING, A., HOFFMANN, S. & WILLBOLD, D. 2020. Lack of GABARAP-Type Proteins Is Accompanied by Altered Golgi Morphology and Surfaceome Composition. *Int J Mol Sci*, 22.
- SATOO, K., NODA, N. N., KUMETA, H., FUJIOKA, Y., MIZUSHIMA, N., OHSUMI, Y. & INAGAKI, F. 2009. The structure of Atg4B-LC3 complex reveals the mechanism of LC3 processing and delipidation during autophagy. *EMBO J*, 28, 1341-50.
- SAYERS, E. W., BARRETT, T., BENSON, D. A., BOLTON, E., BRYANT, S. H., CANESE, K., CHETVERNIN, V., CHURCH, D. M., DICUCCIO, M., FEDERHEN, S., FEOLO, M., FINGERMAN, I. M., GEER, L. Y., HELMBERG, W., KAPUSTIN, Y., LANDSMAN, D., LIPMAN, D. J., LU, Z., MADDEN, T. L., MADEJ, T., MAGLOTT, D. R., MARCHLER-BAUER, A., MILLER, V., MIZRACHI, I., OSTELL, J., PANCHENKO, A., PHAN, L., PRUITT, K. D., SCHULER, G. D., SEQUEIRA, E., SHERRY, S. T., SHUMWAY, M., SIROTKIN, K., SLOTTA, D., SOUVOROV, A., STARCHENKO, G., TATUSOVA, T. A., WAGNER, L., WANG, Y., WILBUR, W. J., YASCHENKO, E. & YE, J. 2011. Database resources of the National Center for Biotechnology Information. *Nucleic Acids Res*, 39, D38-51.
- SAYERS, E. W., BECK, J., BOLTON, E. E., BRISTER, J. R., CHAN, J., COMEAU, D. C., CONNOR, R., DICUCCIO, M., FARRELL, C. M., FELDGARDEN, M., FINE, A. M., FUNK, K., HATCHER, E., HOEPPNER, M., KANE, M., KANNAN, S., KATZ, K. S., KELLY, C., KLIMKE, W., KIM, S., KIMCHI, A., LANDRUM, M., LATHROP, S., LU, Z., MALHEIRO, A., MARCHLER-BAUER, A., MURPHY, T.

- D., PHAN, L., PRASAD, A. B., PUJAR, S., SAWYER, A., SCHMIEDER, E., SCHNEIDER, V. A., SCHOCH, C. L., SHARMA, S., THIBAUD-NISSEN, F., TRAWICK, B. W., VENKATAPATHI, T., WANG, J., PRUITT, K. D. & SHERRY, S. T. 2024. Database resources of the National Center for Biotechnology Information. *Nucleic Acids Res*, 52, D33-D43.
- SCHWALM, M. P., DOPFER, J., KUMAR, A., GRECO, F. A., BAUER, N., LÖHR, F., HEERING, J., CANO, S., LECHNER, S., HANKE, T., BEKIC, I., MORASCH, V., FEARON, D., MARPLES, P. G., TOMLINSON, C. W. E., BRUNELLO, L., SAXENA, K., ADAMS, N., VON-DELFT, F., MÜLLER, S., STOLZ, A., PROSCHAK, E., KUSTER, B., KNAPP, S. & ROGOV, V. V. 2023a. Targeting LC3/GABARAP for degrader development and autophagy modulation. *BioRxiv*.
- SCHWALM, M. P., KNAPP, S. & ROGOV, V. V. 2023b. Toward effective Atg8-based ATTECs: Approaches and perspectives. *J Cell Biochem*.
- SCHWARTEN, M., MOHRLÜDER, J., MA, P., STOLDT, M., THIELMANN, Y., STANGLER, T., HERSCH, N., HOFFMANN, B., MERKEL, R. & WILLBOLD, D. 2009. Nix directly binds to GABARAP: a possible crosstalk between apoptosis and autophagy. *Autophagy*, 5, 690-8.
- SHI, X., YOKOM, A. L., WANG, C., YOUNG, L. N., YOULE, R. J. & HURLEY, J. H. 2020. ULK complex organization in autophagy by a C-shaped FIP200 N-terminal domain dimer. *J Cell Biol*, 219.
- SHPIILKA, T., WEIDBERG, H., PIETROKOVSKI, S. & ELAZAR, Z. 2011. Atg8: an autophagy-related ubiquitin-like protein family. *Genome Biol*, 12, 226.
- SHVETS, E., ABADA, A., WEIDBERG, H. & ELAZAR, Z. 2011. Dissecting the involvement of LC3B and GATE-16 in p62 recruitment into autophagosomes. *Autophagy*, 7, 683-688.
- SIEVERS, F. & HIGGINS, D. G. 2014. Clustal omega. *Curr Protoc Bioinformatics*, 48, 3 13 1-3 13 16.
- SKYTTE RASMUSSEN, M., MOUILLERON, S., KUMAR SHRESTHA, B., WIRTH, M., LEE, R., BOWITZ LARSEN, K., ABUDU PRINCELY, Y., O'REILLY, N., SJOTTEM, E., TOOZE, S. A., LAMARK, T. & JOHANSEN, T. 2017. ATG4B contains a C-terminal LIR motif important for binding and efficient cleavage of mammalian orthologs of yeast Atg8. *Autophagy*, 13, 834-853.
- SLITER, D. A., MARTINEZ, J., HAO, L., CHEN, X., SUN, N., FISCHER, T. D., BURMAN, J. L., LI, Y., ZHANG, Z., NARENDRA, D. P., CAI, H., BORSCHKE, M., KLEIN, C. & YOULE, R. J. 2018. Parkin and PINK1 mitigate STING-induced inflammation. *Nature*, 561, 258-262.
- SOU, Y. S., WAGURI, S., IWATA, J., UENO, T., FUJIMURA, T., HARA, T., SAWADA, N., YAMADA, A., MIZUSHIMA, N., UCHIYAMA, Y., KOMINAMI, E., TANAKA, K. & KOMATSU, M. 2008. The Atg8 conjugation system is indispensable for proper development of autophagic isolation membranes in mice. *Mol Biol Cell*, 19, 4762-75.
- STAMATAKOU, E., WROBEL, L., HILL, S. M., PURI, C., SON, S. M., FUJIMAKI, M., ZHU, Y., SIDDIQI, F., FERNANDEZ-ESTEVEZ, M., MANNI, M. M., PARK, S. J., VILLENEUVE, J. & RUBINSZTEIN, D. C. 2020. Mendelian neurodegenerative disease genes involved in autophagy. *Cell Discov*, 6, 24.
- STANGLER, T., MAYR, L. M. & WILLBOLD, D. 2002. Solution structure of human GABA<sub>A</sub> receptor-associated protein GABARAP - Implications for biological function and its regulation. *J Biol Chem*, 277, 13363-13366.
- STEFFEK, M., HELGASON, E., POPOVYCH, N., ROUGE, L., BRUNING, J. M., LI, K. S., BURDICK, D. J., CAI, J., CRAWFORD, T., XUE, J., DECURTINS, W., FANG, C., GRUBERS, F., HOLLIDAY, M. J., LANGLEY, A., PETERSEN, A., SATZ, A. L., SONG, A., STOFFLER, D., STREBEL, Q., TOM, J. Y. K., SKELTON, N., STABEN, S. T., WICHERT, M., MULVIHILL, M. M. & DUEBER, E. C. 2023. A Multifaceted Hit-Finding Approach Reveals Novel LC3 Family Ligands. *Biochemistry*, 62, 633-644.
- STOLZ, A., PUTYRSKI, M., KUTLE, I., HUBER, J., WANG, C., MAJOR, V., SIDHU, S. S., YOULE, R. J., ROGOV, V. V., DÖTSCH, V., ERNST, A. & DIKIC, I. 2017. Fluorescence-based ATG8 sensors monitor localization and function of LC3/GABARAP proteins. *EMBO J*, 36, 549-564.
- SUGAWARA, K., SUZUKI, N. N., FUJIOKA, Y., MIZUSHIMA, N., OHSUMI, Y. & INAGAKI, F. 2004. The crystal structure of microtubule-associated protein light chain 3, a mammalian homologue of *Saccharomyces cerevisiae* Atg8. *Genes Cells*, 9, 611-8.
- SZALAI, P., HAGEN, L. K., SAETRE, F., LUHR, M., SPONHEIM, M., OVERBYE, A., MILLS, I. G., SEGLEN, P. O. & ENGEDAL, N. 2015. Autophagic bulk sequestration of cytosolic cargo is independent of LC3, but requires GABARAPs. *Exp Cell Res*, 333, 21-38.

- TAKAMURA, A., KOMATSU, M., HARA, T., SAKAMOTO, A., KISHI, C., WAGURI, S., EISHI, Y., HINO, O., TANAKA, K. & MIZUSHIMA, N. 2011. Autophagy-deficient mice develop multiple liver tumors. *Genes Dev*, 25, 795-800.
- TAMARGO-GOMEZ, I., MARTINEZ-GARCIA, G. G., SUAREZ, M. F., REY, V., FUEYO, A., CODINA-MARTINEZ, H., BRETONES, G., CARAVIA, X. M., MOREL, E., DUPONT, N., CABO, R., TOMAS-ZAPICO, C., SOUQUERE, S., PIERRON, G., CODOGNO, P., LOPEZ-OTIN, C., FERNANDEZ, A. F. & MARINO, G. 2021. ATG4D is the main ATG8 delipidating enzyme in mammalian cells and protects against cerebellar neurodegeneration. *Cell Death Differ*, 28, 2651-2672.
- TAN, S., WANG, D., FU, Y., ZHENG, H., LIU, Y. & LU, B. 2023. Targeted clearance of mitochondria by an autophagy-tethering compound (ATTEC) and its potential therapeutic effects. *Sci Bull (Beijing)*, 68, 3013-3026.
- TANIDA, I., KOMATSU, M., UENO, T. & KOMINAMI, E. 2003. GATE-16 and GABARAP are authentic modifiers mediated by Apg7 and Apg3. *Biochem Biophys Res Commun*, 300, 637-44.
- TANIDA, I., TANIDA-MIYAKE, E., KOMATSU, M., UENO, T. & KOMINAMI, E. 2002. Human Apg3p/Aut1p homologue is an authentic E2 enzyme for multiple substrates, GATE-16, GABARAP, and MAP-LC3, and facilitates the conjugation of hApg12p to hApg5p. *J Biol Chem*, 277, 13739-44.
- TANIDA, I., TANIDA-MIYAKE, E., UENO, T. & KOMINAMI, E. 2001. The human homolog of *Saccharomyces cerevisiae* Apg7p is a Protein-activating enzyme for multiple substrates including human Apg12p, GATE-16, GABARAP, and MAP-LC3. *J Biol Chem*, 276, 1701-6.
- TANIDA, I., UENO, T. & KOMINAMI, E. 2014. In vitro assays of lipidation of Mammalian Atg8 homologs. *Curr Protoc Cell Biol*, 64, 11 20 1-13.
- THIELMANN, Y., MOHRLÜDER, J., KOENIG, B. W., STANGLER, T., HARTMANN, R., BECKER, K., HOLTJE, H. D. & WILLBOLD, D. 2008. An indole-binding site is a major determinant of the ligand specificity of the GABA type A receptor-associated protein GABARAP. *ChemBiochem*, 9, 1767-75.
- THIELMANN, Y., WEIERGRÄBER, O. H., MA, P., SCHWARTEN, M., MOHRLÜDER, J. & WILLBOLD, D. 2009. Comparative modeling of human NSF reveals a possible binding mode of GABARAP and GATE-16. *Proteins*, 77, 637-46.
- THUMM, M., EGNER, R., KOCH, B., SCHLUMPBERGER, M., STRAUB, M., VEENHUIS, M. & WOLF, D. H. 1994. Isolation of Autophagocytosis Mutants of *Saccharomyces-Cerevisiae*. *FEBS LETT*, 349, 275-280.
- THURSTON, T. L., RYZHAKOV, G., BLOOR, S., VON MUHLINEN, N. & RANDOW, F. 2009. The TBK1 adaptor and autophagy receptor NDP52 restricts the proliferation of ubiquitin-coated bacteria. *Nat Immunol*, 10, 1215-21.
- TIMIMI, L., WROBEL, A. G., CHIDUZA, G. N., MASLEN, S. L., TORRES-MÉNDEZ, A., MONTANER, B., DAVIS, C., SKEHEL, J. M., RUBINSTEIN, J. L., SCHREIBER, A. & BEALE, R. 2023. The V-ATPase/ATG16L1 axis is controlled by the V1H subunit. *BioRxiv*.
- TOOZE, S. A., ABADA, A. & ELAZAR, Z. 2014. Endocytosis and autophagy: exploitation or cooperation? *Cold Spring Harb Perspect Biol*, 6, a018358.
- TSUBOYAMA, K., KOYAMA-HONDA, I., SAKAMAKI, Y., KOIKE, M., MORISHITA, H. & MIZUSHIMA, N. 2016. The ATG conjugation systems are important for degradation of the inner autophagosomal membrane. *Science*, 354, 1036-1041.
- TSUKADA, M. & OHSUMI, Y. 1993. Isolation and Characterization of Autophagy-Defective Mutants of *Saccharomyces-Cerevisiae*. *FEBS LETT*, 333, 169-174.
- TUMBARELLO, D. A., MANNA, P. T., ALLEN, M., BYCROFT, M., ARDEN, S. D., KENDRICK-JONES, J. & BUSS, F. 2015. The Autophagy Receptor TAX1BP1 and the Molecular Motor Myosin VI Are Required for Clearance of *Salmonella Typhimurium* by Autophagy. *PLoS Pathog*, 11, e1005174.
- ÜFFING, A., GOLD, L., GENSCHE, T., WEIERGRÄBER, O. H., HOFFMANN, S. & WILLBOLD, D. 2024a. Highlighting the hidden: monitoring the avidity-driven association of a fluorescent GABARAP tandem with microtubules in living cells. *Autophagy Reports*, 3.



- ÜFFING, A., WEIERGRÄBER, O. H., SCHWARTEN, M., HOFFMANN, S. & WILLBOLD, D. 2024b. GABARAP interacts with EGFR — supporting the unique role of this hAtg8 protein during receptor trafficking. *FEBS LETT*.
- UHLEN, M., FAGERBERG, L., HALLSTROM, B. M., LINDSKOG, C., OKSVOLD, P., MARDINOGLU, A., SIVERTSSON, A., KAMPF, C., SJOSTEDT, E., ASPLUND, A., OLSSON, I., EDLUND, K., LUNDBERG, E., NAVANI, S., SZIGYARTO, C. A., ODEBERG, J., DJUREINOVIC, D., TAKANEN, J. O., HOBER, S., ALM, T., EDQVIST, P. H., BERLING, H., TEGEL, H., MULDER, J., ROCKBERG, J., NILSSON, P., SCHWENK, J. M., HAMSTEN, M., VON FEILITZEN, K., FORSBERG, M., PERSSON, L., JOHANSSON, F., ZWAHLEN, M., VON HEIJNE, G., NIELSEN, J. & PONTEN, F. 2015. Proteomics. Tissue-based map of the human proteome. *Science*, 347, 1260419.
- UHLEN, M., OKSVOLD, P., FAGERBERG, L., LUNDBERG, E., JONASSON, K., FORSBERG, M., ZWAHLEN, M., KAMPF, C., WESTER, K., HOBER, S., WERNERUS, H., BJORLING, L. & PONTEN, F. 2010. Towards a knowledge-based Human Protein Atlas. *Nat Biotechnol*, 28, 1248-50.
- ULFERTS, R., MARCASSA, E., TIMIMI, L., LEE, L. C., DALEY, A., MONTANER, B., TURNER, S. D., FLOREY, O., BAILLIE, J. K. & BEALE, R. 2021. Subtractive CRISPR screen identifies the ATG16L1/vacuolar ATPase axis as required for non-canonical LC3 lipidation. *CELL REP*, 37.
- VAITES, L. P., PAULO, J. A., HUTTLIN, E. L. & HARPER, J. W. 2018. Systematic Analysis of Human Cells Lacking ATG8 Proteins Uncovers Roles for GABARAPs and the CCZ1/MON1 Regulator C18orf8/RMC1 in Macroautophagic and Selective Autophagic Flux. *Mol Cell Biol*, 38.
- VERBAANDERD, C., MAES, H., SCHAAF, M. B., SUKHATME, V. P., PANTZIARKA, P., SUKHATME, V., AGOSTINIS, P. & BOUCHE, G. 2017. Repurposing Drugs in Oncology (ReDO)-chloroquine and hydroxychloroquine as anti-cancer agents. *Ecancermedicalscience*, 11, 781.
- VERNIER-MAGNIN, S., MULLER, S., SALLOT, M., RADOM, J., MUSARD, J. F., ADAMI, P., DULIEU, P., REMY-MARTIN, J. P., JOUVENOT, M. & FRAICHARD, A. 2001. A novel early estrogen-regulated gene gec1 encodes a protein related to GABARAP. *Biochem Biophys Res Commun*, 284, 118-25.
- VIJAY-KUMAR, S., BUGG, C. E. & COOK, W. J. 1987. Structure of ubiquitin refined at 1.8 Å resolution. *J Mol Biol*, 194, 531-44.
- VON MUHLINEN, N., AKUTSU, M., RAVENHILL, B. J., FOEGLEIN, A., BLOOR, S., RUTHERFORD, T. J., FREUND, S. M., KOMANDER, D. & RANDOW, F. 2012. LC3C, bound selectively by a noncanonical LIR motif in NDP52, is required for antibacterial autophagy. *Mol Cell*, 48, 329-42.
- WANG, H. & OLSEN, R. W. 2000. Binding of the GABA<sub>A</sub> receptor-associated protein (GABARAP) to microtubules and microfilaments suggests involvement of the cytoskeleton in GABARAP–GABA<sub>A</sub> receptor interaction. *J Neurochem*, 75, 644-55.
- WANG, H., SUN, H. Q., ZHU, X., ZHANG, L., ALBANESI, J., LEVINE, B. & YIN, H. 2015. GABARAPs regulate PI4P-dependent autophagosome:lysosome fusion. *Proc Natl Acad Sci U S A*, 112, 7015-20.
- WANG, H. B., BEDFORD, F. K., BRANDON, N. J., MOSS, S. J. & OLSEN, R. W. 1999. GABA<sub>A</sub>-receptor-associated protein links GABA<sub>A</sub> receptors and the cytoskeleton. *Nature*, 397, 69-72.
- WANG, Y., RAMOS, M., JEFFERSON, M., ZHANG, W., BERAZA, N., CARDING, S., POWELL, P. P., STEWART, J. P., MAYER, U. & WILEMAN, T. 2022. Control of infection by LC3-associated phagocytosis, CASM, and detection of raised vacuolar pH by the V-ATPase-ATG16L1 axis. *Sci Adv*, 8, eabn3298.
- WEIDBERG, H., SHPILKA, T., SHVETS, E., ABADA, A., SHIMRON, F. & ELAZAR, Z. 2011. LC3 and GATE-16 N termini mediate membrane fusion processes required for autophagosome biogenesis. *Dev Cell*, 20, 444-54.
- WEIDBERG, H., SHVETS, E., SHPILKA, T., SHIMRON, F., SHINDER, V. & ELAZAR, Z. 2010. LC3 and GATE-16/GABARAP subfamilies are both essential yet act differently in autophagosome biogenesis. *EMBO J*, 29, 1792-1802.
- WEIERGRÄBER, O. H., STANGLER, T., THIELMANN, Y., MOHRLÜDER, J., WIESEHAN, K. & WILLBOLD, D. 2008. Ligand binding mode of GABA<sub>A</sub> receptor-associated protein. *J Mol Biol*, 381, 1320-31.

- WILD, P. F., H.; MCEWAN, D.G.; WAGNER, S.; ROGOV, V.V.; BRADY, N.R.; RICHTER, B.; KORAC, J.; WAIDMANN, O.; CHOUDHARY, C.; DÖTSCH, V.; BUMANN, D.; DIKIC, I. 2011. Phosphorylation of the Autophagy Receptor Optineurin Restricts Salmonella Growth. *Science*, 333.
- WIRTH, M., MOUILLERON, S., ZHANG, W., SJOTTEM, E., PRINCELY ABUDU, Y., JAIN, A., LAURITZ OLSEVIK, H., BRUUN, J. A., RAZI, M., JEFFERIES, H. B. J., LEE, R., JOSHI, D., O'REILLY, N., JOHANSEN, T. & TOOZE, S. A. 2021. Phosphorylation of the LIR Domain of SCOC Modulates ATG8 Binding Affinity and Specificity. *J Mol Biol*, 433, 166987.
- WIRTH, M., ZHANG, W., RAZI, M., NYONI, L., JOSHI, D., O'REILLY, N., JOHANSEN, T., TOOZE, S. A. & MOUILLERON, S. 2019. Molecular determinants regulating selective binding of autophagy adapters and receptors to ATG8 proteins. *Nat Commun*, 10, 2055.
- WU, F., WATANABE, Y., GUO, X. Y., QI, X., WANG, P., ZHAO, H. Y., WANG, Z., FUJIOKA, Y., ZHANG, H., REN, J. Q., FANG, T. C., SHEN, Y. X., FENG, W., HU, J. J., NODA, N. N. & ZHANG, H. 2015. Structural Basis of the Differential Function of the Two *C. elegans* Atg8 Homologs, LGG-1 and LGG-2, in Autophagy. *Mol Cell*, 60, 914-29.
- WU, W., TIAN, W., HU, Z., CHEN, G., HUANG, L., LI, W., ZHANG, X., XUE, P., ZHOU, C., LIU, L., ZHU, Y., ZHANG, X., LI, L., ZHANG, L., SUI, S., ZHAO, B. & FENG, D. 2014. ULK1 translocates to mitochondria and phosphorylates FUNDC1 to regulate mitophagy. *EMBO Rep*, 15, 566-75.
- XIE, X. S., PADRON, D., LIAO, X., WANG, J., ROTH, M. G. & DE BRABANDER, J. K. 2004. Salicylhalamide A inhibits the V0 sector of the V-ATPase through a mechanism distinct from bafilomycin A1. *J Biol Chem*, 279, 19755-63.
- XIN, Y., YU, L., CHEN, Z., ZHENG, L., FU, Q., JIANG, J., ZHANG, P., GONG, R. & ZHAO, S. 2001. Cloning, expression patterns, and chromosome localization of three human and two mouse homologues of GABA<sub>A</sub> receptor-associated protein. *Genomics*, 74, 408-13.
- XU, R., JI, Z., XU, C. & ZHU, J. 2018. The clinical value of using chloroquine or hydroxychloroquine as autophagy inhibitors in the treatment of cancers: A systematic review and meta-analysis. *Medicine (Baltimore)*, 97, e12912.
- XU, Y., ZHOU, P., CHENG, S., LU, Q., NOWAK, K., HOPP, A. K., LI, L., SHI, X., ZHOU, Z., GAO, W., LI, D., HE, H., LIU, X., DING, J., HOTTIGER, M. O. & SHAO, F. 2019. A Bacterial Effector Reveals the V-ATPase-ATG16L1 Axis that Initiates Xenophagy. *Cell*, 178, 552-566 e20.
- XUE, G., XIE, J., HINTERDORFER, M., CIGLER, M., DOTSCH, L., IMRICHOVA, H., LAMPE, P., CHENG, X., ADARIANI, S. R., WINTER, G. E. & WALDMANN, H. 2023. Discovery of a Drug-like, Natural Product-Inspired DCAF11 Ligand Chemotype. *Nat Commun*, 14, 7908.
- YAMAMOTO, H., ZHANG, S. & MIZUSHIMA, N. 2023. Autophagy genes in biology and disease. *Nat Rev Genet*, 24, 382-400.
- YANG, A., RAJESHKUMAR, N. V., WANG, X., YABUUCHI, S., ALEXANDER, B. M., CHU, G. C., VON HOFF, D. D., MAITRA, A. & KIMMELMAN, A. C. 2014. Autophagy is critical for pancreatic tumor growth and progression in tumors with p53 alterations. *Cancer Discov*, 4, 905-13.
- YANG, C. S., LEE, J. S., RODGERS, M., MIN, C. K., LEE, J. Y., KIM, H. J., LEE, K. H., KIM, C. J., OH, B., ZANDI, E., YUE, Z., KRAMNIK, I., LIANG, C. & JUNG, J. U. 2012. Autophagy protein Rubicon mediates phagocytic NADPH oxidase activation in response to microbial infection or TLR stimulation. *Cell Host Microbe*, 11, 264-76.
- YANG, Y. & KLIONSKY, D. J. 2020. Autophagy and disease: unanswered questions. *Cell Death Differ*, 27, 858-871.
- YANG, Z., WILKIE-GRANTHAM, R. P., YANAGI, T., SHU, C. W., MATSUZAWA, S. & REED, J. C. 2015. ATG4B (Autophagin-1) phosphorylation modulates autophagy. *J Biol Chem*, 290, 26549-61.
- YE, J., ZOU, G., ZHU, R., KONG, C., MIAO, C., ZHANG, M., LI, J., XIONG, W. & WANG, C. 2021. Structural basis of GABARAP-mediated GABA<sub>A</sub> receptor trafficking and functions on GABAergic synaptic transmission. *Nat Commun*, 12, 297.
- YUE, Z., JIN, S., YANG, C., LEVINE, A. J. & HEINTZ, N. 2003. Beclin 1, an autophagy gene essential for early embryonic development, is a haploinsufficient tumor suppressor. *Proc Natl Acad Sci U S A*, 100, 15077-82.

- ZHANG, S., YAZAKI, E., SAKAMOTO, H., YAMAMOTO, H. & MIZUSHIMA, N. 2022. Evolutionary diversification of the autophagy-related ubiquitin-like conjugation systems. *Autophagy*, 18, 2969-2984.
- ZHANG, W., NISHIMURA, T., GAHLOT, D., SAITO, C., DAVIS, C., JEFFERIES, H. B. J., SCHREIBER, A., THUKRAL, L. & TOOZE, S. A. 2023. Autophagosome membrane expansion is mediated by the N-terminus and cis-membrane association of human ATG8s. *Elife*, 12.
- ZHENG, Y., QIU, Y., GRACE, C. R. R., LIU, X., KLIONSKY, D. J. & SCHULMAN, B. A. 2019. A switch element in the autophagy E2 Atg3 mediates allosteric regulation across the lipidation cascade. *Nat Commun*, 10, 3600.
- ZHOU, J., RASMUSSEN, N. L., OLSVIK, H. L., AKIMOV, V., HU, Z., EVJEN, G., KAESER-PEBERNARD, S., SANKAR, D. S., ROUBATY, C., VERLHAC, P., VAN DE BEEK, N., REGGIORI, F., ABUDU, Y. P., BLAGOEV, B., LAMARK, T., JOHANSEN, T. & DENGJEL, J. 2023. TBK1 phosphorylation activates LIR-dependent degradation of the inflammation repressor TNIP1. *J Cell Biol*, 222.
- ZHU, Y., MASSEN, S., TERENCE, M., LANG, V., CHEN-LINDNER, S., EILS, R., NOVAK, I., DIKIC, I., HAMACHER-BRADY, A. & BRADY, N. R. 2013. Modulation of serines 17 and 24 in the LC3-interacting region of Bnip3 determines pro-survival mitophagy versus apoptosis. *J Biol Chem*, 288, 1099-1113.